Sheffield Hallam University

A Sheffield Hallam University thesis
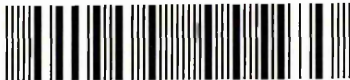
Fines are charged at 50p per hour

2 6 FEB 2007

REFERENCE

ProQuest Number: 10694339

ProQuest 10694339

ProQuest LLC.
789 East Eisenhower Parkway
P.O. Box 1346
Ann Arbor, MI 48106 – 1346

Optimising the airflow performance of ventilators for natural ventilation in buildings

Nelson Chilengwe

A thesis submitted in partial fulfilment of the requirements of
Sheffield Hallam University
for the degree of Doctor of Philosophy

January 2005

Acknowledgements

ABSTRACT

Ventilation is essential if an adequate environment in buildings is to be provided. Natural ventilation is a sustainable method commonly used to achieve this. Natural ventilation can occur from random flow of air through unintentional (adventitious) openings, commonly referred to as *infiltration,* or can be facilitated through purpose-provided openings - commonly called *controlled* natural ventilation. Stringent national and international regulations have led to building structures becoming more and more air-tight so that ventilation is confined to airflow through intentionally provided openings only. These purpose-provided openings typically consist of one or a combination of basic components such as louvers, insect-screens or noise baffles. An extensive literature review indicated that the airflow performance of combinations of such components has neither been thoroughly determined nor fully understood, making it difficult to accurately predict their building performance. This investigation set out to answer some of these questions by employing experimental and computational fluid dynamics (CFD) parametric studies. For the experimental study, a test rig was designed and constructed in accordance with European Standard BS EN 13141-1: 2004. The text rig was designed with sufficient flexibility to enable individual components and combinations of various components to be investigated. Components tested ranged from ordinary slots fabricated from pine wood to commercial ventilators and mesh-screens as are commonly found in natural ventilation applications. The results of this investigation indicate that the overall airflow properties of a ventilator are influenced by the combination of constituent components, the manner in which the components are incorporated into a ventilator and also the direction of airflow through it. A CFD study utilising three-dimensional models of some of the components tested during the experimental phase, and employing the k - ε turbulence representation was facilitated by a commercial software package (FLOVENT). Comparisons between CFD results and experimental data were reasonable and acceptable. A new mathematical approach, based up on experimental results, to analyse the airflow properties of combinations of ventilator components is introduced in this thesis. The proposed equations enable relative assessments of the impacts of each component on the overall airflow performance of a ventilator to be made. Comparisons between results from the proposed equations and those obtained experimentally showed good agreement. Although more work could be done to understand the physical meaning of the equations proposed, the author believes that this investigation has set a foundation for a generic representation of ventilator airflow performance. As such, refinements to the proposed equations would inevitably result if further research into this task is undertaken.

Contents

Chapter 3: Basic Principles of Fluid Flow

Chapter 4: Fundamentals of Airflow through Openings

Chapter 5: Experimental Investigation

Chapter 6: Computational Fluid Dynamics

Chapter 7: Ventilator Airflow Performance Optimisation

Chapter 8: Final Remarks

Bibliography

Appendices

List of Tables

Chapter 2

Chapter 4

Chapter 5

Chapter 6

Chapter 7

Appendix A

List of Figures

Chapter 2

Chapter 3

Chapter 4

Chapter 5

Chapter 6

Chapter 7

Nomenclature

Symbol	Description
A	constant
A$_e$	effective area of an opening
A$_L$	effective leakage area
A$_m$	geometrically measured area
A$_s$	surface area
B	constant
B$_o$	permeability coefficient
b	width of rectangular strip orifice
C	constant
C$_p$	pressure coefficient
c	gas concentration at any instant inside room
c$_o$	gas concentration at time t = 0
c$_{pair}$	specific heat capacity of air
C$_i$	maximum allowable indoor concentration of contaminant
C$_o$	concentration of contaminant in outdoor air
c$_d$	discharge coefficient
c$_v$	coefficient of velocity
C$_z$	discharge coefficient
d	gap thickness
d$_h$	hydraulic diameter
F	normal force
F$_i$	inertia force
F$_s$	shear force
G	generation rate of contaminant in occupied zone
g	gravitational constant (= 9.81)
h	height of observation point
h$_{NPL}$	height of neutral pressure level
I	infiltration rate
K	flow coefficient dependent on geometry of opening
k	pressure loss coefficient
L	length in direction of flow
ℓ	characteristic length
M	momentum of fluid particle
m	mass of particle
m$_r$	mass flow rate
N	air change rate
n	index
p	unkown static pressure at reference height

p_a	ambient pressure
p_o	static pressure at reference plane
p_s	static pressure
p_t	total pressure
p_v	velocity pressure
p_w	wind pressure
Q	volume flow rate
Q_{act}	actual airflow rate
Q_{comp}	airflow rate through component
Q_{heat}	heat flow
Q_L	volume flow rate from low pressure characteristic
Q_{leak}	air leakage
Q_H	volume flow rate from high pressure characteristic
Q_{meas}	measured volume flow rate
Q_{STP}	volume flow rate corrected to standard temperature and pressure
Q_T	total volume flow rate
q_v	volume flow rate across area A
R	regression correlation coefficient
R_{const}	universal gas constant (=287)
Re	Reynolds number
S	surface area of walls and roof
T	temperature at height h
T_a	ambient temperature
T_i	indoor temperature
T_o	outdoor temperature
T_{ref}	temperature at reference height
t	time in seconds
u_o	wind velocity in unrestricted airflow
V	ventilation rate
V_{cont}	control volume
V_r	predicted volume flow rate
V_{50}	leakage airflow rate at 50 Pa
vol	volume of occupied zone
v	velocity at a given point in the flow field
v'	average velocity
w	width of opening
x	horizontal distance along flow path
y	distance normal to the flow
z	distance through crack
α	power law coefficient
β	power law index
ε	rate of dissipation
Δ	change in given quantity
ΔP	pressure difference between two observation points
ΔP_o	unknown pressure difference at reference height
Δp_T	pressure difference due to stack effect
ΔP_r	reference pressure difference
ΔP_T	total pressure difference across an opening
ρ	fluid density
ρ_{air}	air density
ρ_{cold}	density of colder air
ρ_{warm}	density of warmer air
ρ_o	fluid density at reference temperature

μ	dynamic viscosity
θ	angle of inclination
φ	predicted quantity
ν	kinematic viscosity
τ	shear stress

Subscripts

0	reference point
1	observation point 1
2	observation point 2
i	internal
e	external
L	louver
M	mesh
V	ventilator

Abbreviations

AIVC	Air Infiltration and Ventilation Centre
AHU	Air Handling Unit
AM	Applications Manual
ASHRAE	American Society of Heating Ventilation and Air Conditioning Engineers
ASTM	American Society for Testing and Materials
BMS	Building Management System
BRE	Building Research Establishment
BS	British Standard
CEN	Central European Nations
CFD	Computational Fluid Dynamics
CIBSE	Chartered Institution of Building Services Engineers
CO_2	Carbon Dioxide
FA	Free Area
HVAC	Heating Ventilation and Air Conditioning
MDF	Medium Density Fibreboard
NPL	Neutral Pressure Level
ROI	Relative Overall Improvement
TM	Technical Memorundum

Real ventilation is so uncommon that ....the layman usually thinks the object has been attained if some of the windows can be opened.

Ventilating and Warming, Prof. Ernest Jacob, 1894.

Chapter 1

INTRODUCTION

This chapter introduces the background to the investigation reported and highlights the motivation behind this work, including the definition of the application domain through to aims, objectives and outline of the research methodology employed. Some key aspects of the indoor environment and its implications are also briefly explained. The chapter closes with an outline of the chapters forming the rest of this thesis.

1.1 Background

Over the last twenty to thirty years there has been a shift in emphasis in relation to priorities concerning energy and indoor climate in buildings. For instance, in the 1970s the energy crisis led to energy conservation for heating being the key issue of concern in most climates whilst in the 1990s much attention was paid to global energy use, air leakage through building envelopes, comfort and indoor air quality within buildings. Although heat depletion through the building envelope has been greatly reduced, the loss of background ventilation due to infiltration, along with bad HVAC system maintenance and increased pollution, has led to poor indoor air quality and subsequently to building related illnesses.

1.2 Energy and Environmental Impact of Buildings

In developed countries, such as the U.K., buildings consume approximately 50% of all primary energy production [Parrot, *1998*, DEFRA, *2003*] whilst in the U.S. buildings account for more than 36% of primary energy usage - representing about 62% of total U.S. electricity consumption [Rosenberg, *2002,* WBDG, *2004*]. This energy is used for the heating, cooling, lighting, ventilating and other essential activities of building occupants. Since virtually all of this energy is produced from the burning of fossil fuels then buildings also contribute around 50% and 36%, for U.K. and U.S. respectively, of the total carbon dioxide (CO_2) emissions into the atmosphere. In addition, the use of air-

conditioning not only increases building operation costs, but leads to the discharge of refrigerants into the atmosphere. The effluent from fossil fuels and air-conditioning processes may be detrimental on the environment through the effects of global warming and ozone depletion. Therefore, an important strategy in reducing these effects must be to make buildings more energy efficient.

1.3 Indoor Environment: Occupants' Comfort and Health

Given that on average people spend about 90% of their time indoors [Liddament, *1996*] healthy and comfortable indoor environments are essential in sustaining the quality of life. Indoor environmental quality depends on many interrelating factors, not least the physical parameters that define thermal comfort *(temperature, relative humidity, air movement)*, indoor air quality *("freshness" as defined by carbon dioxide level and "cleanliness" as defined by absence of harmful substances i.e. air pollution)*, lighting quality *(mainly day-lighting provisions)*, and acoustics *(noise and vibration aspects)*.

The impact of poor air quality on comfort, health and occupant attitudes often results in occupant dissatisfaction and loss of productivity and revenue. To avoid this negative impact it is essential that buildings be designed and operated to meet basic human requirements for a healthy and comfortable indoor environment while at the same time ensuring low energy consumption. Essentially, ventilation is required to provide a thermally comfortable environment and to dilute pollutants *(allergens, carbon monoxide, carbon dioxide, tobacco smoke, moisture, volatile organic compounds, odours etc)* to levels unlikely to pose a health risk [Ata, *1997*], and to combat condensation. As such, it is vitally important to have an effective ventilation system to help meet occupants' increasing expectations for satisfactory air quality in the indoor environment.

1.4 Sustainable Approach to Building Design

One approach to making buildings more energy efficient is to smartly design and operate them in a way that reduces total energy usage, such as the consumption associated with mechanical ventilation and air-conditioning. This involves either supplementing or replacing these energy-intensive services with more sustainable and environmentally friendly schemes such as natural ventilation systems [Allard, *1998*].

Although the concept of natural ventilation is a familiar one, the successful design of a modern naturally ventilated large building or its incorporation into existing buildings is a complex and comparatively untried process. This process often requires a combination of high tech and low tech solutions and has been found to be most effective if addressed in initial design phases. Any concerns about the external environment must be balanced against the need for an indoor environment that is sustainable.

Several major building projects have been completed in the last ten to fifteen years that would have, traditionally, been designed to be mechanically serviced. Instead, the supply of fresh air was designed to be provided predominantly by natural ventilation systems. Examples of such projects include the Wessex Water Headquarters [Alexander, *2000*] and the Contact Theatre in Manchester [Palmer, *1999*]. Also, studies suggest that naturally ventilated buildings have health benefits for building occupants [Vincent *et al. 1997*].

1.5 Application Domain

At the heart of natural ventilation systems are the facade openings that allow fresh air to flow in and stale air to flow out of a building. These openings can take the form of simple holes or slots, openable windows, trickle ventilators and through-wall ventilators. The design and performance of these openings are critical factors in determining the success of a natural ventilation system because the natural forces that drive fresh air into buildings (the wind and/or thermal buoyancy) are very weak. The pressure difference across an opening will typically be less than 10 Pascal for a naturally ventilated building whereas for a mechanically ventilated building the pressure difference will usually exceed 100 Pascal.

In urban areas natural ventilation openings in buildings (*open windows, trickle ventilators and through-the-wall ventilators*) can lead to several environmental problems, such as noise and poor indoor air quality for building occupants. Such problems can create major obstacles to the widespread implementation of natural ventilation in new and refurbished urban buildings. For example, the design requirements for the airflow performance and acoustic performance of a ventilator are not complimentary. For airflow the requirement is for a large open area with smooth

uninterrupted flow path. For acoustics the requirement is for a small open area with an attenuating multi-bend flow path. There obviously has to be a design compromise if a ventilator is to have both good airflow and good acoustic properties. From an aerodynamic perspective a ventilator can be a combination of relatively large openings (such as louvers) with flow properties independent of the flow rate (Reynolds number independent), and very small openings (such as insect screens) that may have some Reynolds number dependence as indicated in Baker *et al.* (*1986*).

A literature review of ventilator research, including a search of the AIVC database, indicated that previous work in this area tended to investigate either overall ventilator performance, for example Gonzalez, *1984*, Yakubu and Sharples, *1991*, Ayad *1999*, Heiselberg *et al. 2001*, Karava *et al. 2003*, or individual elements such as louvres, screens and meshes in isolation, for example White *et al. 1998*, Maghrabi and Sharples, *1999*, Miguel *et al. 2001*. These observations are also true for the recently completed EU-funded natural ventilation research project NatVent® [NatVent, *1999*]. Such studies have often assessed geometrical dimensions, fluid properties and pressure coefficients in order to determine their impact on the airflow characteristics of the ventilator components in relation to gaining fundamental understanding of the airflow characteristics.

A recent study by the UK's Building Research Establishment (BRE) [White *et al. 1999*] of twenty-one commercial trickle and wall ventilators revealed that the airflow performance of these devices could be more complex than might be envisaged from their relatively simple constructions. Some ventilators performed better than would be predicted from their free area, and others performed worse (*free area* is the physical size of the smallest aperture in the ventilator). The BRE study concluded that these discrepancies might arise from a poor understanding of the interactions between, among other things, internal flow paths, insect screens, filter materials, baffles and louvre blade shape/geometry. However, the BRE study was not required to investigate in a parametric manner the nature of these interactions.

There does not appear to have been a systematic, parametric study of how components within a ventilator system interact with each other to impact upon the final airflow performance. Therefore, part of the motivation for this research stemmed from the need

to gain better understanding of the interactions between the components constituting a ventilator system. The other part resulted from the fact that recent years have seen increasing application of Computational Fluid Dynamics (CFD) as a tool for understanding and predicting the performance of thermal-fluids systems thus offering a competitive and more flexible alternative to full-scale physical modelling. However, at present there is a lack of validated CFD data relating to airflow performance of ventilators for natural ventilation of buildings. On this basis this study set out to test if CFD could be used as a reliable design, analysis and optimisation tool for ventilators.

1.6 Aims and Objectives

The need to understand the interactions between the components in a ventilator and the subsequent impact on airflow performance cannot be over-emphasised. This understanding would enable manufacturers to design ventilators that have as high an airflow performance as possible. For example, a manufacturer of a particular ventilator might be interested to know the relative contributions to flow resistance of louvre blade shape, size and spacing compared to, say, different insect screen mesh sizes or acoustic linings. The parametric experimental studies carried out in this study allowed some of these questions to be answered and design guidance given for individual components.

Discussions with several ventilators manufacturers revealed that optimising the design of a particular ventilator tended to proceed via a series of 'trial and error' experiments with physical prototypes. It is useful for manufacturers to have computer-based tools that enabled them to analyse how changes in the design of individual components affected the overall airflow properties of a ventilator. The suitability of CFD as a potential design tool for this purpose was investigated in the study. Although it was recognised that there are other important ventilator performance issues, such as weather-tightness, day-lighting admittance and noise ingress, this investigation concentrated solely on airflow.

The overall aim of this study was to investigate the airflow performance of ventilators through a parametric analysis based upon experimental measurements and Computational Fluid Dynamics (CFD) modelling.

The specific objectives were as follows:

- To investigate experimentally how individual components in ventilators affect airflow performance

- To develop flow equations to describe the airflow through ventilators

- To compare experimental data with CFD predicted values and develop CFD as a potential design/analysis tool for ventilators

- To develop a methodology to design ventilators with the aim of optimising the overall airflow performance

1.7 Methodology

Investigations on aerodynamic characteristics of a building component essentially involve the task of determining a relationship between the pressure differential and the airflow through the component. Traditionally, *experimental* methods are utilized to collect fundamental data which are then subjected to *analytical* methods in order to derive mathematical models that describe the airflow characteristics. Recent years have seen the rapid development of concepts of tailoring *numerical* methods such as Computational Fluid Dynamics (CFD) to provide fast and accurate predictions of complex airflow problems for ventilation designers and researchers. At present there is a lack of information about possible techniques that could be used in an attempt to *optimise* the airflow performance of ventilators in relation to a set of identified parameters (such as the louvre blade angle or spacing between the louvre and mesh-screen). These methods are applied, developed where necessary, and discussed in detail elsewhere in this thesis.

1.8 Thesis Outline

The intention of this chapter was to set the scene by highlighting the motivation for the investigation, laying down some pointers to the present state of knowledge and outlining the general scope of subject under investigation.

The remainder of this thesis is arranged to cover in sufficient detail some background

theory relating to natural ventilation in buildings and strategies used to implement natural ventilation (*Chapter 2*). *Chapter 3* focuses on the basic principles of fluid flow in general. Following on from *Chapter 3*, the fundamentals of airflow through ventilation openings are outlined in *Chapter 4*, which includes a literature review relating to ventilator openings in general and airflow performance in particular. This chapter also provides an initial look at ventilator airflow performance optimisation.

Details of the test facility, main equipment and set-up used to carry out numerous parametric experiments are given in *Chapter 5* together with an account of the components investigated. The bulk of topics considered in this chapter have also been presented at international conferences and published in a number of prestigious refereed journals either individually or in combination with other material included in this thesis. Computational Fluid Dynamics modelling and simulations including a theoretical background to its application to airflow in buildings are detailed in *Chapter 6*.

Chapter 7 analyses and discusses the experimental results and incorporates detailed comparisons with predictions from CFD and results from other researchers. The strategy employed in attempting to optimise the airflow performance of ventilators for natural ventilation in buildings is presented in detail. Results from this optimisation exercise are included in this chapter together with problems encountered and limitations of the optimisation method used.

The thesis closes (*Chapter 8*) with an overview of the main findings of the investigation including suggestions of design guidelines for ventilator manufacturers and briefly proposes some recommendations of future work for making ventilators more efficient for natural ventilation applications.

Chapter 2

NATURAL VENTILATION IN BUILDINGS

In this chapter various key concepts relating to the design and application of natural ventilation in buildings are introduced. Advantages of natural ventilation over other methods of ventilating buildings are highlighted together with the various strategies utilised in employing natural ventilation. A general overview of natural ventilation openings is also introduced here.

2.1 Background

2.1.1 Why ventilate buildings?

The need for ventilation today is still the same as it has been over many centuries, namely to ensure acceptable indoor air quality (and thermal conditions) within a room or building and to provide a supply of combustion air for fuel-fired heating appliances. Adequate ventilation is essential to replenish oxygen used by occupants, to remove pollutants generated by breathing, for combustion and other household activities, to maintain low odour levels, to discharge heat, to control condensation and to remove emissions from building materials.

What is changing, however, is the means of achieving this need with regard to regional climatic conditions and in accordance with the various Building Regulations imposed by national governments. Typically people spend around 90% of their time in buildings. As such poor ventilation can have an effect on their comfort, health, well-being and productivity. Ventilation is essential if an adequate environment in buildings is to be provided. It usually involves a significant capital and operating expenditure, hence, it is an important consideration in building design.

2.1.2 What is ventilation?

Nowadays, ventilation is considered as the process of providing fresh air or removing stale air at acceptable rates to/from the occupants of a building, rather than the buildings themselves, in order to sustain a good standard of air quality and thermal comfort with minimum capital cost and environmental impact [Awbi, *1998*].

Ventilation may involve one or both of two processes:-

- Where a source of contamination can be readily isolated, air can be exhausted from its immediate vicinity in such a way that contaminants are captured and directed into the exhaust system before they can diffuse into the occupied space. This approach is widely used in industrial applications.

- Where an entire room is a source of contamination, an exhaust system may be used to isolate it from the rest of the building. In removing contaminants in this way, provision must be made for an adequate supply of replacement air.

In most situations the sources of contaminants, usually the occupants themselves and their activities are not readily isolated. The ventilation process then employed is that of dilution. Outdoor air is thoroughly mixed with the air in the occupied space and displaces an equal volume of room air.

2.1.3 How are buildings ventilated?

The process of ventilation consists of the passage of air into the space to be ventilated and out of it again and the distribution of the air during its passage through the ventilated space. At the extremes, two methods, namely mechanical ventilation and natural ventilation, are commonly used to facilitate the process of changing air in an occupied zone. A third method, hybrid ventilation, currently gaining in popularity, combines some aspects of mechanical and natural ventilation systems.

Mechanical ventilation involves the supply of outdoor air to, or removal of room air from, a building using electrically powered fans. There are three basic types of mechanical ventilation systems (Figure 2.1). A *supply-only system* relies on a supply fan to bring outdoor air into a building, raising the air pressure inside the building thus causing an outward flow of air through cracks and openings in the building envelope. An *extract-only or exhaust-only system* works in the opposite way. It employs an extract fan to discharge indoor air to outdoors, thereby lowering the air pressure inside the building so that outdoor air is drawn in through cracks and openings in the building envelope. A *balanced system* simultaneously supplies outdoor air to a building and extracts an approximately equal amount of indoor air.

Supply-only system Exaust-only system Balanced system
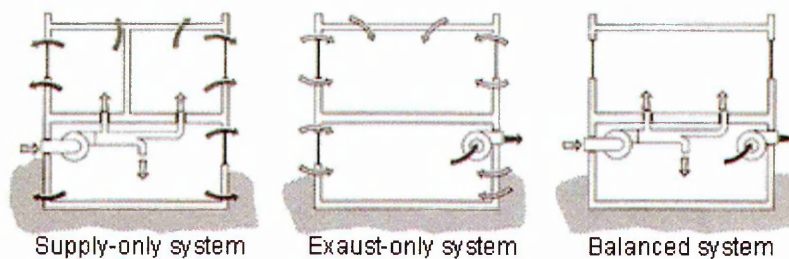
Figure 2.1: Three basic types of mechanical ventilation systems
[Source: Reardon et al. 1990]

Mechanical ventilation systems usually have provision to treat (heat, cool, filter, humidify or dehumidify) the air supplied to the building. Ventilation systems incorporating facilities for air treatment is what is referred to as *air-conditioning*. One of the advantages of mechanical ventilation and air conditioning systems is that they are capable of providing controlled air flow rates and thermal conditions to a space. In addition they normally have provisions for energy recovery from the exhaust air stream. However, they are generally viewed as energy-intensive systems which have a direct burden on the environment since the use of non-renewable energy is often associated with production of environmentally harmful substances.

NATURAL VENTILATION

Following on from the definition of ventilation introduced earlier, natural ventilation can then be defined as a method of achieving ventilation by means of natural forces in which the pressure differential due to wind or the thermal buoyancy effect (or a

combination of both) is used to drive the air through the ventilated space (Figure 2.2) [SPG Media, *2004*].
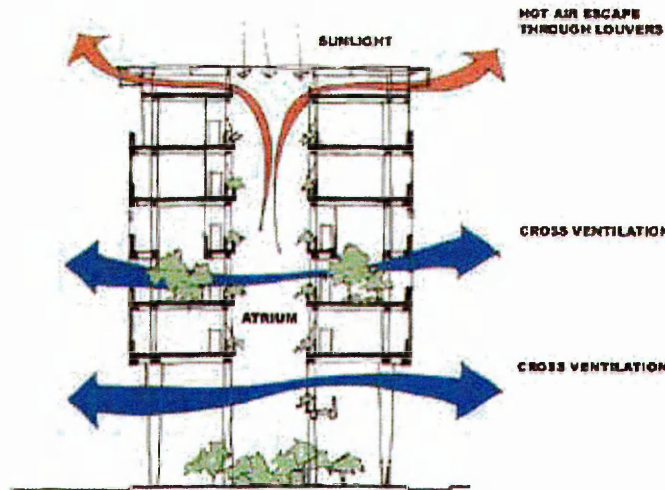
Figure 2.2: Ventilation due to wind and thermal buoyancy

Wind-induced pressures are dependent on the geometry of the building, orientation of the building with respect to the prevailing wind direction, wind speed and the nature of terrain surrounding the building. The pressures due to thermal forces arise from the differences in air density between indoor and outdoor - commonly referred to as the stack effect. When the inside air temperature is greater than the outside air temperature, warm indoor air rises and escapes from the building through high level openings and cooler air is sucked into the building through low level openings by the change in local pressures.

When ventilating a building using natural ventilation, two distinct strategies must be considered - one for the winter and one for the summer. During winter only small air flows are needed (usually 5 - 8 l/s per person) but there is the risk of cold air draughts. During the summer, the main challenge is providing enough air flow to give effective cooling.

HYBRID VENTILATION

Hybrid ventilation systems are two-mode systems that combine the best aspects of natural and mechanical ventilation (Figure 2.3) at different times of the day or season of the year to provide a comfortable indoor environment and good air quality. In hybrid ventilation mechanical and natural forces are combined in such a way that the active

mode reflects the external environment and takes maximum advantage of ambient conditions at any point in time. Hybrid ventilation systems have intelligent control systems that can switch automatically between natural and mechanical modes in order to minimise energy consumption. Advanced hybrid ventilation technology fulfils the high requirements on indoor environmental performance and the increasing need for energy savings and sustainable development by optimising the balance between indoor air quality, thermal comfort, energy use and environmental impact. There are multiple motivations for the interest in hybrid ventilation: the likelihood of a positive response by occupants and a positive impact on productivity, reduced environmental impact and an increased robustness, and/or increased flexibility and adaptability, and financial motivations [Heiselberg: *2002*].
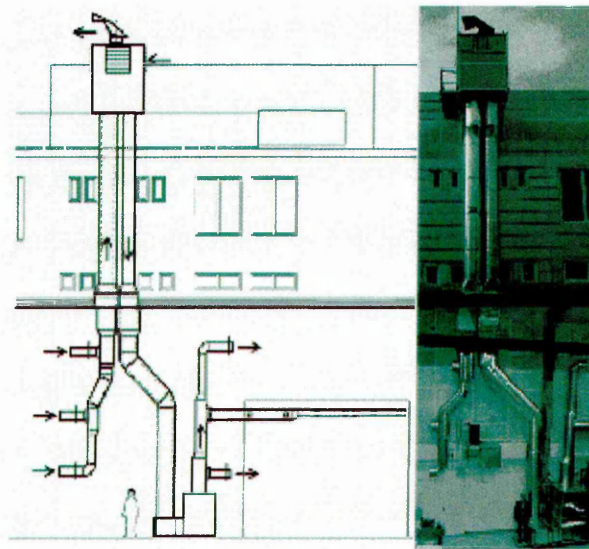
*Figure 2.3: Mechanical and natural ventilation aspects
combined in hybrid systems*

The hybrid ventilation process is very dependent on the outdoor climate, the microclimate around the building, the internal layout of the building, the possible airflow paths through it, as well as the thermal behaviour of the building. Therefore, it is essential that these factors are taken into consideration from the very beginning of the design. In hybrid ventilation design the challenge is to find a solution in which the natural part of the system is used as much as possible, while the mechanical part ensures fulfilment of the requirements in situations where the natural part fails or is less energy efficient. The control strategy plays an important role in this process.

At present one of the major drawbacks to the application of hybrid ventilation is the lack of hybrid ventilation-specific components. As such, development of these components could significantly improve the performance and consequently the uptake of hybrid ventilation.

NIGHT-TIME VENTILATION

During summer, and in some climates where there is sufficient variation of diurnal and outdoor temperatures, and a good prevailing wind, night-time ventilation can be used to cool down the thermal mass of a building. This strategy can save substantial energy by decreasing or eliminating the need for mechanical cooling during daytime occupied periods. Heat gains generated during the day are absorbed by walls, floors and other surfaces then released over a period of time in proportion to the thermal capacity of the materials. During the day, occupants exposed to this chilled thermal mass perceive a cooler environment due to radiative exchange with the low surface temperature of this thermal mass. Challenges to consider in implementing night-time ventilation include security issues, heavy-rain protection, night-time humidity, moisture and condensation control, and pollutant control.

2.1.4 Why natural ventilation?

In developed countries, such as the UK, buildings consume approximately 50% of all primary energy production. This energy is used for heating, cooling, lighting, ventilation and other activities of building occupants. Approximately 30% of the energy delivered to buildings is dissipated in the departing ventilation and exfiltration air stream [Liddament, *1996*]. Since virtually all of this energy is produced from the burning of fossils fuels then buildings contribute around 50% of the total CO_2 emissions into the atmosphere. Discharge of CO_2 into the atmosphere has a significant contribution to global warming. Similarly, the release of refrigerants from air-conditioning systems has historically led to harmful effects on the atmosphere such as ozone depletion.

Therefore, an important strategy in reducing these harmful effects must be to make buildings more energy efficient. Since the energy crisis development in the early 1970s considerable emphasis has been placed on reducing energy usage in buildings in order to conserve energy. Several countries have shown substantial effort towards controlling

present energy consumption by adopting strict requirements on air-tightness and insulation levels. Building structures are becoming more and more air-tight so that ventilation is confined to airflow through intentionally provided openings only, thus leading to the concept of '*Build Tight Ventilate Right*' being recognised as the basis of good design [CIBSE: AM13, *2000*].

An approach to making buildings more energy efficient is to try and reduce the energy consumption associated with mechanical ventilation and air-conditioning. This involves either supplementing or replacing these energy-intensive services with natural ventilation systems. The use of natural ventilation eliminates fan noise from air conditioning and mechanical ventilation plants. Natural ventilation when carefully integrated reduces building construction costs, operation costs, and significantly cuts down on maintenance costs. Further, building occupants perceive natural ventilation to be more comfortable than mechanical ventilation with a likely consequence of improved productivity.

2.2 Driving Forces in Natural Ventilation of Buildings

The driving force for natural ventilation in buildings is the pressure difference across the building envelope. This pressure difference is a result of two important phenomena, namely, *aerodynamic* effects due to the action of wind flowing past the building, and *hydrostatic* (buoyancy) effects resulting from the difference in air density due to temperature between the inside and outside of the building. These phenomena are explained and illustrated in *Sections 2.2.1* and *Section 2.2.2*.

One of the basic problems of design when natural ventilation is adopted is that if the design meets the required standard of ventilation at the mean driving force then the ventilation will be inadequate at lower driving forces and unnecessarily high at higher driving forces, for instance those resulting from high wind speeds. To obtain a more constant rate of airflow under such varying external conditions, the entry of air through cracks around windows and doors must be minimised (by weather-stripping if necessary) and provision made for either automatic or occupant control of the airflow into and out of rooms/buildings.

2.2.1 Wind induced driving forces

Wind effects are usually split into two components i.e. a mean or steady effect and a turbulent one. The steady wind effect creates a field of positive and negative pressures across the building envelope relative to the internal pressure. The pressure field is characterised by turbulence and is dependent on the geometry of the building, orientation of the building with respect to wind direction, wind speed and the nature of the terrain surrounding the building. When the wind meets a facade the flow is slowed down on the windward side, hence the flow finds new paths through and around the facade. Due to this a pressure pattern (Figure 2.4) is developed with different pressures on the different facade elements. Turbulence causes the pressure coefficient to vary over each surface of the building.

Wind velocity profile

Wind pressure field
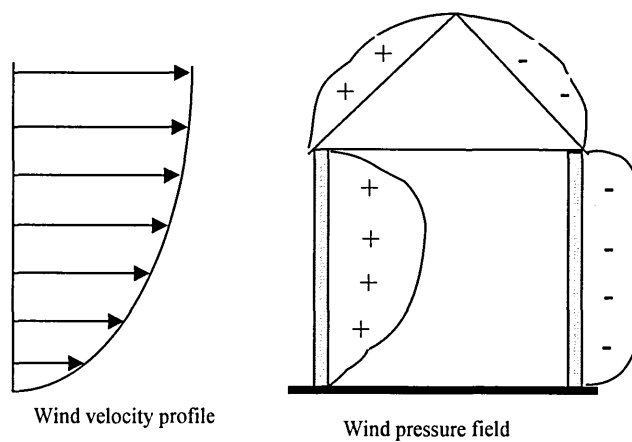
Figure 2.4: Typical pressure distribution due to wind on building envelope

The wind pressure on the exterior building envelope can be expressed as a product of the dynamic pressure and a surface pressure coefficient - derived from the velocity pressure part of the Bernoulli equation:

$$p_W = \frac{1}{2} \rho_{air} c_p u_o^2 \qquad (2.1)$$

where:

p_W = wind pressure

c_p = pressure coefficient

ρ_{air} = air density

u_o = wind velocity in unrestricted air flow

The pressure coefficient, incorporating both the mean and fluctuating/turbulent effects of wind, determines the extent to which the wind pressure is present at a particular spot. A variety of methods for determining the pressure coefficients of building surfaces continue to be well researched and documented for example Grosso *et al. [1995]*, Sharples *[1997]* and Satwiko *et al. [1998]*.

2.2.2 Thermal buoyancy driving forces (stack effect)

The stack effect is produced by thermal buoyancy caused by the difference in density between warm and cold air resulting from variations in temperature between the inside and outside of the building. The difference in density creates buoyancy forces which drive the flow.

During the heating season, the warmer inside air rises and flows out of the building near high level openings. It is replaced by colder outside air which enters the building through low level openings. During the cooling season, the flow directions are reversed and generally less significant because inside-outside temperature differences are smaller. A typical pressure distribution during the heating season is shown in Figure 2.5. The height at which the indoor and outdoor pressures are equal is called the Neutral Pressure Level.
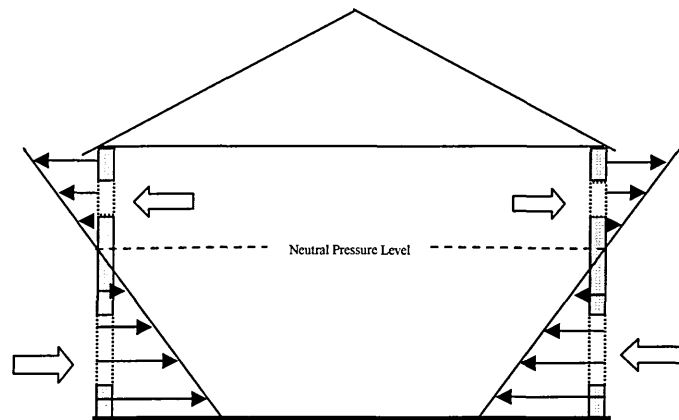
Figure 2.5: Typical pressure distribution due to stack effect

Assuming that the air on each side of the wall is well mixed, the stack pressure difference between air layers of different temperatures at a certain height can be determined from the hydrostatic equation:

$$\Delta p_s = (\rho_{cold} - \rho_{warm}) \, g \, (h - h_{NPL})$$ (2.2)

where:

Δp_s = pressure difference due to stack effect

ρ_{cold} = density of colder air

ρ_{warm} = density of warmer air

g = gravitational constant

h = height of observation point

h_{NPL} = height of neutral pressure level

Pressures are usually measured against a reference pressure, which is normally taken as the ambient pressure - set to zero for convenience.

2.2.3 Combined wind and thermal buoyancy

In most cases natural ventilation occurs as a result of combined wind and stack effects. These effects can complement or oppose each other with the pressure field around the building envelope continually changing in relation to the relative magnitudes of the thermal and wind forces. To accurately gauge the amount of airflow that occurs from the combined effects of wind and thermal buoyancy driving forces, one must superimpose the pressures caused by these mechanisms (Figure 2.6).
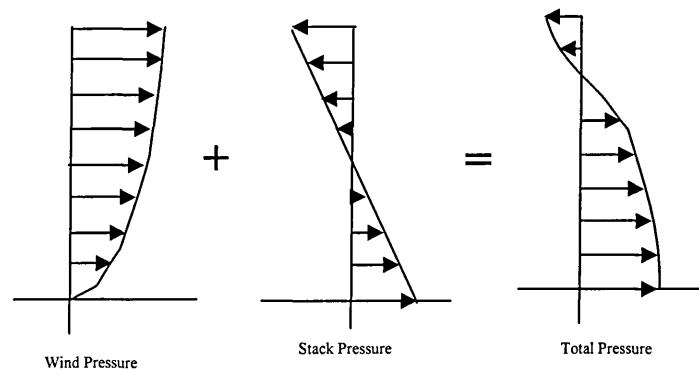
Figure 2.6: Superimposing wind and stack pressures

Airflows caused by these mechanisms are not directly additive because the flow rates are not linearly proportional to the pressure differences. The total pressure difference across an opening at height h is thus written as the sum of the wind and stack pressure minus the unknown pressure difference at reference height Δp_o:

$$\Delta p_t = \frac{1}{2} \rho c_p u_o^2 - (\rho_{cold} - \rho_{warm}) \, g \, (h - h_{NPL}) - \Delta p_o \qquad (2.3)$$

The neutral pressure level is defined as the height at which the pressures on both the inside and outside of the wall are equal. The neutral pressure level is undefined if there is no stack effect.

Wind-induced ventilations seems to become dominant when the wind speed exceeds about 1.8 m/s, that is, the thermal buoyancy effect is small in comparison. On the contrary, when the wind speed is less than 1.8 m/s although the thermal effect is minor it cannot be neglected [Papadakis *et al. 1996*].

2.2.4 Factors that affect the driving forces

The relative importance of the wind and stack pressures in a building is dependent upon several factors which can be classified under three categories. *Climatic* factors such as prevailing external-indoor temperature difference, wind speed and direction. *Configuration* related factors including the shape and height of the building, internal partitions, and size, location and airflow characteristics of inlet and outlet openings. *External physical* effects i.e. the shielding of the building envelope due to obstructing objects such as nearby buildings, landscape and vegetation.

2.3 Natural Ventilation Strategies

Various strategies or combinations of strategies are used to provide natural ventilation in buildings. These strategies take into account several factors such as depth of space with respect to ventilation openings, ceiling height, thermal mass exposed to the space, heat gain and location of building with respect to environmental pollution sources such as traffic noise and airborne pollution. The following paragraphs summarise key aspects of the most widely used strategies, and outline some general rules of thumb that are used to estimate parameters such as the effective depth of ventilation.

2.3.1 Single sided ventilation

This is a method of ventilating a building whereby a simple opening in the form of a window or a ventilation device such as a louvre in a wall is used to allow outdoor air to enter the building and room air to leave either from the same opening or from another opening situated on the same wall (Figure 2.7). Good spacing between openings is needed to generate reliable air change. Single-sided ventilation is generally effective to room depths of between 2 to 2.5 times the room height.
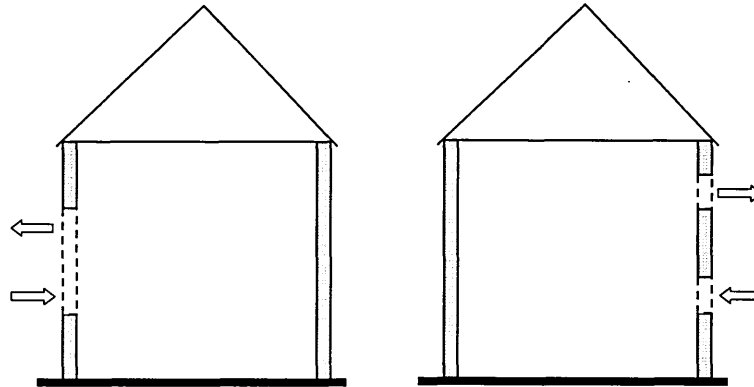
Figure 2.7: Illustration of Single-sided Ventilation

2.3.2 Cross-flow ventilation

Cross-flow ventilation relies on establishing a clearly defined and continuous airflow path between the incoming and outgoing air streams which should pass through the zone of occupancy. Cross-flow ventilation occurs when air enters the room or building from one or more openings on one side and room air leaves through one or more openings on another side of the room or building (Figure 2.8). An open-plan interior is recommended to enhance cross-flow ventilation. When a room has openings on opposite sides, cross ventilation is effective at depths of up to 5 - 6 times the room height.
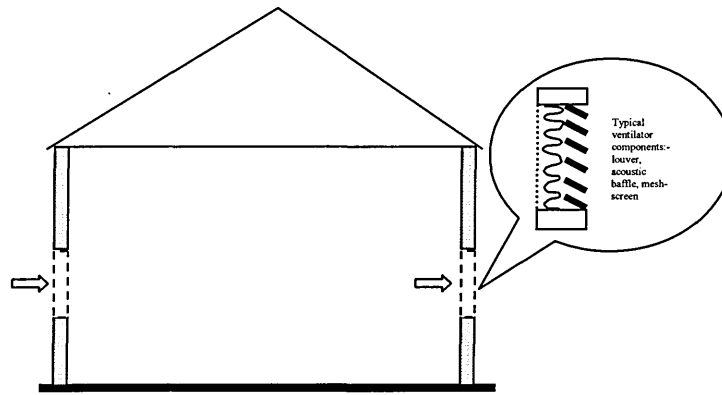
Figure 2.8: Illustration of Cross-flow Ventilation

2.3.3 Stack ventilation

In stack ventilation airflow is driven through the stack by a combination of stack pressure and wind induced suction pressure, with air predominantly entering through purpose provided openings and exhausted through the stack (Figure 2.9).
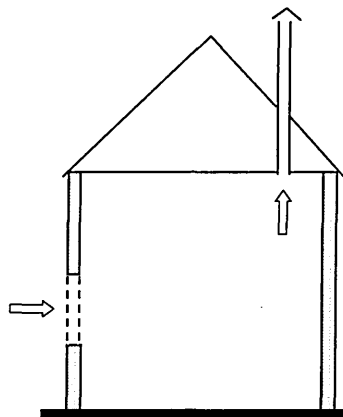
Figure 2.9: Illustration of Stack Ventilation

For stack ventilation in multi-storey buildings the neutral pressure level must be above the window level on the highest floor to be ventilated if air is to flow from the room to the exterior. The top of the stack should be extended to raise the overall height of the stack such that the neutral pressure level is high enough to provide sufficient driving force to draw air out of the building at the top floor [Martin *et al. 2000*].

2.3.4 Solar-induced ventilation

Natural ventilation systems are usually designed on the basis of a buoyancy-driven flow to provide a margin for variation from the expected environmental conditions. In situations where wind assists the buoyancy flow, there should be little difficulty in providing the required airflow rate to the building. However, in cases where the normal buoyancy pressure (resulting from the difference between the internal and external air temperatures) is not sufficient to provide the required ventilation rates then solar-induced ventilation can be a viable alternative.

This technique (Figure 2.10) relies upon the heating of part of the building fabric by solar irradiation resulting into a greater temperature difference, hence, larger airflow rates than in conventional systems which are driven by the air temperature difference between inside and outside of a building.

For all-glass facades, solar chimneys are essentially the glazed manifestation of stack-induced ventilation strategy. Operable windows connect to the vertical "solar shaft". Solar heat gains absorbed within the chimney causes hot air to rise, inducing cross ventilation from the cooler side of the building.
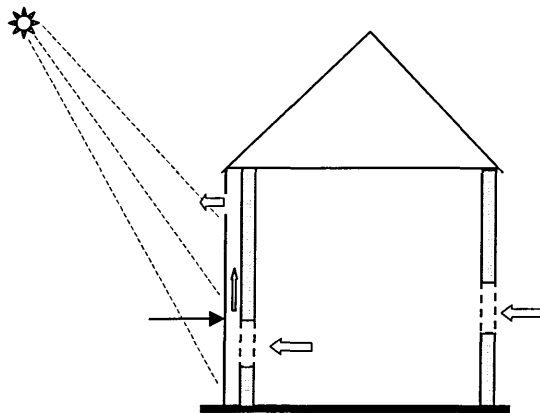
Figure 2.10: Illustration of Solar-induced Ventilation

Stack-induced ventilation through atria works using the same principle as the solar chimney but can serve more functions, for instance smoke extraction and providing daylight to adjacent spaces.

2.4 Natural Ventilation Openings

For many years buildings relied on air leakage through the building envelope to provide indoor-outdoor air exchange. This form of natural ventilation resulting from random flow of air through unintentional openings, commonly referred to as *infiltration*, worked fairly well as buildings tended to be quite leaky and pressure differences between the inside and outside were sufficient to provide a significant amount of air exchange most of the time. However, leaky building envelopes did not always guarantee adequate ventilation and were not energy efficient.

Developments as a result of new products (such as tighter windows and doors, more efficient heating systems) and improved practices resulted in the construction of buildings that were much more airtight. This trend towards greater air-tightness and higher efficiency gave rise to the need for purpose-provided openings. Natural ventilation facilitated by these purpose provided openings is commonly called *controlled* natural ventilation. Airflow through purpose-provided openings can be used to provide adequate ventilation for indoor air quality and thermal comfort control.

The operation of natural ventilation systems (infiltration or controlled ventilation) relies on the presence of suitable inlet and outlet ventilation openings in addition to a continuous airflow path through the ventilated building. Ventilation openings must be provided to meet all anticipated ventilation needs. For instance, they must deliver sufficient air to maintain the indoor air quality in winter and provide adequate airflow in summer to remove expected building heat gains. Airflow openings which facilitate natural ventilation are commonly classified under two categories, namely *adventitious openings* and *purpose-provided openings*. More detailed descriptions of the two types of openings are given in *Section 2.4.1* and *Section 2.4.2*.

A well-designed natural ventilation strategy should combine permanently open vents to provide background ventilation, and controllable openings to meet transient demand. Ventilation openings need to be distributed to eliminate dead zones or pockets that are stagnant and hence high in pollutant levels. Where they are intentionally included, ventilation openings need to be located to allow for unobstructed airflow. Good design can provide some measure of ventilation control in natural ventilation systems, but normally it is necessary for the occupants to adjust ventilation openings to suit demand. The size of ventilation openings is critical to assure proper ventilation rates. On the

other hand, the type of inflow or outflow opening affects the degree of resistance to inflowing air and therefore the ventilation potential.

2.4.1 Adventitious openings

Adventitious openings are normally small openings with a typical dimension less than approximately 10 mm [BS 5925: *1991*]. They include cracks in building fabric, gaps at wall/ceiling, wall/floor interfaces, joints, gaps around doors and windows, openings associated with electric, water, drainage and gas services etc. Adventitious openings are present in every building to a different degree depending on the type of material or components used, method of construction and installation of services. In the past most buildings (especially dwelling type) were adequately ventilated by air leakage through adventitious openings, but in recent years the desire to conserve energy has led to tighter building construction and upgrading of existing stock. This has sometimes been so successful that air leakage can no longer be relied upon as the sole source of ventilation air. As a result purpose-provided openings are often added to meet the recommended ventilation rates.

2.4.2 Purpose-provided openings

Sometimes referred to by the general term *ventilation openings*, purpose-provided openings as the name suggests, are purposely provided and installed to facilitate air supply to or discharge from the building. They range from small openings such as trickle vents and grilles to large openings such as windows and louvre banks. The choice of opening will depend particularly upon the building type and expected usage. Not only must ventilation openings fulfil the ventilation requirements without admitting excessive amounts of noise, rain, dust or insects, but they also need to be reliable, durable, secure, aesthetically pleasing, provide view, admit daylight, control glare, solar gain and limit unwanted air infiltration and heat loss.

Although there is a wide variety of ventilation openings, including windows, wind towers, wind scoops, chimneys, atria etc., to choose from only two types of purpose-provided ventilation openings are considered in this study, namely trickle ventilators and louvered through-the-wall ventilators. The main purpose of trickle ventilators in a building is to provide background ventilation airflow rates - minimum fresh air

requirements sufficient to meet the supply fresh air in winter months. On the other hand, louvered ventilators are used in conjunction with trickle ventilators to combat high pollutant and summer loads.

In the simplest form a trickle ventilator is just a slot or row of holes [CIBSE: AM13, *2000*] fixed with no allowance for control. Some trickle ventilators have some means of being closed, usually by a manually operated slide over the openings. Trickle ventilators can be in the frame, part of the glazed unit or independent of the window usually above it. To minimise resistance to airflow, the main air passage in trickle ventilators (excluding insect screens etc) should have a minimum dimension of 5mm for slots or 8mm for square or circular holes [CIBSE: AM 10, *1997*].

Trickle and louvered through-the-wall ventilators, which together shall be generally referred to as *ventilators* throughout this thesis, normally incorporate various refinements including acoustic treatment and mesh screens to deter insects and birds from entering the building. However, these refinements bring the penalty of increased pressure drop, especially when one takes into account the relatively low driving forces available for natural ventilation. In addition, a major drawback of ventilators is that, when closed, it is difficult to ensure an air-tight seal to limit infiltration/exfiltration.

The number and size of natural ventilation openings in a building envelope will depend on overall ventilation need and the strength of local driving forces. Since the rate of ventilation is dependent on variable driving forces, provision should be made for the occupant to be able to adjust openings to meet demand. In addition local, national and international standards dictate to some extent on provisions to be made in relation to ventilation openings. For instance, the UK Building Regulations have a 'deemed to satisfy' requirement for trickle ventilation in naturally ventilated buildings of 4000mm^2 opening area for floor areas up to 10 m^2 and 400 mm^2 per m^2 of floor area for areas greater than 10 m^2 to be provided in each room [London: HMSO, *1995*].

2.4.3 Controlled air inlets

To eliminate much of the worry associated with sudden changes of wind and external temperatures, some means of automatically controlling ventilation opening sizes during operation are normally incorporated in the design. This is essential to accommodate

various wind speeds and outdoor temperatures, thus ensuring that the indoor air quality and thermal comfort conditions are maintained.

Several types of self regulating ventilators, commonly called *controlled air inlets,* which control the opening area in response to a specific monitored parameter, are becoming commercially available. Controlled air inlets are configured to respond automatically to such parameters as the outdoor temperature, humidity, or air pressure. Some common features of controlled air inlets are as follows:-

- *Pressure sensitive ventilators* - allow a uniform airflow rate to be achieved over a wide pressure range, thus enabling good control of natural ventilation

- *Temperature sensitive ventilators* - the vent opening reduces as the outside air temperature falls

- *Humidity-sensitive ventilators* - the vent opens in response to increased room humidity to assist in moisture removal

The signal from controlled air inlets is usually incorporated into a BMS control strategy. However, to promote user satisfaction the design should allow the ventilator automatic control system to be overridden by the occupant. It must be pointed out that several other factors including weather-tightness, sound insulation, security, safety, controllability, aesthetics, thermal insulation, durability and reliability affect the choice and use of ventilators in naturally ventilated buildings. Whilst some of these issues are mentioned in other parts of this report, most of them are not addressed in this study.

2.4.4 Influence of ventilation openings on indoor air movement

Ventilation openings have a direct influence on the air movement within an occupied space and as such directly affect the indoor air quality and thermal comfort. This influence can be examined in terms of the magnitude of air movement i.e. air speeds - affecting thermal comfort, and also the resulting airflow patterns (affecting contaminant distribution) within the occupied space.

Air inlets should maintain a sufficiently fast inlet air speed so that good air mixing occurs and adequate air circulation within the occupied zone is provided. Occupied zone

air speeds up to 0.5 m/s are comfortable for most people in naturally ventilated buildings, while air speeds between 0.5 m/s and 1 m/s are often acceptable even though people will be aware of the air movement (refer to Table 2.1). However, at 0.8 m/s, hair, loose paper and light objects may start to blow around and annoy people. Air speeds over 1 m/s should be avoided because they create drafts and can be a nuisance [Eley Associates: *2003*].

Table 2.1: Impact of air speed on occupants

Air speed (m/s)	Probable impact on occupants
Up to 0.3	Unnoticed
0.3 to 0.6	Pleasant
0.6 to 1	Generally pleasant but causing a constant awareness of air movement
1 to 1.7	From slightly to annoyingly drafty
Above 1.7	Requires corrective measures if comfort and productivity are to be maintained

source: 2003 Eley Associates - Hawaii Commercial Building Guidelines for Energy Efficiency (Natural ventilation)

Distribution of incoming outdoor air must be even so that all occupied parts of a ventilated space receive an adequate supply. It is the location, design and operation of ventilators that ensures uniform distribution and reduces drafts, uneven temperatures and dead pockets. During cold weather air inlets must direct incoming cool air into the building at high enough velocity to blend it with warm room air before it reaches the occupied zone. During hot weather the inlet must be adjusted to permit a large volume of air to enter the occupied zone to promote air movement past the occupants. Adjustment is also necessary to provide a good airflow pattern within the building.

Figure 2.12 illustrates an example of the airflow patterns resulting from different magnitudes of driving forces [Heiselberg *et al. 2002*] for high level ventilation openings. The characteristics of the driving forces and subsequent nature of airflow, entering the occupied zone (shown dotted), for each path shown in Figure 2.11 are summarised in Table 2.2.
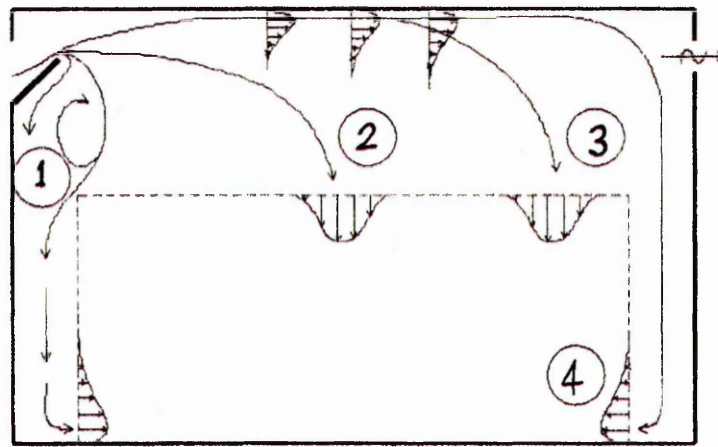
Figure 2.11: Possible airflow patterns in room

Table 2.2: Summary of airflow patterns resulting from driving forces of different magnitudes				
Path		**Driving force properties**		**Nature of airflow**
1		small driving forces or pressure differences (e.g. typically 0.2 - 0.4 Pa) and/or at low outdoor temperature		supply air flow s dow n the w all tow ards the floor
2 and 3		higher pressure differences (typically 4 - 6 Pa) and/or higher outdoor temperature 9 e.g. at an inside/outside temperature difference less than 5K)		supply air acts as a thermal jet
4		during summer w hen the inside/outside temperature difference is very small		supply air acts as an isothermal jet

Source: Adapted from Heiselberg et al. 2002

Several other researchers have investigated either experimentally [Fanger *et al. 1988,* Heiselberg *et al. 2001,* Heiselberg *et al. 2002*], or by computational fluid dynamics means [Ata, *1997*] the characteristics of airflow patterns and in some cases the impact on thermal comfort in occupied spaces resulting from different ventilation opening types and opening strategies.

2.5 Limitations and Disadvantages of Natural Ventilation

The main drawback of natural ventilation systems is the lack of precise control of airflow. Natural ventilation depends on airflow rates and airflow patterns that frequently vary with outdoor conditions (wind and temperature differences) and are difficult to predict. These unreliable driving forces can result in periods of inadequate ventilation (poor indoor air quality) followed by periods of over-ventilation which can cause excessive energy wastage.

Controlling noise and providing natural ventilation are essentially mutually incompatible. For instance, during peak hours of traffic intensity, outdoor air pollution and noise levels may be unacceptable for natural ventilation purposes, especially in highly dense urban environments. Hence, the design for natural ventilation may have opposing requirements in the provision of noise attenuation since noise levels at the façade are difficult to attenuate without seriously affecting the airflow. As a result failure to consider noise control adequately can lead to a building which is functionally unsuitable and thus a disaster. In addition, elimination of debris from outdoors can be a problem in natural ventilation applications since there is limited scope for filtering incoming air due to the very low driving forces.

Natural ventilation is ineffective in reducing the humidity of incoming air, hence this places an upper limit on the application of natural ventilation in warm humid summer months. Also the dependence of natural ventilation on occupants' willingness to operate ventilation openings to regulate thermal comfort presents potential increase in energy usage because of infiltration if the openings are not operated properly. A further consequence would be greater indoor temperature swings than is normal with mechanical ventilation.

Detailed accounts of the limitations and disadvantages of natural ventilation and advice on how to overcome them are well documented in the literature. For example, the NatVent© [*1998*] project recently carried out a study on "*Overcoming technical barriers to low-energy natural ventilation in office type buildings in moderate and cold climates*". The interested reader is referred to this work, centred on seven central and north European countries.

2.6 Practical Considerations for Implementing Natural Ventilation

Providing proper and sufficient natural ventilation requires a "*whole building*" approach. This is a many faceted process that requires an integrated approach to a building systems design, installation, and operation. The following are some of the practical factors that need to be addressed:-

- the building structure should be airtight so that ventilation is confined to airflow through intentionally provided openings only

- ventilation openings should be oriented with respect to the prevailing wind

- rooms should have inlet and outlet openings located in opposing pressure zones

- vegetation and other site buildings should not obstruct inlet openings

- the vertical distance between inlet and outlet opening should take advantage of the stack effect

- low level openings should not be obstructed by furniture and interior partitions

- airflow characteristics of ventilation openings need to be established and understood

- avoid inlet and outlet openings directly across from each other in order to promote more air mixing and improve the effectiveness of the ventilation

- components which require occupant operation and maintenance need to be located where they are readily accessible and replaceable

2.7 Some Design Considerations

When developing the design concept for a naturally ventilated building, the following three basic steps need to be taken [CIBSE: AM10, *1997*]:

- Define the desired airflow pattern from the ventilation inlets openings, through the occupied zone to the outlet openings

- Identify the principal driving forces which facilitate the desired airflow path

- Size and locate the openings so that the required airflow pattern can be delivered under all operating regimes by utilising a suitable control system

2.7.1 Ventilation rates

Ventilation rates are required to determine the sizes of ventilation openings in relation to the required indoor air quality or thermal comfort. Too little ventilation may result in poor indoor air quality, while too much may cause unnecessarily higher heating and cooling loads. Ultimately, the ventilation rate should be sufficient to maintain indoor air quality and thermal comfort requirements to meet the current prevailing demand. The most common methods that are used to determine the ventilation rates include:-

HEAT REMOVAL

The ventilation rate V (m^3/s) required to remove the heat Q (W) from an occupied zone is given by the equation:

$$V = \frac{Q}{c_p \rho (T_i - T_o)}$$

(2.4)

where:

c_p =   specific heat capacity of air (J/kg.K)

ρ =   density of air (kg/m^3)

T_i =   indoor air temperature (K)

T_o =   outdoor air temperature (K)

CONTAMINANT DILUTION

To reduce the concentration of a particular contaminant to a level unlikely to pose a health risk, the ventilation rate V (m^3/s) can be estimated from a decay type equation:

$$V = \frac{A}{C_i - C_o}$$

(2.5)

where:

C_i =   maximum allowable indoor concentration of contaminant

C_o =   concentration of contaminant in outdoor air

A =   rate of generation of contaminant in occupied zone (m^3/s)

Professional institutions and national authorities frequently recommend ventilation rates, for various situations, expressed as air changes per hour. In this case the ventilation rate V (m^3/s) is related to the air change rate N (per hour) by the equation:

$$V = \frac{N.vol}{3600} \qquad (2.6)$$

where:

vol　　=　　volume of occupied zone (m^3)

One major disadvantage of using the fixed air change method is that the air change rate does not vary with the prevailing weather.

2.7.2 Infiltration and air-leakage

The uncontrolled flow of air into a room (*infiltration*) or out of a room (*exfiltration*) through cracks, interstitial spaces (*openings where different materials come together*) and leaks in the building envelope is a result of pressure differences across the building envelope. The infiltration, or exfiltration, rate of a building is dependant upon external weather conditions, equipment operation and occupant activities within the building. Uncontrolled infiltration or ex-filtration can nullify the intended indoor environment and energy conservation control strategy [CIBSE: AM13, *2000*].

The characteristics of this uncontrolled airflow can be determined by measuring the air-leakage of the building envelope, at a reference pressure difference, which describes the relative air-tightness of a building i.e. the resistance of the building envelope to the airflow. For controllable natural ventilation, the air-tightness should not exceed 5 m^3/h per m^2 of permeable envelope area for an imposed pressure differential of 25 Pa across the envelope [CIBSE: AM 10, *1997*]. The air-leakage of a building can be determined by pressurisation, depressurisation or tracer gas methods. Available air-leakage test equipment ranges from blower doors (Figure 2.12) usually used for testing residential type buildings, to large diesel-driven air handlers such as the "Megafan" (Figure 2.13), owned by the Sheffield (UK) based HRS Services Ltd, which can be used for testing large distribution sheds.

Figure 2.12: Internal and external view of blower door
[Source: Sharples and Goodacre, 2004]

Although no simple relationship exists between a building's air-tightness and its air exchange rate, some empirical methods have been developed to estimate the values. A common method is to convert the predicted airflow rate to an equivalent or effective air-leakage area (assumed to be evenly distributed over the building envelope) using the equation:

$$A_L = V_r \frac{\sqrt{\dfrac{\rho}{2.\Delta p_r}}}{C_D} \qquad (2.7)$$

where:

A_L	=	effective leakage area (m^2)
V_r	=	predicted airflow rate at Δp_r (m^3/s)
ρ	=	air density (kg/m^3)
Δp_r	=	reference pressure difference (Pa)
C_D	=	discharge coefficient

An air-leakage test does not provide a measure of the air infiltration rate in a building, and therefore it cannot be used to estimate directly the infiltration rate. A calculation can be carried out to relate the air-leakage at 50 Pa , say, to the air infiltration rate, but this requires some knowledge of the location and nature of the air leakage paths.
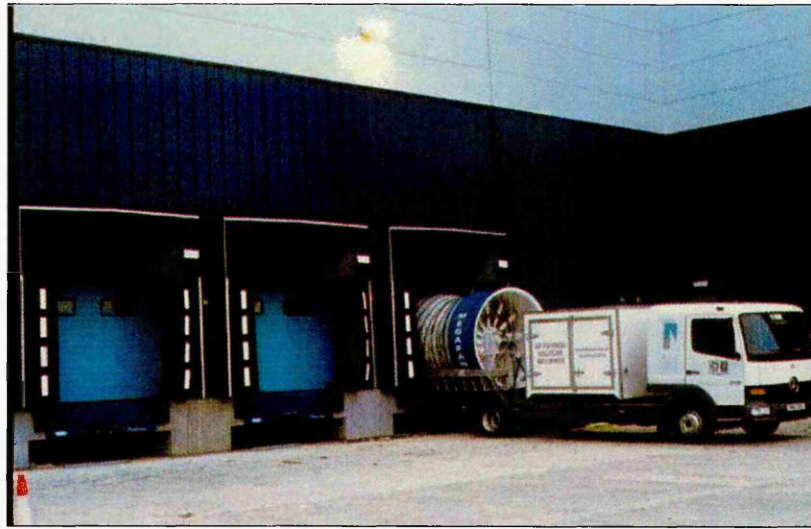
Figure 2.13: Sheffield (UK) HRS Services Ltd "Megafan"

If a direct measure of air infiltration is required, it involves a lengthy and complex test using tracer gases. For average standards of construction and average weather conditions, CIBSE: TM23 [*2000*] recommends a simplified relationship:

$$I = \frac{1}{60}\frac{V_{50}}{S}$$ (2.8)

where:

    I   =   infiltration rate in air changes per hour

    V_{50} =   leakage airflow rate at 50 Pa

    S   =   surface area of walls and roof (m^2)

Where necessary individual building components, such as doors, vents and windows etc., can be pressure-tested in order to derive the leakage areas and flow coefficients. These could be used to determine a more accurate picture of the likely air-leakage performance of the building. For instance, in the Lawrence Berkeley Laboratory (LBL) Model for air-leakage [Kreider *et al*: *1994*], once the total leakage area of the components has been found the infiltration rate I* is related to thermal buoyancy and wind effects by the equation:

$$I^* = A_{leak}\sqrt{a_s \Delta T + a_w v^2}$$ (2.9)

where:

I*	=	infiltration rate (L/s)
A_{leak}	=	total effective leakage area of building (cm^2)
a_s	=	stack coefficient of Table 2.3
ΔT	=	Ti - To (K)
a_w	=	wind coefficient of Table 2.4
v	=	average wind speed (m/s)

Infiltration rates can also be determined by tracer gas techniques. This involves the injection of a tracer gas into a room and then measuring the rate of decay of the gas concentration i.e. the infiltration rate is assumed to be proportional to the rate of loss of tracer gas. The infiltration rate is calculated from the decay equation which after manipulation by integration gives:

$$I = - \frac{vol}{t} \log_e [\frac{c}{c_o}]$$ (2.9)

where:

I	=	infiltration rate (m^3/s)
vol	=	room volume (m^3)
t	=	time (s)
c	=	gas concentration at any instant inside the room
c_o	=	gas concentration at time t = 0

The infiltration I can be calculated from the slope of the graph obtained by plotting the natural logarithm of (c/c_o) against t.

2.8 Concluding Remarks

The above sections provide a detailed discussion of the underlying principles of natural ventilation in buildings. Three main areas are discussed: driving forces effecting natural ventilation, strategies employed in the use of natural ventilation and the importance of ventilation openings. By additionally focussing on design and practical considerations, this chapter helps to put into context the natural mode of ventilating buildings. Key pieces of information to be taken from the theory presented here to be used in the attempt to optimise the airflow performance of ventilators are as follows:

- driving forces in natural ventilation are very low (typically less than 10Pa)

- the design, installation and operation of ventilation openings is critical to the success of any natural ventilation application

- each of the basic components of a ventilator (*louvres, mesh screen, acoustic baffles*) introduces a resistance to airflow which uses up part of the available driving force

Chapter 3

BASIC PRINCIPLES OF FLUID FLOW

This chapter considers some key basic concepts in fluid mechanics including pressure, forces, continuity equations relating to fluid flow with a general aim of getting a feel for flow patterns, pressure variation and shear stresses in airflow with regard to ventilation applications. The mathematical formulation of equations that govern the processes of interest will be discussed only briefly in this chapter. For a complete derivation of the required equations, the reader must turn to standard textbooks such as [Massey, *1998*] on the subject.

3.1 Background

A fluid can be either a gas or liquid and is defined as *a substance that will continuously deform, that is, flow under the action of a shear stress, no matter how small that shear stress maybe* [Kreider, *1994*]. Throughout this report a fluid shall be regarded as a continuum, implying, a hypothetically continuous substance with average effects (pressure, density etc) within a given volume remaining constant or changing smoothly with time [Douglas *et al. 1985*]. Transport phenomena associated with fluid flow are also known as convection or convective mass transfer. Convection may be either natural or forced. Forces acting upon a small part of the fluid govern natural convection, such as flow caused by density differences in natural ventilation applications (see *Section 2.2.2*).

3.2 Flow Visualisation

This section briefly presents general concepts of flow patterns and makes distinctions between different types of fluid flow that are commonly encountered in practice. The intention is to prepare the unfamiliar reader with terms and concepts that will frequently be referred to in other chapters of this thesis, in particular the experimental (*Chapter 5*) and computational fluid dynamics (*Chapter 6*) investigations and results.

3.2.1 Streamlines and flow patterns

It is often desirable to construct lines in the flow field to indicate the speed and direction of flow. Such a construction is called a *flow pattern*, and the lines, called *streamlines*, are defined as *lines drawn through the flow field in such a manner that the velocity vector of the fluid at each and every point on the streamline is tangent to the streamline at that instant* [Douglas *et al. 1985*]. Consequently, a tangent to the curve at any point along the streamline gives the direction of the velocity vector at that point in the flow field. As will be seen later (*Chapter 6*) velocity vectors are a very useful way of indicating flow patterns in computational fluid dynamics results. Consider a flow of water from a slot in the side of a tank (Figure 3.1). The velocity vectors have been sketched at three different positions a, b and c. One can see that the flow pattern is a very effective way of illustrating the geometry of fluid flow.
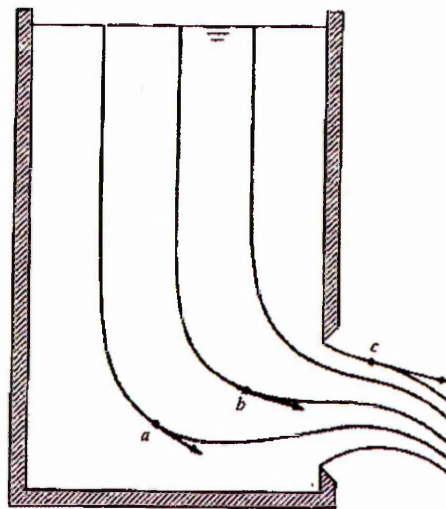
Figure 3.1: Flow from a slot

3.2.2 Uniform and non-uniform flow

In *uniform flow* the velocity does not change from point to point along any streamlines in the flow field. Therefore, it follows that the streamlines must be straight and parallel. If they are not straight, there will be a directional change of velocity. If they are not parallel, there will be a change of speed along the streamlines. The flow pattern for uniform flow between parallel plates is illustrated in Figure 3.2. In *non-uniform flow* the velocity changes from point to point along the streamline. Therefore, the flow pattern consists of streamlines that are either curving in space or converging or diverging.
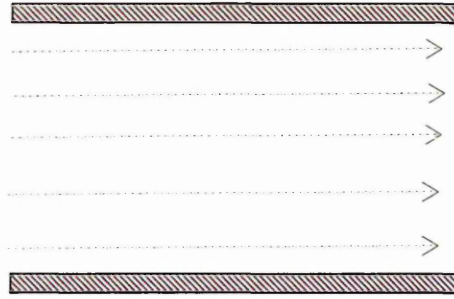
Figure 3.2: Streamlines in flow between parallel plates

3.2.3 Steady and unsteady flow

Another flow classification is based on the variation of velocity with respect to time at a given point in a flow field. If at any given point the velocity does not vary in magnitude or direction with time, then the flow is *steady*. If the velocity of flow does vary with time, the flow is *unsteady*. Steady and unsteady flow conditions are mathematically defined as follows [Douglas *et al. 1985*]:

$$\frac{\partial v}{\partial t} = 0 \ \text{(Steady flow)} \tag{3.1}$$

$$\frac{\partial v}{\partial t} \neq 0 \ \text{(Unsteady flow)} \tag{3.2}$$

where, v is the velocity at a given point in the flow field. For steady flow, the streamlines represent the paths of fluid elements. In unsteady flow the streamline pattern changes in time and the streamlines do not represent the path of a fluid element at any instant. All computational fluid dynamics simulations described in *Chapter 6* were undertaken for steady-state flow conditions.

3.2.4 Laminar and turbulent flow

Turbulent flow is characterised by random fluctuations of velocity and pressure throughout the flow field, with a resulting mixing action caused by eddy currents of varying size within the flow. *Laminar flow*, on the other hand, is devoid of intense mixing phenomena and eddies common to turbulent flow [Massey, *1998*]. Hence, this flow has a very smooth appearance. The effect of turbulence on smooth flow is to add

continuously fluctuating components of velocity to the flow. A general fluid flow index relating to turbulence is the Reynolds number, given by the equation:

$$Re = \frac{v\ell\rho}{\mu} \qquad (3.3)$$

where v is the velocity, ℓ is a characteristic length, ρ is the fluid density and μ is the dynamic viscosity of the fluid. In turbulent flows, there are random local disturbances in the fluid flow pattern about a mean or average fluid velocity [Haines, *1994*]. Resistance to flow is proportional to the square of velocity. A transitional region occurs between laminar and turbulent flows. In this region laminar or turbulent conditions are not always defined. In laminar flows, particles slide smoothly along lines parallel to the wall and resistance to flow varies directly with the velocity [Haines, *1994*]. Figure 3.3 illustrates laminar and turbulent flow patterns within a flow field.
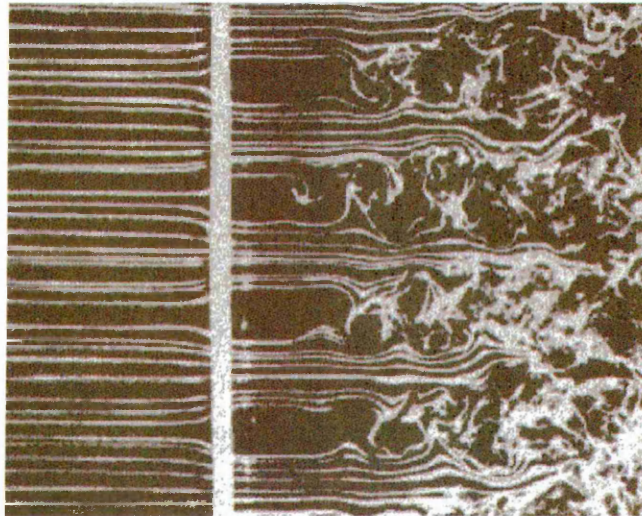
Figure 3.3: Generation of turbulence by a grid[1]
(Source: Milton Van Dyke:1982)

The speed at which the flow changes from laminar to turbulent is not clearly defined and there is a transition zone between the two patterns. Figure 3.4 shows a schematic of the velocity profiles for laminar and turbulent flow.

---

[1] *Smoke wires show a uniform laminar stream passing though a $\frac{1}{16}$ inch plate with $\frac{3}{4}$ inch square perforations. The Reynolds number is 1500 based on the 1 inch mesh size. Instability of the shear layers leads to turbulent flow downstream*

For laminar flow the profile is parabolic, but for turbulent flow the velocity is almost uniform except in the vicinity of the walls. In both cases the velocity at the wall is zero.
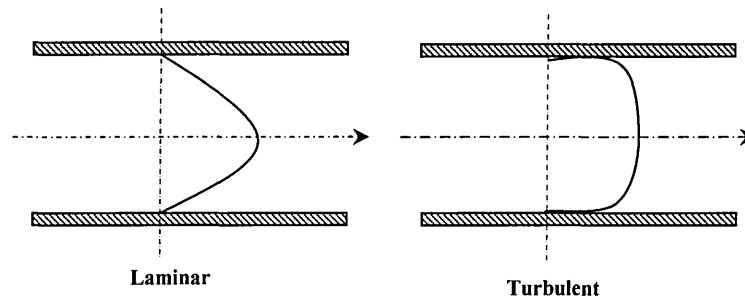
Laminar   Turbulent

Figure 3.4: Schematic representation of velocity profiles

In ventilation applications analytical models such as the power law (*Section 4.7.1*) employ means that directly give an indication of the flow pattern (laminar or turbulent) based up on specific values of indices/exponents.

3.2.5 Flow separation

Flow separation is a condition where the air flowing over a surface no longer remains attached to that surface [Douglas *et al. 1985*]. This results in an effective reduction in the cross sectional area of the flow field. This area reduction is accompanied by an increase in fluid speed which results in a pressure loss. Generally, the flow separates at sharp edges and generates re-circulating flow zones that typically form behind obstacles such as louvre blades or cylindrical bars in a mesh-screen. Examples of recirculation zones formed by air flowing through slots can be seen from the results of CFD simulations given in Figures 6.17 and 6.21. Flow separation creates a type of drag called *pressure drag*. The pressure drag is characterised by the drag coefficient - a function of the object's shape and Reynolds number. Figure 3.5 illustrates the development of flow separation as fluid flows over objects cylindrical wires in a mesh-screen.
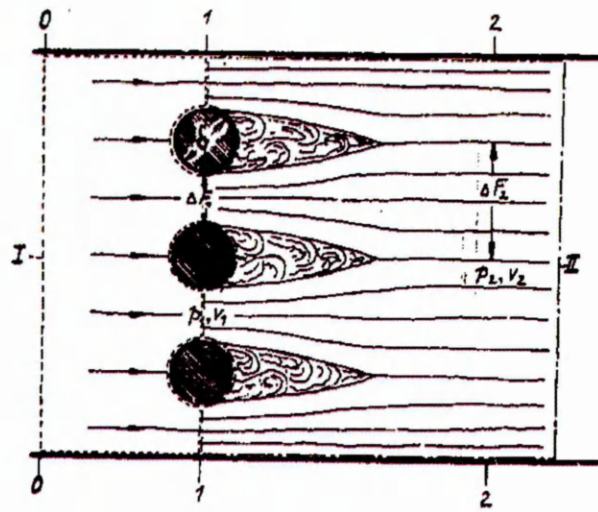
Figure 3.5: Illustration of flow separation in a mesh-screen

3.3 Fluid Forces

In general, fluids exert both normal and tangential forces on surfaces that are in contact with them. However, only fluids with velocity gradients produce shearing forces. A fluid particle in motion obeys the same laws of mechanics as a solid body i.e. the force acting on a particle can be predicted from Newton's law of motion.

3.3.1 Alternative definition of Reynolds number

The inertia force F_i acting on a moving particle is given by the equation:

$$F_i = m\frac{\partial v}{\partial t}$$

(3.4)

where:

m	=	mass of particle (kg)
v	=	velocity (ms^{-1})
t	=	time (s)

In addition to inertia forces fluids in motion also experience viscous forces due to the viscosity of the fluid. The shear stress τ is given by Newton's law of viscosity, which is:

(3.5)

$$\tau = \mu\frac{\partial v}{\partial y}$$

where:

μ =   dynamic (absolute) viscosity of the fluid (Pas^{-1})

y =   distance normal to the flow direction

The shear force (F_s) is given by the equation:

$$F_s = A\tau = \mu A \frac{\partial v}{\partial y} \qquad (3.6)$$

In a moving fluid both of the forces F_i and F_s are significant to different degrees. The ratio F_i/F_s (inertia to viscous forces) is a non-dimensional number called the Reynolds number:

$$R_e = \frac{\rho v y}{\mu} \qquad (3.7)$$

where ρ is the density (kgm^{-3}).

For small values of Re the viscous forces are dominant and this restricts the movement of the fluid particles to follow the main flow direction [Massey, *1998*]. Such a flow is called laminar flow. However, as Re increases the inertia forces acting on the fluid particles dominate the weak shear forces and the flow is said to be turbulent. The transition between laminar to turbulent flow is identified by the value of Re corresponding to the nature of flow and geometry of the object present in the flow.

3.3.2 Momentum of a fluid particle

The momentum of a fluid particle is given by the equation:

$$M = mv \qquad (3.8)$$

If there were a change in momentum (or velocity) of the moving particle, then the force which causes this change is given by:

$$F = \frac{\partial M}{\partial v} = \frac{\partial(mv)}{\partial t} = m\,\partial v \qquad (3.9)$$

where $\tilde{m}$ is the mass flow rate (kgs^{-1}). This equation shows that the force is the rate of change of momentum with respect to time.

3.4 Continuity of Flow

The continuity principle is based on conservation of mass as it applies to flow of fluids and states that the net rate of out flow of mass from a control volume is equal to the rate of decrease of mass within the control volume, expressed mathematically as:

$$\int_{cs} \rho u dA = -\frac{d}{dt} \int_{cv} \rho dV$$

(3.10)

In fluid flow, the law of conservation of mass means that the mass of fluid entering a control volume per unit time is balanced by the mass of fluid leaving a control volume per unit time and change in the mass of fluid in the control volume per unit time i.e:

$$\left(\frac{\partial m}{\partial t}\right)_{in} = \left(\frac{\partial m}{\partial t}\right)_{out} + V\frac{\partial \rho}{\partial t}$$

(3.9)

where:

V = control volume (m^3)

ρ = fluid density (kgm^{-3}).

As will be seen in *Chapter 6* the continuity principle is one of the foundations up on which the governing equations used in CFD are based. For incompressible flow, where air velocities are below the speed at which compressibility effects become important, approximately 70m/s [ASHRAE Fundamentals: *2001*], i.e. when changes in fluid density are small, which is the case for airflow in buildings, the flow continuity can be stated as:

$$\tilde{m} = \rho_1 v_1 A_1 = \rho_2 v_2 A_2$$

(3.12)

and since $\rho_1 = \rho_2$ for incompressible flow, then:

$$Q = v_1 A_1 = v_2 A_2 \qquad\qquad (3.13)$$

where $\tilde{m}$ is the mass flow rate (kgs^{-1}), Q is the volume flow rate (m^{3}s^{-1}), v_1 and v_2 are the inlet and outlet velocities (ms^{-1}) and A_1 and A_2 are the inlet and outlet areas (m^2) normal to the velocity direction.

3.5 Fluid Pressure

Although the most frequently encountered scenario in ventilation applications involves moving fluids (air), for completeness this section briefly describes the effects of pressure in fluids both at rest and those in motion.

3.5.1 Fluids at rest

Static pressure is defined as the stress (force per unit area) normal to a surface at any point on any plane in a fluid at rest [Kreider: *1994*]. Static pressure is the amount of compressive or expansive energy contained in a fluid and is a measure of its potential energy. Static pressure may exist in a fluid at rest or in motion, by transformation into velocity pressure, is the means of producing and maintaining flow against resistance. At every point in a static fluid a certain pressure intensity exists. Specifically, this pressure intensity, usually simply called pressure, is defined as:

$$p = \lim_{\Delta A \to 0} \frac{\Delta F}{\Delta A} = \frac{dF}{dA} \qquad\qquad (3.14)$$

where;

    F = normal force

    A = area of surface

Since a fluid has a density, the pressure within a static column of fluid will increase with depth due to gravity acting on the mass of fluid in the column. The variation in static pressure p_y acting vertically is given by:

$$\partial p_y = -\rho g \partial y \qquad\qquad (3.15)$$

Hence, the static pressure at any horizontal plane (p_y) is:

$$p_y = p_o - y\frac{\partial p}{\partial y}$$

(3.16)

where:

p_o = static pressure at a reference plane

y = vertical distance above the reference plane

For a constant increase in temperature with height $\partial T/\partial y$ i.e.

$$T = T_o - y\partial$$

(3.17)

where:

T_o = temperature at a reference point

T = temperature at a height y

∂T = increase in temperature per m (Km^{-1})

there will be a corresponding decrease in pressure. Using equation (3.16) and the gas law $p = \rho RT$, the vertical variation in pressure due to a uniform increase in temperature becomes:

$$\frac{\partial p}{\partial y} = -\rho_o g\frac{T_o}{T}$$

(3.18)

where:

ρ_o = fluid density at a reference temperature T_o

The pressure difference ΔP between two vertical points 1 and 2 at temperatures T_1 and T_2 separated vertically by a distance y (a situation common in natural ventilation applications) is given by the expression:

$$\Delta P = p_2 - p_1 = \rho_o g T_o y\left[\frac{1}{T_2} - \frac{1}{T_1}\right]$$

(3.19)

- 45 -

3.5.2 Fluids in motion

Flow of any fluid is produced by difference in pressure and the magnitude of the difference in pressure determines the characteristics of flow. The pressure in a moving fluid has a static component and a kinematic component i.e. the total pressure p_t of a moving fluid particle is:

$$p_t = p_v + p_s$$

<div align="right">(3.20)</div>

where:

p_s =   static pressure

p_v =   kinematic or velocity pressure which is $\frac{1}{2}\rho v^2$

In fluid flow there are basically two causes of pressure variation in addition to the weight effect - these are acceleration and viscous resistance. To accelerate a mass of fluid in a given direction, there must be a net force in the direction of acceleration [Massey, *1998*]. Therefore, the pressure must decrease in the direction of acceleration. In addition to acceleration pressure variation is needed to overcome the viscous resistance, which, like friction in solids, acts in opposition to the motion of the fluid.In some cases gravity may also enter the problem.

3.6 Bernoulli's Equation

A basic tool of fluid flow analysis is the Bernoulli relation involving the principle of energy conservation along the flow. Bernoulli equation relates changes in energy in a flowing fluid (kinetic energy, potential energy, energy lost to friction and energy introduced or removed) in terms of heat and work [Douglas *et al. 1985*]. The application of the Bernoulli equation, however, requires the flow to be:-

- Steady
- Incompressible
- Isothermal
- Frictionless

The generalised Bernoulli equation is usually represented by equation 3.21which is derived by considering the energy balance between two sections, such as Section 1 and Section 2 in Figure 3.6, in a flow field:

$$\frac{p}{\rho} + \frac{v^2}{2} + gz = \text{constant} \qquad (3.21)$$

where:

p_1 and p_2	=	static pressure (Pa)
v_1 and v_2	=	velocities (ms^{-1})
ρ_1 and ρ_2	=	fluid densities (kg m^{-3})
z_1 and z_2	=	heights from a datum (m)
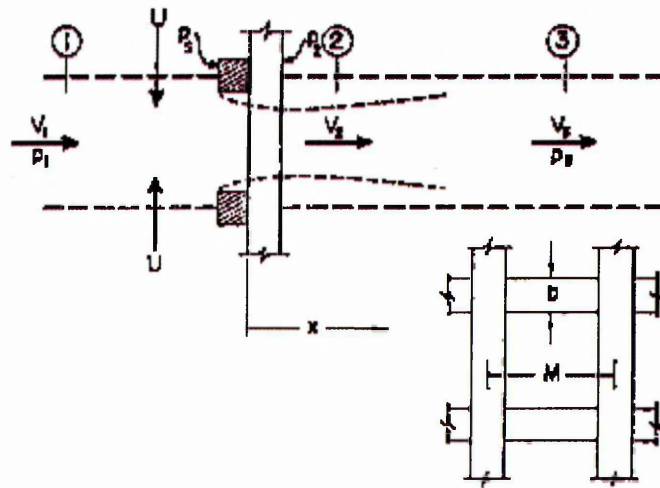
Figure 3.6; Definition sketch for pressure-velocity relationship

The Bernoulli equation is applied along streamlines and hence can be used to predict the pressure distribution within the fluid or the pressure distribution on a body if the flow pattern about the body is known.

3.7 Illustrative Applications

3.7.1 Flow across a sharp-edged orifice

An orifice is a precisely made hole through which fluid may flow. It is a constrictive device that causes change in energy in the form of a loss in static pressure and increased velocity when a fluid flows through the orifice. A small orifice is one in which the variation of head across the hole is small enough to be neglected [Massey, *1998*]. A lot of the principles of air flow through ventilation components such as slots, perforated

plates and mesh-screens can be learned from analysing fluid flow through a simple sharp-edged orifice.

Let Figure 3.7 represent such an orifice with a total pressure in the air stream at point 1 higher than point 2 which is in free space. The flow produces a convergence toward the orifice opening and will reach a maximum velocity at point 2, the smallest area of the stream technically called the *vena-contracta*. The area of the stream at the vena-contracta will be approximately 0.6 times the diameter of the orifice opening. Its location will be a distance downstream equal to about 0.5 times the diameter of the pipe, depending on velocity and size of the orifice [Massey, *1998*].
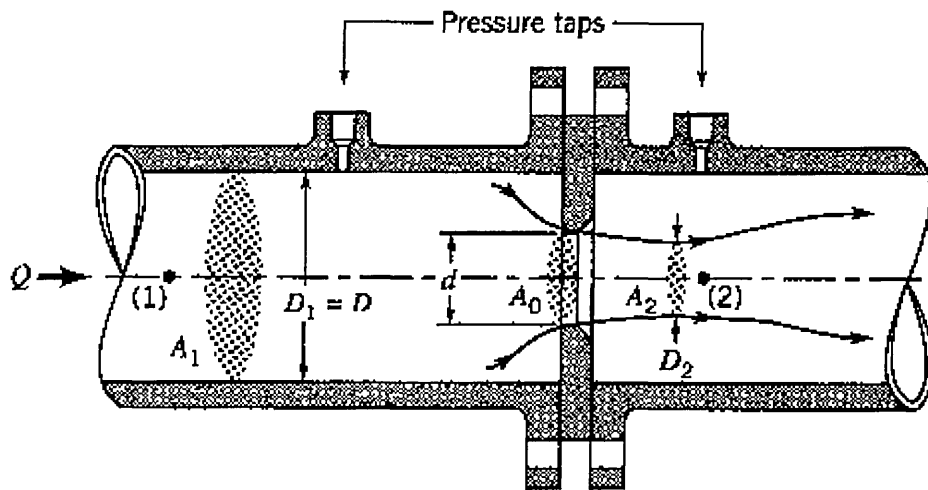
Figure 3.7: Illustration of flow through orifice
[Source: http://bioeng.okstate.edu/home/2000notes/images]

Louvres, for instance, perform in exactly the same way (Figure 3.8) - there is a vena-contracta existing between every louvre blade instead of a single vena-contracta as in the sharp-edge orifice. The sum of the areas of the vena-contractas existing between the louvre blades is termed its *effective area*. When considering a sharp-edge orifice, the effective area will be the area of a single stream at the vena-contracta. The shape, size and number of louvre blades of an air inlet will affect the effective area and location of the vena-contractas, but the basic concept applies regardless of the individual design.
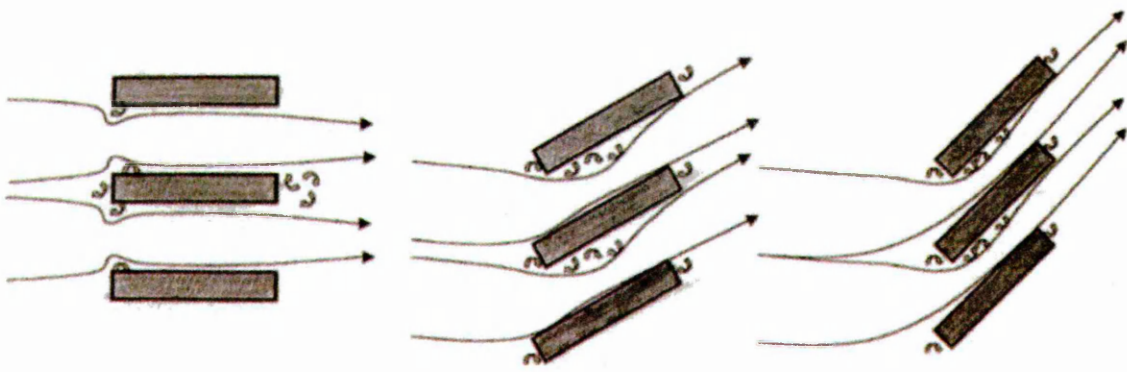
Figure 3.8: Illustration of vena contrata in louvres

The effective area of an air inlet/outlet may be defined by the expression:

$$A_e = A.c$$

(3.22)

where:

A   =   geometrically measure area

c   =   combined coefficient of entry and discharge

The coefficient "c" can only be determined from tests for various components many of which are quite complicated and difficult to measure geometrically. In a flow field the theoretical velocity of the jet is obtained by applying Bernoulli's equation, for instance, to points (1) and (2) in Figure 3.9 to obtain equation (3.23):

Effective b = M − 0,95 D
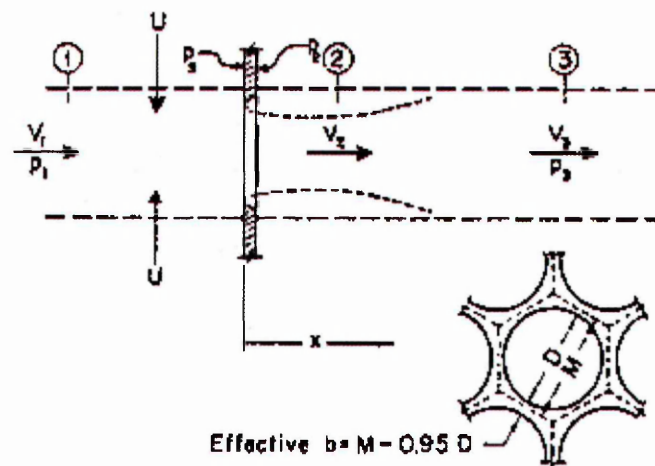
Figure 3.9: Illustration of sharp-edged orifice in perforated plate

$$h + \frac{P_1}{\rho g} = \frac{P_2}{\rho g} + \frac{v^2}{2g} \qquad (3.23)$$

which can be simplified to:

$$v = \sqrt{2gh} \qquad (3.24)$$

COEFFICIENT OF CONTRACTION, COEFFICIENT OF VELOCITY AND DISCHARGE COEFFICIENT

Because of the component of the velocity perpendicular to the axis, the jet will contract after leaving the orifice and the section at which the jet becomes parallel is termed the vena-contracta. The ratio "area of the vena-contracta" to "area of orifice" is called the coefficient of contraction (c_c). Because of friction at the orifice, the velocity at the vena-contracta is slightly less than the theoretical velocity and the ratio "actual velocity of jet" to "theoretical velocity of jet" is called the coefficient of velocity (c_v). If A is the orifice area, the flow rate is given by the equation:

$$Q = c_c \, A \, c_v \, \sqrt{2gh} \qquad (3.25)$$

$$= c_d \, \sqrt{2gh} \qquad (3.26)$$

$$c_d = c_c \cdot c_v \qquad (3.27)$$

c_d is the coefficient of discharge which is the ratio "actual discharge" to "theoretical discharge".

For a well-made, sharp-edged, circular orifice producing free jets, the coefficient of velocity is usually in the range 0.97 to 0.99. The coefficient of contraction for a circular sharp-edged orifice is about 0.61 to 0.66. The coefficient of discharge for a small sharp-edged orifice is usually in the range 0.6 to 0.65 [Massey, 1998].

3.7.2 Flow through rectangular slots

Rectangular slots usually find application as trickle ventilators in natural ventilation schemes. For a large rectangular slot of breadth b (Figure 3.10), the theoretical discharge through an elementary strip of thickness dh is given by equation (3.28):
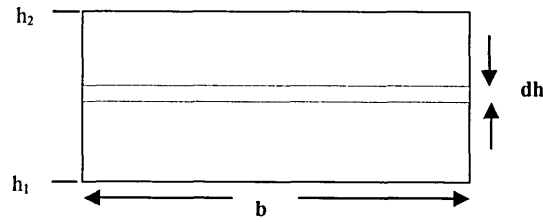
Figure 3.10: Large rectangular strip orifice

$$dQ = b \; dh \; \sqrt{2gh} \tag{3.28}$$

Integrating equation 3.28 gives the total theoretical discharge Q through the slot:

$$Q = b \; \sqrt{2gh} \; \int_{h1}^{h2} h^{-\frac{1}{2}} \; dh \tag{3.29}$$

$$= \frac{2}{3} \; b \; \sqrt{2g} \; \left[h_2^{\frac{3}{2}} - h_1^{\frac{3}{2}} \right] \tag{3.30}$$

Therefore, applying the coefficient of discharge (see *Section 3.7.1*) gives the actual discharge as:

$$Q_T = c_d \; \frac{2}{3} \; b \; \sqrt{2g} \; \left[h_2^{\frac{3}{2}} - h_1^{\frac{3}{2}} \right] \tag{3.31}$$

3.7.3 Flow through mesh-screens

A mesh-screen may be defined as a regular assemblage of elements forming a pervious sheet that is relatively thin in the direction of flow through the mesh-screen [Cornell *et al. 1958*]. Examples are woven round-wire grids with square mesh (Figure 3.11), perforated thin sheets, grids of bars of rectangular cross section etc. One convenient non-dimensional parameter is some measure of the area not blocked by mesh-screen elements as a fraction of the total available flow area - commonly referred to as the *free area ratio*.
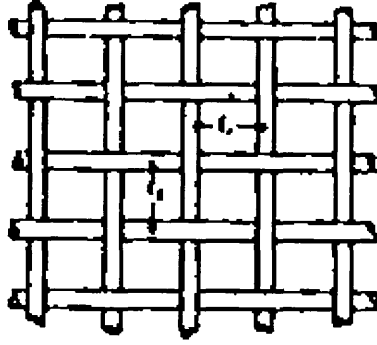
Figure 3.11: Diagrammatic representation of
a typical mesh-screen

Given a plane mesh-screen of certain element type and element arrangement, with a given upstream flow normal to the mesh-screen, the downstream flow conditions, in particular the pressure losses are characterised by the non-dimensional pressure loss coefficient k given by [Taylor *et al. 1944*, Eckert and Pfluger, *1942*, Schubauer, *1950*]:

$$k = \frac{\Delta P_T}{\frac{1}{2}\rho u^2} \qquad (3.32a)$$

Richards *et al.* (*1999*) describe the situation as follows. If u is the mean velocity of a fluid of density ρ through a mesh-screen placed at right angles to the stream and if P1 and P2 are the pressures in front of and behind the mesh-screen, the porosity of the mesh-screen is generally characterised by means of a resistance coefficient k given by the equation:

$$k = \frac{P_1 - P_2}{\frac{1}{2}\rho u^2} \qquad (3.32b)$$

When a fluid stream approaches a mesh-screen with velocity u at an angle, the pressure drop under these conditions is determined by the normal component of the approach velocity. The loss coefficient k is a function of the free area ratio of the structure, the type of construction and the Reynolds number. The effect of each of these factors on the loss coefficient has been investigated to some extent [Annand *1953*, Miguel *et al. 1997*, Richards *et al. 1999*], however, this subject is beyond the scope of the work reported

here. Equation 3.32 was used to estimate the resistance coefficient for representing the mesh-screen in the CFD models (*Section 6.8.6*).

3.7.4 Flow between parallel plates

The theoretical analysis presented in this section is later (*Section 6.6.5*) used to validated the CFD simulation method. Here, a two dimensional incompressible steady-state fluid flow between two parallel plates separated by a distance h (see Figure 3.12) is considered with a constant pressure gradient dp/dx applied to the flow.
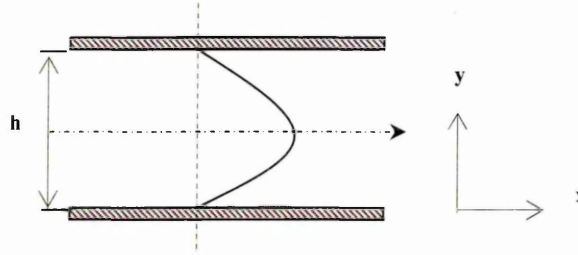
Figure 3.12: Illustration of flow between parallel plates

The simplified momentum equation yields:

$$\frac{1}{\rho}\frac{dp}{dx} = \nu\frac{d^2u}{dy^2}$$

(3.33)

where: ν is the kinematic viscosity.

Considering flow properties as functions of y only, with both plates at rest, the fluid motion is caused by the application of pressure gradient (dp/dx), in this case the velocity profile is a parabola with its vertex (corresponding to the maximum velocity) mid-way between the planes as is to be expected from symmetry. The velocity profile is given by the equation:

$$u\,(y) = \frac{1}{2\mu}\frac{dp}{dx}\,y\,(y-h)$$

(3.34)

The longitudinal pressure gradient along the channel is equal to:

$$\frac{dp}{dx} = -\frac{3\mu u_{average}}{h^2} \tag{3.35}$$

The equation of continuity then suggests that $\partial v/\partial x = 0$, so that the velocity is a function of z only. The pressure gradient is given by the expression:

$$\frac{\partial p(x)}{\partial x} = \mu \frac{\partial^2 v(z)}{\partial z^2} \tag{3.36}$$

Supposing that the pressure decreases with increasing x, this gives:

$$-\frac{\partial p}{\partial x} = \text{const} = \frac{\Delta p}{\Delta x} > 0 \tag{3.37}$$

If both plates are stationary:
$$v(z=0) = 0 = v(z=h) \tag{3.38}$$

which gives:

$$v(z) = \frac{\Delta p}{\Delta x} \frac{z(h-z)}{2\upsilon} = 6\,v' \frac{z}{h} \left(1 - \frac{z}{h}\right) \tag{3.39}$$

where, the average velocity v' is given by:

$$v' = \frac{1}{h} \int_0^h v(z)dz = \frac{\Delta p}{\Delta x} \frac{h^2}{12\upsilon} \tag{3.40}$$

The total discharge is given by the expression:

$$Q = -\frac{bh^3}{12\mu} \left(\frac{\Delta p}{\Delta x}\right) \tag{3.41}$$

Where the pressure changes from p_1 to p_2 over a finite length L in the direction of flow - $\dfrac{\Delta p}{\Delta x}$ maybe replaced by $-(p_2 - p_1) / L = (p_1 - p_2) / L$. Then equation 3.41 becomes:

$$Q = \frac{(p_1 - p_2)bh^3}{12\mu L}$$
(3.42)

b is a fixed breadth. Equation 3.42 is often called on in discussing problems of the leakage of fluid through small gaps.

3.7.5 Flow through air permeable materials

Permeable materials can be found in ventilation applications in various forms including very fine mesh-screens and acoustic linings. An air permeable material permits air to flow through it when a pressure difference acts across it. The permeability, determined by the structure of the material, is a property that states the degree of easiness for a fluid to pass through the material under the influence of a pressure gradient [Kronvall, *1980*]. The fluid permeability coefficient is defined by the equation:

$$B_0 = - \frac{q_v}{A} \cdot \frac{\mu}{grad.p}$$
(3.43)

where:

B_0 = permeability coefficient, (m^2)

A = cross-sectional area, (m^2)

q_v = volume flow rate across A, (m^3/s)

μ = dynamic viscosity, (Ns/m^2)

p = total pressure, (Pa)

3.8 Concluding Remarks

This chapter provided a basis of understanding the nature and patterns of fluid flow process and presented a methodology with which to predict them qualitatively and quantitatively. These tools can be used by the designer of an engineering device such as a ventilator to assess airflow performance. In addition, they provide a basis on which the designer is able to choose the optimum design from among a number of alternative possibilities. For additional detail on fluid mechanics, the reader is referred to Massey,

[1998], Douglas *et al. [1985]* or CIBSE: Guide C *[2001]* and ASHRAE: Fundamentals Handbook, *[2001]* which have a significant summarized presentation of the topic.

Chapter 4

FUNDAMENTALS OF AIRFLOW

THROUGH OPENINGS

The main aim of ventilation is to provide a clean, healthy and comfortable atmosphere for the occupants as well as to refresh the building. Ventilation is qualified as "natural" if it has no energy consumption associated with the use of fans. The question of natural ventilation has focussed the attention of investigators over the last few decades on three main areas:

- internal convective flow in buildings

- external wind and thermal effects

- design of external devices, natural ventilators, aiming to improve the ventilation process

4.1 Scope of Investigation

With respect to natural ventilators, considerable effort has been expended in improving their airflow performance. As will be seen from the sections in this chapter, the work of various researchers may be noted together with the research developed or sponsored by several manufacturers of ventilators for natural ventilation applications. Natural ventilation of a building is made up from two sources, namely, air entering/exiting a room through cracks, such as those around doors and windows (adventitious ventilation or infiltration) and air entry/exit through intentional purpose-provided openings such as trickle ventilators and louvers. As indicated in the earlier chapters, it is the airflow performance of the latter type of openings that is the subject of this thesis. As a prerequisite in the assessment of the airflow performance of ventilators for natural ventilation in buildings this project surveyed the available literature for techniques and methods of characterising or predicting the airflow performance of ventilators. This chapter evaluates the available literature in the context of the research discussed in this thesis. A review of ventilators for natural ventilation applications from various angles follows and includes:-

- developments in the design of ventilators

- theoretical models that have been used to characterise the airflow through ventilators

- experimental methods that have been employed to determine the airflow performance of ventilators

A separate literature review relating to application of Computation Fluid Dynamics (CFD) methods to the prediction or estimation of airflow properties of ventilators is included in *Chapter 6*. Other important considerations, such as ventilator maintenance requirements, capital and installation costs, are beyond the scope of this investigation and hence, although they are mentioned from time to time, they are not discussed in detail in this thesis.

4.2 Developments in Ventilator Design

Ventilators of different types and configurations have found widespread application in the natural ventilation of buildings. Over the years, the purpose of ventilators has generally evolved with advances in technology. Substantial effort has been directed towards the improvement of design of ventilators in response to various factors associated with their application. As early as the mid-1970's [Tipping and Tickner, *1974*] ventilators were being developed in response to the desirability of *reducing draughts* and *supply of air* to rooms that were to be sound proofed against *entry of external noise*. More recently, prior to the mid 1990's, ventilators that could provide *night-time ventilation* and be left safely open at night without risking *weather damage* or *intruders* getting into the building were not readily available [Webb *et al. 1998*]. In this respect a Partners in Technology project part funded by the Department of Environment, Transport and the Regions (UK) and carried out by Willan Building Services, Oscar Faber Applied Research and the Building Research Establishment (BRE) aimed to design, install and test such a prototype night ventilator. This design had to take into account several factors including *weather resistance* (particularly to driving rain), resistance to the *ingress of insects, building security, controllability* (either locally - manual or electric) or centrally (via Building Energy Management Systems), and the need for minimal maintenance and durability [Webb *et al. 1998*]. Post-testing, the practitioners also noted that the prototype needed further research to

improve *draught proofing, noise attenuation* and *controllability* before the ventilator could be marketed. The factors highlighted (*italics* in the above paragraph) are commented on in the following sections.

4.2.1 Design for provision of airflow

During the early years ventilators were generally in the form of a simple air grating or a flue. With fixed opening sizes, these were installed in rooms to provide sufficient and, often, excessive amounts of outdoor air for breathing and fuel burning applications [Bedford, *1943*]. Figure 4.1 shows an example of an early type of air grating.
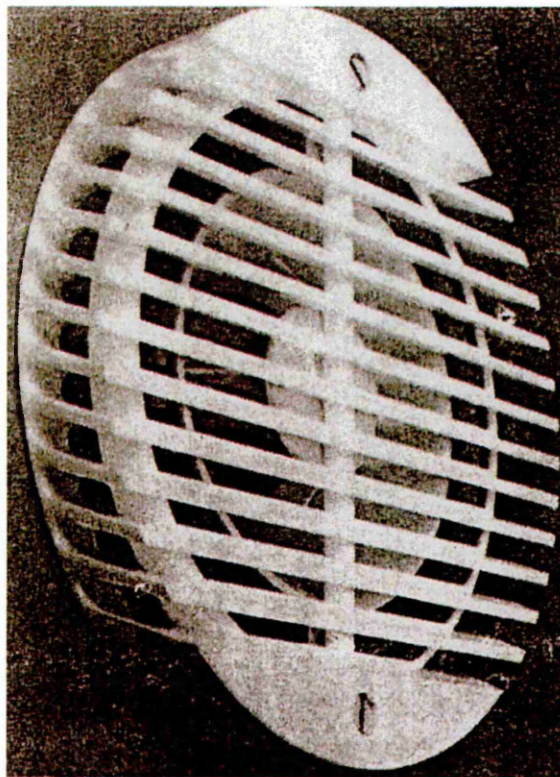
Figure 4.1: Example of air grating
[Source: Tipping & Tickner, 1974]

As time has elapsed more complex types of ventilators, usually incorporating moveable parts (examples can be seen in Figures 4.2 and 4.5 - 4.7), have been developed. The type shown in Figure 4.2 was used to provide natural ventilation in Regent House, Weston-Super-Mare (UK) in 1995 and comprised of insulated ventilators with mesh-screens and louvers [Webb and Kolokotroni, *1996*].
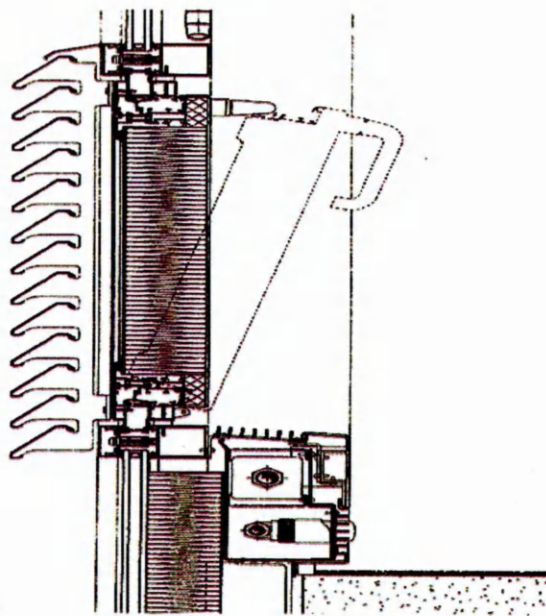
Figure 4.2: Section through louver also showing perimeter heating [Source: Webb & Kolokotroni, 1996]

4.2.2 Design for elimination of draughts

The design factors have also attracted interest from researchers with an aim to improve the airflow performance of ventilators for several decades. For instance, Tipping and Tickner [*1974*] investigated the construction and performance of ventilators developed in response to the desirability of reducing draughts (caused by the presence of the ventilator) and the need to supply air to a room that was to be sound proofed against entry of external noise. Figure 4.3 shows one such window ventilator whose room-side vanes sloped upwards to deflect incoming air towards the ceiling to avoid draughts in the occupied areas of rooms.

EXTERIOR   DIFFUSION   INTERIOR
GRILLE   CONE   GRILLE
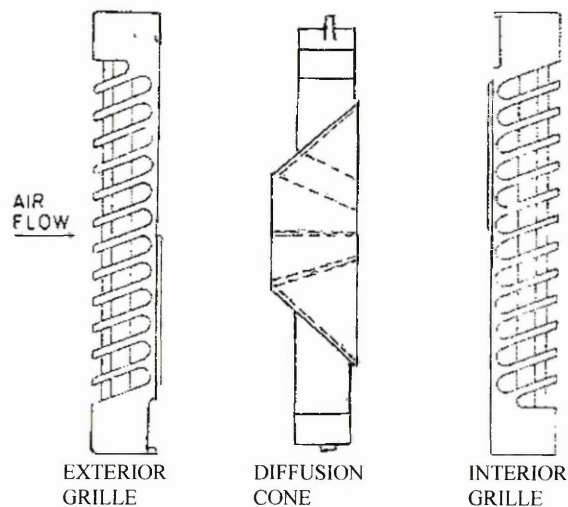
Figure 4.3: Components of ventilator showing upward sloping interior vanes [Source: Tipping & Tickner, 1974]

- 60 -

4.2.3 Design for noise reduction

Passive and trickle ventilators can have an adverse effect on the sound insulation of buildings. In urban areas natural ventilation openings in buildings (*open windows, trickle ventilators and through-the-wall ventilators*) can create several environmental problems, such as noise (from road traffic, aircraft and other external sources) and poor indoor air quality for building occupants. Such problems can create major obstacles to the widespread implementation of natural ventilation in new and refurbished urban buildings. For example, the design requirements for the airflow performance and acoustic performance of a ventilator are not complimentary. For airflow the requirement is for a large open area with smooth uninterrupted flow path. For acoustics the requirement is for a small open area with an attenuating multi-bend flow path. There is therefore a conflict between acoustic and ventilation requirements. Hence, there obviously has to be a design compromise if a ventilator is to have both good airflow and good acoustic properties. To gain an insight on the magnitude of this adverse effect several researchers [Joro, *1990*, White *et al. 1999*, Ajiboye, *1998*, De Salis *et al. 2002,* Kang and Brocklesby, *2003*] have undertaken acoustic measurements and field assessments on ventilators/naturally ventilated buildings.
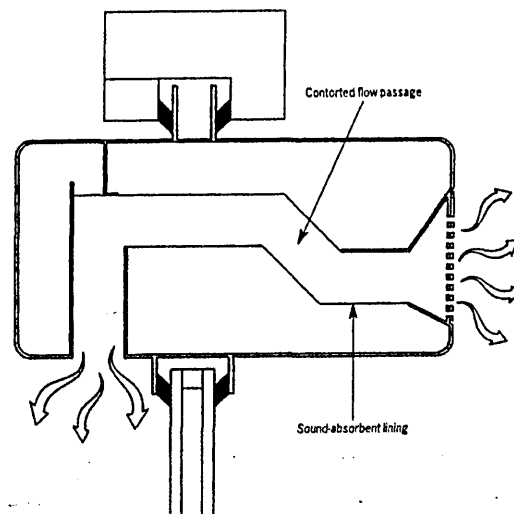
Figure 4.4: Schematic of acoustic vent

[Souce: Ross et al. 2003]

One of the trends towards "tighter" building construction is the sound insulation of rooms in buildings situated in areas of high noise incidence. The implications of these sound insulation requirements on ventilators and methods of reducing noise transmitted through ventilators have been, and continue to be, investigated. The acoustic performance of any ventilator is compromised when it is open and will vary with the

free area. However, this can be mitigated to some extent by specialist design. Improved sound attenuation is mainly achieved by adding sound-absorbent linings to internal surfaces of the flow passage(s) and sometimes also by designing contorted flow passages (Figure 4.4) [Ross *et al.* *2003*]. The sound attenuating performance of ordinary ventilators may also be improved to some extent by fitting external and internal acoustic hoods in place of the standard item (Figure 4.5).
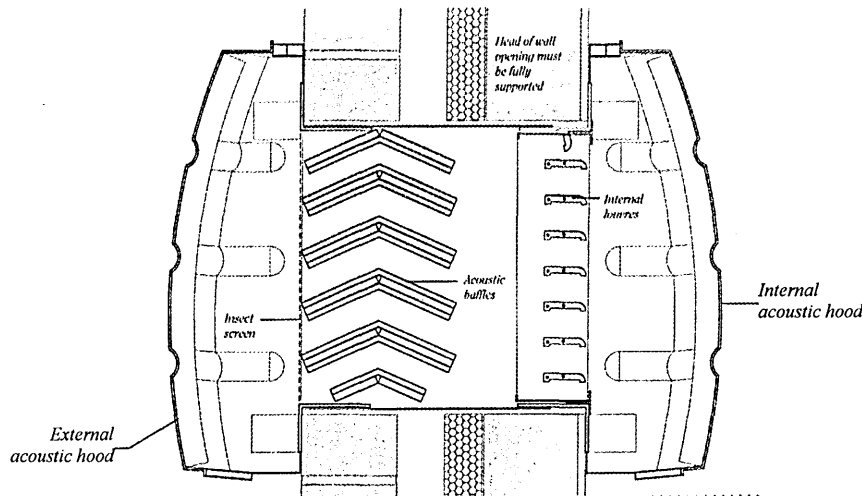
Figure 4.5: Acoustic ventilator with external and internal hoods

[Source: Passivent Ltd Product Catalogue, November 2000]

4.2.4 Design for control

Satisfactory ventilation rates can often be achieved by a natural system in which pressure differentials due to wind or the stack effect (or combination of both) is used to drive the air [Hitchin and Wilson, *1967*]. However, one of the basic problems of design when natural ventilation is adopted is that if the design meets the required standard of ventilation at the mean wind speed then the ventilation will be inadequate at lower wind speeds and unnecessarily high at high wind speeds. Thus, to obtain a more constant rate of airflow under such varying external conditions, provision must be made for either automatic or occupant (manual) control of the airflow into and out of buildings [Bedford, *1943*]. Where manual control is the preferred option due to several factors, including cost, provision needs to be made (e.g. pull-chords to open or close trickle ventilators) for occupants to operate ventilators when necessary. This, however, requires occupants to learn to anticipate the need for daytime cooling rather than waiting for it to get too hot before opening the ventilators [Webb and Kolokotroni, *1996*]. On the other hand, advances in technology have led to the emergence of intelligent ventilators

commonly referred to as *Controlled Airflow Inlets*. This type of ventilator can be integrated with the Building Management Control System and can be configured to automatically respond to various modes of control such as pressure, temperature, humidity or airborne pollutants in order to maintain a constant natural supply of airflow independent of wind pressure and pressure differences due to buoyancy. An outline of the range and availability of Controlled Airflow Inlets can be found in De Gidds [*1997*] where he recommends their application to natural ventilation of buildings in relation to overcoming problems of draughts and stuffiness, and also energy efficient design of buildings. A schematic example of one such passive controlled inlet patented by the Dutch firm Compri is shown in Figure 4.6.
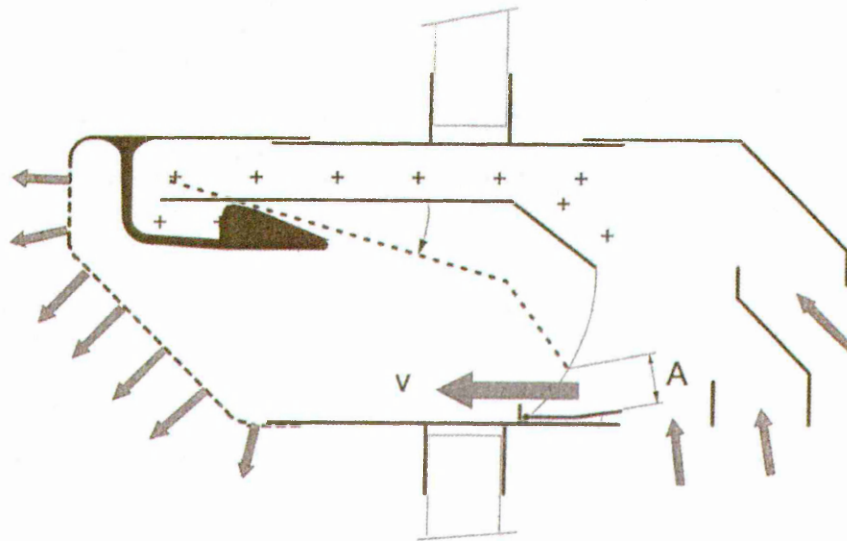
Figure 4.6: Pressure controlled ventilator
[Source: De Gidds, NATVENT WP3.2 Report, 1997]

Another example of a pressure controlled ventilator is shown in Figure 4.7. This ventilator has an interior part with fixed opening area and exterior flap which moves according to the pressure difference across it in order to control the exact amount of air passing through. For low-pressure differential, the flap moves to create a large inlet area whilst for high pressure differential, the flap moves to reduce the inlet area restricting the air from passing through. In this way the air flow is passively controlled since a pre-specified amount of air is passing through the ventilator [Karava *et al. 2003*].
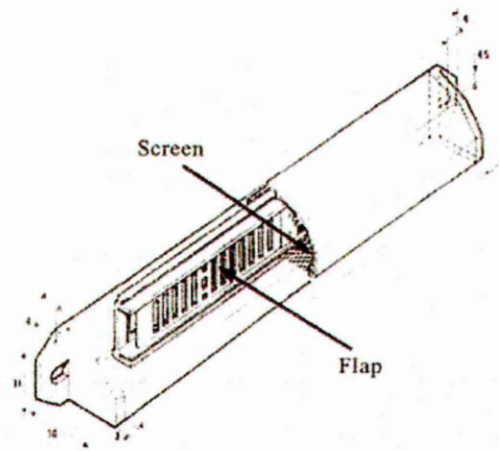
Figure 4.7: Pressure controlled ventilator

[Source: Karava et al. 2003)]

The importance of controls can be summed up from a field study of the thermal comfort of workers (including information about the use of building controls) in a naturally ventilated building by Raja *et al.* [*2001*] which concluded that the availability of controls and their appropriate use is key to better performance of the building and for improving occupant satisfaction.

4.2.5 Design for aesthetics

Aesthetics, often included on the list of engineering and architectural design considerations, is another important factor that is normally taken into account when designing and manufacturing ventilators. Commenting on a new window ventilator, Tipping and Tickner [*1974*] stated that it was developed with an industrial design consultant retained to provide advice on the *external appearance of the ventilator*. More recently, Bevan [*1997*] indicated that "*the ventilator prototype* (Figure 4.8) *tested at the Building Research Establishment (BRE) was ugly and that once its efficiency was established a more aesthetically pleasing version would be developed*". Colour and materials finish (plastic, metallic etc.) are other factors that are normally associated with aesthetics. However, these elements are beyond the scope of this investigation and hence, they are not discussed in any detail.
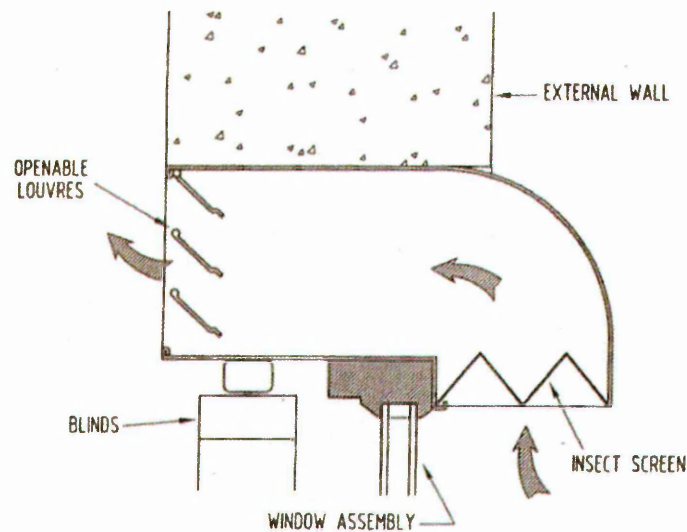
*Figure 4.8: Section through prototype ventilator developed
and test at the BRE [Source: Bevan, 1997]*

4.2.6 Design for elimination of security risk

Building cooling by natural ventilation relies on large openings in the building facade to allow the displacement of warm indoor air with relatively cool air from outside. Night cooling (see also *Section 4.2.8*) exploits this basic physical process whereby heat retained in the structure of the building is dissipated at night. However, the simple solution of opening all office windows at night and leaving the building empty is clearly a security risk [Bevan, *1997*]. During the last decade ventilators have been designed with a requirement to eliminate security risk and weather damage (see also *Section 4.2.7*) as high priority factors [Webb *et al*. *1998*]. Common methods of minimising or eliminating the risk of intruders include limiting the size of openings during unoccupied periods, and incorporating mesh-screens/bars on ventilation openings.

4.2.7 Design for elimination of weather damage

The prevention of water entry in a building by systems of hoods and rain deflector elements is an essential feature of a satisfactory ventilator. However, in certain cases the presence of such preventive devices obstructs to some extent the flow of air and reduces the efficiency of the ventilator in its primary function of supplying or removing air to/from a building [Cousin, *1969*]. Several other methods of minimising or eliminating water entry through ventilators are utilised. Some ventilators incorporate complex controls that close the ventilators when rain sensors are triggered [Bevan, *1997*]. The window ventilator (Figure 4.3) had an exterior grille mounted with the vanes sloping

downwards to facilitate this function of preventing water entry through the ventilator. Further, some ventilators incorporate "rain hooks" on each vane or blade to help prevent rain from entering through the ventilator. Rain hooks are simply protrusions extending across the width of each vane/blade.

4.2.8 Design for night cooling

The need to focus on energy saving in existing buildings has led to the use of *night cooling* through natural ventilation. Night cooling depends on the low night-time temperatures and utilises the buildings thermal mass to achieve lower indoor temperatures on the following day and thus provide a more comfortable environment for occupants. Night cooling has steadily been gaining popularity as evidenced from increasing interest shown towards the review in methods of designing and operating ventilators. Webb *et al.* [*1996, 1998*] investigated the effectiveness of a night cooling strategy for a refurbished 1950 office building with the results indicating an improvement in the provision of a more comfortable working environment for occupants. For night-time ventilation some form of automatic control system is desirable to prevent the ingress of rain, to ensure the building will be cooled down when necessary and to prevent over cooling. For instance, if overnight ventilation is not stopped early enough, it could lead to too low temperatures at the beginning of the occupancy period [Gratia *et al. 2004*].

4.3 Ventilator Airflow Performance Assessment

In parallel to increased interest in the development of ventilators the question has arisen regarding standardised methods of establishing the true performance of ventilators. From a manufacturing point of view the main method employed has been based on determining the effective area of the ventilator [Bedford *1943*, Tipping and Tickner *1974*]. Recent studies [e.g. White *et al. 1999*] have highlighted the performance of ventilators as being dictated mainly by the open area of the aperture. Most standards and regulations in the UK specify ventilation and air supply openings in terms of a *free area* (also often referred to as *open area*). Free area is simply the physical size of the smallest aperture in a ventilator. For an ordinary grille with many holes, the free area is the sum of the areas of all the individual holes. Whilst free area is relatively easy to calculate it does not necessarily reflect the airflow performance which a vent will achieve. The more complicated and/or contorted the airflow passages in a ventilator, the

less air will flow through for a given pressure difference. So, two different vents with the same free area will not necessarily have the same airflow performance [White *et al. 1999*]. Areas of simple thin-plate openings having standard geometrical shapes may be assessed by direct measurement, but openings of such a type are rare in practice. Where the ventilator has any complication in design, such as a louver or a grille, it is difficult to assess its area of opening and some experimental methods become necessary. The area derived by these means is often called the *equivalent area* of the airflow component. Airflow performance of such a ventilator is then assessed by implicitly comparing it with a thin-plate sharp-edged circular orifice. *Equivalent area* is a better measure of airflow performance. The equivalent area of a vent is measured on an airflow test rig and it is defined as the area of a single sharp-edged hole (in a thin plate) that passes the same air volume flow rate and at the same applied pressure difference as the vent being tested.

Although the specification of a size of opening is the only parameter which is under the control of the specifier, specification of the opening size is in itself an inadequate criterion for the representation of the airflow performance of a ventilator. What is required is a specification of the rate of airflow through the opening and the pressure difference across it in addition to its size. Other performance assessments previously used for airflow components involved measurements of, say, the air speed attained at a given distance from the centre of a ventilator unit. An example can be found in the work of Tipping and Tickner [*1974*] mentioned earlier, which examined the performance of ventilator units with the benchmark being the velocity attained at a certain distance from the centre of the unit. For instance, in relation to the window ventilator (shown in Figure 4.3) they arrived at a performance of 0.34m/s at 500 mm away from the centre of the unit. This was then compared against the velocity (0.9m/s) achieved by a simple louvered ventilator requiring the same diameter hole in the window and delivering the same volume flow rate.

4.4 Regulations and Standards

Installation standards and general workmanship have an impact on the use of ventilators for natural ventilation in buildings. It is well known that poor building air-tightness results in excessive air infiltration and resultant uncontrolled energy loss. Armed with this knowledge, many countries have introduced regulations and guidance towards improvement in building air-tightness whilst ensuring that this is done without

detriment to the indoor air quality. However, National and International code requirements regarding smoke, noise and fire transfer present challenges to the designer of a natural ventilation system. The difference in philosophy between countries regarding ventilation and the way the requirements are described in the Building Regulations have a large influence on the design and performance of ventilators. An interesting example can be found in De Gidds [*1997*] where he indicated in relation to Controlled Airflow Inlets that "*in France air inlets may not be fully closed whilst for The Netherlands they must be completely closable*" and also that "*in The Netherlands the controllability of these inlets must be between 1 and 25 Pa, while in France the control may be at about 20 Pa*". The following paragraphs briefly comment on some regulations and standards relevant to airflow through ventilators in naturally ventilated buildings.

4.4.1 Airflow provisions

As far back as the early 1940's, there are reports [Bedford, *1943*] of the London City Council By-laws requiring that any room used as an office or for habitation, if not ventilated by a mechanical ventilation system installed in the building, was to have a flue or other aperture of specified area to provide air exchange with the outside air. More recently [Kolokotroni *et al. 1997*, White *et al. 1998*], the UK Building Regulations recommend provision of external openings with open areas of 4000 mm^2 in rooms with floor areas less than 10 m^2, and 400 mm^2 per m^2 of floor area for those rooms which are larger, as sufficient provision for background ventilation. Approved Document Part F1 (UK) Building Regulations prescribes requirements of openable area for back ground ventilation.

4.4.2 Component airflow performance

The need to establish or substantiate the performance of airflow components has been around for many years. However, until recently there has been a lack of guidance on methods and procedures for testing these components. The use of the variety of methods that have been previously employed (such as those based on the specification of a free area) often resulted in discrepancies being observed with regard to the reported performance of the airflow components. For instance, an over-optimistic assessment by manufacturers and subsequent publication of free areas [White *et al. 1999*] and, variations in manufacturing and installation tolerances [Cockroft and Robertson, *1976*]

have been reported as some of the reasons why actual characteristics of ventilator components vary considerably between samples. The introduction and adoption of international standards such as BS EN 13141-1:*2004* by CEN member countries alleviates the problem of assessing and reporting the performance of airflow components. This standard specifies laboratory methods for testing ventilator devices. The test generally consists of measuring several volume flow rates induced through a device by the applied static pressure difference to define the flow rate/pressure characteristic curve. The American standard [ASTM E783:*1993*] for field measurements of air leakage through installed windows and doors is also based on the same principle.

4.5 Theoretical Models

The airflow through openings for natural ventilation applications is governed by two important phenomena, namely aerodynamic effects (resulting from effects of wind flowing past buildings) and hydrostatic action due to buoyancy effects generated by temperature differences. Airflow through openings is encouraged by a variety of factors which can be broadly classified into two groups; those which induce steady flow by virtue of their mean values (mean wind pressures on the building surfaces and effect of indoor/outdoor temperature differences), and those whose effect is due to their fluctuating nature. The behaviour of airflow through ventilation openings as a function of these factors has been investigated by several researchers [Cockroft and Robertson *1976*, Kronvall *1980*, Etheridge and Stanway *1988*] and found to be quite complex.

Other researchers [e.g. Baker *et al. 1986A*, Yakubu and Sharples *1991*, Maghrabi and Sharples *1999*] have directed their effort towards the study of airflow performance of ventilator openings in an attempt to establish methods to predict the flow characteristics. These prediction methods have resulted in a variety of procedures ranging from simple single equation models to sophisticated models employing measured data or even numerical techniques. Generally, the aim is to establish a relationship between the airflow resulting from a pressure difference applied across an opening. Two such models (power law and quadratic, discussed in *Section 4.7*) have found universal recognition although they have given rise to the widest differences of opinion over the last 25 years. There is still an on-going debate as to which method can be used to cover the range of parameters encountered in natural ventilation applications.

4.6 Experimental Methods

Estimation methods in building ventilation tend to rely upon simple experimental data and general assumptions since precise calculations of unsteady flow characteristics of openings within buildings are rarely known. Hence, frequently it is more preferable to undertake laboratory measurements as the steady flow characteristic is a significant parameter to establish any ventilation measurements. Researchers have employed experimental methods to estimate various coefficients to be used in conjunction with their proposed theoretical models for prediction of airflow characteristics of openings. Others have used experimental methods as a means of examining the validity of theoretical models. Literature is available [Etheridge *1977*, McGrath and Howarth *1984*] on airflow characteristics of real leakage paths. Such characteristics have often been measured using pressurisation or depressurisation techniques. Other investigators [Hopkins and Hansford *1974*, Baker *et al.* *1986B*, Baker *et al.* *1987*] have used laboratory fabricated model cracks of different geometry to represent typical building cracks. In general such studies have established coefficients and equations that can be used to represent the airflow characteristics of cracks. In many cases the relationships have been found to depend on various factors including the characteristic dimensions and shape of the airflow path, and the resulting coefficients have normally been found to be functions of the Reynolds number. Although conflicting in nature, the data derived from the studies on cracks has no doubt provided useful information from which investigations of airflow through components such as mesh-screens, perforated plates, louvers etc have benefited.

4.6.1 Airflow through cracks

Similarities between airflow in purpose-provided openings for natural ventilation and infiltration through adventitious openings has led researchers to study airflow through cracks such as those occurring around windows and doors in order to understand the airflow characteristics resulting from natural forces (wind and temperature differences). Several proposals have been put forward to characterise the airflow through such components. Some evidence [Dick, *1950*] suggested that the flow rate is approximately proportional to the square root of the pressure drop:

$$Q = A \sqrt{\Delta P} \qquad\qquad (4.1)$$

where A is a constant proportional to the effective leakage area of the crack. However, in practice the relationship does not fit available data and is not strictly true for all types of cracks and their geometries and pressure differentials [Hopkins and Hansford, *1974*]. Hopkins and Hansford [*1974*] and Peterson [*1982*] suggested the use of equations of the form:

$$\Delta P = \text{constant}.V^n \tag{4.2}$$

to describe crack flows, where V is the volume flow rate and the index n had a fixed value of 1.6. Etheridge [*1977*] points out that equations of this type (Equation 4.1 and Equation 4.2) lack generality because they are not dimensionally homogeneous i.e. they do not obey Reynolds law of similitude, and indicated that Equation 4.3 below more adequately estimates the open areas of a wide range of real full-scale components and successfully described the flow through them regardless of the flow direction.

$$\frac{1}{C_z^{\,2}} = B\frac{z}{d_h}.\frac{1}{R_{ey}} + C \tag{4.3}$$

where C_z is the discharge coefficient, z is the distance through the crack, d_h is the hydraulic diameter, R_{ey} is the Reynolds number, and B and C are constants.

Some researchers prefer to describe laminar and turbulent flows separately. For instance, for very small openings where the flow is assumed to be laminar the pressure drop is represented by the Couette flow equation (Equation 4.4) [Awbi, *1998*]:

$$\Delta P = \frac{12\mu l}{bh^3}Q \tag{4.4}$$

where *l* is the depth of opening in the flow direction, Q is the flow rate through the opening, *b* is the width of the opening, *h* is the height of the opening and μ is the dynamic viscosity. For turbulent flow through large openings the pressure drop is given by the equation:

$$\Delta P = 0.5\left[\frac{Q}{C_d A}\right]^2 \tag{4.5}$$

where the discharge coefficient (C_d) depends on the sharpness of the opening and the Reynolds number of the flow. For sharp openings $C_d = 0.6$ approximately, which is independent of the Reynolds number [Awbi, *1998*]. If the flow is transitional, i.e. neither fully laminar nor fully turbulent, Awbi [1998] suggests the use of the power equation:-

$$\Delta P = \left[\frac{Q}{KL}\right]^{\frac{1}{n}} \tag{4.6}$$

where K is a flow coefficient which is dependent on the geometry of the opening, L is the length of opening and n ($0.6 \leq n \leq 0.7$) is a flow exponent dependent on the flow regime.

It appears as though the use of the quadratic equation (Equation 4.7) below:

$$\Delta P = AQ^2 + BQ \tag{4.7}$$

was first proposed to describe the flow characteristics of components in the discussion following the presentation by Dick [*1949*]. The results of Baker *et al.* [*1987*] together with previous data and earlier suggestions [Etheridge *1984*] led Baker *et al.* [*1987*] to conclude that a theoretical quadratic model of crack flow obtained from the same parallel plate theory as Equation 4.3 was a more practical alternative to the more general non-dimensional solutions found in Equation 4.3 since adequate estimates of the parameters A and B:

$$A = \frac{\rho C}{2d^2 l^2} \tag{4.8}$$

$$B = \frac{12 \mu z}{l d^3} \tag{4.9}$$

can be readily obtained by quadratic regression analysis of experimental data. According to Baker *et al.* [*1987*] the pressure difference (ΔP) is the total pressure drop allowing for edge effects due to skin friction along the dimension z in the direction of flow, d is the gap thickness between plates, l is the breadth of the plates, μ is the dynamic viscosity (Pa s), ρ is the fluid density and C is a dimensionless constant.

4.6.2 Airflow through mesh-screens

Mesh-screens have found widespread application in many engineering branches ranging from aeronautics to ventilation and air conditioning of buildings. Mesh-screens are used in airflow systems for a variety of important duties including production of uniformity of the velocity distribution, reduction of turbulence of the air-stream, production of artificially high turbulence, introduction of known pressure drops into experimental systems [Annand *1953*] and control of dust and insect entrance into buildings [Miguel *1998*]. The most common types of screen used in ventilation applications are the square-mesh lattice formed of round wires or straight bars and the perforated plate. The relative scale of any pattern is best described by the open area ratio i.e. the fractional degree to which the screen allows fluid to flow through it. The use of mesh-screens is accompanied by the introduction of a resistance in a system, and in practice slight irregularities in the texture of the mesh-screen generally produce both spatial and time variations of flow on the downstream side. As this resistance (or pressure loss) frequently limits the effectiveness of the installation, it is thus a factor of primary importance. Therefore, for all these applications it is desirable to be able to estimate the airflow characteristics which will be produced by a given mesh-screen. The general problem of the flow through mesh-screens has been widely investigated and is well documented in studies such as Taylor and Davies [*1944*], Simmons and Cowdrey [*1945*], Baines and Peterson [*1951*], Cornell [*1958*], Morgan [*1962*], Baker *et al.* [*1986A*], Idelchik [*1989*], Miguel [*1998*], and Richards and Robinson [*1999*]. Many of these studies have attempted to relate a pressure drop coefficient to the geometry of the mesh-screen (usually expressed in terms of the porosity or free/open area) and the flow conditions represented by the Reynolds number (e.g. Figure 4.9 - Source: Richards *et. al. 1999*).

An experimental determination of the aerodynamic resistance of a porous screen is usually made from the difference of pressure measured across the two sides when the screen is held transversely to an air current. The pressure drop across a mesh-screen is commonly represented as a resistance coefficient "k" via the expression [Eckert and Pfluger *1942*, Baines and Peterson *1951*, Morgan *1962*]:-

$$\Delta P = \frac{1}{2} k \rho v^2 \qquad (4.10)$$
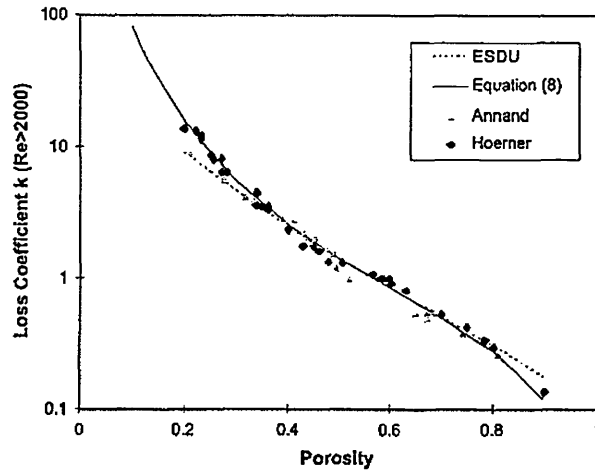
Figure 4.9: Loss coefficient for round wire mesh-screens[A]

It is not uncommon to fit pressure-flow equations to data from experiments on mesh-screens. Miguel *et al* [*1998*] tested a variety of such screens (Table 4.1) and obtained excellent curve fits by using a second order polynomial to relate the pressure drop (ΔP) to the air velocity (u) through the mesh-screen.

In a study on perforated plate screens subjected to small pressure differences Baker *et al.* [*1986A*] related the mean flow velocity to the pressure differential by considering the sum of the pressure drops due to skin friction and end effects, and arrived at the expression:-

$$\Delta P = \frac{32\rho\upsilon l}{d^2}v + 0.75\rho v^2 \qquad (4.11)$$

These experimental and theoretical studies on perforated screens at small pressure differences suggested that the theory was relevant to natural ventilation of buildings and to the design of many types of deliberate ventilation openings such as trickle ventilators and eaves ventilators [Baker *et al. 1986A*].

[A]*The figure shows data derived from Annand ("The resistance to air flow of wire gauzes" - J. Roy. Aeronaut. Soc 57 (1953) 141 - 146) and Hooerner (Fluid Dynamic Drag, published by the author, 1965) for round wire mesh-screens at high Reynolds numbers. Also shown is the correlation given by ESDU item 72009 (Engineering Science Data Unit, London 1972) which fits most of the data shown but does not behave at low and high porosities in the manner expected [Richards et al 1999].*

Mesh-screen specifications and best fit equation for second order polynomial $\left(\Delta P = Au^2 + Bu\right)$

Description	Porosity (m^2/m^2)	A	B	Correlation coefficient
Polyester rectangular mesh	0.04±0.004	2869.81	189.72	0.98
Parallel polyethylene strips held by thread (irregular mesh)	0.04±0.006	3261.12	202.36	0.98
Polyethylene rectangular mesh	0.07±0.003	715.75	126.44	0.99
Polyester irregular mesh	0.07±0.005	801.18	134.07	0.98
Woven screen regular mesh	0.14±0.014	82.297	31.168	0.99
Parallel polyethylene strips held by thread (irregular mesh)	0.14±0.011	83.272	31.438	0.99
Woven screen regular mesh	0.25±0.010	18.015	17.712	0.99
Woven screen regular mesh	0.36±0.016	7.637	15.001	0.98
Polyester irregular mesh	0.36±0.015	7.563	14.816	0.98
Polyester rectangular mesh	0.5±0.009	1.556	2.503	0.99
Polyester rectangular mesh	0.63±0.015	0.9112	2.285	0.98
Polyester irregular mesh	0.63±0.035	0.9053	2.299	0.99
Polyester irregular mesh	0.89±0.018	0.3667	1.605	0.99
Woven screen regular mesh	0.9±0.022	0.3524	1.548	0.97

[Adapted from A.F. Miguel, *1998*]

It is evident from the above paragraphs that much progress has been made in understanding the underlying physical phenomena of flow through mesh-screens. However, information on how such mesh-screens affect the airflow characteristic when used in combination with other ventilator components is very scarce or non-existent. Hence, there is a clear need for research focussing on this area. It is evident that most experiments on mesh-screens are confined to the case of gauzes possessing geometrical symmetry about the plane of flow. However, from the reviewed literature, there is no experimental evidence that if the gauze were rotated in its plane the downstream flow would remain in the same direction or even in the plane containing the upstream flow and the perpendicular to the gauze. It seems that for simplicity, it is generally assumed that the gauze has aerodynamic properties which are rotationally symmetrical about the perpendicular to its plane.

4.6.3 Airflow through whole ventilator units

There are some reports available [Tipping and Tickner, *1974*, Gonzalez *1984*, Yakubu and Sharples, *1991*, Oliveira and Bittencourt *1998*, Maghrabi and Sharples, *1999*, Nielsen *et al.* *2000*, Heiselberg *et al.* *2000,* Karava *et al.* *2003*] on studies that have investigated the airflow characteristics of whole ventilator units for natural ventilation applications in order to gain fundamental understanding of the airflow characteristics. In relation to the investigation in this thesis perhaps the work of Yakubu and Sharples [*1991*] on modulated louver windows can be regarded as the earliest attempt to apply proposals from crack flow theory to a louver system similar to the ones used in this study. Yakubu and Sharples [*1991*] adapted the quadratic equation (Equations 4.7 - 4.9) to account for louver blade inclinations through the use of revised coefficients:

$$A_\theta = \frac{\rho C}{2d^2 l^2} \frac{1}{\cos^4 \theta} \qquad (4.12)$$

$$B_\theta = \frac{12 \mu z}{l d^3} \frac{1}{\cos^4 \theta} \qquad (4.13)$$

where θ is the louver blade inclination angle from the horizontal. However, the predicted dependence of the pressure drop on $\cos^4 \theta$ was not substantiated from their experimental results. They attributed this to an indication of a more complex relationship between the pressure difference at blade angle θ and the pressure difference when the blades were horizontal than that suggested by simple parallel plate flow theory. Follow on work by Maghrabi [*2001*] on modulated window louvers, similar to the ones used by Yakubu and Sharples, extended the investigation by assessing the influence of various louver configurations (including variations of louver blade inclination angles, depth of louvers, gap between louver blades, and ratio of aperture to depth) on the pressure-flow characteristics. Maghrabi found that the major enhancement in pressure differential was not due to an individual louver geometric variable but rather to the combination of variables that would comprehensively describe ΔP. Like Yakubu and Sharples, Maghrabi made no consideration for the use of modulated louver windows in combination with other ventilator components such as insect screens or acoustic linings.

4.6.4 Discharge coefficients

Computation of natural ventilation airflow through components is most commonly made using Equation 4.14 which describes the airflow through an equivalent sharp-edge orifice opening [Mathew and Rouseau *1994*, Awbi *1994*, Heiselberg *et al. 2001*, Karaval *et al. 2003*]:

$$Q = C_d A \sqrt{\frac{2\Delta P}{\rho}} \qquad (4.14)$$

This equation utilises discharge coefficients C_d that are usually regarded as being constant. In the absence of better information, a generally accepted value for the discharge coefficient of a sharp-edged large opening is $C_d = 0.6 \pm 0.1$ [Flourentzou *et al. 1998*]. C_d is a characteristic parameter for a specific opening. It takes both the contraction and the friction loss into account, and depends on the geometry of the opening and flow Reynolds number. Discharge coefficients quantify the airflow efficiency of an opening or alternatively the airflow resistance of openings. Reported results such as [Heiselberg *et al. 2000*] indicate that discharge coefficients vary (Figure 4.10) considerably with the size of the opening area, opening type and driving force e.g. temperature difference. Hence, the use of constant values needs to be treated with care as misuse could lead to serious errors in the prediction of airflow capacity of the ventilation openings.
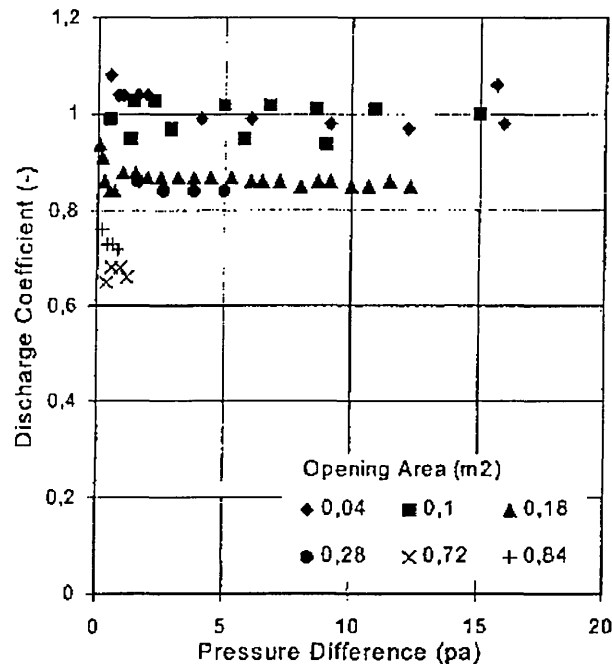
Figure 4.10: C_d variation with ΔP for windows

[Source: Heiselberg et al. 2000]

Although researchers, for example [Baker *et al.* *1986B*, Baker *et al.* *1987*, Idelchik *1989*, Nielsen *et al.* *2000*], have employed differing techniques to determine empirical coefficients, the common basis or reference seems to be the application of data traditionally used for fluid flow in pipes and flow between parallel plates to problems concerning airflow in building components [Kronvall, *1980*]. This has generally been achieved through simplifications such as basing models on only the steady state conditions resulting in deviations from actual conditions that would occur when air flows across openings in the real world. Consequently, such simplifications often lead to inaccuracies in the proposed models. While a large number of coefficients relating to a variety of individual ventilator components can be found in the reference work of Idelchik [*1989*], there is a lack of data which have been measured on combinations of these components as is typical in natural ventilation applications.

4.7 Analytical Methods

In order to maintain a continuous flow of air in an enclosed space some motive power is required to drive the air through ventilation openings. In natural ventilation applications this motive power is derived from wind or thermal buoyancy and takes the form of a pressure difference across the opening. Some means of expressing this motive power in relation to the resulting airflow rate is therefore required. The primary requirement of such a flow equation is that it should give a good representation of the flow characteristic of openings over a wide range of pressures [Etheridge, *1998*]. Ventilation designers and researchers often attempt to estimate the motive power spent in producing velocity in the inlet, altering velocity as the inlet varies in size, producing velocity in the outlet and over-coming friction in any straight lengths within the opening [Shaw, *1907*]. Two forms of flow equation are usually used to describe the flow through component openings and background cracks, namely the *power law* and *quadratic formulations*. The coefficients derived from experiments (*Section 4.6*) are usually also used to transform the experimental findings into one of the two forms of representing the flow equation [McGrath and Howarth *1984*, Baker *et al.* *1987*, Yakubu and Sharples *1991*, Maghrabi and Sharples *1999*]. This provides a basis of representing data in a form that allows direct comparison of experimental findings. The form of the pressure-flow relationship for building envelopes has been a topic of debate for many years. Whilst many researchers [Walker *et al.* *1998*, Liddament, *1987*] have expressed preference for the power law equation others [Baker *et al.* *1986B*, Etheridge *1998*] argue that the

power law is flawed because it is not dimensionally homogeneous and the constant n does, in fact, vary as the flow rate varies. That aside, the power law has gained almost universal acceptance for building envelope leakage in measurement standards, ventilation standards and many infiltration models [Walker *et al.* *1998*].

4.7.1 Power law equations

For most practical purposes the versatile power law is used to estimate the motive power (ΔP) resulting into an airflow (Q) through a ventilation opening. The power law takes the form:

$$Q = \alpha \Delta P^{\beta} \tag{4.15}$$

where α and β are constants which are assumed to depend only on the geometry of the ventilation opening. Some researchers [Haghighat and Rao, *1991*] have, however, suggested the dependence of α on the Reynolds number and geometry of the opening. The flow exponent β normally assumes values such that 0.5 (turbulent flow) $\leq \beta \leq 1.0$ (laminar flow).

4.7.2 Quadratic type equations

The alternative common method of estimating flow characteristics is the quadratic equation which takes the form:

$$\Delta p = aQ^2 + bQ \tag{4.16}$$

resulting from a combination of fully developed laminar flow and turbulent flow. Here "a" (Pa s^2/m^6) is the coefficient for entry, exit and turbulent flow losses and "b" (Pa s/m^3) is a flow coefficient for fully developed laminar friction losses [Dick *1949*, Walker *et al.* *1998*] and both are normally assumed to be constant. The quadratic relationship between airflow rate (Q) and pressure difference (ΔP) has been expressed in terms of geometric parameters of parallel-plate ventilation openings by [Baker *et al.* *1987*] using the equation:

$$\Delta P = \frac{12\mu z}{wd^3} Q + \frac{\rho c}{2d^2 w^2} Q^2 \tag{4.17}$$

where ΔP is the total pressure drop allowing for edge effects due to skin friction along the dimension z in the flow direction, c is a dimensionless constant, d is the gap thickness, w is the breadth, μ is the dynamic viscosity and ρ is the fluid density.

Although the quadratic formulation disregards the existence of a critical velocity of transition between streamline and turbulent flow, it has the practical advantage that at both extremes i.e. Q tending towards 0, and Q tending towards infinity, it gives the correct forms corresponding respectively to laminar flow and to complete turbulence [Baker *et al. 1987*]. However, Etheridge [*1998*] indicates that the second order term of the flow rate (Q^2) is primarily due to turbulent flow. Etheridge suggests that to a large extent it represents the pressure decrease at the inlet which is not recovered at the outlet of the opening, because the flow emerges in the form of a jet. This, Etheridge says, is due to flow separation at the outlet which occurs irrespective of whether or not the subsequent jet is laminar or turbulent.

It is argued that the quadratic equation overcomes some of the drawbacks of the power law. However, for several years there has been an ongoing debate as to which equation provides better results. Arguments in favour of the power law e.g. [Peterson, *1982*] are based on the fact that it has been shown many times to give good agreement with measured leakage characteristics, although it is generally accepted that the concept of a constant value of the exponent is an approximation. Arguments in favour of the quadratic equation are based on the fact that at very low flow rates the relationship between airflow and pressure difference will tend to become linear [Etheridge *1984*]. Comparisons between the power law and the quadratic formulations e.g. [Etheridge *1984*] show that the two equations differ by the greatest amounts at low pressures (Figure 4.11).
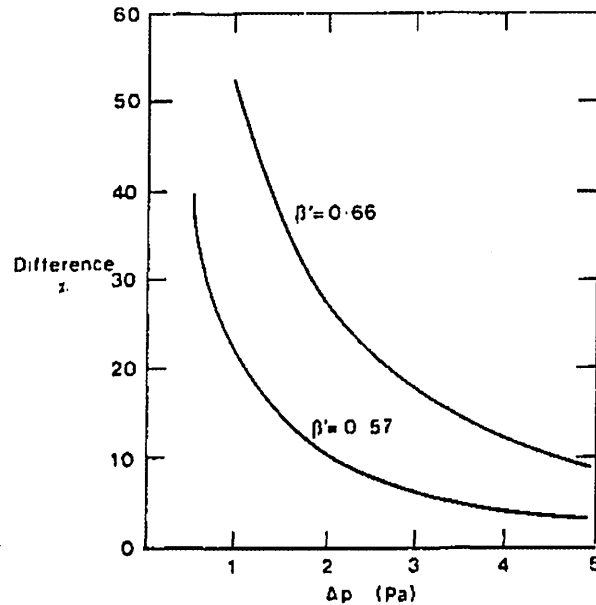
Figure 4.11: Percentage differences between power law
and quadratic equations at low pressures[B]
[Source: Etheridge, 1984]

In their comparison of the power law to the quadratic formulation for field and laboratory measurements of flows through building envelopes Walker *et al.* [*1998*] found the power law to better represent the relationship between pressure and flow for buildings with small cracks only, combinations of small building envelope cracks and large holes and laboratory measurements of furnace flues.

4.8 Review of Airflow through Ventilator Openings Research

This section presents an overview of the studies available in the literature on the subject of airflow characteristics and performance of ventilators for natural ventilation applications. In particular a few of these studies that contributed to the direction and procedures of this investigation are outlined and commented on to some greater detail. These consist of results from field studies, full scale experimental studies and from numerical models.

[B]*β' is the exponent obtained by curve fitting a power law to quadratic equation data [Etheridge 1984].*

Although natural ventilation is conceptually the simplest and cheapest option to cool a building (if implemented correctly), it is also the most difficult to control, since the driving forces and thus the airflow rates vary constantly with the weather. Airflow characteristics of openings in relation to very low driving forces and the effect of wind and temperature differences on ventilation have previously been investigated [Dick 1949, Dick 1950, Awbi 1994, Hunt and Linden 1999,]. In addition, several studies on different types of natural ventilation schemes [CIBSE:AM10 1997, Etheridge 2002] are available in the literature. Some researchers such as [Webb et al. 1998] have investigated the use of purpose-provided openings in order to determine/assess their effectiveness. An earlier example is an investigation by Bedford et al. [1943] to assess the effectiveness of purpose-provided openings in providing adequate and controlled background ventilation in naturally ventilated buildings. They examined the effect of air gratings used in dwellings, in particular two blocks of flats of volume 700 cubic feet (block A) and 1165 cubic feet (block B). Their results (Table 4.2) indicated that with the air gratings open the background ventilation increased by about 50% compared to that when the ventilators were closed.

Table 4.2: Effect of small air gratings on ventilation of unheated rooms

Flats	Average ventilation rate (air changes per hour) with air grating		Percentage increase due to open air grating
	Open	Closed	
Block A	0.83 (22)	0.55 (17)	51
Block B	1.04 (10)	0.71 (12)	46

[Source: Bedford et al. 1943 - scanned and retained in original form to give "historical feel" to investigation]

Perera et al. [1993] also reported positive results in their study to determine whether permanent controllable ventilators could provide adequate background ventilation for occupants in large commercial buildings.

Although ventilators (trickle and through-wall) are significant ways in which air is transferred from one zone of a building to another or to outside, the airflow characteristics of these openings are not fully understood. Further, the pressure difference across the opening will in practice depend upon its location in a building, on the time of year, wind speed and direction, temperature difference between inside and

outside. The opening will therefore experience a considerable range of pressure differences and hence will transmit a wide range of air flows. Nevertheless, general airflows in building components is of great interest as is shown by many previous experimental, field and theoretical investigations in this area and the elementary models already proposed therein to describe the airflow characteristics. Previous work and several other researchers have concentrated on flow through individual components. In addition, the flow path in real ventilators is a combination of individual components (normally) of differing airflow characteristics in series (and perhaps in parallel) with each other. In such cases the electric resistance series analogy has often found application to ventilator components as shown in Kronvall *[1980]*, Aynsley *[1988]* and Walker *et al. [1998]*. A number of studies have focussed on the airflow characteristics of ventilation openings in relation to the type, size, shape and location of openings on the building facade for example [Couzin *1969* and Gratia *et al. 2003*], or in relation to surrounding landscape and vegetation etc. Others have studied how airflow characteristics of ventilation openings affect airflow patterns in rooms. The study by Evans *[1979]* highlights some interesting findings in this respect. Evans found that:-

i) The type of the inlet opening and its location in a wall determine the initial airflow pattern through a room. Airflow patterns resulting from typical windows and openings are shown in Figure 4.12 and Figure 4.13. Typical airflow patterns are shown in section and plan assuming a wind perpendicular to the plane of the window wall.
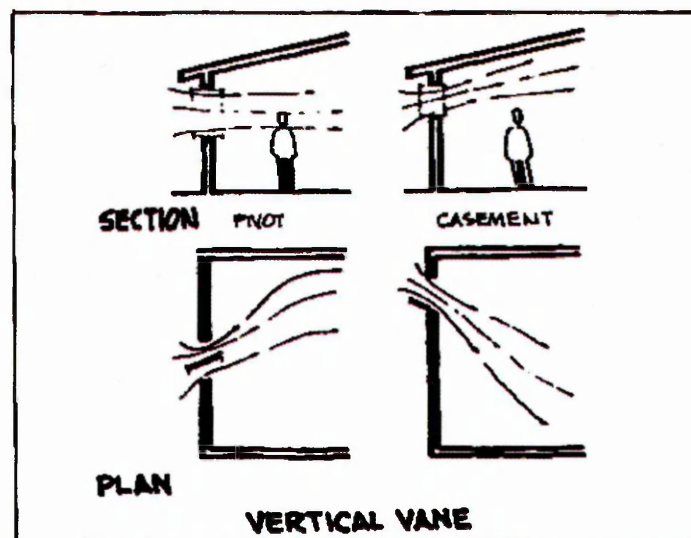
Figure 4.12: Airflow pattern resulting from vertical vane window
[Source: Evans, 1979]
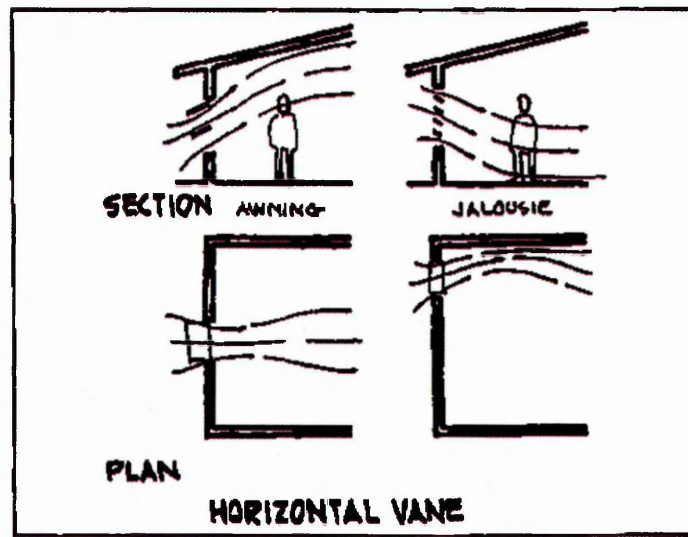
Figure 4.13: Airflow pattern resulting from horizontal vane window

[Source: Evans, 1979]

ii) The relative size of the inlet opening is the principal determinant of the speed with which the air moves through a building (Figure 4.14).
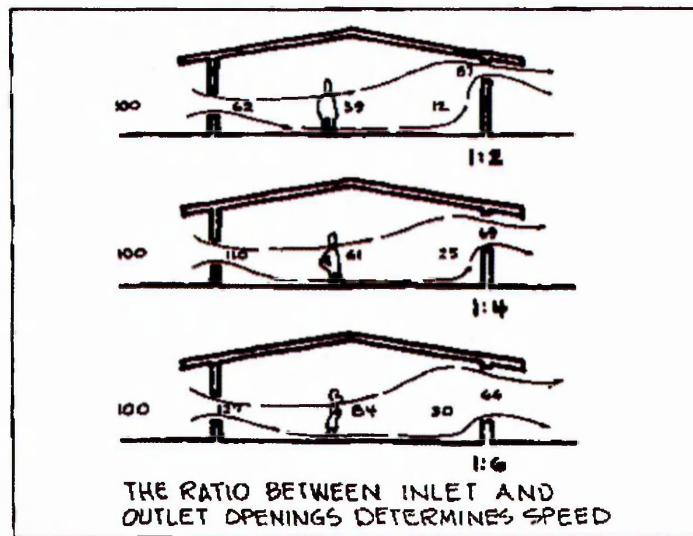
Figure 4.14: Increased outlet size in relation to the inlet size,

results in increased air speeds [Source: Evans, 1979]

Figure 4.14 shows air speeds through typical building sections as tested in the wind tunnel [Evans, *1979*]. The oncoming air speed is indicated as 100, and the inside air speeds are expressed as percentages of this outside speed. The diagram clearly indicates a substantial gain in inside speed as the size of the outlet is increased while holding the inlet size constant.

From the foregoing sections, it is clear that at the heart of natural ventilation are facade openings which facilitate the movement of air into and out of buildings. Despite the wealth of data available on bulk air movement through buildings, information concerning airflow performance of the ventilation openings is very scarce. Relatively little detailed information appears to be available on the subject of ventilator airflow performance. A literature review of ventilator research, including a search of the AIVC database, indicated that previous work in this area tended to investigate either overall ventilator performance, for example [Gonzalez *1984*, Yakubu and Sharples *1991*, Ayad *1999*, Heiselberg *et al.* *2001*, Karava *et al.* *2003*], or individual elements such as louvers, screens and meshes in isolation, for example [Baker *et al 1986A*, White *et al.* *1998*, Maghrabi and Sharples *1999*, Miguel *et al.* *2001*]. These observations are also true for the recently completed EU-funded natural ventilation research project NatVent[®] [NatVent *1999*]. Such studies have included louvers, mesh-screens, trickle ventilators etc and have often assessed geometrical dimensions, fluid properties and pressure coefficients in order to determine the airflow characteristics of these airflow components.

A recent study of through-the-wall ventilators at the Building Research Establishment [White *et al.* *1999*] revealed that ventilator performance was a more complex parameter than would be perceived from the relatively simple construction of the ventilators. For example, the airflow performance of some of the ventilators tested was found to be better than would be predicted from standard orifice plate theory. The acoustic performance of some ventilators with tortuous, sound attenuating paths was found to be worse than would be expected from theory. The BRE suggested that these discrepancies might arise from poor understanding of the impact of, amongst others, complex internal flow paths, insect screens, filter material, baffles and louver blade geometry. Although the BRE study listed the airflow properties of all the ventilators tested (revealing their variable performances) it made no attempt to understand the individual parameters that were influencing these performances. Consequently, the study produced no guidance on improving the design of ventilators. In this regard, further studies/research to understand the airflow performance of ventilators is necessary if their use in natural ventilation applications is to be promoted. Prior to the BRE work on ventilators, and in a totally independent study, Oliveira and Bittencourt [*1998*] in their investigation identified a lack of information regarding ventilation performance presented by typical openings, particularly the porous components like louvered windows and mosquito screens. The

results from their full-scale room assessment of air velocities gave some indication of the impact of ventilator components (louvers and mosquito screens) on airflow properties. For instance, Figure 4.15 shows that the airflow resistance through the louvered window was about 70% of that found for the open window.
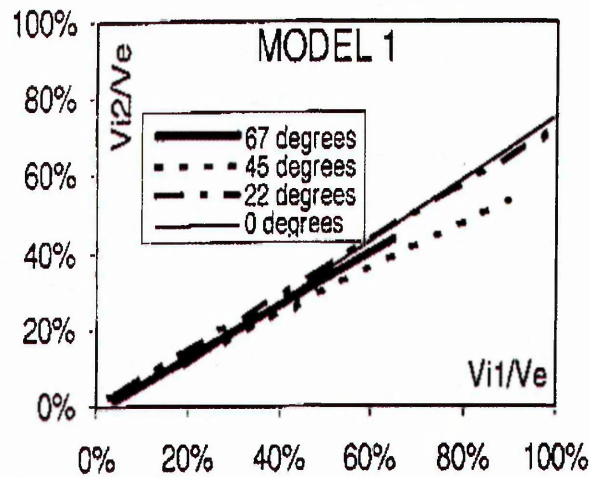
Figure 4.15: Comparison of airflow resistance for the opening window and the louvered one
[Source: Oliveira & Bittencourt, 1998]

The use of a mosquito screen together with the louvered window resulted in a flow around 60% of that found for the open window (Figure 4.16), considering wind incidence close to the normal to the window (0° and 22°). For oblique wind incidence (45° and 67°) the flow was reduced to about 40%.
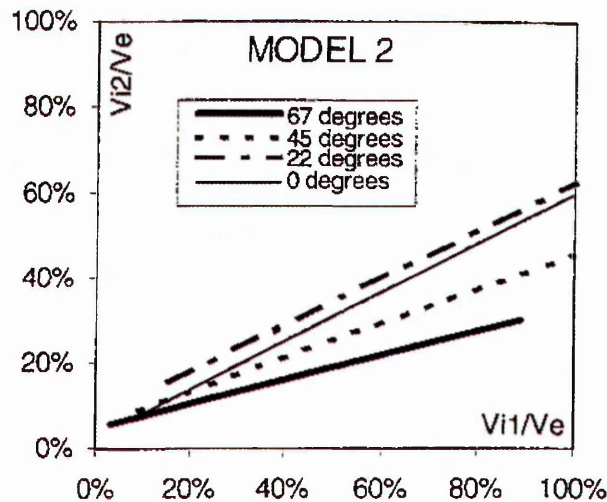
Figure 4.16: Comparison of airflow resistance for the opening window and the louvered window with mosquito screen
[Source: Oliveira & Bittencourt, 1998]

These findings suggest that components such as mesh-screens and acoustic linings could have a significant influence on the overall airflow properties of ventilators. Hence, there is a need for further research aimed at understanding the ventilation performance of various types of purpose-provided ventilation openings and their constituent components. The study by Miguel and Silva [*2000*] is also of interest and relevance in this regard in that they investigated the effect of flow path (apertures of different size and geometry, and mesh-screen filters) characteristics on mass flows within enclosures. They found a strong influence on mass flow characteristics within the enclosure, and therefore indoor climate. However, no attempt was made to separate and understand the impact of each component (aperture and filter screen).

4.8.1 Ventilator component testing in the laboratory

Laboratory studies are an important first step in establishing appropriate boundary conditions for ventilator analysis. The laboratory environment is much more controllable, making it possible to investigate the suitability of assumptions made regarding ventilator boundary conditions. Over the past few decades the "*airflow chamber*" test rig (Figure 4.17) employed by several researchers [Tutt *1955*, Hopkins and Hansford *1974*, Baker *et al.* *1987*, Yakubu and Sharples *1991*, Maghrabi *2000*, Chilengwe and Sharples *2002*] to assess the airflow characteristics of the ventilator components has generally consisted of an airtight plenum box and an air handling unit connected to the plenum chamber via some form of ducting.
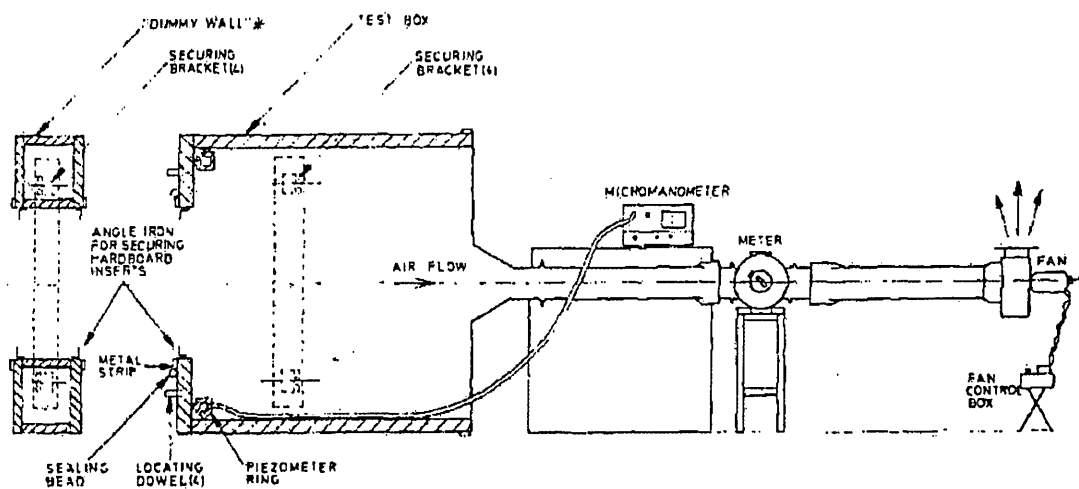
Figure 4.17: Airflow chamber test rig typically used for testing ventilator components
[Source: Hopkins & Hansford, 1974]

However, there has not been any consistence in the size of plenum chamber used by various researchers. The recent publication of the European Standard (BS En 13141-1: *2004*) has in a way given some guidance on the dimensions of plenum chamber to be used in relation to the particular size of ventilator components tested. That aside, it is very difficult to see what alternative method could rival the *airflow chamber* for ease of producing readings in the laboratory. Two key aspects relating to the use of the airflow chamber method of testing components are briefly commented on below.

TEST RIG AIR LEAKAGE

While the variation of air leakage with pressure from test rigs is widely appreciated and several practitioners have noted this quantitatively for their particular test rigs, very few quantitative observations under conditions of laboratory usage have been published. Although some studies consider the air leakage to be sufficiently minimised or eliminated by sealing test rig joints with draught-proof materials, for example Yakubu and Sharples [*1991*], it is an important factor that could influence the derived airflow characteristic of components tested in the laboratory if not taken into account. Several researchers utilising the airflow chamber have generally estimated, one way or another, the background leakage from the test rig in order to determine the actual airflow rate through the component tested. Some investigators [for example McGrath and Howarth *1984*, Karava *et al. 2003*] have adopted the approach of establishing actual airflow rate through the test component at each pressure difference by taking measurements with the test component unsealed initially and then subtracting the figure obtained from the measured value when the test component is sealed. Others [Baker *et al. 1987*] have used curve fits to experimental test rig air-leakage data covering the range of pressure differentials expected during actual component testing. The derived equation is then used to obtain the specific background leakage rate at a particular pressure difference. This method was followed in this investigation. A few researchers, for example Maghrabi [*2000*], have adopted a single value of air- leakage measured at high pressure drops and used it to calculate actual flows at various pressure differentials. This approach possibly leads to an under-estimation of actual flows at lower pressure difference and should be avoided.

The dependence of airflow characteristics of components on flow direction has previously been investigated, for instance McGrath and Howarth [*1984*] and Ward and Sharples [*1982*]. This factor can have a significant impact on resulting airflow characteristics if not taken into account. As an example, Baker *et al.* [*1986*] in their experimental work relating to leakage through components/cracks represented by laboratory fabricated L-shaped asymmetric cracks with arms of unequal length found differences of up to 20% (at pressure differences of 10 Pa across the cracks) by reversing the flow direction through the crack (Figure 4.18).
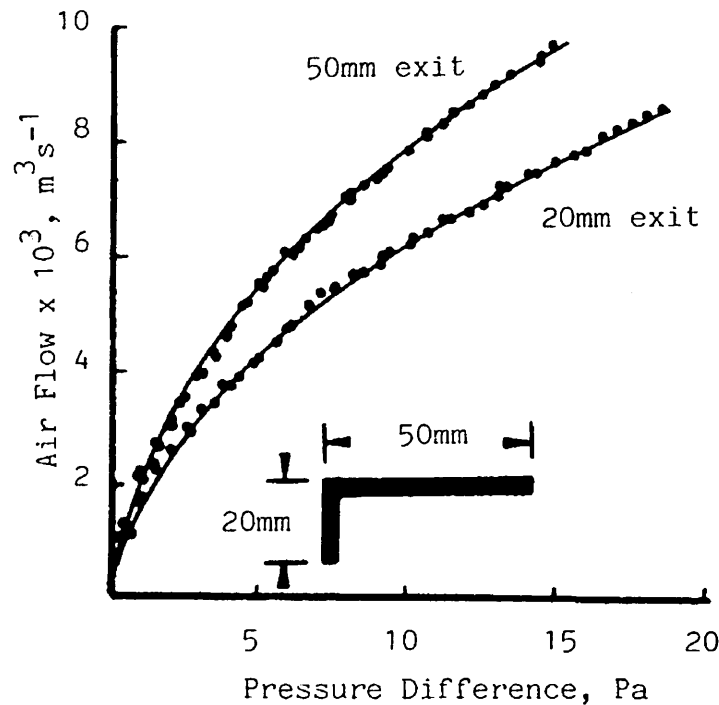
Figure 4.18: Flow-pressure difference curves for 6mm thickness
L-shaped crack, showing effect of flow reversal
[Source: Baker et al. 1986]

In relation to whole ventilator units, the geometry of the internal flow-path, the inclination of louver blades and the location of mesh-screens and acoustic linings are features that stop the ventilator being aerodynamically symmetrical for different flow directions. However, previous work [Yakubu and Sharples, *1991* and Maghrabi, *2000*] which employed louvers similar to the ones forming the basis of this thesis did not assess the effect of reversing the flow direction.

4.9 Concluding Remarks

The preceding sections have highlighted a lack of existing data on the airflow performance of individual components used in combination to form a ventilator for natural ventilation applications. This clearly suggests a need for further research into the impact on airflow properties of ventilator component combinations. Very little work appears to have been done on the impact of mesh-screen/louver combinations and hence this is addressed as a part of this research. This lack of knowledge calls for an improved understanding of airflow performance of ventilator components used in combination with each other with respect to the low pressure differentials that drive the flow in natural ventilation systems. In the available literature, a good agreement does exist on the prediction of airflow characteristics through individual components (such as louvers, mesh-screens etc) using power law and quadratic formulations/regressions. Nevertheless a large uncertainty due to lack of sufficient studies remains on the definition of the discharge coefficient in relation to a combination of ventilator components. A real lack of knowledge exists on the behaviour of ventilators (combinations of components) or airflow characteristics especially in relation to low pressure differentials typical in natural ventilation applications. However, some studies/experiments do exist on individual components and these serve as an excellent starting point in any attempt to investigate and quantify the impact of individual components on the overall airflow performance of ventilators. This survey strengthens the impression that further experimental observations are needed if the effects of individual components commonly used in ventilators were to be predicted. The key findings from the literature review were as follows:-

1) Principles guiding airflow by natural forces are well documented. However, knowledge of the performance of individual openings is rather limited and is based on theoretical assumptions of the main driving forces, effective areas and airflow within rooms.

2) There is evidence that ventilators provide an effective method of providing background ventilation into buildings. However, not much attention has been paid to their airflow performance characteristics in relation to the low driving forces such as those in natural ventilation applications.

3)   Basically two forms of flow equation (the quadratic and the power law formulations) are usually used to describe the relationship between airflow and pressure differences across airflow paths. However, at present there is no agreement amongst researchers regarding which model can universally be employed to fully describe flow through the different types of airflow openings occurring in practice.

4)   Various techniques are used to determine values of the empirical coefficients associated with the two forms of flow equation. From the literature, it seems the most common method is the use of data traditionally used for fluid flow in pipes and flow between parallel plates.

5)   Determination of the coefficients is normally achieved through simplifications, such as basing models on only the steady state conditions from data usually derived from laboratory experiments employing the airflow chamber test rig. In practice this approach possibly leads to deviations from actual conditions occurring when air flows across openings, hence, leading to inaccuracies in the proposed models.

6)   Many researchers have highlighted the need and requirement for more work regarding factors that influence airflow (such as insect screens, filter materials, baffles and louver blade shape etc). More studies are needed to provide reliable design data for computation of natural ventilation through purpose-provided openings, as that can improve the ventilation design methods to a level where they can match the design methods of air inlets in mechanical ventilation.

RESEARCH QUESTION

In the light of the above deficit in current knowledge on airflow characteristics of ventilator components acting together, the key question to be answered by this investigation has been broken down to include the following aspects:-

- to quantify the impact of each component on the overall airflow performance of the ventilator

- to shed some light on the task of optimising the airflow performance of ventilators as a result of complicated interactions between flow properties of individual constituent components of a ventilator

- to investigate the possibility of introducing universal parametric models to describe the airflow characteristics of ventilators optimised in relation to low driving forces typical in natural ventilation applications

Chapter 5

EXPERIMENTAL INVESTIGATION

5.1 Introduction

This chapter is arranged in three main parts. The first section describing the equipment and experimental test rigs used is followed by detailed descriptions of the components tested. The latter part of the chapter outlines results obtained from various experimental investigations undertaken. The experiments were aimed at establishing relationships between pressure differentials applied across a ventilator component and resulting airflow rates for each given configuration.

5.2 Experiments

5.2.1 Experimental test rig and instruments

The experimental test rig, shown schematically in Figure 5.1, used to assess the airflow characteristics of ventilator components consisted of an airtight plenum chamber, variable speed fan and laminar flow meter. Other instruments used were micromanometers, velocimeters and a barometer. These components are briefly described in this section.
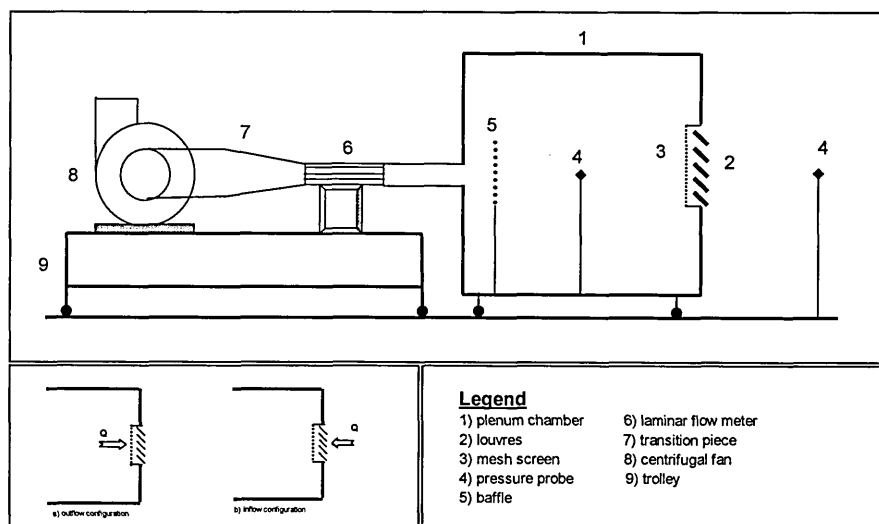
Figure 5.1: Schematic representation of experimental set-up

Two types of plenum chambers made from wooden blocks and panels - designed and constructed in accordance with the requirements of BS EN 13141-1: *2004* - were used in the investigation. The first one was a large 2.4m x 2.4m x 1.2m deep plenum chamber (Figure 5.2) which was used to test large wooden and aluminium type louver banks. The second plenum chamber was a 1m x 1m x 1m box (Figure 5.3) used to test smaller components such as slots and trickle ventilators. Each chamber had provision for easily mounting and removing test pieces. In addition, each had an access door complete with a clear perspex glass viewing panel. Inside each plenum chamber was a fine mesh baffle (Figure 5.4) to damp turbulent flows and allow a uniform distribution of airflow past the internal pressure differential probe and onto the louver face.
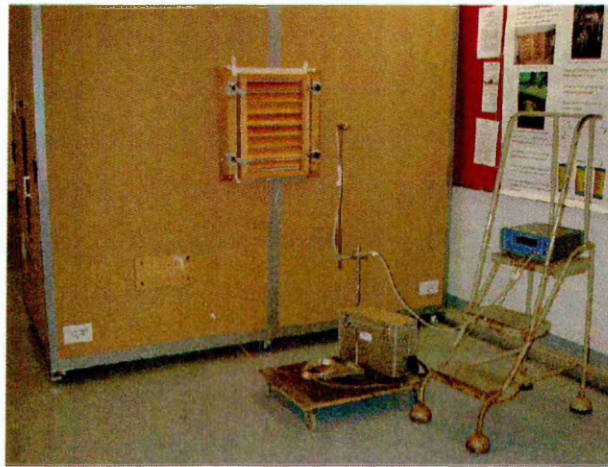
Figure 5.2: Ventilator end of 2.4m x 2.4m x 1.2m
plenum chamber
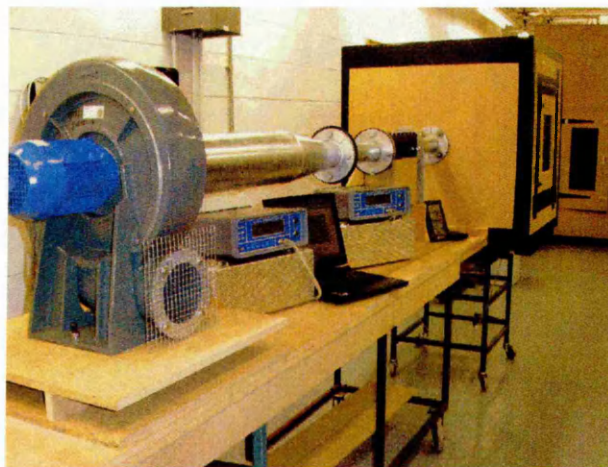
Figure 5.3: 1m x 1m x 1m plenum chamber

*Figure 5.4: View inside plenum chamber showing fine
mesh baffle and pressure differential probe*

AIR HANDLING UNIT

The air handling unit (AHU) (Figure 5.5) included a Soler & Palau type COT 130.240v/400v/3ph/50Hz variable speed centrifugal fan (Beatson Fans & Motors Ltd). The centrifugal fan was fitted with an Excal inverter type SFS 150/240v 1ph input 240v 3ph output controller. The AHU was connected to the plenum chamber via galvanised steel ductwork.
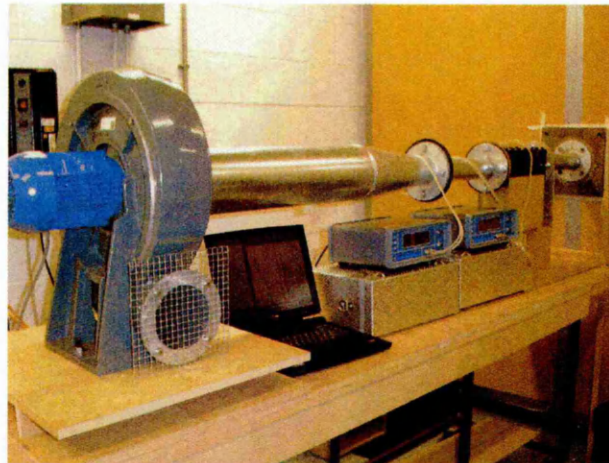
Figure 5.5: Experimental test rig air handling unit

LAMINAR FLOW METER

A high accuracy Furness FC050 laminar flow meter installed within the AHU ductwork was used to measure the airflow rate through the test rig. The laminar flow meter had a linear relationship between pressure differential and airflow rate. This relationship was verified (Figure 5.6) at the beginning of the experimental phase of the investigation.
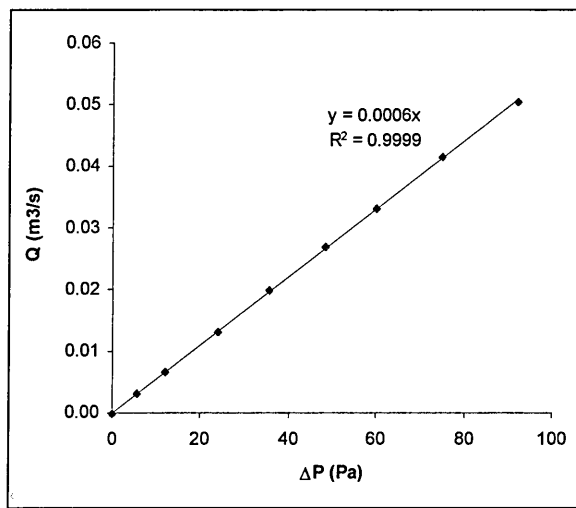
Figure 5.6: Relationship between pressure differential and airflow rate for laminar flow meter

MICROMANOMETERS

Pre-calibrated FC0510 Furness digital micromanometers were used to measure the pressure differences applied across the test piece and the laminar flow meter. The manufacturer quotes the accuracy of the micromanometers as ± 0.25% for pressure differentials and ± 0.0003 m³/s for volume flow rates.

A potential source of significant experimental error associated with measured parameters was that resulting from fluctuations in room air movement due to the air-conditioning system serving the laboratory. However, this was ignored in the analysis because the main focus was to establish relative airflow properties between various ventilator components. Further justification of this approach is given in *Section 5.5*.

5.2.2 Experimental method

In accordance with current practice the experimental method employed generally involved subjecting a ventilator component(s) to a pressure differential and noting the resulting airflow rate. This method is recommended in BS 13141-1: *2004* and has widely been used by several researchers over the years [Hansford and Hopkins *1974*, McGrath and Howarth *1984*, Baker *et al. 1987*, Yakubu and Sharples *1991*, Etheridge and Sandberg *1996*, Maghrabi and Sharples, *2000*]. The general experimental procedure followed in this investigation is illustrated in Figure 5.7 below. Additional specific steps or variations to the general procedure for experiments undertaken are detailed in the relevant sections (*Section 5.4.1* to *Section 5.4.12*) where applicable.
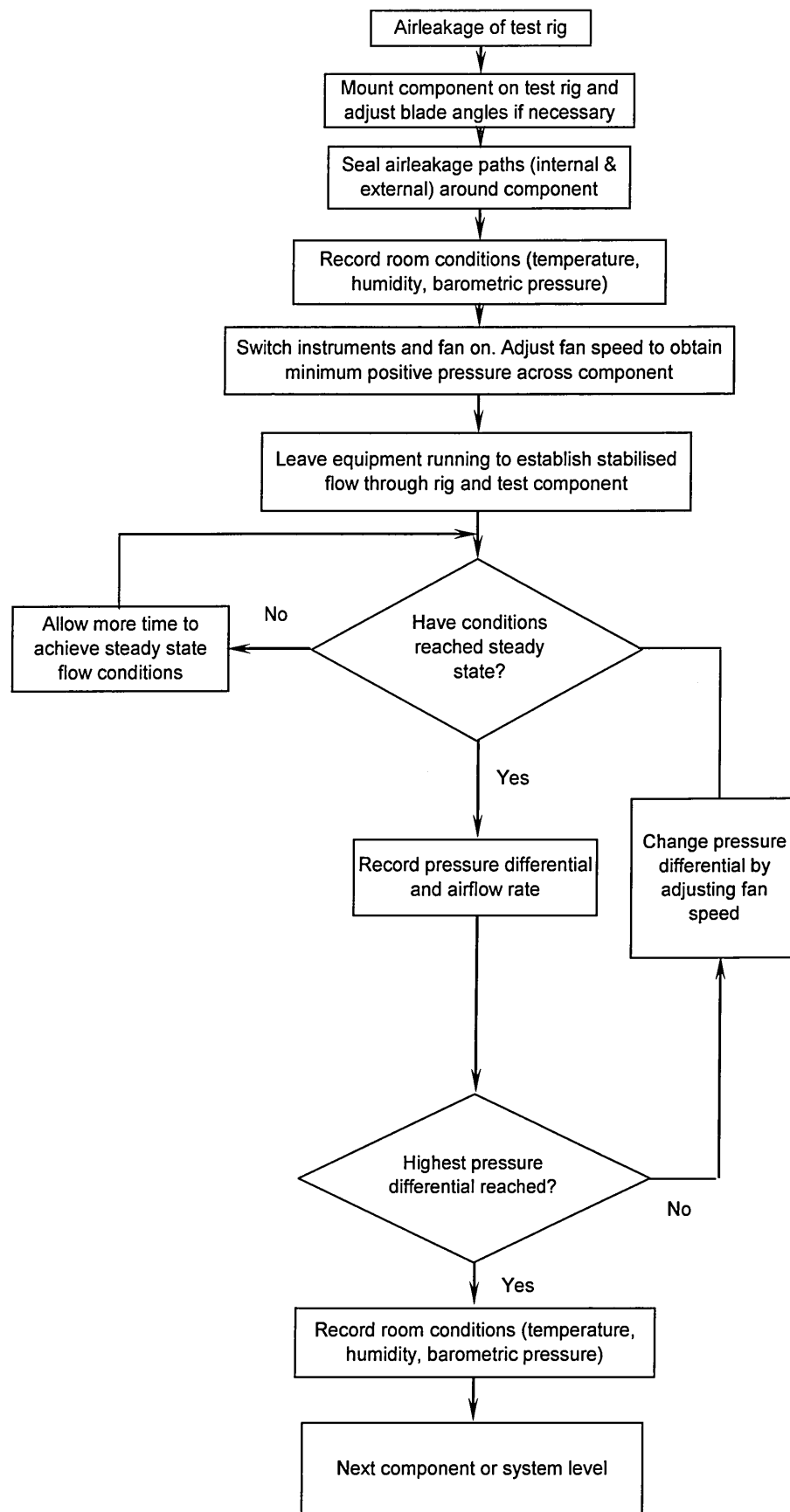
Figure 5.7: General experimental procedure flow chart

5.2.3 Validation of experimental procedure

A pilot investigation [Chilengwe and Sharples, *2001*] was carried out on some of the wooden louver banks (see *Section 5.3.2*), and results compared with those obtained from a previous independent study [Maghrabi and Sharples, *2000*] under similar conditions. This served both as a basis of familiarisation with the instrumentation and as validation for the experimental procedure employed in this investigation. The validation of the experimental procedure was on the basis of obtaining good agreement between the two sets of experimental data (Figure 5.8 below).
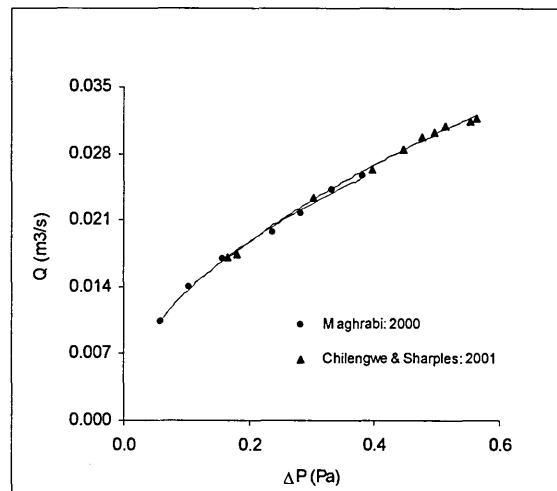
Figure 5.8: Comparison of typical measured data between
Maghrabi [2000] & Chilengwe & Sharples [2001]

5.2.4 Data reduction

In general, airflow is three-dimensional in the sense that flow parameters (velocity, pressure etc.) vary in all three coordinate directions. However, the experiments undertaken in this investigation assumed that pressure losses across ventilator components were one-directional and occurred in the direction of the airflow through the component. In all cases the approaching airflow was considered to be perpendicular to the face of the ventilator component. This assumption was necessary in order to reduce the amount of data that needed to be collected for analysis.

5.2.5 Data correction to standard air conditions

The measured airflow rate at each pressure differential was corrected to standard temperature and pressure (20°C and 101 325 Pa) by taking into account the prevailing thermal conditions (temperature, humidity, barometric pressure) in the laboratory at the time of each test. Data correction was achieved by using Equation 5.1 [BS EN 13141-1: *2004*]:

$$Q_{stp} = Q_{meas} \cdot \frac{293}{273 + T_a} \cdot \frac{P_a}{101325} \qquad (5.1)$$

where:

P_a	=	ambient pressure (Pa)
T_a	=	ambient temperature (°C)
Q_{meas}	=	measured airflow rate (m³/s)
Q_{stp}	=	corrected airflow rate (m³/s)

Correction to standard air conditions accounted for air density differences resulting from different ambient conditions, therefore, facilitated direct comparison of parameters measured under different thermal conditions.

5.2.6 Range of investigation parameters

Ambient conditions in the laboratory during the measurement phase were within the following ranges:-

Air temperature:	18 to 27 °C
Ambient pressure:	96 800 to 102 000 Pa
Relative humidity:	27 to 48% RH

Pressure differentials generated across ventilator components during the investigation generally ranged from 0 to 10 Pa depending on the type of component being tested. Obtaining these pressure differences experimentally was relatively easy with the capacity of the AHU used. However, for certain components the open area of the product being tested was sufficiently large that although the fan could produce the required airflow rate to generate pressures in excess of 10 Pa, the measuring instruments in particular the laminar flow metre, had a limitation of the maximum airflow rate, hence for these products it was not possible to achieve pressure differences up to 10 Pa.

5.3 Components Investigated

Several components are used in ventilators for natural ventilation applications. At present the airflow performance of these ventilators is not well understood and in some cases data relating to them is non-existent. In such situations it is essential to resort to basic elements such as slots and orifices to gain some indication of how components behave when incorporated into a ventilator. This section describes various components that were investigated in this study.

5.3.1 Ordinary slots

Two sets of laboratory-manufactured slots were used to investigated the basic airflow performance of ordinary slots. Set (B) , illustrated in Figure 5.9, consisted of 6 fixed height (12mm) slots with varying depths ranging from 6mm to 36mm. Set (A), illustrated in Figure 5.10, consisted of 6 fixed depth (12mm) slots with varying heights ranging from 6mm to 36mm.
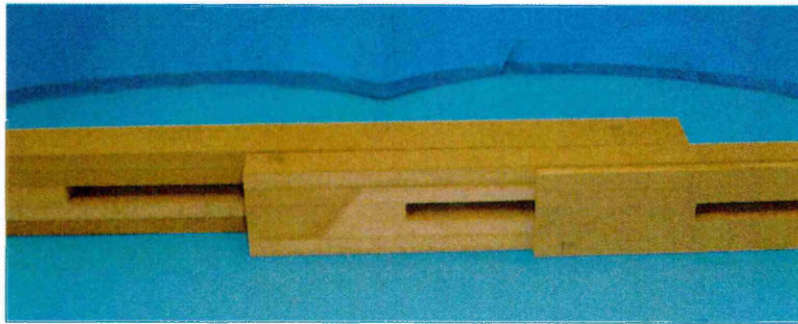
Figure 5.9: Fixed height- varying depth ordinary slots
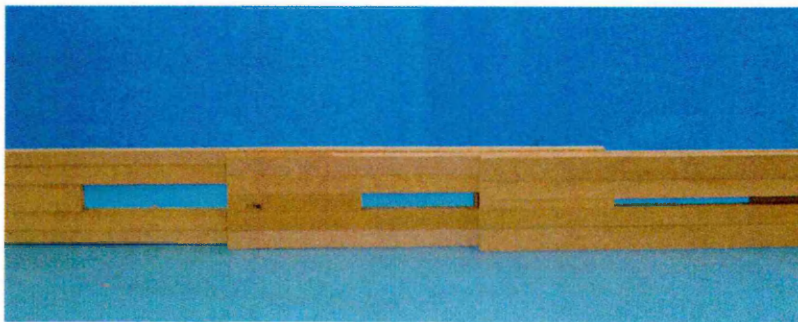
Figure 5.10: Fixed depth- varying height ordinary slots

The slots, made from smooth MDF wooden boards, were used both in isolation and in combination with a fine insect screen type round-wire mesh (with each hole measuring 0.2 mm x 0.2 mm) to assess the resulting airflow characteristics.

5.3.2 Wooden louvers

Two full-size smooth pinewood louver banks each with overall frame dimensions of 480 mm high x 320 mm wide were used in the investigation. These dimensions represent actual ventilator sizes commonly used in Middle Eastern countries [Maghrabi, *2000*]. The first louver bank, referred to as louver 1, had 15 blades with a gap of 20 mm between blades measured when the blades were in a horizontal position. Each blade measured 60 mm deep and was 10 mm thick.

Figure 5.11: Pinewood louver bank

The second louver bank (louver 2), shown in Figure 5.11, had 8 blades with a gap of 50 mm between blades measured when the blades were in a horizontal position. Each blade measured 80 mm deep and was 10 mm thick. Each louver bank was fitted with a mechanism that allowed louver blades to be inclined and adjusted to the desired angle. The two louver banks formed the basis of the experimental procedure validation described in *Section 5.2.3*. An extensive study of the effect of the various louver parameters (depth (L), blade spacing (d), number of louver blades (N), and ratio (d/L)) is reported in [Maghrabi, *2000*] and was not the subject of this investigation. Here the focus was on the interaction of combinations of different ventilator components.

5.3.3 Commercial louvers

Three commercial aluminium louver banks, illustrated in Figure 5.12, each measuring 495 mm x 495 mm x 130 mm deep were used in the investigation. The first louver bank, referred to as Louver X, had 5 blades each inclined at 45° with a 100 mm gap between the blades. The second (Louver Y) and third (Louver Z) louver banks were very similar to each other and had 6 blades, each inclined at 45° with a 75 mm gap. Louver Z incorporated an additional offset or "rain hook" on each blade which is intended to provide additional protection against water ingress during operation in actual buildings.

Figure 5.12: Illustration of commercial louver bank

5.3.4 Square round-wire meshes

The pattern of screens used in conjunction with the pinewood louver banks was of a woven-square mesh lattice formed from round wires evenly spaced in both the vertical and horizontal directions (Figure 5.13). These were locally obtained from a commercial supplier.
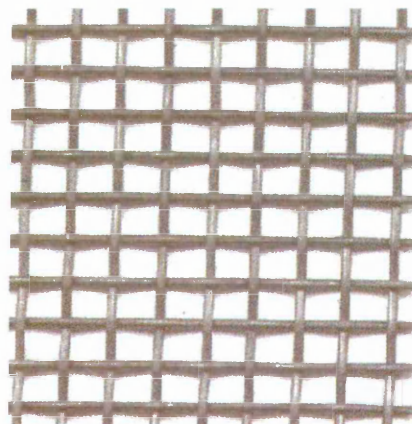
Figure 5.13: Square grid round-wire meshes

Three types of wire-mesh, detailed in Table 5.1, were used in the investigation. The free area of the mesh-screens used were 35%, 50% and 70% - determined by calculation from measurements of the grid and wire thickness undertaken on an "OMT" Toolmakers Microscope (Sheffield Hallam University, Materials Engineering laboratory).

Table 5.1:
Details of round wire meshes used in investigation

Mesh	Construcion type	Average wire dia (mm)	Holes in 320mm x 480mm	Equivalent open area (m2)	Free Area (%)
1	woven square	0.599	95256	0.056	35
2	woven square	0.921	34126	0.077	50
3	woven square	1.618	8475	0.104	70

5.3.5 Polygon-type meshes

Two mesh types each mounted into a frame measuring 450 mm x 450 mm were used in conjunction with the aluminium commercial louver banks. The first mesh (Figure 5.14) was a thin polyethylene type insect-screen of hexagon-shaped orifices with a free area of 45%. The second mesh (Figure 5.15) was a polygon-shaped orifice welded steel strip bird-guard with a free area of 65%.

Figure 5.14: Insect screen mesh
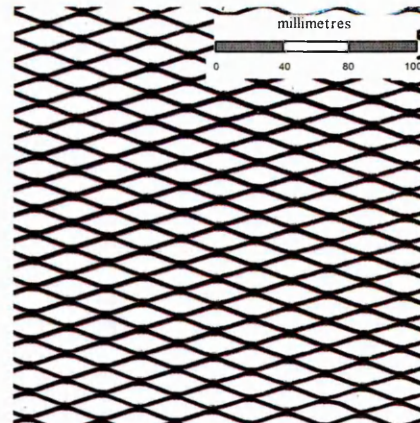
Figure 5.15: Bird guard mesh

The mesh frame design was such that meshes could be attached onto the back of the aluminium louvers (35mm from the blades) and held in position by two easily adjustable screws. Close examination of these meshes revealed that the hole pattern was not geometrically square. Further, discussions with a reputable ventilator manufacturer indicated that no particular attention is paid to the orientation of meshes incorporated in ventilators. One aspect of this investigation examined (*Section 5.4.11*) the impact on airflow properties of rotating these non-square meshes.

5.4 Experimental Results and Discussion

The aim of this part of the chapter is to cover the range of laboratory experiments undertaken during the investigation and point out aspects of the ventilator components that could be used in an attempt to optimise the airflow performance of the ventilator. The core of the identification of such aspects was the steady state measurement of airflow through a ventilator component resulting from an applied pressure differential across it. A range of experiments carried out are detailed in the following sections.

5.4.1 Measured airflow characteristics of ventilators

Ventilator components, or combination of components, were subjected to a range of pressure differentials by increasing the fan speed up to maximum and then decreasing from maximum (at each stage ensuring that the pressure differential reading was as close as experimentally possible to that recorded when the fan speed was being increased). All measurements were recorded when flow conditions appeared to have stabilized. The two sets of readings were taken and then averaged, corrected to standard temperature and pressure (*Section 5.2.5*) and corrected for background air leakage from the test rig (*Section 5.4.3*) to determine the actual airflow prior to obtaining ventilator airflow characteristics of a particular component. The pressure drop across the component was measured as the difference in pressure measured by static probes, one placed centrally inside the plenum chamber and the other located on the outside at half-a-metre away from the plenum chamber face (Figure 5.1). Readings were taken for airflow in both directions i.e. pressurisation and depressurisation of the plenum chamber. The subsequent analysis treated each flow direction separately.

5.4.2 Derived airflow characteristics of ventilators

In most practical situations the geometry of the ventilator flow path cannot be measured and only the airflow characteristic is of interest [Etheridge and Sandberg, *1996*]. Generally, the means of determining the airflow characteristic of a ventilator component involves establishing a pressure difference ΔP across the component, measuring the consequent airflow Q through it and then deducing a relationship between ΔP and Q. The usual way of presenting airflow characteristics of ventilator components is via a graph of actual airflow passing through a component and the pressure differential

causing the airflow. The resulting airflow characteristics of ventilator components are then described by either the power law (Equation 5.2) or the quadratic (Equation 5.3) functions:-

$$Q = \alpha \, (\Delta p)^{\beta} \qquad (5.2)$$

$$\Delta P = aQ^2 + bQ \qquad (5.3)$$

For some of the ventilator parameter studies this investigation employed both approaches with an interim objective of determining which of the two models best described the measured data for each particular case. This provided a basis of representing data in a form that allowed direct comparison of experimental findings for different ventilator components.

5.4.3 Air-leakage characteristics of the test rigs

All obvious air-leakage paths in the test rigs were sealed with tape and thereafter the background air-leakage of each test rig was measured over the same range of pressure differences used during the performance testing of the various specimens. The airflow rate through the laminar flow element and pressure differential between the inside and outside of each plenum chamber were measured for various fan speeds. The air-leakage characteristic of each test rig was then derived for both power law and quadratic models (Table 5.2). "R" in Table 5.2 and elsewhere in this report represents the regression analysis correlation coefficient.

Table 5.2:
Airleakage characteristics of test rigs

Test Rig Plenum Chamber	Configuration	Power law			Quadratic		
		α	β	R	a	b	R
1m x 1m x 1m	depressurisation	0.00001	0.9296	99.05	$4x10^7$	114518	99.85
2.4m x 2.4m x 1.2m	pressurisation	0.0001	0.913	98.34	$7.4x10^5$	8609.7	97.57
2.4m x 2.4m x 1.2m	depressurisation	0.00006	0.8468	99.97	$2x10^6$	26641	99.98

These air-leakage characteristics were then used to determine the actual airflow rate (Q_{act}) through a particular ventilator component using Equation 5.4:

$$Q_{act} = Q_{comp} - Q_{leak}$$

$$(5.4)$$

where Q_{comp} and Q_{leak} are respectively the airflow rate through the component and air-leakage from the test rig at a given pressure differential, both of which were individually corrected to standard temperature and pressure prior to finding Q_{act}.

Although the British standard BS EN 13141-1:*2004* requires the background leakage of a test rig to be determined, it was noted that the maximum air-leakage rate (< 1 l/s at 100 Pa) quoted therein does not relate to a given size of plenum chamber. This makes it difficult to compare leakage rates from test rigs of different dimensions. As such a suggestion would be to express the leakage as a rate per m^2 of surface area or per m^3 of volume of a given plenum chamber. This then allows direct comparison between plenum chambers of different dimensions. As the leakage rate is dependant on the pressure differential between the inside and outside of the test rig it was essential to derive leakage characteristics over the whole range of pressure differentials encountered during specimen testing. This approach, recommended by Etheridge and Sandberg [*1996*], has also previously been employed by some researchers [Baker *et al.* 1987] and gives a more accurate representation of air leakage at each specific value of pressure differential, than that obtained by using a single value of air leakage over the whole range of pressure differentials as in [Maghrabi, *2000*].

5.4.4 Airflow performance of ordinary slots

Experimental measurements were carried out on simple rectangular slots as a basis of gaining fundamental knowledge of airflow through various types of ventilator airflow paths, in particular deliberate ventilation openings such as trickle ventilators. This served as a starting point of gaining some indication of how components such as louvers would behave when incorporated into a ventilator. This study employed general natural ventilation theory to predict how these components would behave when subjected to the range of pressure differentials expected in natural ventilation applications i.e. 0 to say 10 Pa. The study investigated via a series of laboratory experiments variations in airflow performance characteristics of simple ventilators comprising rectangular slots and a fine round-wire mesh-screen. The main objectives were to investigate and quantify variations in airflow performance in relation to the range of pressure differentials expected and also with regard to changes in dimensions of the ventilator. It has been suggested [Baker *et al.* 1987, Etheridge *2002*] that the quadratic equation (Equation 5.3) is more suitable for estimation of flow through crack type openings as it

provides a more accurate assessment than the power law. Therefore, the analysis in this section employed the quadratic approach.

RESULTS

Figures 5.16 - 5.17 show graphical representations of the results obtained to illustrate variations of airflow characteristics of slots over the range of pressure differentials common in natural ventilation applications. In these graphs a relative airflow (Q/Q_{12}) has been used and is defined as the ratio of the airflow rate (Q) for a given slot size to the airflow rate (Q_{12}) for the slot with both depth and height equal to 12mm at a particular pressure differential. The 12mm slot was chosen as reference simply because it happened to be the intersection between the two sets of slots used in this study. To appreciate the connection between relative airflow performance, dimensions of slots and pressure differential the graphs of meshed/unmeshed slots are aligned side by side and plotted to the same scale for ease of comparison.
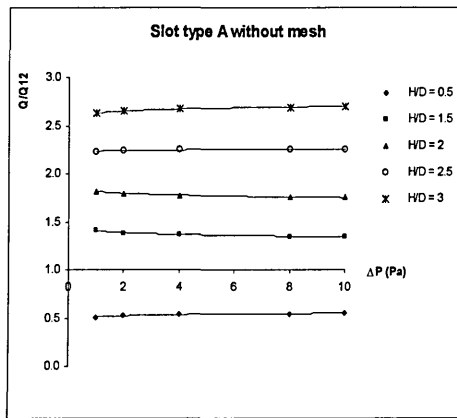
Figure 5.16: Q/Q_{12} as a function of ΔP for slot type A without mesh
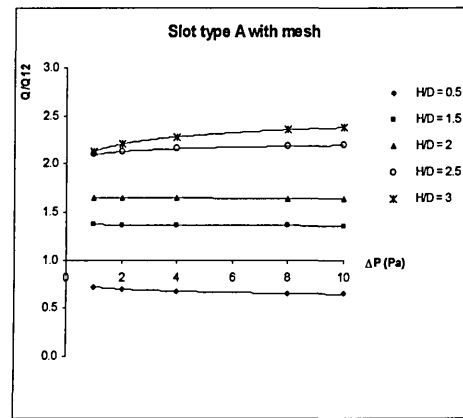
Figure 5.17: Q/Q_{12} as a function of ΔP for slot type A with fine mesh
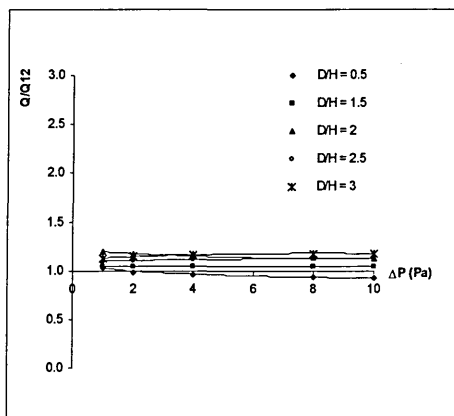
Figure 5.18: Q/Q_{12} as function of ΔP for slot type B without mesh
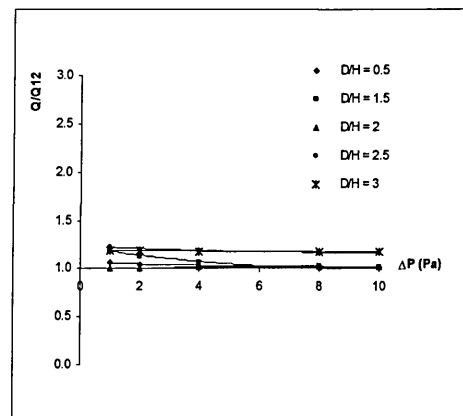
Figure 5.19: Q/Q_{12} as a function of ΔP for slot type B with fine mesh

-107-

Figures 5.20 - 5.23 below illustrate variations of the relative airflow (Q/Q_{12}) characteristics with respect to the height-depth ratio (H/D) (type A) and depth-height (D/H) ratio (type B) of slots used in isolation and also in combination with a mesh-screen.
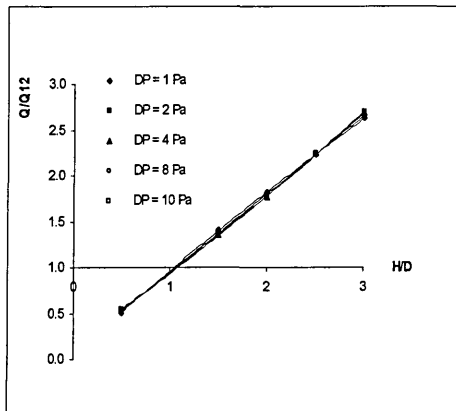
Figure 5.20: Q/Q_{12} as a function of H/D for slot type A without mesh
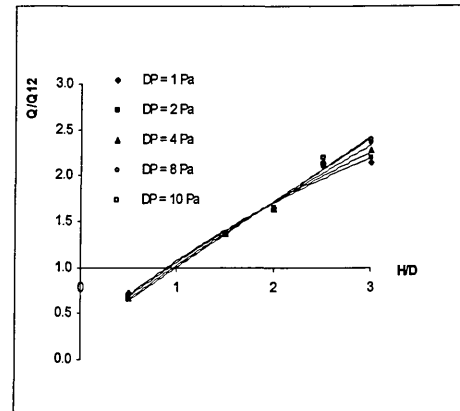
Figure 5.21: Q/Q_{12} as a function of H/D for slot type A with fine mesh
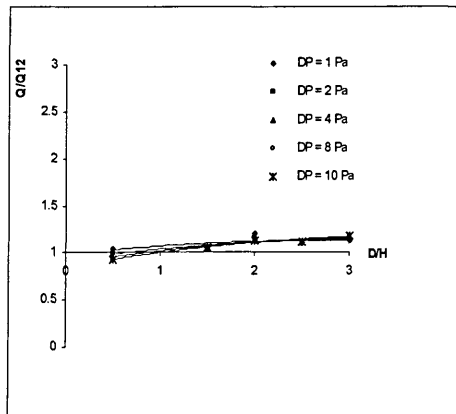
Figure 5.22: Q/Q_{12} as a function of D/H for slot type B without mesh
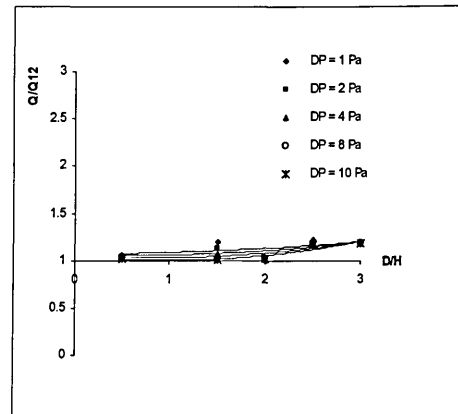
Figure 5.23: Q/Q_{12} as a function of D/H for slot type B with fine mesh

DISCUSSION

Regression analysis quadratic curve fits to measured data resulted in correlation coefficients better than 0.99 in all cases considered. For slots of fixed depth and varying heights (slot type A), Figure 5.16 and Figure 5.17 revealed that the cases with and without a mesh-screen were slightly influenced by pressure at low pressure differentials (say < 2 Pa). The influence of the pressure on the relative airflow characteristic was less significant at pressure differentials higher than 2 Pa. For slot type A it is evident that addition of a mesh-screen to the slots did not affect the relative airflow performance in a linear manner i.e. contrary to general expectation, the resulting airflow ratios where different (averaging just under 10%) between meshed and

unmeshed slots. The relative airflows for unmeshed slots were generally higher than the corresponding meshed configurations throughout the range of natural ventilation pressure differentials. For meshed slots the airflow performance for H/D = 3 approaches that of H/D = 2.5. Similarly the relative airflow performance at H/D = 2 approaches that at H/D = 1.5 when the slots are meshed. Slots of fixed height and varying depths (slot type B) revealed a more flatter relative airflow characteristic with increasing pressure differential (Figure 5.18 and Figure 5.19). Here again the effect of the pressure appears to be more significant at lower pressures. The difference between the relative airflows for meshed and unmeshed slots is too small to appreciate from the graphical representation, hence a summary of average values for all depth-to-height ratios is presented in Table 5.3.

Table 5.3:
Variation of relative airflow (Q/Q12) with pressure differential for slot type B

	1Pa	2Pa	4Pa	8Pa	10Pa
unmeshed	1.10	1.09	1.09	1.08	1.08
meshed	1.13	1.12	1.10	1.08	1.08

Figure 5.20 and Figure 5.21 show the variation of relative airflow with increasing height-depth ratio for slots type A. The relative airflow appears to be independent of the pressure differential for unmeshed slots. This suggests that a single line chosen for some intermediate pressure differential could be used to represent the various relative airflow characteristics without introducing significant errors. It is clear from Figure 5.20 that the relative airflow of the unmeshed slots was totally independent of the pressure differential at H/D = 2.5. Figure 5.21 shows that addition of a mesh-screen to the slots introduced some dependence on the pressure differential with variations being bigger (11% between 1Pa and 10Pa) at H/D = 3. With a mesh-screen, the slots appear to give a relative airflow performance totally independent of the pressure differential at H/D = 2.

On the other hand for slot type B, Figure 5.22 and Figure 5.23 suggest less variation of the relative airflow with respect to the depth-height ratio. For both cases (with and without a mesh-screen) there is some dependence on pressure differentials at low D/H ratios. At D/H ratios above 2.5 the graphs suggest that the relative airflow performance could be represented by a single curve without introducing many errors. The above analysis can also be applied to ventilator components in hybrid ventilation systems as suggested in Chilengwe and Sharples [2004].

From the analysis/discussion above it emerges that the characteristic equations of the simple rectangular slots and meshes are not only influenced by the pressure range from which they are derived but also by the constituent components. The results obtained suggest that by quantifying and understanding the impact of combining components in a ventilator general solution airflow characteristics can be deduced to represent the performance of ventilators over the range of pressure differentials encountered in natural ventilation systems. Such information would be useful in any attempt to optimise the overall airflow performance of ventilator. In addition, the use of a representative general solution could reduce the number of parameters to be considered in the optimisation exercise. To avoid significant errors the general solution could incorporate some methods to adapt resulting airflow characteristics to account for variations in pressure differentials and dimensional parameters for a given ventilator.

5.4.5 Airflow performance of louvers

Measurements were carried out to establish the airflow characteristics of wooden louver banks for three louver blade inclinations angles (0°, 30° and 60°), and for commercial aluminium louvers all of which had a fixed blade inclination angle of 45°. Experimental and derived data for the aluminium louvers is given in Table 5.4. Experimental and derived data for wooden louvers is given in Table 5.5 and Table A.1 in the appendices.

A quick check of regression coefficients suggests that for both aluminium and wooden louvers without meshes, ventilator flows were marginally more accurately described by power law equations. Comparison between power law and quadratic correlation coefficients gave differences of less than 1% in all cases.

Table 5.4:
Experimental and derived data for aluminium louvers (depressurisation)

Louver Type	Insect-screen ΔP	Insect-screen Q	Bird guard ΔP	Bird guard Q	No Mesh ΔP	No Mesh Q	Insect-screen (derived)	Bird guard (derived)	No Mesh (derived)	Regression coefficients	
X	0.030	0.0082	0.005	0.0046	0.015	0.0114	0.0702	0.0698	0.0813	α	Power Law
	0.067	0.0129	0.046	0.0119	0.069	0.0200					
	0.131	0.0201	0.096	0.1927	0.156	0.0298	0.6324	0.5434	0.5033	β	
	0.260	0.0302	0.222	0.0288	0.321	0.0417					
	0.456	0.0407	0.419	0.0406	0.557	0.0568	99.65	99.16	99.53	R	
	0.714	0.0545	0.653	0.0525	0.814	0.0716	60.331	66.656	51.571	a	Quadratic
	1.029	0.0693	1.028	0.0693	1.043	0.0870					
	1.357	0.0840	1.379	0.0871	1.239	0.0997	10.291	9.2611	6.9269	b	
	1.703	0.1009	1.672	0.1015	1.373	0.1088					
	2.019	0.1192	1.965	0.1179	1.472	0.1170	99.05	99.09	98.7	R	
	2.183	0.1296	2.143	0.1279	1.588	0.1268					
Y	0.013	0.0073	0.013	0.0074	0.013	0.0082	0.0737	0.0763	0.0936	α	Power Law
	0.042	0.0126	0.042	0.0128	0.027	0.0132					
	0.130	0.0215	0.103	0.0207	0.068	0.0226	0.5675	0.5924	0.5519	β	
	0.273	0.0328	0.239	0.0314	0.105	0.0315					
	0.466	0.0432	0.418	0.0436	0.267	0.0436	98.95	99.3	99.46	R	
	0.708	0.0565	0.672	0.0569	0.464	0.0579	56.023	62.293	65.46	a	Quadratic
	1.000	0.0723	0.987	0.0730	0.697	0.0727					
	1.341	0.0883	1.313	0.0895	0.933	0.0888	9.431	8.4799	4.2868	b	
	1.568	0.1024	1.578	0.1034	1.144	0.1028					
	1.739	0.1141	1.816	0.1192	1.391	0.1196	99.01	98.94	99.13	R	
	2.006	0.1291	1.986	0.1291	1.558	0.1304					
Z	0.028	0.0072					0.0849	0.0863	0.0904	α	Power Law
	0.057	0.0122	0.054	0.0113							
	0.130	0.0211	0.115	0.0202	0.061	0.0209	0.6924	0.6866	0.5273	β	
	0.220	0.0306	0.185	0.0310	0.134	0.0317					
	0.352	0.0419	0.372	0.0425	0.227	0.0420	99.86	99.45	100	R	
	0.577	0.0564	0.568	0.0557	0.401	0.0565	41.217	39.705	110.55	a	Quadratic
	0.842	0.0722	0.817	0.0723	0.602	0.0701					
	1.113	0.0897	1.049	0.0862	0.939	0.0884	8.1451	8.0245	1.0024	b	
	1.307	0.1030	1.273	0.1031	1.287	0.1043					
	1.516	0.1188	1.504	0.1200	1.649	0.1200	99.2	98.99	99.98	R	
	1.660	0.1305	1.595	0.1287	1.903	0.1281					

Table 5.5: Experimental and derived data for wooden Louver 1 with various mesh sizes at 0° and 60° blade inclinations

Experimental data

Louver Blade Inclination (deg)	Mesh Free Area (%) 35		50		70		100	
	ΔP (Pa)	Q (m3/s)	ΔP (Pa)	Q (m3/s)	ΔP (Pa)	Q (m3/s)	ΔP (Pa)	Q (m3/s)
0	0.044	0.0054	0.025	0.0112	0.029	0.0123	0.022	0.0127
	0.115	0.0127	0.075	0.0205	0.078	0.0221	0.054	0.0218
	0.213	0.0218	0.135	0.0312	0.178	0.0333	0.126	0.0329
	0.380	0.0325	0.249	0.0435	0.290	0.0463	0.196	0.0453
	0.596	0.0451	0.372	0.0583	0.421	0.0613	0.316	0.0599
	0.885	0.0608	0.515	0.0740	0.562	0.0764	0.456	0.0775
	1.189	0.0778	0.667	0.0899	0.719	0.0923	0.591	0.0913
	1.361	0.0913	0.801	0.1044	0.836	0.1061	0.688	0.1053
	1.586	0.1062	0.993	0.1279	0.974	0.1226	0.786	0.1220
60	0.070	0.0052	0.041	0.0052	0.049	0.0077	0.037	0.0077
	0.215	0.0123	0.133	0.0120	0.130	0.0129	0.104	0.0125
	0.473	0.0206	0.360	0.0207	0.376	0.0225	0.289	0.0217
	0.983	0.0321	0.812	0.0327	0.741	0.0327	0.645	0.0319
	1.611	0.0436	1.375	0.0446	1.241	0.0437	1.206	0.0443
	2.486	0.0583	2.143	0.0591	1.978	0.0586	1.881	0.0578
	3.452	0.0744	2.964	0.0748	2.826	0.0763	2.757	0.0753
	4.297	0.0896	3.702	0.0894	3.486	0.0915	3.433	0.0901
	5.021	0.1033	4.342	0.1035	4.035	0.1052	4.021	0.1040

Derived data

Louver Blade Inclination (deg)	Regression coefficients		Mesh Free Area (%) 35	50	70	100
0	Power Law	α	0.0691	0.1106	0.1046	0.1223
		β	0.8054	0.6449	0.6203	0.6054
		R	99.81	99.65	99.41	99.67
	Quadratic	a	34.686	39.880	25.584	39.653
		b	12.021	4.032	5.217	2.784
		R	99.39	99.53	99.24	99.41
60	Power Law	α	0.0320	0.0377	0.0401	0.0419
		β	0.6767	0.6193	0.5710	0.5335
		R	99.83	99.75	99.62	99.62
	Quadratic	a	232.910	226.320	195.180	229.250
		b	28.329	21.996	20.666	17.605
		R	99.38	99.26	99.02	98.98

5.4.6 Airflow performance of meshes

Mesh-screens are used in airflow systems for a variety of important duties, including production of uniformity of the velocity distribution, reduction of turbulence of the airstream, production of artificially high turbulence, introduction of known pressure drops into experimental systems [Annand, *1953*] and control of dust and insect entrance into buildings [Miguel and Silva, *2000*]. For all these applications it is desirable to be able to estimate the airflow characteristics which will be produced by a given mesh-screen. Although the general problem of the flow through meshes has been widely investigated, information on how the mesh-screens affect the airflow performance when used in combination with other ventilator components is very scarce or non-existent. This lack of data was an important driver for this study. Power law and quadratic formulations for various meshes used in the investigation were derived from measured data (Table 5.6).

Table 5.6: Derived parameters for various mesh screens

Mesh type	Free area (%)	Power law			Quadratic		
		α	β	R	a	b	R
Wooven round wire	70	0.5181	0.7947	97.5	2.69	0.9875	97.5
	50	0.4704	0.8336	93.7	4.80	0.9924	97.9
	35	0.0985	0.8151	99.7	8.76	8.2088	99.7
Polyethelyne insect screen	45	0.1304	0.6394	99.6	30.15	3.3163	98.7
Welded steel strip bird-guard	65	0.1207	0.5337	99.3	36.41	2.6082	99.1

Airflow characteristics of a fine mesh-screen (used in combination with slots - *Section 5.4.4*) of fixed width and varying heights were also determined for a range of mesh-screen heights. The airflow characteristic of the mesh-screen with fixed width was found to be dependant on the height of mesh-screen used, and independent of the pressure differential i.e. for a given mesh-screen height the ratio of the airflow rate through the mesh-screen relative to the airflow rate through the smallest height used (6mm) remained constant throughout the range of pressure differentials considered. A non-dimensional relationship between relative heights and relative airflow rates was derived by regression analysis (Figure 5.16) for which a linear function fitted the data with a correlation coefficient of 98%.
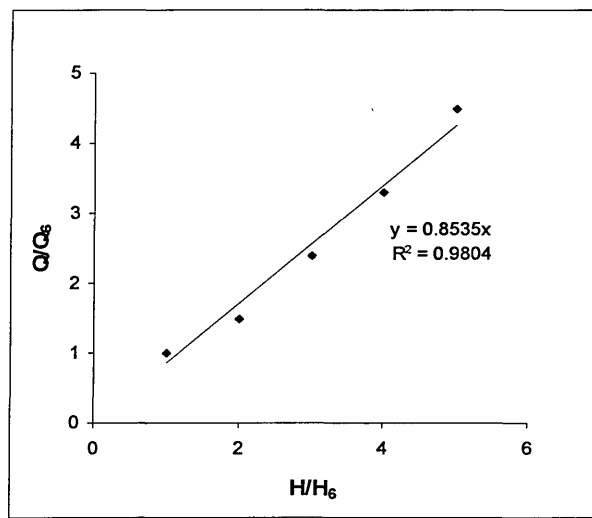
*Figure 5.24: Non-dimensional relationship between relative
heights (H/H₆) and relative flows (Q/Q₆) through a fine mesh*

COMMENT

It is evident from Figure 5.24 that the airflow through the mesh-screen suffered a 15%
reduction in performance compared to that theoretically expected, whereby doubling the
mesh-screen height (for a fixed width) results in double the airflow. Such information
can be useful for ventilator manufacturers in that it could be used to assess flow
properties of differently sized meshes without necessarily having the actual physical
size of the mesh-screen. In addition, armed with this data the impact on the airflow
performance of ventilators can be more accurately quantified and accounted for when
the mesh-screen is used in combination with other ventilator components.

5.4.7 Airflow performance of louver-mesh combinations

To assess the impact of louver-mesh combinations on the overall airflow performance
of ventilators, parametric measurements were undertaken for combinations of mesh-
screens and louvers (see also Chilengwe and Sharples, *2002*). Experimental data and
derived regression coefficients for various louver-mesh combinations can be found in
Table 5.3, Table 5.4 above and Table A1.1 in the appendices. Figure 5.25 and Figure
5.26 show the airflow characteristics of Louver 1 used in isolation and in combination
with a round wire mesh-screen of 35% free area for horizontal and 60° louver blade
angles.
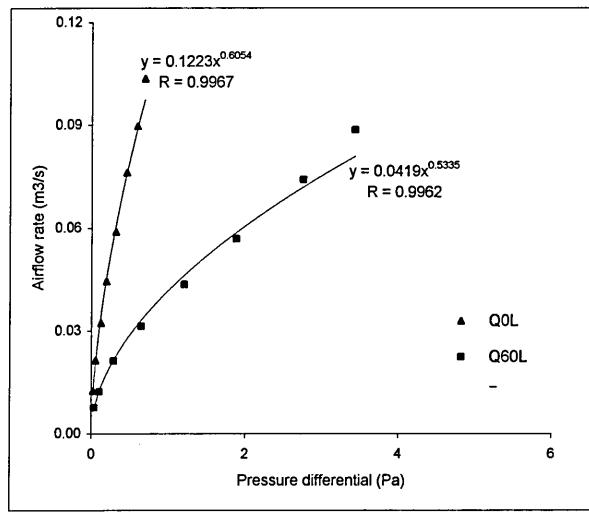
Figure 5.25: Airflow characteristics of unmeshed louvers - horizontal louver (Q0L) and 60°louver (Q60L)
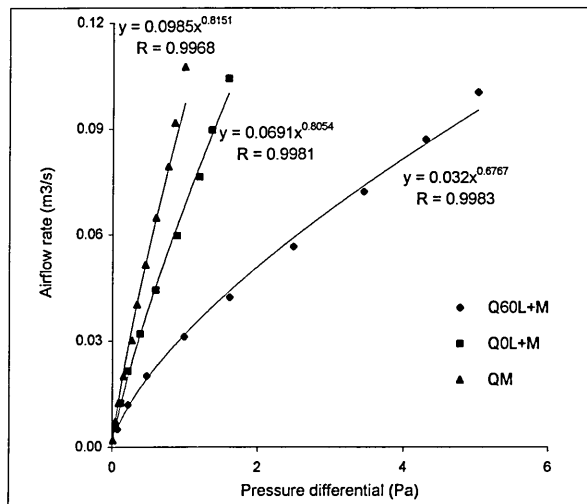
Figure 5.26: Airflow characteristics of meshed louvers - horizontal louver with mesh(Q0L+M); 60°louver with mesh (Q60L+M) and mesh only (QM)

The airflow properties resulting from a combination of components within a ventilator can be analysed by using the electrical analogy of resistances in series [Kronvall, *1980*]. For an arrangement such as components in a ventilator, it follows that if two components are connected to each other in series the flow rate in each component is the same as that for the total system i.e.

$$Q_V(\Delta P_V) = Q_M(\Delta P_M) = Q_L(\Delta P_L) \qquad (5.5)$$

and,

$$\Delta P_V(Q) = \Delta P_M(Q) + \Delta P_L(Q) \qquad (5.6)$$

-115-

where ΔP and Q have their usual meanings and the subscripts V, M and L stand for ventilator, mesh-screen and louver respectively. The applicability of this concept to airflow properties resulting from louver-mesh combinations was examined using wooden Louver 1 and round-wire meshes of different free areas. Further, it was possible to assess individual component (mesh-screen and louvers) contribution to the overall resistance to airflow through the ventilator when the components are used in combination.

RESULTS

Table 5.7 and Table 5.8 show comparisons of individual and combined airflows at selected pressure differentials for horizontal and 60° inclined louver blades. The airflow performance of the combined unit relative to the airflow performance of the louver used in isolation is presented for various pressure differentials. Table 5.9 and Table 5.10 show comparisons of individual and combined pressure losses at selected airflow rates for horizontal and 60° inclined louver blades. Data in these tables was used to examine the validity of the electrical analogy of resistances in series with respect to louver-mesh combinations. The contribution of the mesh-screen to the overall resistance of the combined unit was examined and the results obtained are given in Table 5.11 and Table 5.12 for horizontal and 60° inclined louver blades respectively.

DISCUSSION

It was apparent from the analysis (Table 5.7 and Table 5.8) that the individual airflow performances of the mesh-screen and louver components were always better than the overall airflow performance of the combined units. However, it is interesting to note that airflow characteristics of combined units are not obtained by direct/arithmetic addition of the characteristics of meshes and louvers in isolation (Table 5.9 and Table 5.10). From Tables 5.7 and 5.8 it can be seen that with the exception of the combined unit with a 35% free-area mesh-screen when the blades are horizontal, the cases examined indicate that the combined louver/mesh unit airflow properties generally were closer to those of the louver used in isolation than those for the mesh-screen.

-116-

Table 5.7: Comparison of individual and combined flows Q (m3/s) for horizontal blades (depressurisation)

	Louver 1 with 35% FA mesh					Louver 1 with 50% FA mesh					Louver 1 with 70% FA mesh			
ΔP (Pa)	Q_M	Q_L	Q_{M+L}	$\frac{Q_{M+L}}{Q_L}$ (%)	ΔP (Pa)	Q_M	Q_L	Q_{M+L}	$\frac{Q_{M+L}}{Q_L}$ (%)	ΔP (Pa)	Q_M	Q_L	Q_{M+L}	$\frac{Q_{M+L}}{Q_L}$ (%)
0.05	0.009	0.020	0.006	31	0.025	0.039	0.020	0.016	80	0.025	0.045	0.020	0.016	82
0.25	0.032	0.053	0.023	43	0.15	0.148	0.053	0.045	86	0.15	0.186	0.053	0.044	84
0.5	0.056	0.080	0.040	49	0.3	0.264	0.080	0.071	88	0.3	0.342	0.080	0.068	85
1.2	0.114	0.137	0.080	59	0.5	0.548	0.137	0.124	91	0.5	0.738	0.137	0.117	86
1.5	0.136	0.156	0.096	61	0.8	0.660	0.156	0.144	92	0.8	0.898	0.156	0.135	86
2	0.172	0.186	0.121	65	1	0.838	0.186	0.173	93	1	1.157	0.186	0.161	86

Table 5.8: Comparison of individual and combined flows Q (m3/s) for 60° inclined blades (depressurisation)

	Louver 1 with 35% FA mesh					Louver 1 with 50% FA mesh					Louver 1 with 70% FA mesh			
ΔP (Pa)	Q_M	Q_L	Q_{M+L}	$\frac{Q_{M+L}}{Q_L}$ (%)	ΔP (Pa)	Q_M	Q_L	Q_{M+L}	$\frac{Q_{M+L}}{Q_L}$ (%)	ΔP (Pa)	Q_M	Q_L	Q_{M+L}	$\frac{Q_{M+L}}{Q_L}$ (%)
0.05	0.009	0.008	0.004	50	0.025	0.039	0.008	0.006	70	0.025	0.045	0.008	0.007	86
0.25	0.032	0.020	0.013	63	0.15	0.148	0.020	0.016	80	0.15	0.186	0.020	0.018	91
0.5	0.056	0.029	0.020	69	0.3	0.264	0.029	0.025	85	0.3	0.342	0.029	0.027	93
1.2	0.114	0.046	0.036	78	0.5	0.548	0.046	0.042	91	0.5	0.738	0.046	0.044	96
1.5	0.136	0.052	0.042	81	0.8	0.660	0.052	0.048	93	0.8	0.898	0.052	0.051	97
2	0.172	0.061	0.051	84	1	0.838	0.061	0.058	95	1	1.157	0.061	0.060	98

Table 5.9: Comparison of individual and combined pressure losses horizontal blades (depressurisation)

Q (m3/s)	Louver 1 with 35% FA mesh					Louver 1 with 50% FA mesh					Louver 1 with 70% FA mesh				
	ΔPL	ΔPM	ΔPM+L	ΔPM+ΔPL	$\frac{\Delta P_M + \Delta P_L}{\Delta P_{M+L}}$ (%)	ΔPL	ΔPM	ΔPM+L	ΔPM+ΔPL	$\frac{\Delta P_M + \Delta P_L}{\Delta P_{M+L}}$ (%)	ΔPL	ΔPM	ΔPM+L	ΔPM+ΔPL	$\frac{\Delta P_M + \Delta P_L}{\Delta P_{M+L}}$ (%)
0.005	0.005	0.025	0.038	0.030	78	0.005	0.004	0.008	0.009	114	0.005	0.004	0.007	0.009	123
0.025	0.073	0.183	0.283	0.256	90	0.073	0.030	0.100	0.102	103	0.073	0.026	0.100	0.098	99
0.05	0.228	0.432	0.669	0.660	99	0.228	0.068	0.292	0.296	101	0.228	0.056	0.304	0.284	93
0.075	0.446	0.714	1.107	1.160	105	0.446	0.111	0.548	0.556	102	0.446	0.089	0.585	0.535	91
0.1	0.717	1.020	1.582	1.737	110	0.717	0.156	0.855	0.873	102	0.717	0.123	0.930	0.841	90
0.15	1.401	1.686	2.618	3.087	118	1.401	0.254	1.604	1.655	103	1.401	0.196	1.788	1.597	89

Table 5.10: Comparison of individual and combined pressure losses for 60° inclined blades (depressurisation)

Q (m3/s)	Louver 1 with 35% FA mesh					Louver 1 with 50% FA mesh					Louver 1 with 70% FA mesh				
	ΔPL	ΔPM	ΔPM+L	ΔPM+ΔPL	$\frac{\Delta P_M + \Delta P_L}{\Delta P_{M+L}}$ (%)	ΔPL	ΔPM	ΔPM+L	ΔPM+ΔPL	$\frac{\Delta P_M + \Delta P_L}{\Delta P_{M+L}}$ (%)	ΔPL	ΔPM	ΔPM+L	ΔPM+ΔPL	$\frac{\Delta P_M + \Delta P_L}{\Delta P_{M+L}}$ (%)
0.005	0.019	0.025	0.064	0.044	68	0.019	0.004	0.038	0.023	60	0.019	0.004	0.026	0.023	87
0.025	0.380	0.183	0.694	0.563	81	0.380	0.030	0.515	0.409	79	0.380	0.026	0.437	0.405	93
0.05	1.393	0.432	1.934	1.825	94	1.393	0.068	1.578	1.461	93	1.393	0.056	1.472	1.449	98
0.075	2.978	0.714	3.521	3.692	105	2.978	0.111	3.036	3.089	102	2.978	0.089	2.994	3.067	102
0.1	5.107	1.020	5.386	6.127	114	5.107	0.156	4.832	5.263	109	5.107	0.123	4.955	5.230	106
0.15	10.919	1.686	9.806	12.605	129	10.919	0.254	9.299	11.173	120	10.919	0.196	10.079	11.115	110

Table 5.11: Contribution of mesh to overall resistance of combined unit for horizontal blades

Q (m3/s)	Louver 1 with 35% FA mesh				Louver 1 with 50% FA mesh				Louver 1 with 70% FA mesh			
	ΔPL	ΔPM	ΔPM+L	$\frac{\Delta P_{M+L} - \Delta PL}{\Delta P_{M+L}}\%$	ΔPL	ΔPM	ΔPM+L	$\frac{\Delta P_{M+L} - \Delta PL}{\Delta P_{M+L}}\%$	ΔPL	ΔPM	ΔPM+L	$\frac{\Delta P_{M+L} - \Delta PL}{\Delta P_{M+L}}\%$
0.005	0.005	0.025	0.038	87	0.005	0.004	0.008	38	0.005	0.004	0.007	32
0.025	0.073	0.183	0.283	74	0.073	0.030	0.100	27	0.073	0.026	0.100	27
0.050	0.228	0.432	0.669	66	0.228	0.068	0.292	22	0.228	0.056	0.304	25
0.075	0.446	0.714	1.107	60	0.446	0.111	0.548	19	0.446	0.089	0.585	24

Table 5.12: Contribution of mesh to overall resistance of combined unit for 60° inclined blades

Q (m3/s)	60 deg blades with 35% FA mesh				60 deg blades with 50% FA mesh				60 deg blades with 70% FA mesh			
	ΔPL	ΔPM	ΔPM+L	$\frac{\Delta P_{M+L} - \Delta PL}{\Delta P_{M+L}}\%$	ΔPL	ΔPM	ΔPM+L	$\frac{\Delta P_{M+L} - \Delta PL}{\Delta P_{M+L}}\%$	ΔPL	ΔPM	ΔPM+L	$\frac{\Delta P_{M+L} - \Delta PL}{\Delta P_{M+L}}\%$
0.005	0.019	0.025	0.064	71	0.019	0.004	0.038	51	0.019	0.004	0.026	29
0.025	0.380	0.183	0.694	45	0.380	0.030	0.515	26	0.380	0.026	0.437	13
0.050	1.393	0.432	1.934	28	1.393	0.068	1.578	12	1.393	0.056	1.472	5
0.075	2.978	0.714	3.521	15	2.978	0.111	3.036	2	2.978	0.089	2.994	1

In all cases the airflow performance of the combined unit relative to the airflow performance of the louver improved with increasing pressure differential. Comparison between horizontal and inclined louver blades indicates that airflow performance of combined units with the 35% and 70% free-area mesh-screens approaches that of the louver when the blades are inclined, whereas for the 50% free-area mesh-screen the variation changes only slightly. In relation to the electrical analogy of resistances in series the results obtained (Table 5.9 and Table 5.10) for both horizontal and inclined blades suggest that, with the flow rate known, the total pressure drop across the combined unit is not simply calculated by adding the pressure drops of the constituent components. For the combined unit with a 35% free-area mesh-screen, both horizontal and inclined blades show that that electrical analogy under-predicts the total pressure drop at low airflow rates whilst at higher airflow rates it over-predicts the total pressure drop with a turning point occurring between 0.05 m^3/s and 0.075 m^3/s. This trend was repeated for combined units with the 50% and 70% free-area mesh-screens when the louver blades were inclined. The combined unit with 50% free-area mesh-screen and horizontal blades only slightly over-predicted the total pressure drop (with an over-prediction range of 1 to 3%, ignoring the value at 0.005 m^3/s) throughout the range of airflow rates considered. On the other hand, for the combined unit with a 70% free-area mesh-screen the electrical analogy consistently under-predicted the total pressure drop. Here again the over-prediction at 0.005 m^3/s is ignored. The high values corresponding to 0.005 m^3/s can be attributed to fluctuations resulting from turbulence in the test rig when measurements were taken. Tables 5.11 and 5.12 show that the impact of the mesh-screen on the total pressure drop of the combined unit was greatest with the 35% free-area mesh-screen. For horizontal louver blades, the addition of this mesh-screen accounted for an average 71% of the total pressure drop for the combined unit for airflow rates ranging from 0.005 m^3/s to 0.075 m^3/s. With blades inclined at 60° the impact of the mesh-screen reduced to approximately 40%. The impact of the 50% and 70% free-area mesh-screen was relatively low for horizontal blades - averaging 27% for the same respective airflow rates. When the louver blades were inclined to 60°, the two mesh-screen affected the combined unit rather differently with the influence of the 50% free-area mesh-screen reducing only slightly to an average of 22% whilst that of the 70% free area mesh-screen reduced to 12%.

This investigation sought to gain a better understanding of how mesh-screen and louver components in ventilators interact. Although a basic arrangement was used in this study it still emerged that even for simple systems the resulting airflow properties of combined components are rather complex. As seen here the interactions and impacts of meshes on the overall airflow performance of ventilators could not be intuitively estimated. These findings are in agreement with the conclusions from the Building Research Establishment study (White *et al.* 1999) that even for very simple arrangements of ventilators (as in this work) the aerodynamic interactions are not straightforward to quantify. The magnitudes of the flow losses associated with the meshes indicate that applying a simple blockage correction factor to allow for a mesh-screen will lead to an overestimate of the associated loss. It is possible that this is because the mesh-screen blockage does not consist of one homogeneous area but rather an array of narrow, relatively aerodynamic wires that would not offer the same flow resistance.

5.4.8 Effect of separation between louver and mesh

The effect of locating a mesh-screen relative to louver blades and how this affects the overall airflow performance of the ventilator was investigated by inserting wooden spacer frames of identical width and height to the wooden louver frame dimensions (Figure 5.27).

Figure 5.27: Spacer between louver and mesh

Spacer frames of thickness 3, 6, 9, 12 and 15 mm were used in combination with Louver 1 for horizontal and 60° louver blade inclinations and a round-wire mesh-screen of 35% free-area. Measurements were also taken when the mesh-screen was placed adjacent to the louver frame without a spacer in-between (0mm spacer).

RESULTS/DISCUSSION

Applying power law regressions to measured sets of pressure differential (ΔP) and resulting airflow (Q) for all the separations (spacer thickness) gave correlation coefficients greater than 99.6 % in all cases. Using these power law characteristic equations Q values were calculated for pressure differentials in the range 0 - 10 Pa in steps of 0.05 Pa resulting in 200 pressure differential levels. This level of accuracy was considered adequate taking into account the uncertainties that occur in problem definition likely to be encountered in natural ventilation practice [Chilengwe and Sharples, *2002* and *2003B*]. The data generated (see Table 5.13 for sample values at selected pressure differentials) was then used to establish a *Relative Overall Improvement* (R.O.I.) of the ventilator as a result of each separation. *Relative Overall Improvement* at given pressure differential is here defined as:-

(5.7)

$$Relative\ Overall\ Improvement\ (R.O.I.) = \frac{Q_{highest}}{Q_{lowest}}$$

It was found that a separation between louver and mesh-screen improved the overall airflow performance of the ventilator depending on the pressure differential (Figure 5.28) and the size of spacer used. For instance for the 60° louver blade angle only over the ΔP range 1.05 - 1.75 Pa did all the separations perform better than 0 mm separation.

Table 5.13:
60° Louver blade and 35% FA mesh

ΔP (Pa)	Q_{15} (l/s)	Q_{12} (l/s)	Q_9 (l/s)	Q_6 (l/s)	Q_3 (l/s)	Q_0 (l/s)	R.O.I.
0.05	4.67	4.20	4.56	4.22	4.41	4.21	1.112
0.2	11.52	10.75	11.29	10.80	11.19	10.77	1.072
0.5	20.94	20.00	20.58	20.08	20.72	20.02	1.047
1	32.90	32.00	32.40	32.10	33.00	32.00	1.031
1.5	42.85	42.12	42.25	42.24	43.33	42.10	1.029
3	67.33	67.39	66.52	67.54	69.02	67.30	1.038
5	93.94	95.28	92.95	95.45	97.28	95.09	1.047
8	127.62	131.03	126.44	131.22	133.39	130.70	1.055
10	147.60	152.42	146.33	152.62	154.96	152.00	1.059
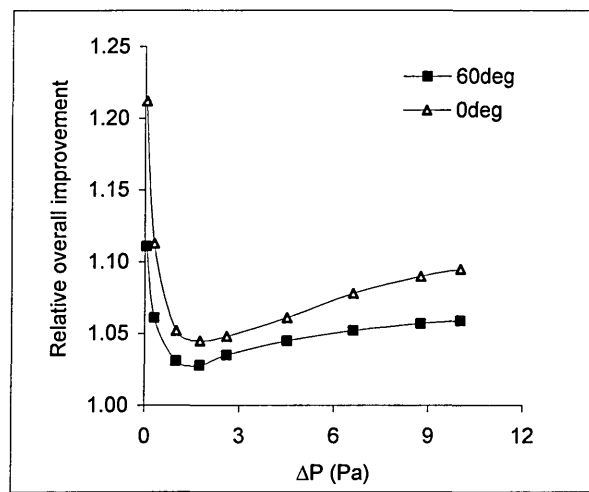
Fig. 5.28: Relative overall improvement as a function of ΔP

Further it was interesting to note that for both louvre angles eight clearly distinct categories for ranking the effect of separation emerged from the 200 levels of pressure differentials within the range 0 - 10 Pa. Table 5.14 summarizes the key findings for the two louver blade inclination angles.

Table 5.14:
Summary of effect of separation for Louver 1 with a 35% free area mesh

Horizontal louver blades	60° inclined louver blades
For ΔP's up to 0.7 Pa a 12 mm separation is most effective	For ΔP's up to 0.85 Pa a 15 mm separation is most effective
For ΔP's up to 1 Pa a 0mm separation is least effective	For ΔP's up to 1 Pa a 12 mm separation is least effective
Between 0.75 Pa and 3.15 Pa a 15 mm separation is most effective, whilst above 3.2 Pa a 0 mm separation is most effective	Between 0.9 Pa and 10 Pa a 3 mm separation is most effective
Above 1 Pa a 3 mm separation is least effective	Between 1.05 Pa and 1.75 Pa a 0 mm separation is least effective whilst above 1.8 Pa a 9 mm separation is least effective
Relative Overall Improvement ranged from 4.7% to 21.2% with an average of 7.2%	Relative Overall Improvement ranged from 2.8% to 11.2% with an average of 4.7%
Over the whole range of ΔP's considered the following categories of ranking the relative improvement emerged:-	Over the whole range of ΔP's considered the following categories of ranking the relative improvement emerged:-

Horizontal louver blades — (separation mm) Increasing effectiveness → ; (separation mm) Increasing ΔP ↓

0	3	9	6	15	12
0	3	6	9	12	15
3	0	6	9	12	15
3	6	0	9	12	15
3	6	0	12	9	15
3	6	12	9	0	15
3	6	12	9	15	0
3	6	12	15	9	0

60° inclined louver blades — (separation mm) Increasing effectiveness → ; (separation mm) Increasing ΔP ↓

12	0	6	3	9	15
12	0	6	9	3	15
12	0	6	9	15	3
0	12	6	9	15	3
0	12	9	6	15	3
9	0	12	6	15	3
9	0	12	15	15	3
9	15	0	12	6	3

-123-

Although there was only a limited range over which all separations performed better than 0 mm separation, the results indicate that for a given louver-mesh screen combination there is a particular separation that is most efficient for the passage of air through the ventilator for a given range of ΔP. Depending upon the pressure range and spacing between louver and mesh-screen, relative overall improvement in ventilator performance was found to be as high as 21% for horizontal louver blades [Chilengwe and Sharples, *2002*]. Generally, relative overall improvement for horizontal blades was higher than that for inclined louver blades at similar pressure differentials. This investigation highlighted the fact that by carefully considering the relative locations of components in a ventilator, appreciable improvements in the airflow performance can be achieved which could result in improved airflow patterns within a room. Higher improvements occur for horizontal blades compared to inclined blades. This can be attributed to the fact that the more aerodynamically efficient horizontal blades are more sensitive to the position of the mesh-screen than inclined blades which suffer weaker flows through relatively higher resistance.

5.4.9 Directional airflow performance of ventilators

One feature of natural ventilation is that depending upon the prevailing climatic or thermal conditions the airflow through a ventilator can be bi-directional. Aerodynamically, the ventilator, depending upon its construction may not perform in the same way for the two different flow directions (Figure 5.29).

a) Outflow configuration   b) Inflow configuration
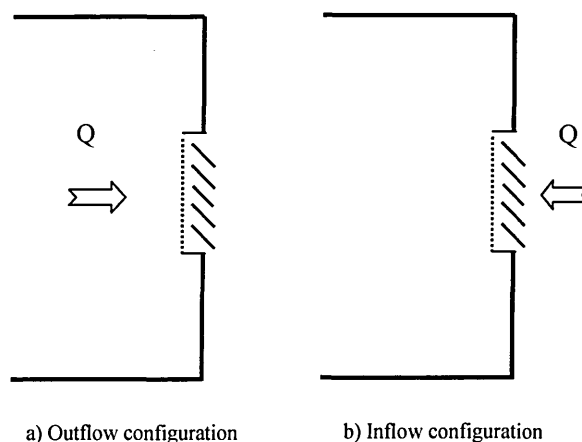
Figure 5.29: Illustration of directional airflow

The geometry of the internal flow-path, the inclination of louver blades and the location of meshes and acoustic linings are features that stop the ventilator being aerodynamically symmetrical for different flow directions. This section describes a series of experimental measurements on commercial louver ventilators (see *Section 5.3.3* and *Section 5.3.5* for details of the components used) that investigated the influence that flow direction and magnitude of pressure differentials can have on airflow performance. Experimental data obtained was also compared with Computational Fluid Dynamics predicted values of airflow parameters (*Chapter 7*).

RESULTS/DISCUSSION

The results obtained (Table 5.15) show that for a given pressure differential (ΔP) across the ventilator component the resulting airflow for inlet configurations was different from that obtained for outlet configurations. The majority of the cases shown in Table 5.15 indicate that the ventilator performed better in outlet configuration than it did in the corresponding inlet configuration. The results further show that the percentage difference between the outlet flow rate and inlet flow rate relative to the inlet flow rate was greater at low pressure differentials than at higher pressure differentials. Figures 5.30, 5.31 and 5.32 show the airflow performance of outlet configurations relative to inlet configurations plotted as functions of pressure differentials across louver/mesh combinations. Here again it is evident that the effect of flow direction was more significant at low pressure differences and gradually levels off as ΔP increases. It is interesting to note that the graph obtained for louver X is different from those for louver Y and louver Z. An explanation of these differences is that airflow performance is significantly affected by variations in ventilator geometry i.e. louver Y and louver Z which gave similar graphs were also geometrically similar except for the "rain hooks" on each blade of Louver Z (see *Section 5.3.3*). It was also interesting to note that in all three cases the graph of the ventilator with a bird guard mesh-screen intersected the one with an insect screen somewhere between 1 Pa and 1.5 Pa. This suggests that there is a ΔP between these limits at which the airflow performances of the two ventilators are equal. However, bearing in mind that the two meshes used in this investigation had different geometries it is not surprising that the characteristics of the two ventilators intersected [Sharples and Chilengwe, *2003*].

Table 5.15:
Measured air flow rates for inlet and outlet configurations at various pressure drops

Louvre	Mesh type	Pressure drop across louvre ΔP = 0.05 (Pa)			Pressure drop across louvre ΔP = 0.25 (Pa)			Pressure drop across louvre ΔP = 0.5 (Pa)			Pressure drop across louvre ΔP = 1.5 (Pa)			Pressure drop across louvre ΔP = 2 (Pa)		
		Inlet Qi (l/s)	Outlet Qo (l/s)	$\frac{Qo-Qi}{Qi}$ (%)	Inlet Qi (l/s)	Outlet Qo (l/s)	$\frac{Qo-Qi}{Qi}$ (%)	Inlet Qi (l/s)	Outlet Qo (l/s)	$\frac{Qo-Qi}{Qi}$ (%)	Inlet Qi (l/s)	Outlet Qo (l/s)	$\frac{Qo-Qi}{Qi}$ (%)	Inlet Qi (l/s)	Outlet Qo (l/s)	$\frac{Qo-Qi}{Qi}$ (%)
X	no mesh	18.02	17.70	-1.8	41.83	42.68	2.0	60.12	62.36	3.7	106.8	113.7	6.5	124.17	133.09	7.2
	bird guard	13.87	15.26	10.0	33.72	36.46	8.1	49.44	53.06	7.3	90.7	96.1	6.0	106.30	112.33	5.7
	insect screen	10.78	9.10	-15.6	29.81	28.25	-5.2	46.20	46.03	-0.4	92.5	99.8	7.9	110.97	122.19	10.1
Y	no mesh	18.28	22.10	20.9	44.44	47.69	7.3	65.14	66.42	2.0	119.5	112.3	-6.0	140.00	128.83	-8.0
	bird guard	13.19	17.05	29.3	34.22	39.92	16.7	51.60	57.60	11.6	98.9	103.0	4.1	117.30	119.89	2.2
	insect screen	13.73	15.80	15.1	34.23	37.64	10.0	50.74	54.70	7.8	94.7	98.9	4.5	111.45	115.54	3.7
Z	no mesh	18.85	23.60	25.2	44.05	51.94	17.9	63.49	72.97	14.9	113.3	125.0	10.4	131.87	143.99	9.2
	bird guard	11.17	19.10	71.0	33.74	43.24	28.2	54.30	61.47	13.2	115.5	107.4	-7.0	140.67	124.26	-11.7
	insect screen	10.81	14.73	36.3	32.93	37.65	14.3	53.22	56.40	6.0	113.9	107.0	-6.0	138.97	126.60	-8.9
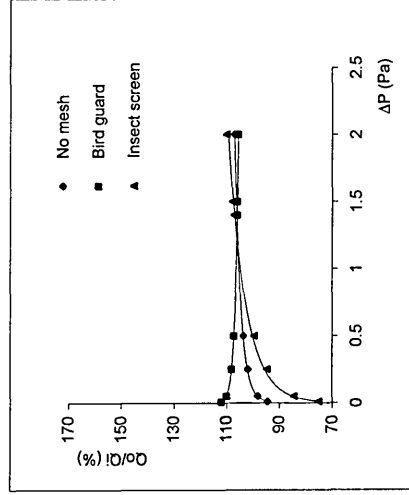
Fig.5.30: Qo/Qi as a function of ΔP for louver X
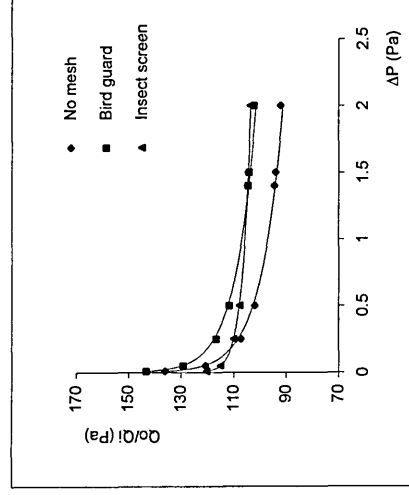
Fig.5.31: Qo/Qi as a function of ΔP for louver Y
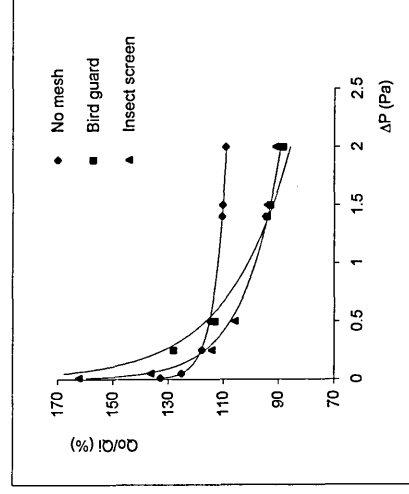
Fig.5.32: Qo/Qi as a function of ΔP for louver Z

The findings of this investigation revealed that airflow through ventilators is influenced by the flow direction, with the influence being more pronounced at low pressure differentials than at high pressure differentials. Therefore, where prevailing climatic conditions are reasonably steady it might prove beneficial in naturally ventilated buildings to have differently designed inlet and outlet ventilators. Hence, it is essential to treat the inlet and outlet configurations as independent systems in any attempt to optimise the airflow performance of a given ventilator.

5.4.10 Low and high pressure ventilator characteristics

The wind and buoyancy pressure driving forces for natural ventilation of buildings are very low, typically less than 10 Pa. Depending upon the prevailing climatic and thermal conditions or even the location of a building on a site in relation to other surrounding buildings and landscape the predominant pressure force incident on a purpose-provided natural ventilation opening can either be closer to the lower range of pressure differentials (< 2 Pa) or vary over a wider range of higher pressures (2 - 10 Pa). This study investigated via a series of experiments variations in power law characteristic equations of ventilators derived from low pressure measurements, relatively higher (typical) pressures and those derived by considering the whole pressure range. For the ventilation designer, this kind of information is important because the nature of the driving forces incident up on the ventilator has a direct impact on the thermal comfort of occupants of the room being ventilated. However, such information is not readily available. To this effect the aim of this study was to investigate and quantify via a series of experiments variations in characteristic equations of ventilators, derived from low pressure measurements, relatively higher pressures and those derived by considering the whole pressure range [Chilengwe and Sharples, *2003A*].

Figures 5.33 to 5.35 show typical power law regressions for wooden Louver 1 with blades at 0° and 60° used in combination with a 35% free-area mesh-screen.

$y = 0.0684x^{0.7997}$
$R^2 = 0.9971$

$y = 0.0318x^{0.6712}$
$R^2 = 0.9971$
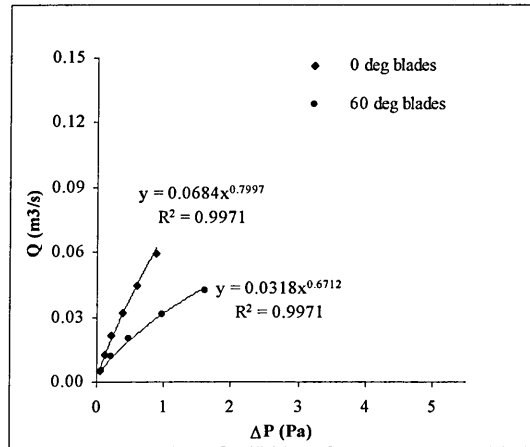
Figure 5.33: Low pressure airflow characteristic

$y = 0.0666x^{0.9731}$
$R^2 = 0.9988$

$y = 0.029x^{0.7556}$
$R^2 = 0.9964$
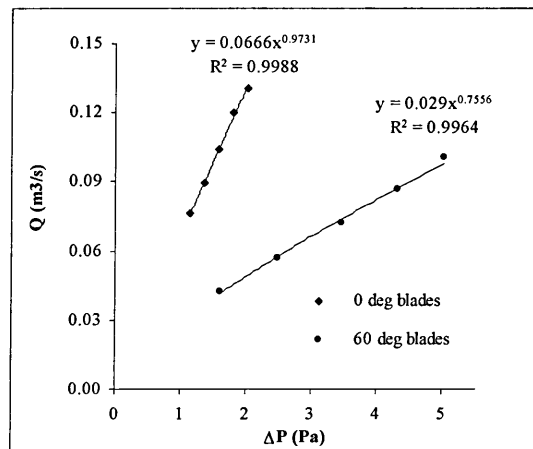
Figure 5.34: High pressure airflow characteristic

$y = 0.0702x^{0.8139}$
$R^2 = 0.9981$

$y = 0.032x^{0.6767}$
$R^2 = 0.9983$
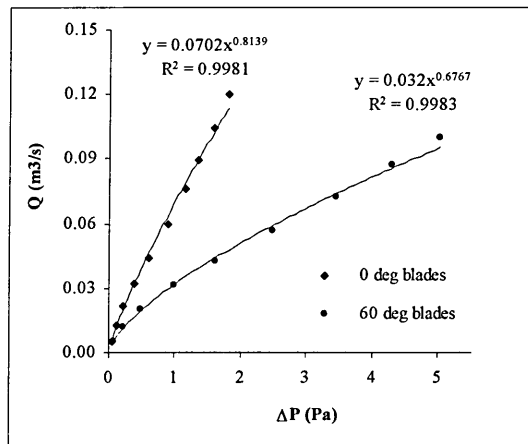
Figure 5.35: Overall pressure range airflow characteristic

-128-

Power law regressions for meshed louvres at various blade angles

Louvre angle (deg)	ΔP range	35% FA mesh			50% FA mesh		
		α	β	R	α	β	R
0	L	0.068	0.800	99.71	0.111	0.645	99.56
	H	0.067	0.973	99.88	-	-	-
	O	0.070	0.814	99.81	0.111	0.645	99.65
60	L	0.032	0.671	99.71	0.037	0.611	99.59
	H	0.029	0.756	99.64	0.033	0.758	99.22
	O	0.032	0.677	99.83	0.038	0.628	99.64
Louvre angle (deg)	ΔP range	70% FA mesh			100% FA mesh		
		α	β	R	α	β	R
60	L	0.037	0.532	99.99	0.039	0.499	99.92
	H	0.035	0.770	99.13	0.037	0.737	98.95
	O	0.416	0.596	99.22	0.044	0.558	99.17
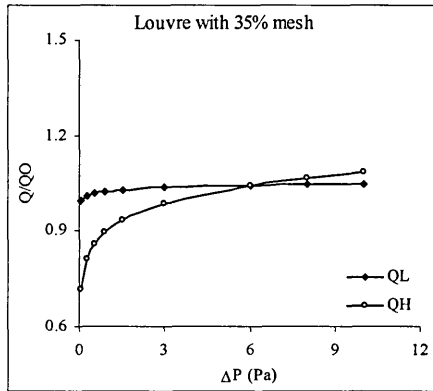
Figure 5.36: Ratio of Q_L and Q_H with respect to Q_O for 35% FA mesh
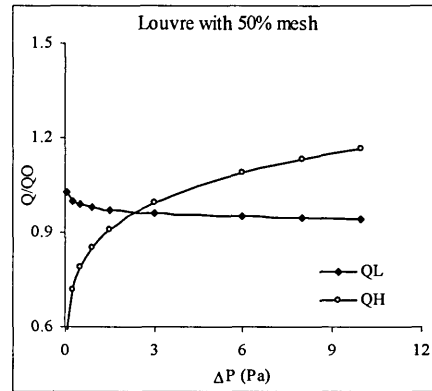
Figure 5.37: Ratio of Q_L and Q_H with respect to Q_O for 50% FA mesh
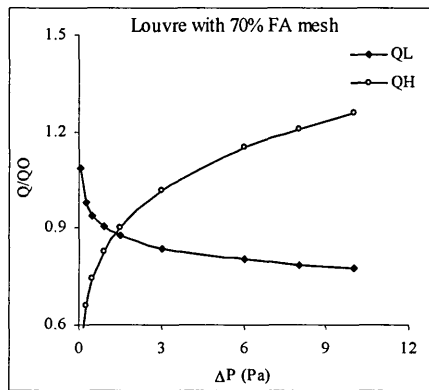
Figure 5.38: Ratio of Q_L and Q_H with respect to Q_O for 70% FA mesh
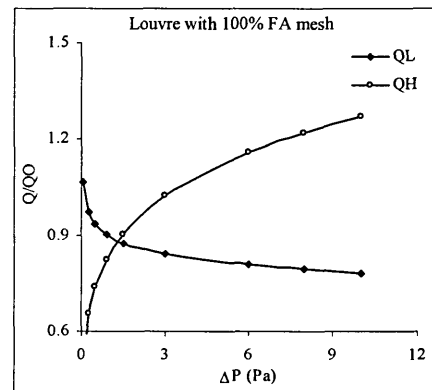
Figure 5.39: Ratio of Q_L and Q_H with respect to Q_O for 100% FA mesh

Comparison of air flow rates Q (m3/s) from low and high ΔP (Pa) equations for louver with 60 deg blades

ΔP (Pa)	35% FA mesh				50% FA mesh				70% FA mesh				100% FA mesh			
	Q_L	Q_H	Q_L/Q_O	Q_H/Q_O	Q_L	Q_H	Q_L/Q_O	Q_H/Q_O	Q_L	Q_H	Q_L/Q_O	Q_H/Q_O	Q_L	Q_H	Q_L/Q_O	Q_H/Q_O
0.05	0.004	0.003	1.01	0.72	0.006	0.003	1.03	0.59	0.008	0.003	1.09	0.50	0.009	0.004	1.07	0.49
0.25	0.013	0.010	1.00	0.81	0.016	0.012	1.00	0.72	0.018	0.012	0.98	0.66	0.020	0.013	0.97	0.65
0.5	0.020	0.017	1.00	0.86	0.024	0.020	0.99	0.79	0.026	0.021	0.94	0.75	0.028	0.022	0.93	0.74
0.9	0.030	0.027	0.99	0.90	0.035	0.030	0.98	0.85	0.035	0.032	0.91	0.83	0.037	0.034	0.90	0.82
1.5	0.042	0.039	0.99	0.94	0.048	0.045	0.97	0.91	0.046	0.048	0.88	0.90	0.048	0.049	0.88	0.90
3	0.066	0.067	0.99	0.99	0.073	0.076	0.96	1.00	0.067	0.082	0.84	1.02	0.068	0.082	0.84	1.02
6	0.106	0.112	0.98	1.04	0.112	0.128	0.95	1.09	0.097	0.139	0.80	1.15	0.096	0.137	0.81	1.16
8	0.128	0.140	0.98	1.07	0.133	0.160	0.95	1.13	0.113	0.174	0.79	1.21	0.110	0.170	0.79	1.22
10	0.149	0.165	0.98	1.09	0.153	0.189	0.94	1.17	0.127	0.206	0.78	1.26	0.123	0.200	0.78	1.27
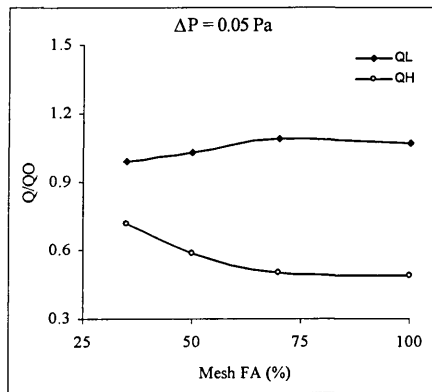
Figure 5.40: Ratio of Q_L and Q_H with respect to Q_O for $\Delta P = 0.05Pa$
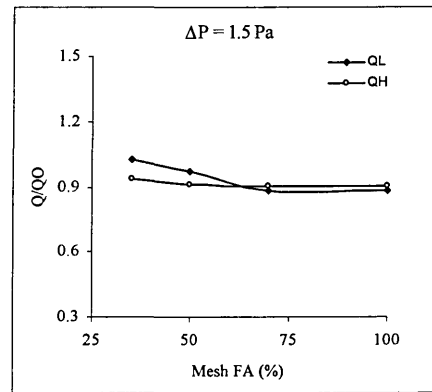
Figure 5.41: Ratio of Q_L and Q_H with respect to Q_O for $\Delta P = 1.5Pa$
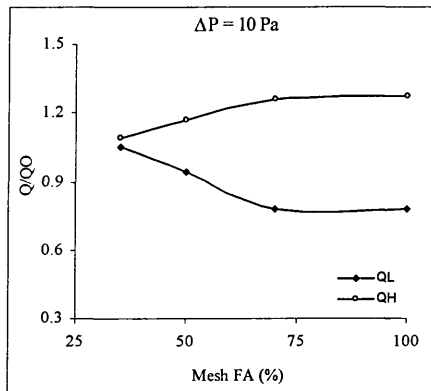
Figure 5.42: Ratio of Q_L and Q_H with respect to Q_O for $\Delta P = 10Pa$

Table 5.18:
Variations in derived airflow rates for louver with 35% FA mesh

ΔP (Pa)	Blade angle (deg)	Q_L (m3/s)	Q_H (m3/s)	Q_O (m3/s)	$\frac{Q_O-Q_L}{Q_O}$ (%)	$\frac{Q_O-Q_H}{Q_O}$ (%)
1	0	0.068	0.066	0.07	2.29	5.71
	60	0.033	0.029	0.032	-3.13	9.38
10	0	0.431	0.658	0.457	5.69	-43.98
	60	0.161	0.165	0.152	-5.92	-8.55
20	0	0.751	1.313	0.804	6.59	-63.31
	60	0.258	0.279	0.243	-6.17	-14.81

Table 5.16 shows the coefficients obtained from power law regressions of low pressure (< 1 Pa) and high pressure (> 1 Pa) together with those obtained by fitting the power law to the whole range of pressure achieved during experimental measurements i.e. 0 - 6 Pa. Data for the horizontal blades with 50%, 70% and 100% mesh-screens is not given

in Table 5.16 because for these combinations the maximum pressure differentials achieved during experiments were less than 1 Pa, hence, there was no high pressure readings for comparison. Using these power law correlation relationships airflow rates Q_L (low pressure) and Q_H (high pressure) were derived, by extrapolation, for selected pressure differentials in the range 0 - 10 Pa (Table 5.17) and compared with respect to the airflow (Q_O) obtained from the overall pressure differential characteristic equation in order to assess the differences that occurred based upon which pressure range was used for generating the airflow characteristic equation. Figures 5.36 to 5.39 show the variation of the ratios Q_L/Q_O and Q_H/Q_O as functions of pressure differential ΔP for the louver used in combination with mesh-screens of 35%, 50%, 70% and 100% (no mesh-screen) free-areas. Figures 5.40 to 5.42 show how the ratios Q_L/Q_O and Q_H/Q_O vary with mesh-screen free area at selected pressure differentials. Table 5.18 quantifies the variations in airflow rates derived from low/high pressure characteristic equations relative to those obtained from whole pressure range data at selected ΔP's for the ventilator - louver at 0° and 60° blade angles with a 35% free-area mesh-screen.

DISCUSSION

The results indicate that the pressure range used during experimental measurements influenced the generated airflow characteristic. The influence was dependent upon the pressure differential and the components such as louvers and mesh-screens which made up the ventilator. It is clear from the results that over the range of pressure differentials typical in natural ventilation applications, whilst over-predictions of up to 27% can be introduced in ventilator airflow calculations under-predictions can be as much as 51% depending upon the pressure range used in determining the characteristic equation. The deviation in airflow rates predicted from the high pressure characteristic equation change from under-prediction at low ΔP's to over-predictions with increasing pressure differentials with the turning point generally occurring between 1.5 Pa and 3 Pa. On the other hand the deviation in airflow rates predicted from the low pressure characteristic generally decreased from over-prediction at low ΔP's to under-prediction with increasing pressure differential. This was true for the cases considered except for the 35% free-area mesh-screen (Figure 5.36) which showed a converging trend between the low and high pressure characteristic equation as the pressure differential was increased. In relation to mesh-screens, at 0.05 Pa the low pressure characteristic equation resulted

-131-

in an under-prediction of airflow at low free-area ratios which slightly increased with increasing free-area ratios. The high pressure characteristic equation on the other hand resulted in under-prediction of airflows for all mesh-screen free-area ratios. On the contrary, at 10 Pa the opposite was true. In both cases the under-prediction/over-prediction was constant at mesh-screen free areas above 70% (Figure 5.40 and Figure 5.42). At 1.5 Pa (Figure 5.41) there was very close agreement between the low and high pressure characteristic equations for all the mesh-screen free areas considered. The variations in predicted airflow rates ranged from 2.29% to 63.31%. It can be seen (Table 5.18) that the airflow rates predicted from the high pressure equation were always greater than those from the low pressure characteristic equation at the pressure differentials considered for both louver blade angles. The 60° blade arrangement over-predicted the airflow at given pressure differential whilst the 0° arrangement under-predicted the airflow.

The low pressure equation showed less variation (2.29% - 6.59%) as the pressure differential was increased from 1 to 20 Pa than the high pressure equation (5.71% - 63.31%).

CONCLUSION

The results obtained indicate that the characteristic equation was not only influenced by the constituent components of the ventilator but also the pressure range from which it was generated. This study highlighted the need to understand how the airflow characteristic of a ventilator is influenced by the pressure range from which it was generated. Although only a basic arrangement was used it was still sufficient enough to bring to light the dependence of the characteristic of a ventilator on pressure range under consideration and the components that make up the ventilator - louvers and mesh-screen in this case. These findings coupled with the fact that ventilation openings cannot be considered in isolation from the rest of the building, and from the effects even of other buildings and objects emerging in the immediate surroundings (direct impact on pressure differential to which a given ventilator would be exposed), suggest that the design and operation of natural ventilation need to incorporate some methods to adapt resulting airflow rates. This would account for variations in pressure differentials thus ensuring that a given ventilator maintains a consistent airflow pattern over the whole

range of pressure differentials encountered. A possible solution would, for instance, involve ventilator manufacturers incorporating means of adapting the configuration of a ventilator in relation to prevailing climatic and thermal conditions. A simple and easy way to implement this method of adaptation would be the option of adjusting the location of the mesh-screen within a ventilator to vary the resulting airflow performance (*Section 5.4.8*). This would in turn ensure that a given ventilator maintains a consistent airflow pattern over the whole range of pressure differentials encountered in natural ventilation applications thus resulting in improved controllability, impact on comfort and indoor air quality.

5.4.11 Effect of rotating non-square meshes

Tests were carried out on the aluminium louver banks (described in *Section 5.3.3*) used individually and in combination with the insect-screen and the bird guard mesh-screen described in *Section 5.3.5*. An assessment was undertaken to establish the effect of rotating non-square mesh-screen through 90° (Figure 5.43 and Figure 5.44) on the overall airflow performance of the ventilator. This investigation stemmed from discussions with a reputable ventilator manufacturer which revealed that no particular attention is paid to the orientation of meshes incorporated in ventilators. Therefore, this study attempted to quantify differences in airflow properties resulting from different mesh-screen orientations.
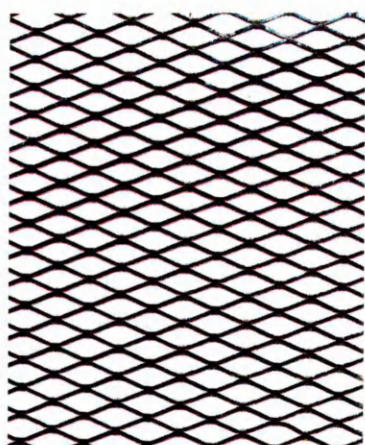
Figure 5.43: Bird guard mesh arrangement

Figure 5.44: Bird guard mesh rotated 90°

Table 5.19 shows a comparison of airflow performance of various ventilators as a result of rotating the mesh-screen through 90° from the usual configuration. This assessment was necessary as the meshes did not have a geometrically even pattern. It can be seen from Table 5.19 that the orientation of uneven meshes in ventilators can result in significant differences in airflow performance (as high as 36%) hence, requires careful consideration by ventilator designers.

An assessment of the airflow performance in relation to the orientation of the meshes on the ventilators compared to the arrangement where the mesh-screen is rotated through 90° indicated differences of more than 20% in some cases. The arrangement with the rotated mesh-screen gave the worst performance.

Table 5.19:
Comparison of airflow rates Q (m3/s) resulting from mesh rotation on various ventilators

Louvre	Mesh type	Louvre face velocity 0.05m/s			Louvre face velocity 0.25m/s			Louvre face velocity 0.5m/s		
		Mesh normal	Mesh 90°	max. % difference	Mesh normal	Mesh 90°	max. % difference	Mesh normal	Mesh 90°	max. % difference
X	insect screen	0.0117	0.0107	9.3	0.0501	0.0497	0.8	0.0952	0.0979	2.8
	bird guard	0.0097	0.0093	4.3	0.0485	0.0475	2.1	0.0984	0.0969	1.5
Y	insect screen	0.011	0.0098	12.2	0.05323	0.05	4.6	0.1043	0.1028	1.5
	bird guard	0.0124	0.0091	36.3	0.053	0.0435	21.8	0.1001	0.0863	16
Z	insect screen	0.0091	0.0085	7.1	0.0552	0.0528	4.5	0.1227	0.1184	3.6
	bird guard	0.0096	0.0127	32.3	0.0561	0.0566	0.9	0.1218	0.109	11.7

For the insect screen the average deviations ranged from 2.6% at a louver face velocity of 0.5ms/ to 9.5 at louver face velocity equal to 0.05m/s. The average deviation at 0.25 m/s louver face velocity was 3.3%. On the hand the average deviations for the bird guard ranged from 8.2% at louver face velocity 0.25 m/s to 24.5% at louver face velocity 0.05 m/s. The average deviation at louver face velocity 0.5 m/s was 9.7%.

5.4.12 Establishment of boundary conditions for use in CFD investigations

The pressure drop caused by the presence of ventilators can be split into two major elements, namely, the frictional forces resulting from the roughness of solid surfaces, and inertia losses due to velocity changes resulting from angled louver blades and other variations in size of the flow path within the ventilator. Surface roughness is caused by

irregularities in the profile of the surface and it is a property of the surface on which the flow behaviour in the transition and turbulent zones depends to a considerable degree. Generally, surface roughness is determined from geometrical measurements of the surface finish. It was necessary to determine the surface roughness of louvers since it was needed as one of the input parameters for CFD modelling (*Chapter 6*).

Some CFD studies, for example [Maghrabi, *2000*], ignore the roughness of surfaces over which air flows in their simulation models. Although this is acceptable for bulk air movement investigations, for detailed investigation of airflow on a more or less microscopic scale it is important to incorporate roughness of surfaces to reflect reality. For this investigation the roughness of the material (extruded aluminium) used to make louvers tested in this investigation was taken into account in the CFD simulation model, and was accurately measured at Sheffield Hallam University *(Materials Engineering laboratory)*. Roughness measurements were carried out on a Taylor Hobson Laser Form Talysurf MK 1 (2 micron radius stylus) surface texture machine. Figure 5.45 shows typical results of the surface roughness measurements.
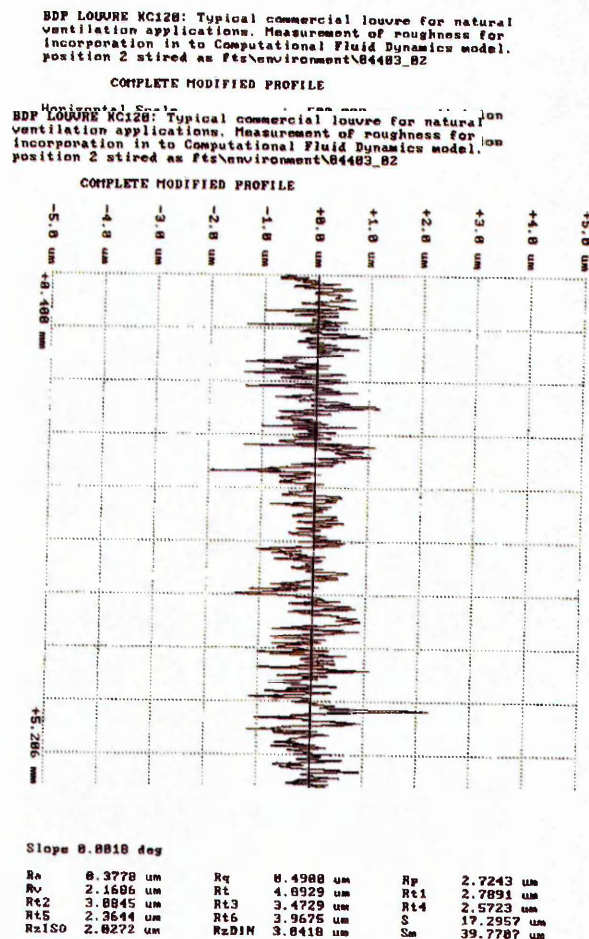
Figure 5.45: Typical results from aluminium
louver surface roughness measurement

From a number of measurements carried out, an average roughness value Ra = 0.3756 micron was adopted for incorporation into the CFD model for all simulations (*Chapter 6*). Detailed discussion and guidance on various aspects relating to surface roughness and its measurement was beyond the scope of this study. For the interested reader British Standard BS1134 and the book "*Exploring Surface Texture*" by H Dagnall are excellent starting points to explore the subject.

5.5 Concluding Remarks

This chapter set out to describe various ventilator components, and a number of experimental measurements which formed the basis of the investigation. Based on these measurements, airflow characteristics were derived using the power law and quadratic models of representation. Key findings from the experiments showed that the airflow properties are not obtained by simple arithmetic addition of the properties of the individual components included in a ventilator. Further, the investigation revealed that the airflow performance of ventilators is affected by various factors including the type of mesh-screen used, free area ratio of the mesh-screen, location of the mesh-screen relative to the louver blades, inclination angle of the louver blades, direction of airflow through the ventilator, range of pressure differential used to derive the airflow characteristic and the orientation of the mesh-screen, where a non-square configuration is used. The differences between repeated tests for a selection of measurements carried out on different days throughout the experimental phase of the investigation were generally within ±1% . This repeatability was also achieved when results from tests on commercial ventilators were compared with those obtained independently from a similar test rig by a reputable UK based ventilator manufacturer. In addition, as the main interest was in establishing relative variations in airflow performance of ventilator components it was assumed that deviations in test results due to external influences such as room air movement were similar for various measurements. For these reasons it was not necessary to conduct a detailed uncertainty analysis to determine the propagation of error of individual measurements.

Findings from the experiments described in this chapter will form the basis upon which further analysis will be carried out (*Chapter 7*) with a view to optimising the airflow performance of a given ventilator.

Chapter 6

COMPUTATIONAL FLUID DYNAMICS

6.1 Introduction

Computational Fluid Dynamics (CFD) is one discipline falling under the broad heading of computer-aided engineering and comprises a mathematical-based approach to engineering product and process design, analysis and manufacture. CFD has as its objective the representation of a fluid flow problem by mathematical equations based on the fundamental laws of physics and numerical solution of those equations to predict the variation of the relevant parameters within the flow field [Jones and Whittle, *1992*]. The calculus problem of solving a coupled system of non-linear partial differential equations for variables of interest (e.g. velocity, pressure, temperature) is transformed into an algebraic problem of solving a large system of simultaneous linear equations for discrete unknowns that represent a thermal-fluids system; the latter is amenable to numerical solution on a digital computer [O'Rourke *et al. 1997*]. One of the main advantages of CFD is that it provides a cost effective method to predict the whole flow field in buildings [Lu, Howarth and Jeary, *1997*]. This chapter has a three-fold purpose:-

- To provide a basic technical foundation for CFD and its use in ventilation studies *(Sections 6.2 - 6.5)*
- To highlight some of the key features of FLOVENT, the CFD software used in this investigation *(Section 6.6)*
- To present parametric case studies on the investigation of the influence of various components in a ventilator *(Section 6.7 - 6.9)*

6.2 Fundamentals of Computational Fluid Dynamics

Over the last three decades CFD calculation of thermal-fluid flows has become more common. This has heightened enormously the interest in CFD among engineers, as most fluid-flow problems encountered in industry are so complex that the only method of analysis to which they are amenable is CFD. Thus, although use of CFD began some

fifty years ago, it is difficult to find problems in fluid dynamics to which computer solution has not been brought to bear. The advent of three dimensional calculations has increased the engineering relevance of CFD, but many obstacles remain to be overcome before CFD realises its full potential as an engineering design tool. The main advantages of CFD over conventional experimental studies/physical models are substantial reductions in lead times and development cost, availability to study systems where experiments are not possible, and ease of performing a large range of parametric studies for optimisation. A detailed comparison of the strengths and weaknesses of CFD relative to alternative procedures can be found in Etheridge and Sandberg [*1996*]. The governing equations of fluid dynamics and an introduction to CFD techniques for their solution are described in the following sections.

6.2.1 Definition of CFD

Computational Fluid Dynamics can be summarised by the following definitions [Veersteeg and Malalasekera, *1995*]:

- The *computational* part of CFD means using computers to solve the equations which predict the Fluid Dynamics. This can be compared with other methods, such as full or part scale mock-ups.

- *Fluid* means any substance which cannot remain at rest under a sliding, or shearing stress.

- *Dynamics* is the study of objects in motion and the forces involved.

6.2.2 Governing equations

The governing equations of fluid dynamics represent the *conservation of mass*, *Newton's second law of motion* (force equals mass times acceleration) and the *first law of thermodynamics* (total energy, in all its forms, must be conserved) for a fluid continuum. In the 19th Century two scientists, Navier and Stokes, described the equations for a viscous, compressible fluid, which are now known as the Navier-Stokes Equations. In CFD applications these equations form a set of Differential Equations which can usefully be written in the general form [Lu, Howarth *et al. 1996*, Pollock and Stribling, *1989*]:

-138-

$$\frac{\partial}{\partial t}\rho\varphi + div(\rho\nabla\varphi) = div(\Gamma_\varphi grad\varphi) + S_\varphi \qquad (6.1)$$

In words,

Rate of increase of φ of fluid element		Net rate of flow of φ out of fluid element		Rate of increase of φ due to diffusion		Rate of increase of φ due to sources
	+		=		+	

where ρ is the density, ∇ is the velocity vector, Γ_φ is the diffusion coefficient and S_φ is the source or sink and the variable φ represents any of the predicted quantities such as fluid velocity, temperature, pressure or concentration of chemical species at any point in the three-dimensional model. This equation is derived by considering a small or finite volume of fluid. Though deceptively simple, only the emergence of ever-faster computers over the past two decades has made it possible to solve the real world problems governed by this equation.

6.2.3 Turbulence models

A common physical complexity encountered in engineering situations is turbulence, as engineering flows typically are characterised by high Reynolds number. Details of the turbulent motion are too small-scale in character to be directly amenable to analytical treatment, and in any case it is not the detailed fluctuations, but the time-averaged consequences which interest the engineer even when the mean flow is unsteady. Most flows of practical interest have features whose relevant spatial and temporal scales span many orders of magnitude. These effects of small scale unresolvable features of the large-scale average flow features of interest are in CFD modelled through modifications to the governing partial differential equations, generally through *turbulence models* with a penalty of necessarily introducing imprecision. By a *model of turbulence* is meant a set of equations which, when solved with the mean flow equations (averaged Navier-Stokes and other conservation equations), allows calculation of the relevant correlations and so simulates the behaviour of real fluids in important respects. The most popular turbulence models in engineering design calculations are the so called two-equation models [Jones and Whittle, *1992*]. The $k - \varepsilon$ turbulence model is by far the most

widely used two-equation eddy-viscosity turbulence model. In this model the turbulent viscosity (μ_t) is given by the expression:

$$\mu_t = \frac{c_\mu \rho k^2}{\varepsilon} \qquad (6.2)$$

where c_μ is a constant, ρ is the density of the fluid, k is the turbulent kinetic energy, and ε is its rate of dissipation. The parameters k and ε are obtained by solving two additional differential equations with an associated drawback of increased computational demand. Typical turbulent constants associated with the k - ε model can be found in many published articles, for instance Lu and Howarth [*1996*], or other sources such as relevant CFD software specific user manuals.

6.2.4 Discretization

Analysis of the flow in a thermal-fluid system is normally done by numerical techniques (see *Section 6.2.5*) of which various methods are available. However, which ever technique is applied it is necessary to discretize the flow domain into control volumes or elements and to use discretization equations to represent the physics of flow within each of the control volumes or elements. Discretization is the method by which the flow domain is subdivided into control volumes or elements (the subdivision is called a grid or mesh) to which numerical techniques maybe applied to obtain approximations of the transport equations *[Roache, 1998]*. Careful consideration is needed with regard to the selection of an appropriate discretization system. A technique is required which identifies each element within the discretized space and identifies its relationship with adjacent cells. Also attention is required with respect to the coarseness of the network, the representation of the boundaries and coping with regions within the network in which high velocity, temperature or pollutant concentration gradients occur. A range of grid systems has been designed to cope with these various aspects and includes; uniform orthogonal grid, non-uniform orthogonal grid, body fitted and curvilinear coordinate system grids [Liddament, *1991*].

6.2.5 Numerical methods

Numerical methods for CFD are mostly concerned with the solution of systems of partial differential equations. These equations must be classified prior to attempting their solution. In the process of discretization of the fluid equations a continuously varying fluid flow field, which has an infinite number of degrees of freedom, is represented by a finite set of data using one of the discrete equations of the *finite-difference, finite-volume, finite-element* and other associated concepts of numerical stability and accuracy [O'Rourke *et al. 1997*]. Finite-difference and finite-volume methods are more popular than finite-element in CFD because they are generally more economical in computational time [Awbi, *1991*]. In finite-difference methods the entire fluid region of interest is divided into non-overlapping cells, and approximate values of the fluid variables are stored in each cell. Derivatives are approximated by taking differences between the variable values in neighbouring cells. As in finite-difference methods, finite-volume methods subdivide the computational region into a mesh of cells, but finite-volume cells can be arbitrary quadrilaterals in two-dimensions, hexahedra in three-dimensions or indeed any shape enclosed by a set of corner points. In contrast, finite-difference methods are defined on grids that are obtained using orthogonal curvilinear coordinate systems. Finite-volume methods approximate forms of the fluid equations that are integrated over these cells which are also known as control volumes. These integrals or partial derivatives are replaced by linear algebraic equations which are then solved by numerical analysis techniques to obtain values of the flow variables at discrete points in time and space [Ata, *1996*]. Iterative solution methods are then applied to calculate a sequence of approximations that converge to the solution. The iterative nature of the calculation methods and the need to solve thousands of equations which are required to represent a reasonably detailed description of the flow and temperature fields means that substantial computing power is needed [Jones & Whittle, *1992*]. The exact solution is rarely obtained, but calculations are terminated when either the difference between successive iterates or the residual is acceptably small.

6.3 The CFD Procedure

There is a growing commercial market for CFD software packages in addition to a variety that are already available. However, regardless of the software being used there is a clearly defined set of stages that make up a CFD analysis process. Figure 6.1 below highlights the main stages (procedures) which must be employed and accomplished in modelling and simulation in order to generate a CFD solution. Besides countless articles in archival journals such as the Internal Journal of Computational Fluid Dynamics, there are entire books such as Shaw [*1992*] devoted to the CFD procedure therefore, in the following sections each stage is only briefly described.

```
        ┌──────────────┐
        │  Geometry    │
        │  definition  │
        └──────────────┘
               │
               ▼
        ┌──────────────┐
        │Grid generation│
        │ and problem  │
        │specification │
        └──────────────┘
               │
               ▼
        ┌──────────────┐
        │Flow solution │
        │ computation  │
        └──────────────┘
               │
               ▼
           ◇ Evaluate CFD
    NO      results:
           requirements
              met?
               │ YES
               ▼
        ┌──────────────┐
        │To next component or│
        │  system level │
        └──────────────┘
```
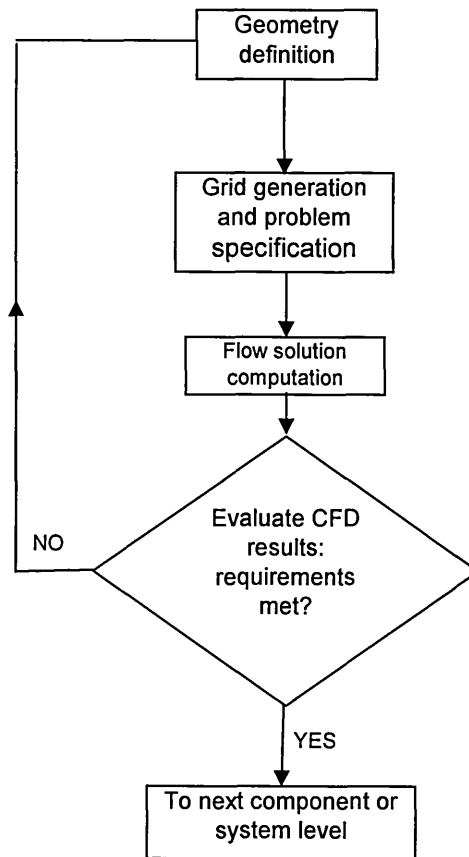
Figure 6.1: CFD procedure flow chart

6.3.1 Geometry definition

CFD simulations require the generation or acquisition of geometric data which describe the bounding surfaces of the actual flow field. This involves the definition of the overall size and shape of the computational domain, and key objects present in the flow field which are later used for attaching boundary conditions relating to friction, contaminants, heat and mass transfer. It is necessary to identify the locations of any supply and extract

terminals, obstructions within the flow field and to define surfaces of differing characteristics. For a particular physical configuration boundary conditions are defined which provide a geometric representation of the boundary surfaces of the three-dimensional computational domain. In recent years, the use of three-dimensional CAD geometry models is increasing as the preferred method for geometric representation. However, a drawback of acquiring geometry in this way is that there may be too much geometric detail to be practical for CFD analysis. Hence, in order to enable efficient use of CFD the correct balance between simplification and accuracy is a key requirement in using CFD software [Cadserver website, *2002*].

6.3.2 Grid generation and problem specification

Before applying CFD calculation methods a computational grid or mesh must be generated that fills the flow domain and conforms to its boundaries. It is the distribution of the grid points in the flow domain that defines the positions where the flow variables are calculated. In addition, the flow rates, velocities and temperatures of the supply air, heat transfer processes occurring at surfaces and within the space, and if required the location and release rates of any contaminants are specified at this stage. The grid is the structure on which the numerical solution is built i.e. it is a set of points to which the partial differential equations governing fluid flow in the domain can be applied. *Grid generation* can be described as the act of specifying the physical configuration to be simulated and dividing it up into a three dimensional mesh containing a sufficient number of small regions known as control volume cells so that the Navier-Stokes partial differential equations can be solved iteratively.

Generally a specified grid must satisfy three requirements:

- It must be compatible with the selected flow solver

- It must be sufficiently fine to satisfy accuracy requirements

- It must be sufficiently coarse to satisfy computational resource limitations

Figure 6.2 shows examples of grids used in CFD calculations.
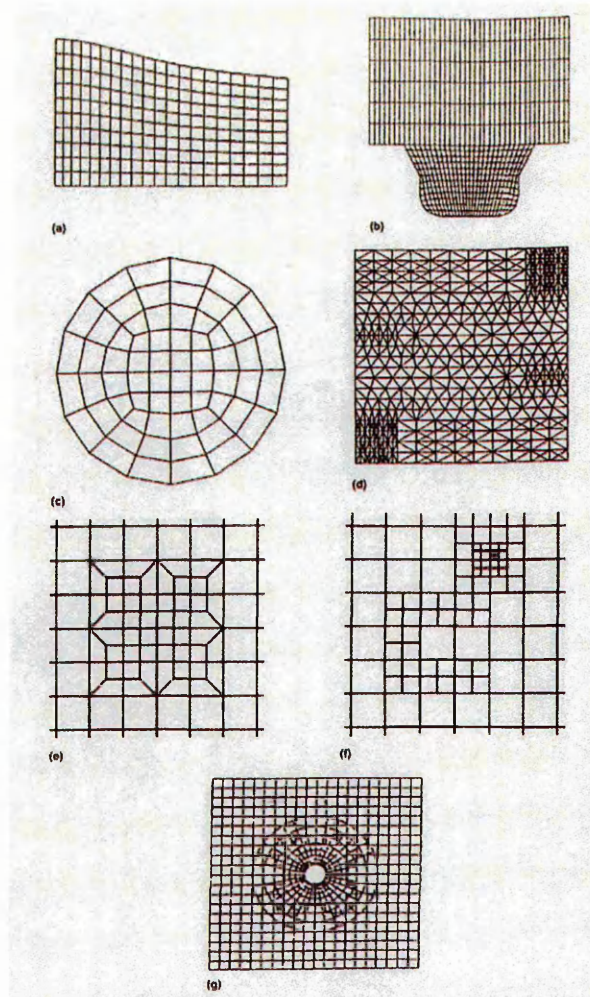
Figure 6.2: Examples of grids used in CFD calculations [A]

[Source: O' Rourke et al, 1997]

Most CFD packages provide the user with inbuilt features to modify the grid to suit the situation being modelled and improve resolution at locations of specific interest. Two types of mesh modification are commonly used, namely *mesh enrichment* and *mesh adaptation*. Mesh enrichment (Figure 6.3) is where additional points are placed within the domain at locations of specific interest. On the other hand, mesh adaptation (Figure 6.4) is where the topology of the mesh stays the same but the mesh points are moved so that the density of points is increased where required.

[A] *Two-dimension examples are shown for clarity. (a) A structured grid. (b) A block-structured grid. (c) An unstructured hexahedral (quadrilateral) grid. (d) An unstructured tetrathedral (triangular) grid. (e) Local mesh refinement via a transition region on an unstructured hexahedral grid. (f) Local mesh refinement via cell splitting on an unstructured hexahedral grid. (g) A chimera grid, [O' Rourke et al, 1997].*
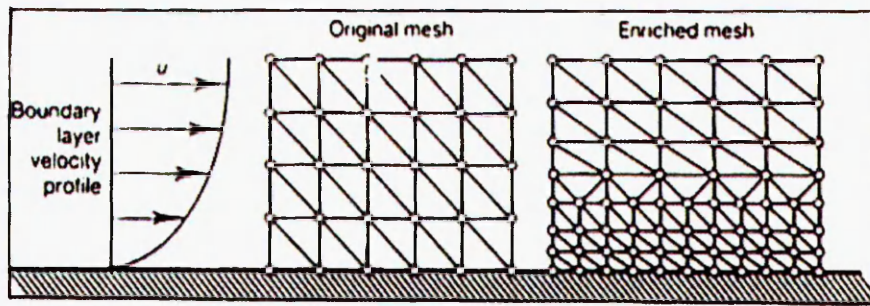
Figure 6.3: Mesh enrichment
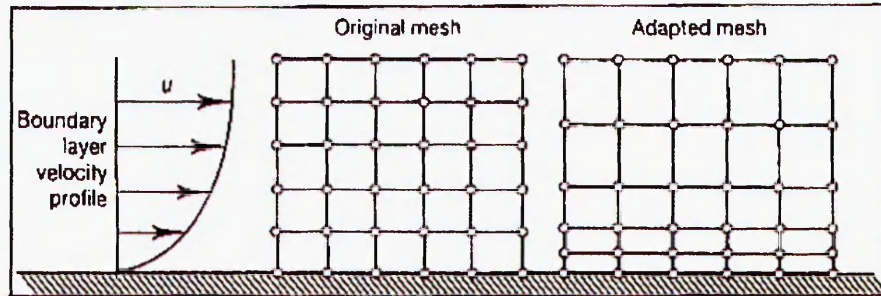
Figure 6.4: Mesh adaptation

The software FLOVENT, used in the present investigation, incorporates such features which are referred to as *localise* and *inflate* functions. Localisation provides the capability to have localised grid spaces associated with objects and regions. Inflation allows the user to specify a grid region outside the limits of the defined grid space which can be particularly useful in controlling near-wall grid sizes. This is helpful when one attempts to capture the gradients associated with the near-wall boundary layer flows or sudden contraction and expansion losses at the inlet and exit of a heat sink [FLOMERICS, *2002*]. The ideal procedure of carrying out a computation is to initially generate a relatively coarse grid to procure a solution fairly quickly and establish some confidence in the modelling and the approach being taken, then to refine the grid to improve resolution and accuracy [Jones and Whittle, *1992*]. Generally, the finer the grid the greater the accuracy of the solution, although a high quality mesh is considered to be one that yields high numerical accuracy for low computational effort (memory and CPU time). This is quantified by performing multiple computations of a single flow configuration using different grids, and computing the error in each with respect to a benchmark numerical or experimental solution.

6.3.3 Flow solution and solution control methods

Application of a mesh and boundary conditions to a computational domain, together with initial conditions and fluid properties, specify the actual flow problem that is to be solved [Shaw, *1992*]. Numerical Simulation is the process of applying a mathematical model to the defined geometrical configuration and then computing a solution. In most CFD codes numerical simulation of fluid flow and heat transfer equations involves the solution of partial differential equations which are linearized to a set of algebraic equations which for the finite-volume method are given by the general form:

$$(a_p - S'_p)\varphi_p = \Sigma_n \, a_n \varphi_n \; + \; S_p \qquad\qquad (6.3)$$

where coefficients $a_n = D_n \alpha(|Pe_n|) + [[0, \pm C_n]]$ and $a_p = \Sigma_n a_n$, indices p and n denote the central computation grid point and its neighbouring points respectively C and D indicate the strength of the convection and diffusion, $\alpha(|Pe_n|)$ is a weighting function, and the symbol $[[a, b]]$ denotes the greater of a and b.

The algebraic equations are solved by code in an iterative manner using a tri-diagonal matrix algorithm and the velocities and pressures are calculated via SIMPLE (Semi-Implicit Method for Pressure Linked Equations) algorithms of Patankar and Spalding (*1972*) [Alamdari *et al. 1991*]. The SIMPLE algorithm provides a means of correcting a computed intermediate pressure (and velocity) field to enforce mass continuity [Jones and Whittle, *1992*]. The solution for each variable will depend upon the solution for each and every variable in the neighbouring cells and vice-versa. Detailed descriptions and derivations of the numerical analysis techniques can be found in standard Numerical Methods text books such as Patankar *[1980]* and Roache *[1998]*. Basically, the solution method is iterative resulting in a set of errors. At the end of each iteration the errors for each variable are summed. A solution is reached when the sums of the errors, from all cells, for each and all the variables, reach a predetermined and acceptable level. It is worth noting that the governing equations are rather complex, as they are non-linear and highly coupled, and can be time-dependent. This means that the possibilities for some error creeping into the solution procedure are great, leading to a simulation that will not converge or to a set of results that are not very good [Shaw, *1992*]. These problems can to some extent be reduced by user experience. On the other

hand, CFD software codes contain a number of techniques both automatic and manual, which can be used to monitor the progress of the solution and take any action necessary to improve both convergence rate and quality of results. These include false time step relaxation, linear under relaxation, successive over-relaxation, temperature block correction and the conjugate gradient solver. Descriptions and application of these methods can be found in user handbooks and application manuals of the relevant software. Further, by looking at the results produced it is possible to see if a simulation is a good one. If it is not then the flow specification might be incorrect, or the mesh might not be suitable for the flow being modelled, or a conceptual mistake could have been made at the beginning of the analysis process.

6.3.4 Post processing and synthesis

When some results have been obtained they must be analysed, first to check that the solution is satisfactory and then to determine the actual flow data that is required from the simulation. CFD analyses generate so much data that, quite often, the only way of analysing it over the whole domain is to use some form of graphical representation. As such, good quality graphics-based post processing diagnostics are needed to extract relevant physical information from the vast quantity of numerical data. Viewing and making sense of vast quantities of three dimensional data that are generated in CFD is comparatively a challenging task. Many software packages have been developed for this purpose, both for structured and unstructured grids. In general all provide considerable flexibility in setting model orientation, in passing cutting planes through computed solution, and in displaying the computed vector and scalar fields. Such direct inspection of the computed fields provides detailed insight into flow structure in the same sense as a high resolution flow visualisation experiment. An attractive element of CFD solutions is that the generated fluid flow information includes visual representation of pressure distribution and velocity fields (such as those shown in Figure 6.5 and Figure 6.6) within the flow domain. The visual representation of the pressure distribution and velocity field provides vital information in revealing patterns that would otherwise be very difficult to discern if presented in the form of strings of digits.

Velocity Vectors at X = 1.16 m
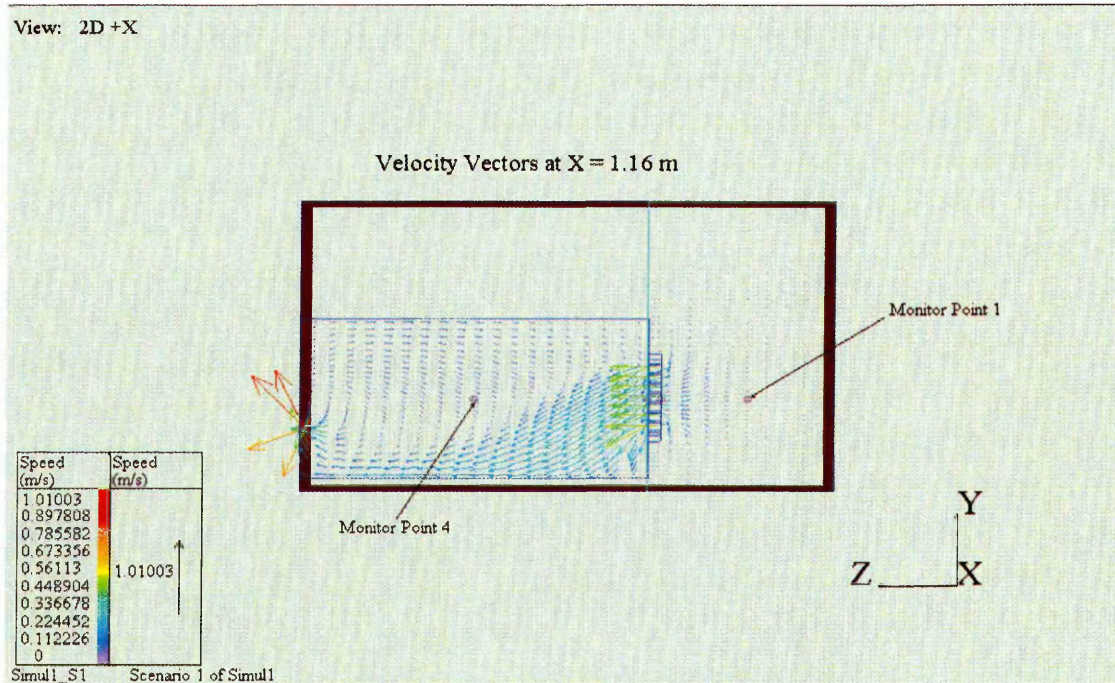
Figure 6.5: Example velocity vectors from CFD simulation

Velocity Contour at X = 1.16
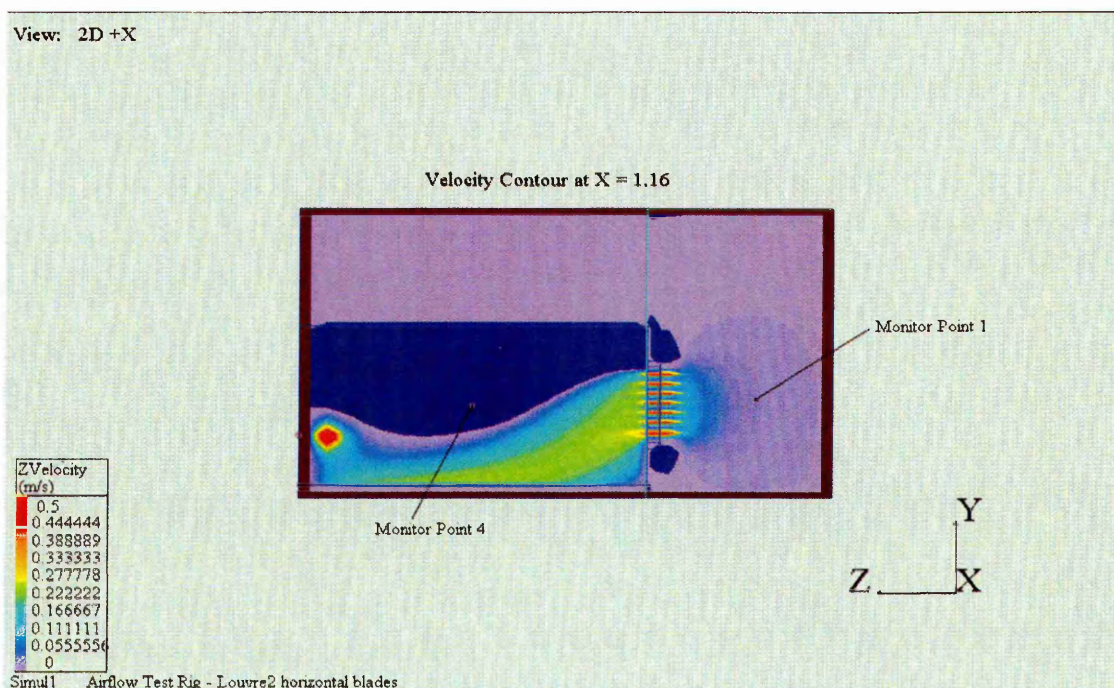
Figure 6.6: Example velocity contour from CFD simulation

Note: Figure 6.5 and Figure 6.6 were obtained from an early pilot study by the author on CFD modelling of airflow through wooden ventilators with horizontal blades.

6.4 Application of CFD to airflow in/around buildings

The movement of air in and around buildings has a major influence on a wide range of issues including comfort, health and safety, and on the efficiency and effectiveness of space heating, cooling and ventilation. The prediction and engineering of air movement is a complex subject. Physical modelling has traditionally provided means of evaluating air movement in and around buildings although in many cases cost and time-scale preclude its use. Recent years have seen increasing application of CFD as a tool for prediction of airflow as it appears to offer a competitive and more flexible alternative [Jones and Whittle, *1992*]. This has mainly been attributed to the cost of computer hardware always reducing while its performance is increasing and software is becoming more user-friendly. The use of the CFD method to simulate air movement in buildings has contributed to the understanding of flow features in buildings [Lu, Howarth and Jeary, *1997*].

CFD applied to airflow within buildings has the potential to predict detailed velocity, pressure and temperature distributions from which interpretations relating to thermal comfort and energy use can be made [Jones and Whittle, *1992*]. Predictions of chemical species/contaminant distributions can lead to interpretations relating to indoor air quality and ventilation efficiency. On the other hand, data relating to heat transfer processes can lead to interpretations of the effectiveness and efficiency of energy distribution in the occupied space. It is believed that the study by Nielsen in the mid-1970's, of flow in conditioned rooms was one of the first to predict air movement and heat transfer in buildings using CFD methods [Jones and Whittle, *1992*, Weathers and Spitler, *1998*]. More recently, CFD methods have found application in a variety of investigations including bulk air movement, thermal comfort, indoor air quality in rooms [Ata *1997*, Ayad *1999*, Jiang and Chen *2001*], natural ventilation of enclosed spaces [Fracastoro *et al. 2000*, Alloca *et al. 2003*], impact of airflow profile on indoor air quality [Sekhar and Willem *2004*], and studies relating to the movement and distribution of aerosols particles/contaminants [Lu and Howarth *1996* and Howarth *et al. 1997*]. A limitation in this regard is that in most of these computational approaches emphasis has been placed on simulating the airflow in and/or around buildings, while airflow through ventilator components (especially in natural ventilation applications) has received relatively little attention.

6.4.1 Assessment of CFD use as tool in airflow investigations

During the early adaptation of CFD to the Building Services industry, many models were set up to assess the suitability of application of CFD to the building environmental design. For instance, Jones and Whittle [*1992*] investigated issues in the context of the status and capabilities of CFD simulation of airflow within buildings, and identified the positive benefits that CFD could contribute to the design and evaluation of the indoor environment. The use of CFD in airflow investigation has also been recommended from the point of view of the contextual complexity of the actual physical phenomena and methods have been suggested e.g. Iannone *[1999]* which allow projects to evolve in small increments beginning at the idea stage whilst at the same time considering the relation between building form, fluid dynamics and the indoor environmental performance of the system. Some studies such as Holmes and Whittle *[1987]* have reviewed some of the problems associated with the application and validation of CFD codes and highlighted some suggestions of how a user can ensure that the physical processes are being modelled realistically. More recently, CFD is finding wide spread application to the study of natural ventilation related phenomena. Fracastoro *et al [2000]* investigated and verified the applicability of CFD transient 2-D analysis to a simple, yet complex, phenomenon of thermal and fluid dynamic fields resulting from the mere action of indoor-outdoor temperature difference following the opening of a window in a single-side ventilated enclosure. A common problem highlighted in many of the studies employing computer tools to evaluate physical phenomena is a lack of reliable data which can be used for validation of the proposed methods.

6.4.2 Natural ventilation airflow studies employing CFD

Natural ventilation contributes to a sustainable environment by reducing energy use in buildings. During the past few years, many studies on natural ventilation have been undertaken utilising CFD to investigate certain features, such as its driving forces [Straw *et al. 2000*, Alloca *et al. 2003*], flow characteristics [Etheridge, *2000*], air movement and distribution of CO_2 in naturally ventilated offices [Awbi, *1996*] or even large spaces such as atria [Alexander *et al. 1996*, Awbi, *1996*, Kato *et al. 1995*]. Cockroft and Robertson [*1976*] studied wind-driven ventilation through a single opening subjected to a turbulent impinging air stream, neglecting buoyancy effects. They derived a simple theoretical wind model to predict this type of airflow. The model

was then compared with experiments from a full-scale model. The results from this study, however, only provided an indication of the magnitudes of airflows that wind may generate and concluded that further analysis and experiments were needed. Buoyancy driven convective heat flows have also received some attention from researchers for example Lu, Howarth and Jeary [*1997*] used CFD to predict a three-dimensional airflow field and temperature distribution in a full-scale enclosure and validated the predicted parameters by measured data from an independent study carried out by one of the researchers [Howarth, *1985*]. The simulated and observed airflow patterns and temperature fields showed good agreement. On the other hand CFD has not always been successful in predicting natural ventilation physical phenomena. An example can be found in Dascalaki *et al. [1999]* where amongst other techniques, CFD failed to accurately describe local turbulent motion resulting from the non-uniform pressure difference distribution at the level of the opening in the case of single-sided ventilation. They indicate that the uncertainty in the definition of boundary conditions as well as spatial and temporal variations due to the turbulence models employed in CFD codes limited the accuracy of the results.

6.4.3 Problems associated with the use of CFD

Although CFD can quickly and easily be utilised to predict airflow and to carry out parametric studies, its accuracy and quality of results rely heavily on accurate setting up of the simulation model and specification of boundary conditions governing the flow field. Whilst various studies [Holmes and Whittle *1987*, Peppes *et al. 1997*] have highlighted problems associated with setting up and running CFD simulations, a few [Holmes and Whittle *1987*, Huo *et al. 2000*] have also offered advice and solutions for overcoming some of the difficulties encountered in the application of CFD techniques in building ventilation. Gosman [*1999*] provides an overview of the capabilities and limitations of CFD and acknowledges that although it is already being used for diverse applications in the built environment, CFD's full capabilities and potential are still far from being exploited. Further, it is essential to carry out sensitivity analyses to ensure that the resolution of the flow mesh is not influencing the results. However, at present there is a lack of grid convergence studies and no uniformity in the reporting of results achieving grid-independence.

Perhaps the most important consideration is the selection of boundary conditions, which can have a major impact on the results. Therefore, it is necessary to validate CFD results and to conduct more CFD studies on boundary conditions.

6.5 Review of Application of CFD to Airflow through Openings Research

As far as the CFD study of airflow performance of ventilators and their associated components for natural ventilation applications is concerned, in addition to there being very little information available in the literature, validation studies comparing CFD and physical model testing are very rare. This section presents an overview of the studies available in the literature on the application of CFD in investigations of the airflow performance of ventilation openings. In particular a few of these studies that contributed to the direction and procedures of this investigation are outlined and commented up on to some greater detail.

Early airflow studies through ventilator components concentrated mainly on flows through horizontal inter-zonal openings. For instance, Peppes *et al. [1997]* employed a CFD code utilising the finite-volume method and incorporating a low-Reynolds k-ϵ two equation turbulence model to simulate the cases undertaken in the study. Comparison between the experimental data and their simulation results was reported as encouraging agreement despite difficulties related with turbulence models, geometry, experimental errors and detailed determination of boundary conditions. Their investigation highlighted a lack of studies with respect to natural convective conditions and indicated that very few systematic experimental data are available in the literature. They also pointed to some difficulties encountered in relation to convergence and simplification of boundary conditions, and proposed further investigations of these factors to enhance the accuracy of the model.

Some practitioners such as Fracastoro *et al. [2000]* have undertaken transient analysis of natural ventilation provided by a single opening when only indoor-out door temperature differences are present. Their study employing FLUENT software verified the applicability of CFD transient 2-D analysis to a simple, yet complex phenomenon such as the evolution of thermal and fluid dynamic fields following the opening of a window under the mere action of indoor-outdoor temperature difference. Experiments

were also carried out on a naturally (single-side) ventilated enclosure with only thermal effects taken into account. The CFD results (after correction) were found to agree with other engineering models.

Only a few studies e.g. Southall and McEvoy *[2000]* have been reported that have investigated operation of ventilator openings under various conditions including different configurations. However, limited progress has been made in analysing different component contributions to the overall airflow performance of ventilators. This is a consequence of the lack of sufficient experimental data which can be used for validating the numerical results. Perhaps the work of Sharples and Maghrabi *[2000]* on modulated louver windows can be regarded as the closest attempt to apply CFD methods to a louver system similar to the ones used in this study. In their investigation, Sharples and Maghrabi *[2000]* undertook CFD simulations of different wooden louver configurations and successfully predicted air velocities in the region close to room side of the louvers. They employed the k-ε turbulence model and indicated the need for further CFD simulations and the need to identify appropriate boundary conditions. An extensive literature search revealed a lack of information on the use of CFD to investigate the interactions between components in a ventilator. Consequently, in a pilot study of interactions between airflow components Sharples and Chilengwe *[2001]* investigated the suitability of using CFD to predict the impact of mesh-screens and louvers on the overall airflow performance of ventilators. In this study louvers similar to the ones used by Sharples and Maghrabi were modelled using the FLOVENT software. Although differences between experimental and CFD predicted parameters were found to be quite large (up to 34%) the study highlighted difficulties in prescribing suitable boundary conditions associated with modelling mesh-screens so as to achieve full-convergence within reasonable simulation time scales. This pilot study formed a basis for future investigations which were subsequently extended to commercial aluminium louver systems. The details of these investigations are presented in *Section 6.8* of this thesis.

6.6 Description of the Simulation Model

A CFD model is a predictive tool that enables engineers and researchers to analyse the climatic conditions within and around buildings. The objective of the analysis is basically to understand the flow pattern, air velocity, temperature distribution, smoke or

airborne contaminant concentration and movement, pressure distribution etc which then enables the design to be improved [Alamdari and Seymour, *1993*]. Numerical simulations offer a detailed picture of the temperature spatial distribution and the airflow field. This data can be used for analysing the contribution of various components in a ventilator to the general ventilating performance of the ventilator. In this investigation the modelling and simulations were carried out using the software FLOVENT. The main reasons for selecting the FLOVENT software were:-

i) It is an established package that was originally developed specifically for building services applications and has since been widely used by industry and for research

ii) The author's familiarity and experience of using FLOVENT in the Design Industry

iii) Availability of FLOVENT software on site at the time of commencement of the present investigation

The following sections describe the role of FLOVENT in the investigations of this thesis in addition to explaining some key aspects of how the model was developed.

6.6.1 FLOVENT modelling and its role in this research

Simulation of heat and airflow in FLOVENT involves solving of the fundamental conservation equations for mass, momentum and energy using the finite volume technique, based up on a structured Cartesian co-ordinate system. Like many airflow simulation commercial CFD tools FLOVENT incorporates a pre-process (*drawing board*), a solver and post-processor (*visualisation*) module arrangement collectively referred to as the "project". The pre-processor handles all tasks that take place before the numerical solution process is started. This includes setting up of the geometry of the flow problem, grid generation, specification of initial and boundary conditions, setting up of fluid and material properties, and numerical control parameters. The solver is the part of the program that solves the numerical equations for the problem under consideration. Although the operation of the solver program is little seen by the user, it is the core of any CFD software system as it contains sequences for data transfer and storage allocation, formulation of the finite volume equations, iterative solution of finite

volume equations, termination of iterations and output of the results. The post processor, as mentioned earlier, facilitates graphical viewing of the results. As a large number of points is created within the flow domain and several variables are stored at these points, computer graphics are often the most useful means of displaying results such as velocity vectors and contour plots of scalar variables such as pressure. In FLOVENT the various modules can easily be accessed and controlled from a structured Project Manager module. Detailed descriptions of each module and how they operate can be found in FLOVENT online documentation (www.flovent.co.uk) and other application manuals such as the [FLOVENT software Lecture Notes, *2001*]. In this investigation FLOVENT was used for three main functions, namely:

- To examine the basic performance of ventilators by carrying out computations on some commercial ventilators
- To investigate and explore the effect of mesh-screens by undertaking computations for different mesh-screen free-areas i.e. operating conditions of ventilators (*initial and boundary conditions*)
- To show a possible direction of using CFD to optimise the performance of ventilators by varying some parameters and then comparing the obtained results with those of the other cases

6.6.2 Simulation model domain and adopted grid

Generally, the computational domain consisted of a wind tunnel to represent the actual plenum chamber on which experimental measurements were carried out. The wind tunnel had a fixed flow outlet of 100% free area at one end coinciding with the domain boundary; an intermediate solid partition into which various ventilators were inserted; and an open face inlet located on the domain boundary at some distance away from the partition. Location of the inlet in this manner enabled FLOVENT to establish its own boundary conditions at the ventilator inlet face. In addition it represented the airflow resulting from fan pressurisation/depressurisation when the fan was operating at a given speed and was used to vary the airflow rate through the ventilators. The sides of the wind tunnel were assumed to be far enough from the ventilator so as not to influence the airflow through the ventilator. These were modelled as symmetry boundaries hence there was no need to specify friction in addition to computational savings being made by avoiding fine grids at the wind tunnel walls. Monitor points were included in the

base model to represent pressure sensors/probes used during the experimental measurement phase. It is at these monitor points that parameters were obtained in order to assess the airflow characteristics of the ventilator components. Specific elements of the computational domains and the computational grid systems used in the simulations for each case study are described in the relevant sections below. Because the grid is a discrete representation of the continuous field phenomena, the accuracy and numerical stability of simulation depends on the choice of grid. To assess the grid dependency of the computational results comparisons were made of selected parameters for a number of grid densities for each ventilator type. Details of the grid sensitivity assessments are given in the relevant sections below.

6.6.3 Boundary conditions

When solving any system of partial differential equations it is the boundary conditions, together with the initial conditions specific to the problem at hand, that determine the exact solution. Some common boundary conditions are met when solving fluid flow problems with computers. These include velocity profiles, which will affect the momentum equations, pressure and mass flow which generally influence the continuity equation, and turbulence variables such as the turbulence kinetic energy and its rate of dissipation. These conditions have to be applied at a variety of boundaries such as solid walls, inlets, outlets and symmetry boundaries. A complete problem prescription for CFD thus requires, in addition to geometry and grid definition, the specification of initial and boundary conditions for all flow variables, fluid properties, and any model and numerical parameters. The accuracy of any CFD output is extremely sensitive to the assumptions made about the initial conditions and boundary conditions. Because both geometry and grid information are available at grid generation stage, this is the most natural time to assign values for initial conditions and material properties and surfaces for boundary conditions (e.g. specify which surfaces represent walls, inflow boundaries etc.). For natural ventilation in the real world these conditions are difficult to establish due to the random fluctuations in the ambient air temperatures and wind pressures. Therefore, laboratory studies are an important first step in establishing appropriate boundary conditions for CFD application in ventilation analysis. The laboratory environment is much more controllable, making it possible to investigate the suitability of assumptions made regarding ventilator boundary conditions.

6.6.4 Turbulence model selected for application in this research

It was stated earlier in this chapter that the effects of small scale unresolvable features of the large-scale average flow features of interest are in CFD modelled through modifications to the governing partial differential equations, through *turbulence models* with a penalty of necessarily introducing imprecision. There are four turbulence models available in FLOVENT for simulating turbulent fluid flow, *namely revised algebraic*, *LVEL algebraic*, *two-parameter* $k - \varepsilon$ and *revised two-parameter* $k - \varepsilon$. The revised $k - \varepsilon$ model (with turbulent constants left at FLOVENT default settings) , selected for application in this investigation following discussions with FLOVENT user-support team, calculates the turbulent viscosity for the cells not immediately adjacent to solid surfaces as a function of the kinetic energy of turbulence (k) and its rate of dissipation (ε). The two field variables are determined by the solution of two additional differential equations which these variables satisfy [FLOVENT online documentation - Turbulence, *2003*]. In addition the literature review indicated that the $k - \varepsilon$ model is the most widely used [Jones and Whittle, *1992*] and most widely validated method [Southall and McEvoy, *2000*] to represent turbulence for most building related applications.

6.6.5 Validation of simulation method

Various stages of the CFD analysis process have been described in *Section 6.3*. This section demonstrates how the whole process is used to produce a CFD simulation. The work in this section was used as validation for modelling and simulation using FLOVENT in addition to gaining some confidence that the program produces accurate results compared to known analytical solutions. A *simple flow between parallel plates* (see *Section 3.7.4*) was modelled and simulated in FLOVENT, and the results were compared with those generated by Shaw *[1992]* using a different commercial software package called PHOENICS. PHOENICS (also used by Chilengwe, *[1994]*) has been available since 1981 and is written by CHAM Ltd of Wimbledon (England). It is a CFD software package which, like FLOVENT, uses a finite volume method to solve the governing equations on a staggered grid which has a regular topology.

FLOW SPECIFICATION

Two thin parallel plates of length L (m) and distance h (m) apart were placed horizontally in a flow which, well upstream of the plates, has a constant velocity in the horizontal direction (Figure 6.7).
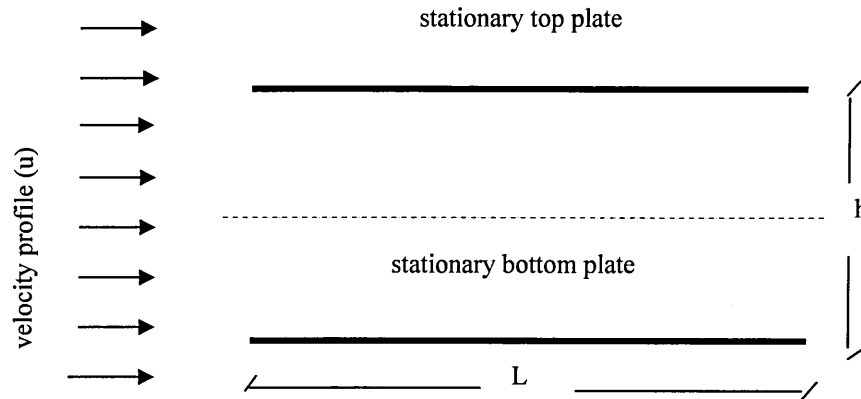
Figure 6.7: Specification of flow between parallel plates

The following assumptions were taken:-

- the plates are so thin that flow ahead of the plates is not affected by them

- flow above the top plate and below the bottom plate is not considered

- the plates are both stationary solid walls

- the flow is steady-state

BUILDING A MESH

A mesh must fit within the domain in such a way that the variations in flow variables can be calculated as accurately as possible. For the flow situation considered, there is a boundary layer on each of the plates due to shearing of the fluid caused by friction. In addition at some distance downstream of the inlet the flow becomes fully developed and is effectively one-dimensional. In the vertical direction, between the plates the velocity profile is parabolic at the outlet and so it varies throughout the vertical distance. An initial grid with 10 cells equally spaced between the lower plate and the symmetry plane, and 10 cells down the length of the plates (similar to Shaw, *1992*) was used. Along the length the grid was biased with more cells placed near the inlet in order to capture the rapid changes in velocity at the inlet. To improve the accuracy of the results

-158-

and to ensure grid-independence a total of 420 cells was used in the final FLOVENT model.

BOUNDARY CONDITIONS

The distance between the plates was taken to be 1 m and the length of the plates to be 20 m, hence the computational domain was 0.5 m high (taking symmetry at the centre line between plates). The properties of the system fluid also needed specification. For simplicity, the density was taken to be 1 kg/m^3 and the absolute viscosity was 1 kg/ms.

ANALYTICAL SOLUTION

When the flow is fully developed the Navier-Stokes equation can be simplified. If the flow is steady and has the velocity characteristics given above, then the momentum in the direction of flow (x-momentum) can be written as (see also *Section 3.7.4*):

$$-\frac{\partial p}{\partial x} + \frac{\partial}{\partial y}\left(\mu\frac{\partial u}{\partial y}\right) = 0 \qquad (6.5)$$

and the vertical momentum (y-momentum) can be written as:

$$\frac{\partial p}{\partial y} = 0 \qquad (6.6)$$

Equation (6.6) shows that the pressure is a function of x only and so when Equation (6.5) is integrated with respect to y the pressure derivative can be taken to be a constant. This gives:-

$$\mu\frac{\partial u}{\partial y} = \frac{\partial p}{\partial x}y + A_1 \qquad (6.7)$$

where A_1 is a constant or a function of x only. Further integration with respect to y gives:-

$$\mu u = \frac{\partial p}{\partial x}\frac{y^2}{2} + A_1 y + B_1 \qquad (6.8)$$

where B_1 is also a constant or a function of x.

The values of A_1 and B_1 can be determined by applying boundary conditions for the velocity at the two plates. Now, the horizontal velocity component u is zero at the plates i.e. u = 0 at y = 0 and y = h, where h is the distance between the plates, and so Equation (6.8) becomes:-

$$\mu u = \frac{\partial p}{\partial x}\frac{y^2}{2} - \frac{\partial p}{\partial x}\frac{hy}{2} = \frac{y}{2}(y-h)\frac{\partial p}{\partial x}$$

(6.9)

which describes a parabolic velocity profile (see also *Section 3.7.4*).

The mass flow in and out of the system can now be calculated. For an inlet velocity of 1 m/s and a density of 1 kg/m^3, the mass flow per unit area is simply h and this must be the mass flow at the outlet too. Integrating the velocity expression in Equation 6.9 to obtain mass flow at the outlet:

$$h = \int_{y=0}^{h} u\,dy = \frac{1}{\mu}\left\{ + \frac{\partial p}{\partial x}\frac{h^3}{6} - \frac{\partial p}{\partial x}\frac{h^3}{4} - \right\}$$

(6.10)

which can be rearranged to give an expression for the pressure gradient:

$$\frac{\partial p}{\partial x} = -12.0\frac{\mu}{h^2}$$

(6.11)

Equation (6.11) enables the pressure gradient for a fully developed flow to be found for a given mass flow rate, and this can be used in Equation (6.9) to give the fully developed velocity profile for the same flow. These quantities were then compared with the values calculated by the CFD program. Near the outlet (velocity field is fully developed and flow is one-dimensional) the exact values of the pressure gradient and the velocity profile can be determined. From Equation (6.11) substituting for the viscosity and domain height, the pressure gradient was found to be:

$$\frac{\partial p}{\partial x} = -12.0$$

(6.12)

and the velocity profile was found from Equation (6.9) as:

$$u = 6.0(y - y^2)$$

(6.13)

-160-

Validation of the FLOVENT modelling/simulation for this investigation was on the basis of obtaining good agreement between the FLOVENT predicted values, analytical solution and also Shaw's PHOENICS results.

RUNNING THE NUMERICAL SOLUTION

Apart from setting the number of iterations for the simulation, all other numerical solution control parameters such as termination residual values were automatically determined by the software. A converged solution was obtained in under 1300 iterations within a time frame of about 5 minutes on a Toshiba P4 laptop.

SIMULATION RESULTS

From the converged simulation the following was found:-

- Using the pressure field data, the pressure gradient near the outlet was determined to be -12.21 and -12.11 near the symmetry plane (y = 0.475 m) and near the bottom plate (y = 0.025 m) respectively. This compares well with the value (-12.55) obtained by Shaw using PHOENICS and also the analytical solution i.e. -12.0.

- As can be seen from Figure 6.8 the velocity profile develops into a fully developed profile moving downstream from the inlet, in line with the expectations.

- The closeness of the FLOVENT simulation results to the analytical and PHOENICS solutions can be judged from Table 6.1 showing the x-velocities at the outlet. The results in Table 6.1 show that there was only a small error, which was worse near the plate and difference between the three schemes being too small for a useful graphical comparison.
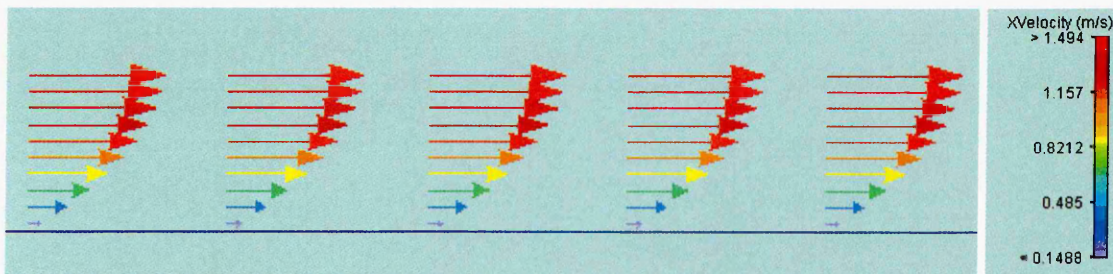
Figure 6.8: Part FLOVENT results showing fully-developed parabolic velocity profile

y	analytical (va)	PHOENICS (vp)	FLOVENT (vf)	$\left(\dfrac{va-vf}{va}\right)(\%)$	$\left(\dfrac{vf-vp}{vp}\right)(\%)$
0.025	0.146	0.109	0.149	-2.26	26.99
0.075	0.416	0.388	0.418	-0.46	7.15
0.125	0.656	0.639	0.657	-0.11	2.70
0.175	0.866	0.858	0.866	0.03	0.89
0.225	1.046	1.047	1.045	0.10	-0.19
0.275	1.196	1.204	1.194	0.17	-0.84
0.325	1.316	1.329	1.313	0.23	-1.22
0.375	1.406	1.423	1.403	0.21	-1.43
0.425	1.466	1.486	1.463	0.20	-1.57
0.475	1.496	1.517	1.492	0.27	-1.68

In a way, the excellent agreement shown by the results was not surprising, because a very simple flow problem was used. On the other hand, simple as the problem was, it served its function of demonstrating the CFD analysis process and also provided a confidence-basis for further modelling and simulations undertaken in this investigation.

6.7 Steady-State Simulations of Airflow through Slots

This section describes and presents details of steady-state simulations that were conducted on the airflow through simple slots of varying dimensions (described in *Section 5.3.1*). Basic CFD simulations where conducted in 3-D and for flow only (with thermal calculations disabled) on full-size slots with and without a mesh-screen (described in *Section 5.3.1*). The simulations were carried out using FLOVENT which was used as a numerical wind tunnel. The intent was to compare the computational results with some of the experimental findings detailed in *Chapter 5*.

6.7.1 Case study I: Ordinary slots of varying depths

SIMULATED CASES

A computational study was conducted of the airflow through slots of fixed height (12 mm) and fixed width (300 mm) but varying depths (Type B slots) over a range of pressure differentials typical in natural ventilation applications. Six configurations of slots without a mesh -screen were investigated to simulate the operation of the actual Type B slots used in the experimental study (*Chapter 5*). The analysed cases are tabulated in Table 6.2 together with key boundary conditions used during the simulations.

It was necessary to investigate variable depths of the slots as variation of depth in actual ventilators contributes to the length of flow path and hence the total resistance to airflow across the ventilator. Therefore, it is important to understand what impact the depth of the ventilator has on the airflow performance. It follows therefore that it is important to assess and determine the optimum depth of the ventilator, although this to a large extent is dictated by the site conditions i.e. thickness of wall/partition into which the ventilator is to be installed. The depth of a ventilator can be critical in natural ventilation applications where the pressure differentials driving the flow are relatively low (typically less than 10 Pa). This computational study attempted to understand how the airflow performance varies in relation to the depth of slots.

Table 6.2:
Simulated cases for slots of varying depth

Case No.	Slot Reference	Slot depth (mm)	Slot height (mm)	Boundary Conditions	
				Airflow Rates (m3/s)	Mesh-screen
1	B6	36	12		
2	B5	30	12	For each case at least 7 levels of airflow rates in the range 0 - 0.0105m^3/s were simulated. This range of flow rates covered the ΔPs typical in experimental findings.	slots modelled without mesh-screen
3	B4	24	12		
4	B3	18	12		
5	B2	12	12		
6	B1	6	12		

COMPUTATIONAL DOMAIN

A three-dimensional computational domain was used to predict differential pressures across the slot for a range of airflow rates through it. The model used for the simulations consisted of a uniform velocity profile inflow at one end of the domain and a static free stream opening at the opposite end to represent the outflow boundary. The complete computational domain of the model is shown in Figure 6.9.

Figure 6.9: Computational domain for variable depth slots

For each configuration the simulation model included a fixed flow smart part (inlet) to facilitate varying of the airflow rate. The slot was represented by a gap between two solid cuboids which were configured to represent the height and depth of the actual slot being modelled. Simulation airflow rates were set to match those from corresponding experimental tests after correction to standard temperature and pressure. The primary data produced from these simulations were pressure differentials (along the central Z-plane) which were later (*Chapter 7*) used for comparison with experimental results.

GRID

The solution was initially developed on a coarse grid that contained one half of the grid points of the fine mesh in the flow (X) and cross-flow (Y and Z) directions. Once the solution converged on the coarse grid, it was resolved with a medium grid that included one quarter more of the grid points in both flow and cross-flow directions. After convergence was obtained on the medium grid, the solution was refined and converged on the fine grid shown in Figure 6.10. The fine grid was set with spacing decreasing upstream of the slot and increasing downstream of the slot whilst being kept uniform vertically. A refined mesh was necessary near, and on either side of, the slot because in this area large gradients of the solution variables were anticipated. The fine grid contained approximately 82000 cells. Grid sensitivity results are discussed in Sub-section "Simulation Results and Analysis" below.
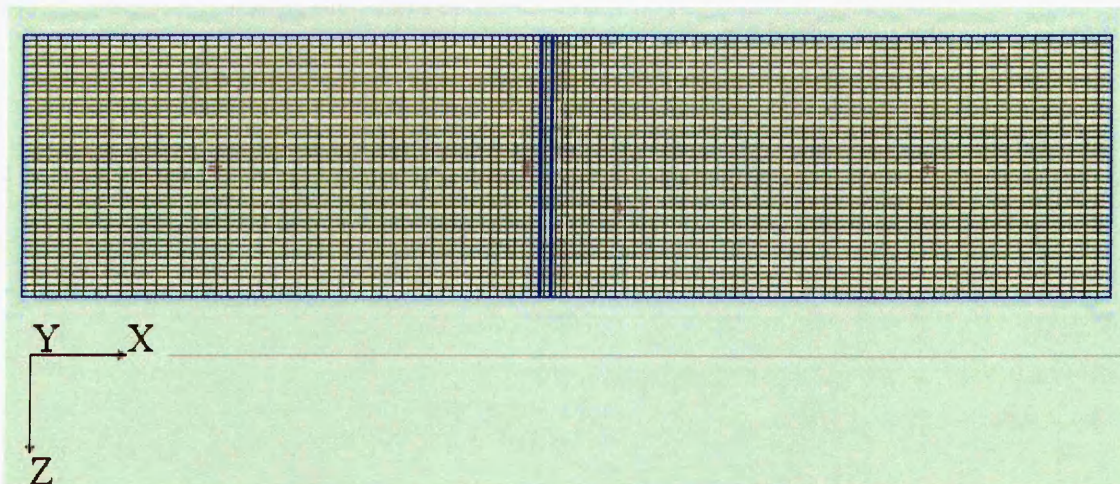
Figure 6.10: Computational (X-Z plane) fine grid for slots of varying depth

NUMERICAL SOLUTION

Computational simulations were run through a range of flow rates resulting in ΔPs typical of the experimental conditions. Power law regressions of experimentally measured data on the slots (*Chapter 5*) resulted in power law indices close to the value 0.5. From the theory, this suggests a turbulent nature of flow and as such the simulations were solved for turbulent as opposed to laminar flow. This approach to modelling provided information about the flow characteristics of the slots and a good estimate of performance quantities. The execution time was about 140 minutes for each case solved on a Toshiba P4 laptop with 1.7 GHz processor speed and 512 MB RAM. The pressure data produced by FLOVENT were absolute pressures within each cell. In this investigation it was the pressure differences across slots that were important and this was the parameter used for comparison with experimental results. In addition airflow information from the simulations included visual representation of the pressure distribution and velocity field in the computational domain.

SOLUTION CONTROL AND CONVERGENCE

In the simulations 2000 - 3000 iterations were allowed for each case. A solution performance and residual history were used to monitor convergence as the solution developed at each grid level. Most cases simulated achieved full convergence whereby *the residual errors in the transport equations reached an acceptably low-level [FLOVENT Manual, 1999] calculated automatically by the code*. A typical solution history for a fully converged case is shown in Figure 6.11.
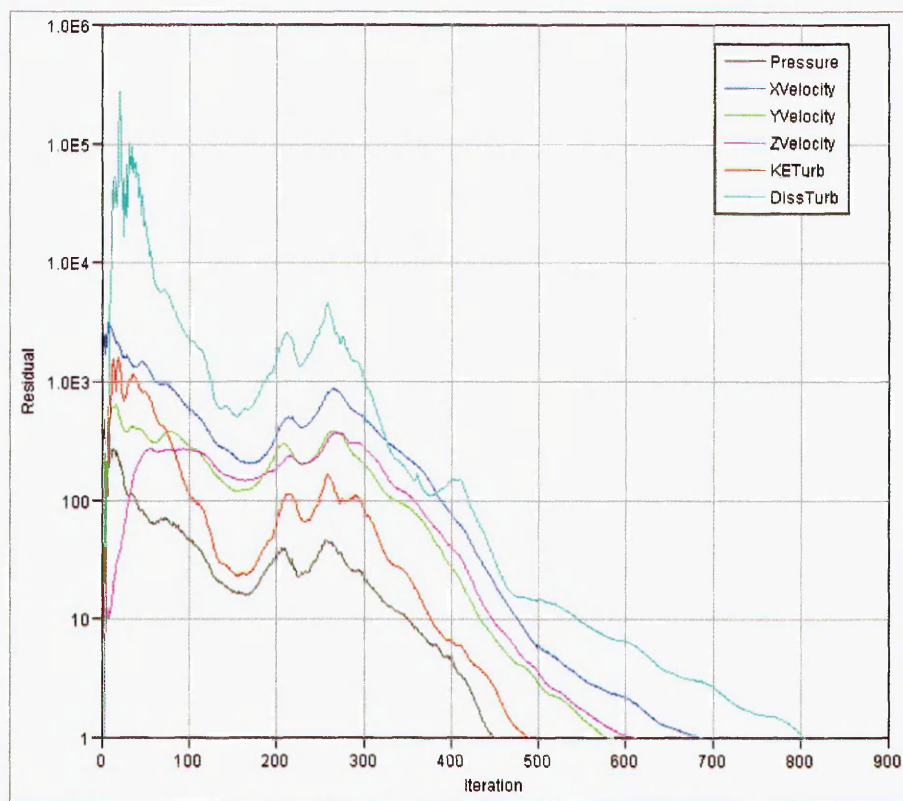
Figure 6.11: Typical fully converged solution history for slots of varying depth

However, a few cases of slots modelled at airflow rates below 0.002m³/s did not achieve full convergence as defined above but rather settled to an oscillating residual that could not be reduced through further calculations, variation of relaxation factors or other solution control options. For these cases a secondary convergence criteria was used to assess convergence as advised by and following discussions with the FLOVENT User-support team. This secondary convergence criteria required the *error residuals to drop 3 - 4 orders of magnitude and that variables at monitor points achieved stable values and variation between iterations for solved variables were small enough to be neglected.*

A typical oscillating solution convergence history is shown in Figure 6.12. In all oscillating solution cases the secondary convergence criteria was met. For instance in the example shown in Figure 6.12 the oscillating residuals dropped 5 orders of magnitude and remained nearly constant for 1200 iterations beyond the point where the residual error in the other variables had dropped to the full-convergence level.
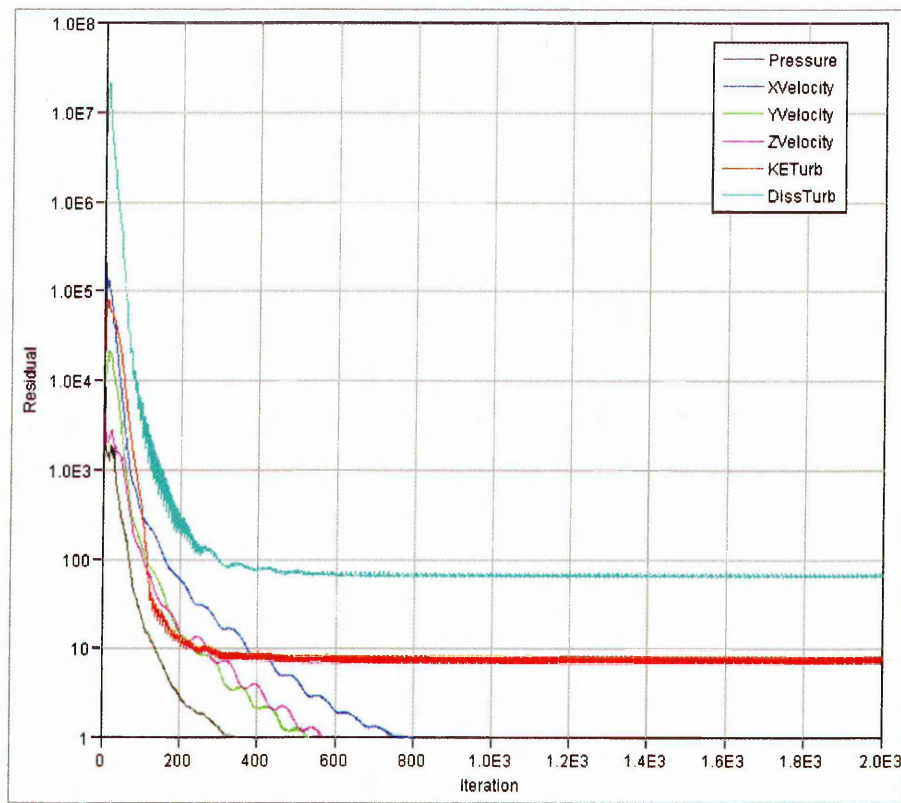
Figure 6.12: Typical oscillating solution convergence history for slots of varying depth

This phenomenon was interpreted as representing the unstable nature of flows being simulated and an inadequacy in the simple simulation model in accurately resolving the turbulence occurring in the actual physical situation. Hence it was accepted as such rather than as an indication of an error in code or data input to the model. In all cases no adjustments to false time-steps were required in the simulations.

SIMULATION RESULTS AND ANALYSIS

A grid mesh and solution convergence study was conducted for selected computational simulations. The grid sequencing (coarse, medium, fine) was used to estimate the dependence of the solution on the grid density of the computational domain. A grid sensitivity study for the solutions developed at low, medium and high flow rates is included as a representative example of the evaluation of solution dependency on grid density completed for each computational case. Predicted pressure differentials at each grid density level are shown in Figure 6.13.
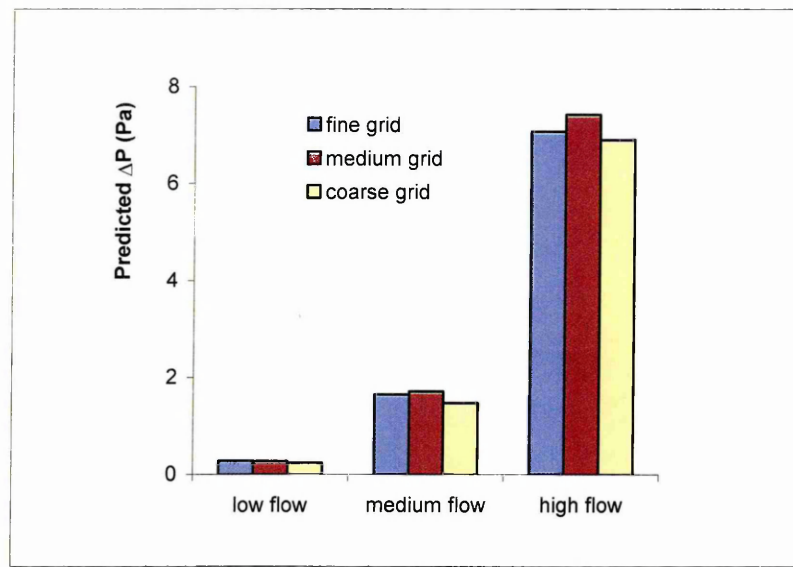
Figure 6.13: Effect of grid density on predicted ΔP at low, medium and high flow rates

For the low flow rates the predicted ΔP changed 11 % from the coarse to medium grid refinement and was negligibly different (0.4%) at the fine grid refinement. At medium flow rates the predicted ΔP changed 13 % from the coarse to medium grid refinement and only 3% at the fine grid refinement. Finally for high flow rates the predicted ΔP changed 7 % from the coarse to medium grid refinement and 4% at the fine grid refinement. The minimal changes in predicted ΔP between the medium and fine grid densities indicate that the solution was minimally dependent on the number of grid points used to develop the solution. This level of accuracy was considered adequate taking into account the other uncertainties in problem definition likely to be encountered in natural ventilation applications in practice.

It was mentioned earlier that seven levels of airflow rates within the range zero to $0.0105 m^3/s$ were simulated for each slot. Pressure differentials corresponding to these flow rates were obtained from the CFD solution and used to derive power law and quadratic formulation coefficients and indices. The results obtained are tabulated in Table 6.3 together with the associated correlation coefficients. Power law and quadratic formulations were explained in *Section 4.7* but are repeated here as Equation 6.4 and Equation 6.5 respectively, for ease of reference when reading Table 6.3:

$$Q = \alpha \, (\Delta P)^{\beta} \tag{6.4}$$

$$\Delta P = aQ^2 + bQ \tag{6.5}$$

Table 6.3:
Power law and quadratic formulation coefficients and indices derived from CFD predicted pressure differentials

Case No.	Slot ref.	Mesh-screen	Power law			Quadratic		
			α	β	R	a	b	R
1	B6	no mesh-screen used	0.0038	0.5081	100	67826	9.777	100
2	B5		0.0038	0.507	100	66119	14.764	100
3	B4		0.0038	0.5076	100	67070	6.111	100
4	B3		0.0038	0.5062	99.89	66252	11.008	99.99
5	B2		0.0038	0.5122	99.97	65384	9.111	100
6	B1		0.0038	0.5133	99.92	68299	-1.059	99.96

The results given in Table 6.3 will be compared with experimental findings (see *Chapter 5*) in the following chapter. Further insight into the simulation results of airflow through slots was obtained from graphical plots of velocity vectors and contours in planes cutting through the computational domain. Typical results of the computed profiles on selected planes in the computational domain are presented in Figures 6.14 to 6.25 to enable visualisation of parameters. It can be seen from Figures 6.14 to 6.25 that changes in parameters such as velocities are confined primarily to regions in the vicinity of the slot. Away from the slot, velocities are nearly uniform or change only very slightly. The arrows in the vector plots denote the velocity vectors in both magnitude and direction whilst the different colours in the contour plots represent different magnitudes of velocities. The general magnitude of the velocity can be seen to increase as the air flows through the slot in all cases. Generally, the results indicate that small changes in depth of the slot did not have a significant effect on airflow velocities on the downstream side of the slot.
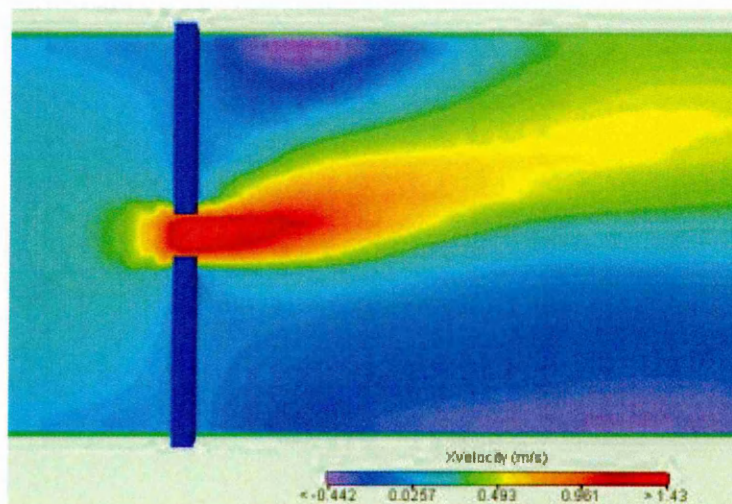
Figure 6.14: X-Velocity contours for slot B1 at 1.5 m/s
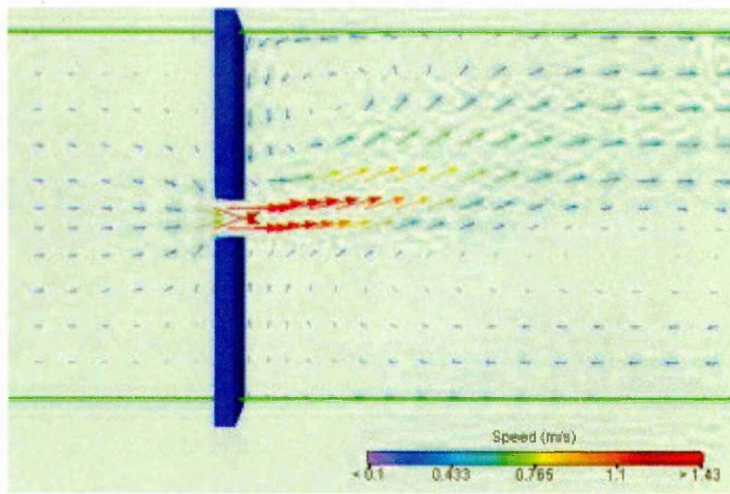
Figure 6.15: Velocity vectors for slot B1 at 1.5m/s
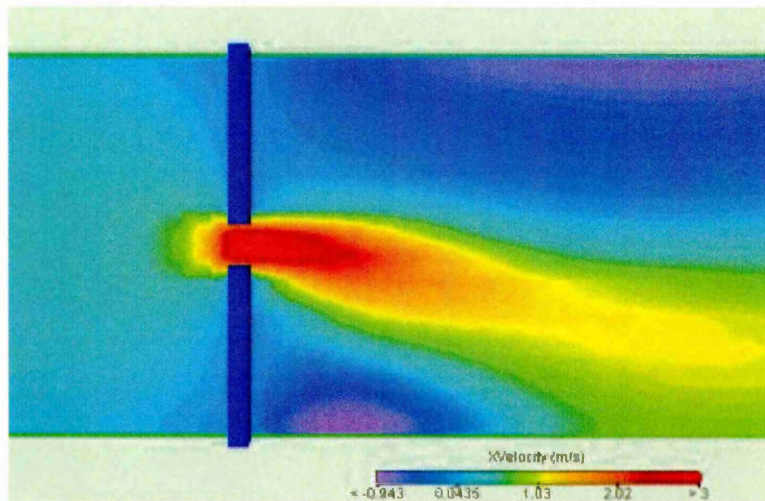
Figure 6.16: X-Velocity contours for slot B1 at 3m/s
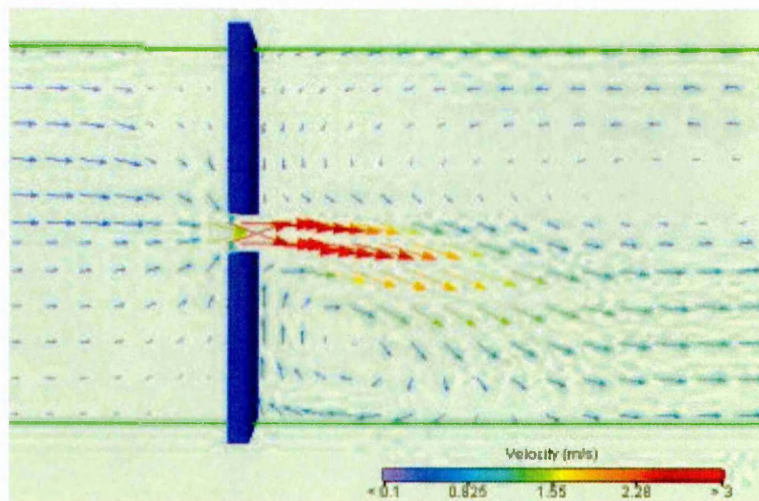
Figure 6.17: Velocity vectors for slot B1 at 3m/s
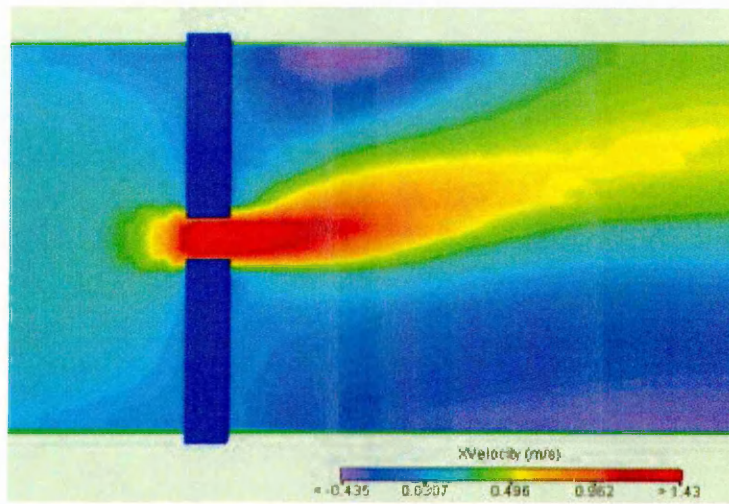
Figure 6.18: X-Velocity contours for slot B2 at 1.5m/s
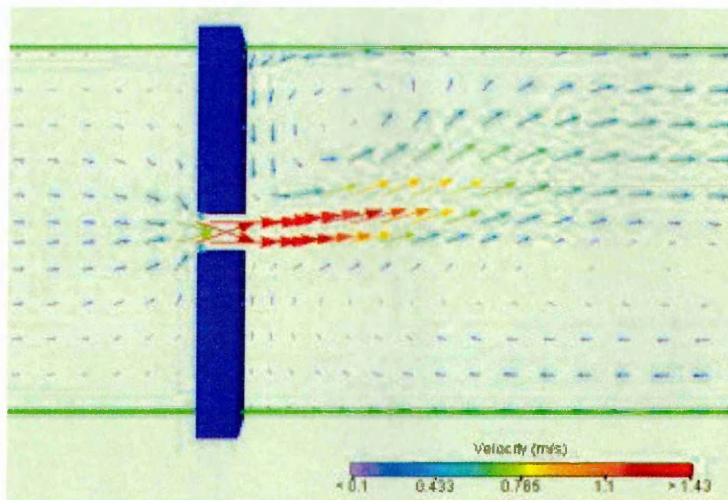
Figure 6.19: Velocity vectors for slot B2 at 1.5m/s
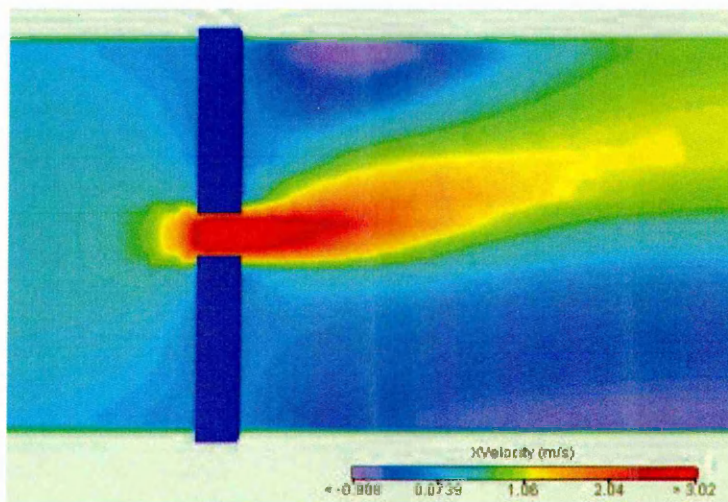
Figure 6.20: X-Velocity contours for B2 at 3m/s
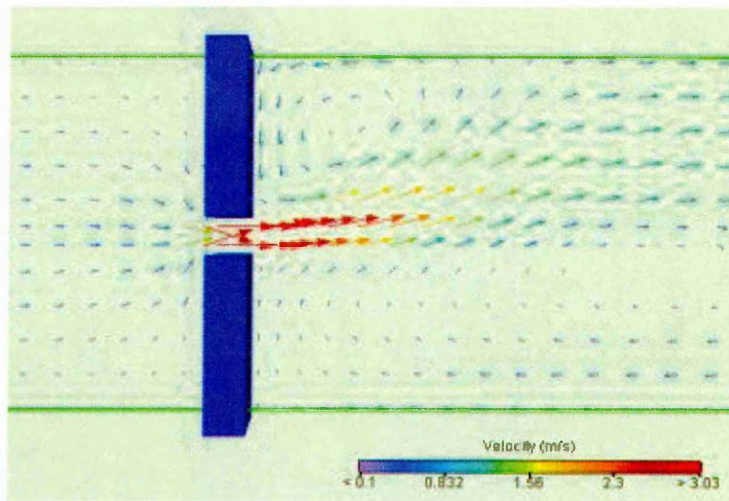
Figure 6.21: Velocity vectors for slot B2 at 3m/s
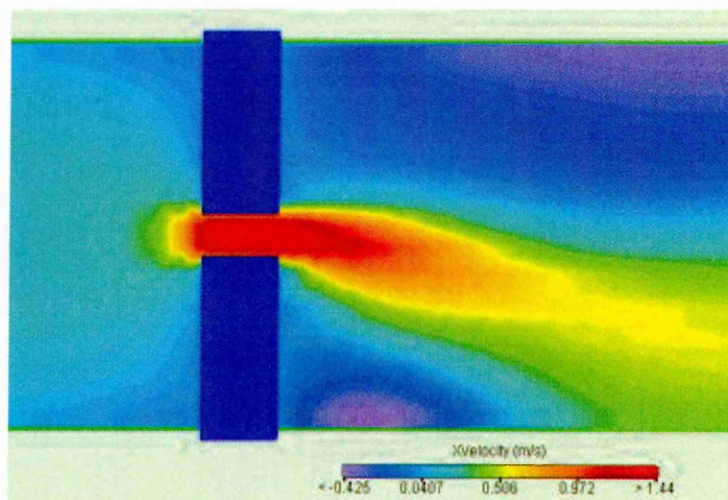
Figure 6.22: X-Velocity contours for B4 at 1.5m/s
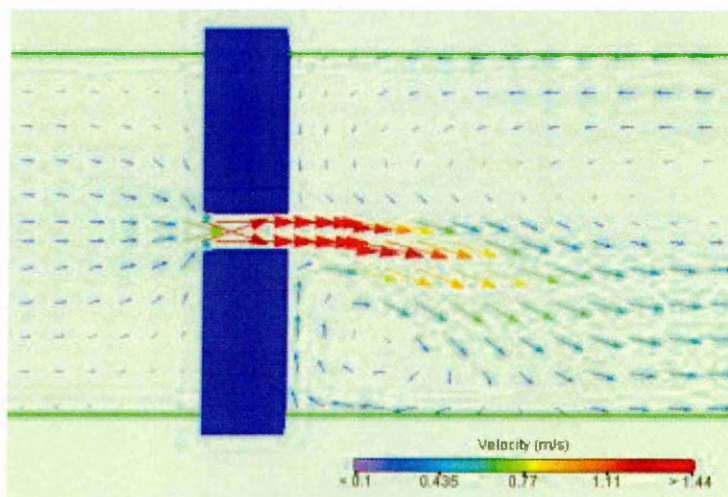
Figure 6.23: Velocity vectors for slot B4 at 1.5m/s
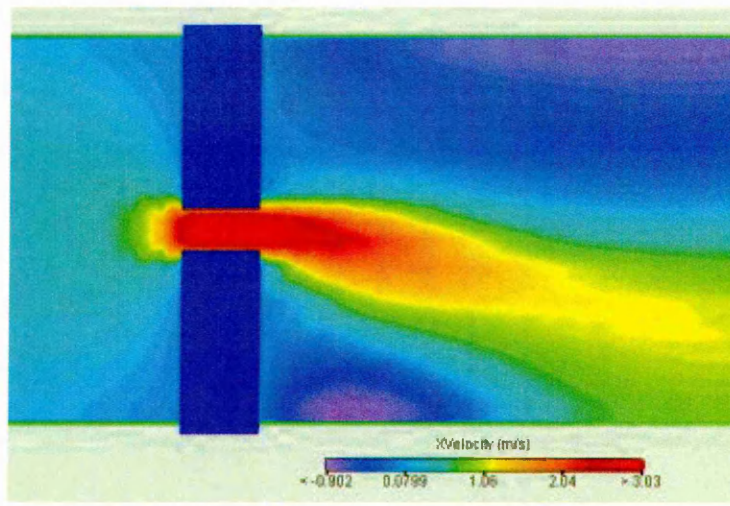
Figure 6.24: X-Velocity contours for slot B4 at 3m/s
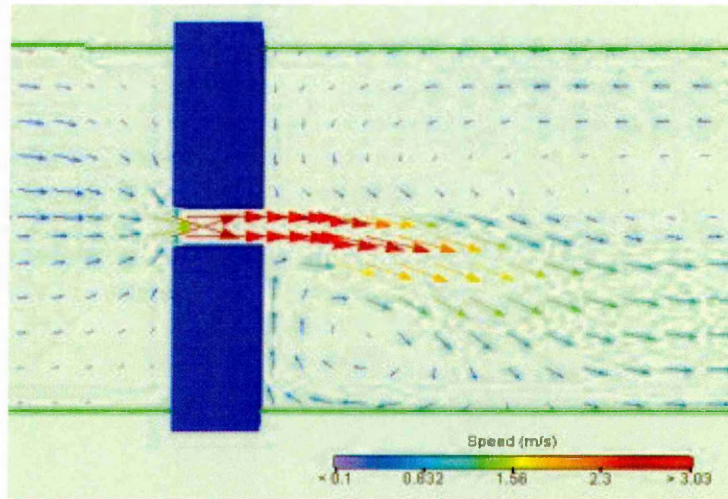
Figure 6.25: Velocity vectors for slot B4 at 3m/s

Velocity plots (vectors and contours) for the central z-axis (X-Y plane) were taken through the computational domain for which airflow approaching the slots at face velocities of 1.5 m/s and 3 m/s was considered and compared for slot B1 (D = 6mm), slot B2 (D = 12mm) and slot B4 (D = 24mm). Two main airflow profiles emerged when the three slots were subjected to the two face velocities in turn. The first pattern exhibited an upward shifting profile of the airflow coming off the slots, as can be seen in Figures 6.14, 6.15, 6.18, 6.19, 6.20, and 6.21, whilst the second pattern exhibited a downward shifting profile (Figures 6.16, 6.17 and 6.22 - 6.25). Close examination of the velocity vectors revealed that in both cases (upward and downward shifts) there was a recirculation zone either above or below the centreline on the downstream side of the slot. It is clear that the existence of the recirculation zone led to entrainment of air on the discharge side of the slot thus causing the upward or downward shift in airflow

-173-

profile. Initially this was perceived as being caused by unsymmetrical gridding vertically, however, careful examination of the grid patches in the computational domain discounted this view. The only other explanations causing the recirculation zone could possibly stem from either the fact at very low airflow rates it was not possible to achieve full convergence of the numerical solution or insufficient grid representation in the CFD model. The patterns of airflow obtained from the simulations could be examined physically on actual slots by means such as smoke tests however this was beyond the scope of the current investigation and is strongly recommended for future studies.

For now comparisons of the airflow patterns resulting from simulations for slots B1, B2 and B4 will proceed on the assumption that the numerical solution is correct. At the lower face velocity of 1.5m/s the airflow profile exhibited an upward shift at slot depths of 6mm and 12mm (Figures 6.14, 6.15, 6.18 and 6.19). At a slot depth of 24mm the airflow profile for the 1.5m/s face velocity swings to a downward deflection (Figure 6.22 and Figure 6.23). Taking the number of *red arrows* coming off each slot as a measure, it can be seen that for the 6mm slot the airflow profile is deflected upwards almost immediately upon discharge from the slot i.e. second arrow - Figure 6.15. When the slot depth was increased to 12mm the upward deflection appeared to be delayed until the third arrow downstream of the slot (Figure 6.19). For a depth of 24mm the deflection (downwards in this case) did not occur until the fifth arrow (Figure 6.23). This was in line with the expectations whereby as the depth is increased the slot tends to straighten the air flowing through it.

At the higher face velocity (3m/s) the airflow pattern for slot B2 (Figure 6.20 and Figure 6.21) was similar to that at 1.5m/s. However, for the reduced slot depth of 6mm the airflow profile (Figure 6.16 and Figure 6.17) exhibited an opposite trend to the one at 1.5m/s i.e. a downward deflection as was the case for the slot with a depth of 24mm (Figure 6.24 and Figure 6.25). Here again using the *red-arrow measure*, it can be seen (Figures 6.17, 6.21 and 6.25) that for both slots B1 and B2 the deflection of the airflow profile from horizontal starts to occur on the second arrow. This indicates that at the higher face velocity the small increase in slot depth from 6mm to 12mm has little influence on the distance from the slot at which the airflow profile deflection from horizontal starts to occur. On the other hand for the 24mm slot the deflection does not

occur until the fifth or sixth arrow. Bearing in mind that the velocity arrows from the computational domain are deduced from grid cells that are only a few millimetres wide, these findings suggest that the depth of the slot, or ventilator in a real building, has some influence on the direction/pattern of airflow within the occupied zone. However, the onset of the deflection from horizontal of the airflow profile is little influenced by small changes in the depth of the slot/ventilator. Although the airflow profiles obtained from the simulations on slots are not of immediate interest in the optimisation of the airflow performance of ventilators, information derived from such studies could be useful in the assessment of sensor locations relative to natural ventilation openings.

The effect of varying the depth-to-height (D/H) ratio of the slots is shown in Table 6.4 and Figure 6.26. Three basic performance parameters were used in the discussion of the results i.e. airflow rate level (low, medium and high), relative pressure differential $(\Delta P/\Delta P_{12})$ and depth-to-height ratio (D/H). A relative airflow $(\Delta P/\Delta P_{12})$ has been used and is here defined as *the ratio of the pressure drop (ΔP) for a given slot size to the pressure drop (ΔP₁₂) for the slot with both depth and height equal to 12mm at a particular flow rate*. The 12mm slot was a natural choice for reference because its depth-to-height ratio was equal to one and thus this slot was set to be the intersection between the two sets of slots used in the investigation. Having a common slot between the two sets considered would also facilitate cross-comparison of airflow parameters.

Table 6.4:

Variation of relative ΔP/ΔP12 with slot dept-to-height ratio

D/H	low flow (=0.5m/s)	medium flow (=1.5m/s)	High flow (=3m/s)
0.5	1.06	1.04	1.03
1.5	1	1.01	1.02
2	1.02	1.01	1.01
2.5	1.03	1.02	1.03
3	1.04	1.04	1.04
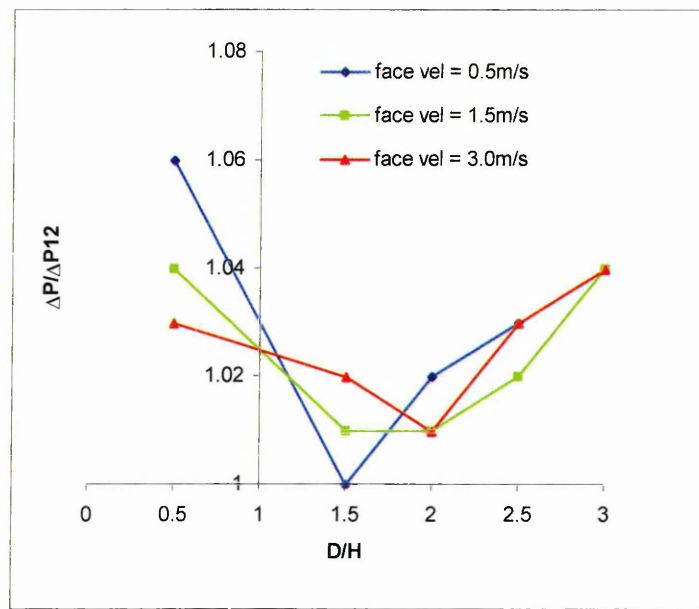
Figure 6.26: Variation of relative ΔP with slot depth-to-height (D/H) ratio

The variation of the CFD predicted relative pressure differential ($\Delta P/\Delta P_{12}$) with slot depth-to-height ratio (D/H) is graphically shown in Figure 6.26 where the data from Table 6.4 are plotted as discrete points joined by straight lines to show the trends. The variation was assessed for three levels of airflow rates (low, medium and high) through the slots, corresponding to face velocities of approximately 0.5 m/s, 1.5 m/s and 3 m/s respectively. It can be seen from Figure 6.26 that all levels of flow had a relative pressure differential greater than one and had similar trends over the D/H ratios considered. The results show that variation in relative pressure differential for the low, medium and high flow levels was greatest at D/H = 0.5. For the low flow level the minimum relative pressure differential occurred at D/H = 1.5 and then rose with increasing D/H. Similarly for the medium flow level the minimum occurred at D/H = 1.5 but stayed constant (horizontal line) until D/H = 2 when it started rising with increasing D/H. The medium flow level attained the same relative pressure differential at D/H = 0.5 and D/H = 3. On the other hand, the high flow level trend fell from D/H = 0.5 to D/H = 2 where it started to rise. The medium and high flow relative pressure differential trends appeared to vary less over the range of D/H ratios considered compared with the low flow trend. This behaviour was expected and can be attributed to stronger flows which were well established throughout the cells of the computational domain at the medium and high flow levels unlike the lower level of flow rates. Variation of relative pressure differential for the three levels of flow relative to the D/H ratios appeared to be more significant at values of D/H less than 1.5. Interestingly the

-176-

low flow and medium flow trends differed by a constant margin (parallel lines) between D/H = 2 and D/H = 2.5. From D/H = 2.5 to D/H = 3 the low flow level and high flow level had exactly the same trend i.e. superimposed lines. From D/H = 2.5 the three flow level trends converged with increasing D/H ratio with the three flow level trends attaining the same relative pressure differential at D/H = 3. This implies that at D/H = 3 there would be no variation in relative pressure differential, and hence airflow performance, as the flow changed from low to high levels through a given slot. With reference to natural ventilation this suggests that to avoid penalties in ventilator airflow performance due to fluctuations over the range of operation, care must be taken when designing the airflow path with low D/H ratio to ensure that the airflow performance remains as uniform/constant as possible. In addition, identifying points (or dimensions of ventilators) at which the relative pressure differential remains constant as the flow level varies over the range of operation would ensure that the airflow performance stays constant.

6.7.2 Case Study II: Ordinary slots of varying heights

SIMULATED CASES

A computational study was conducted of the airflow through slots of fixed depth (12 mm) and width (300 mm) but varying heights (Type A slots) over a range of pressure differentials typical in natural ventilation applications. Ten configurations of slots (with and without a mesh-screen) were investigated to simulate the operation of the actual Type A slots used in the experimental study (*Chapter 5*). The analysed cases are tabulated in Table 6.5 together with key boundary conditions used during the simulations. It was necessary to investigate variable heights of the slots as variation of height in actual ventilators provides larger/smaller area necessary for increased/decreased volumetric flow rate of air during operation. This action prevents any increase/decrease in back pressure that would affect the airflow through the ventilator and helps to maintain performance over a wide range of pressure differentials. This can be critical in natural ventilation applications where the pressure differentials driving the flow are relatively low (typically less than 10 Pa). A ventilator will normally encounter large variations in back pressure over the operation range.

Case No.	Slot Reference	Slot height (mm)	Slot depth (mm)	Boundary Conditions	
				Airflow Rates (m3/s)	Mesh-screen
1	A6	36	12	For each case at least 7 levels of airflow rates in the range 0 - 0.025m³/s were simulated. The airflow rate set for each slot was selected from this range so as to achieve ΔPs typical in experimental findings.	slots modelled without mesh-screen
2	A5	30	12		
3	A4	24	12		
4	A3	18	12		
5	A2	12	12		
6	A1	6	12		
7	A6	36	12	same as above	mesh-screen modelled as a planar resistance smart-part (available in FLOVENT) to represent the pressure loss via the loss coefficient k.
8	A4	24	12		
9	A2	12	12		
10	A1	6	12		

Generally, these variations are handled with a variable area ventilator that adjusts some dimensions to changes in the back pressure. This computational study attempted to understand how the airflow performance varies in relation to varying slot dimensions.

COMPUTATIONAL DOMAIN

A three-dimensional computational domain was used to predict differential pressures across the slot for a range of airflow rates through it. The model used for the simulations consisted of a uniform velocity profile inflow at one end of the domain and a static free stream opening at the opposite end to represent the outflow boundary. The complete computational domain of the model is shown in Figure 6.27.
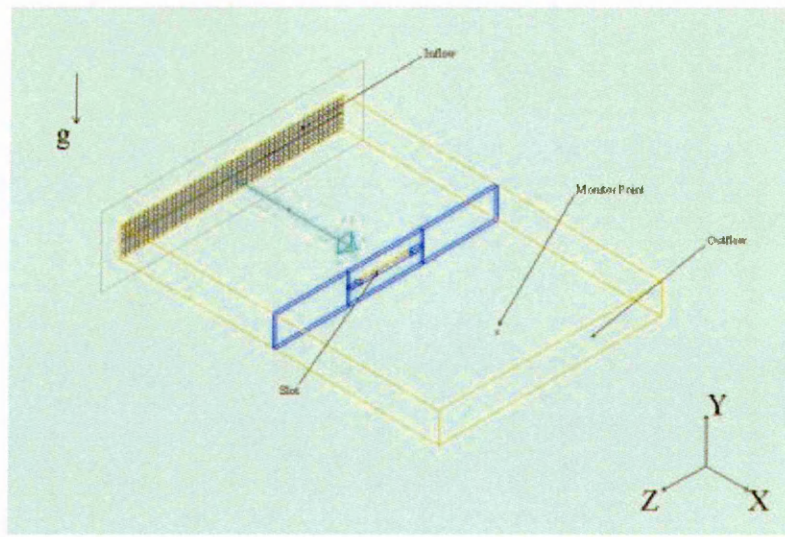
Figure 6.27: Computational domain for slots of varying heights

GRID

The solution was initially developed on a coarse grid that contained one half of the grid points of the fine mesh in the flow (X) and cross-flow (Y and Z) directions. Once the solution converged on the coarse grid, it was resolved with a medium grid that included one quarter more of the grid points in both flow and cross-flow directions. After convergence was obtained on the medium grid, the solution was refined and converged on the fine grid shown in Figure 6.28. The fine grid was set with spacing decreasing upstream of the slot and increasing downstream of the slot whilst being kept uniform vertically and across the slot (Y and Z-directions). A refined mesh was necessary near, and on either side of, the slot because in this area large gradients of the solution variables were anticipated. The fine grid contained approximately 52000 cells.
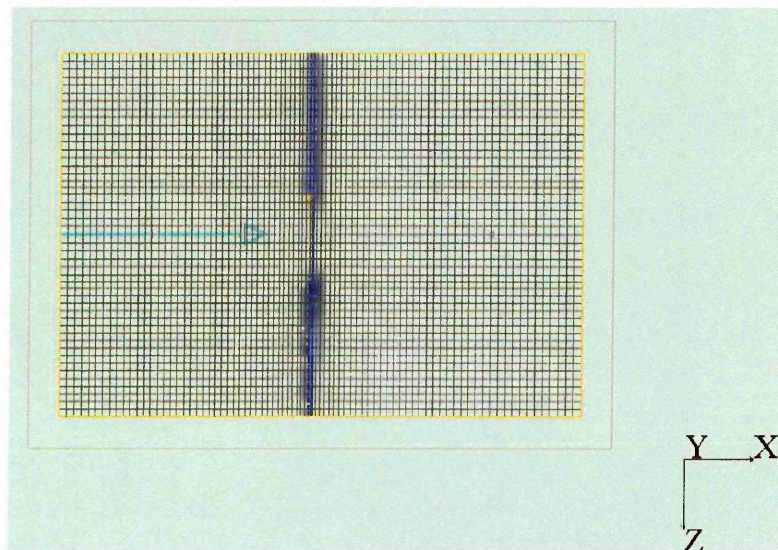
Figure 6.28: Grid distribution in X-Z plane

-179-

NUMERICAL SOLUTION

Computational simulations were run through a range of flow rates resulting in ΔPs typical of the experimental conditions. Power law regressions of experimentally measured data on the slots (*Chapter 5*) resulted in power law indices close to the value 0.5. From the theory, this suggests a turbulent nature of flow and as such the simulations were solved for turbulent as opposed to laminar flow. This approach to modelling provided information about the flow characteristics of the slots and a good estimate of their performance quantities. The execution time was about 200 minutes for each case solved on a Toshiba P4 laptop with 1.7 GHz processor speed and 512 MB RAM. The pressure data produced by FLOVENT were absolute pressures within each cell. In this investigation it was the pressure differences across slots that were important and this was the parameter used for comparison with experimental results. In addition airflow information from the simulations included visual representation of the pressure distribution and velocity field in the computational domain.

SOLUTION CONTROL AND CONVERGENCE

In the simulations 2000 - 3000 iterations were allowed for each case. A solution performance and residual history were used to monitor convergence as the solution developed at each grid level. All cases simulated achieved convergence based on the criteria described in *Section 6.7.1*. Slots modelled without a mesh-screen generally achieved full convergence whilst those incorporating a mesh-screen had the Rate of Dissipation of Turbulence (DissTurb) residual oscillating at residual values less than 10.

A typical solution history for an oscillating case is shown in Figure 6.29. It was mentioned earlier that seven levels of airflow rates within the range zero to 0.025 m^3/s were simulated for each slot. These were selected and suitably spaced to cover the range of ΔPs between one and 10 Pascals. The pressure differentials corresponding to these flow rates were obtained from the CFD solution and used to derive power law and quadratic formulation coefficients and indices. The results obtained are tabulated in Table 6.6 together with correlation coefficients associated with fitting the power law and quadratic functions to the predicted data.
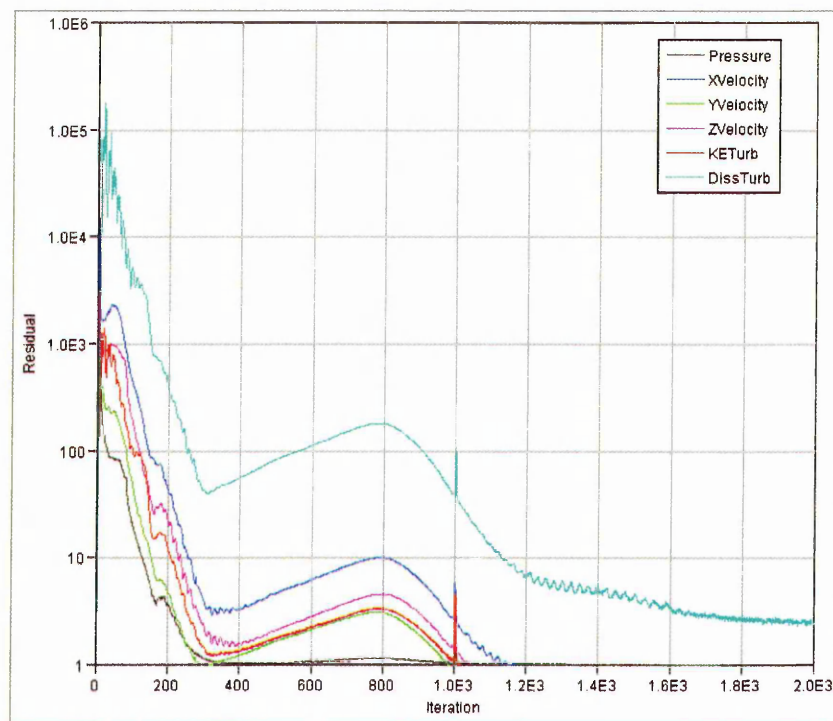
Figure 6.29: Typical fully converged solution residual

history for slots of varying heights

Table 6.6:

Power law and quadratic formulation coefficients and indices derived from CFD predicted pressure differentials

Case No.	Slot ref.	Mesh-screen	Power law			Quadratic		
			α	ß	R	a	b	R
1	A6		0.0076	0.5027	99.97	16498	6.497	100
2	A5		0.0065	0.5034	100	23631	1.812	100
3	A4	no mesh-screen used	0.0055	0.4986	99.99	34777	-20.223	99.9
4	A3		0.0042	0.4779	99.12	57853	20.123	99.88
5	A2		0.0028	0.5082	99.92	119115	53.045	99.91
6	A1		0.0014	0.5719	99.53	256442	544.490	99.6
7	A6		0.0035	0.4962	99.99	87870	-38.571	99.95
8	A5		0.0032	0.4999	100	100878	-0.582	100
9	A4	slots with fine mesh-screen	0.0025	0.4951	99.99	163572	1.097	100
10	A3		0.0021	0.5007	100	236416	1.819	100
9	A2		0.0014	0.5005	100	533745	1.868	100
10	A1		0.0009	0.4954	99.94	1000000	120.010	99.9

The results given in Table 6.6 will be compared with experimental findings in *Chapter 7*. Typical results of the simulations are also presented graphically in Figures 6.30 to 6.59 to enable visualisation of parameters on selected planes in the computational domain.
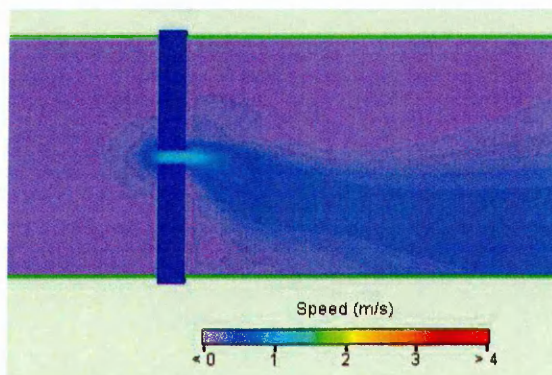
Figure 6.30: Speed contour forSlotA1 with mesh-screen at ΔP = 5Pa
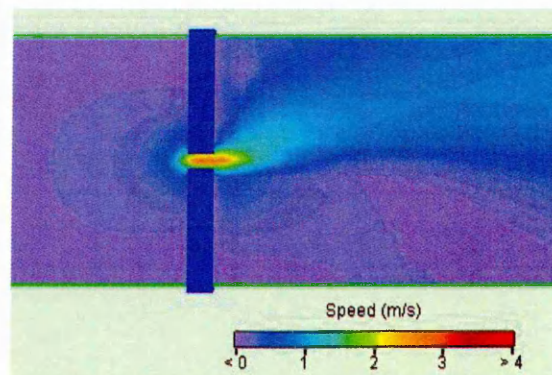
Figure 6.31: Speed contour forSlotA1 without mesh-screen at ΔP = 5Pa
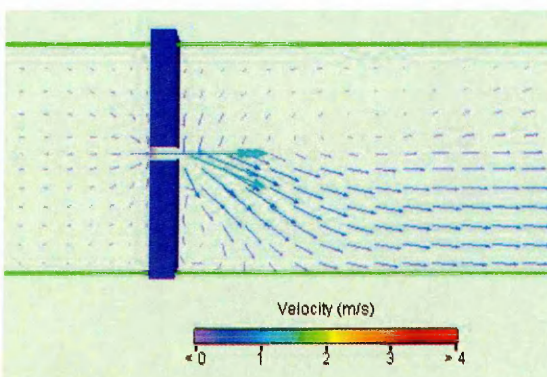
Figure 6.32: Velocity vectors forSlotA1 with mesh-screen at ΔP = 5Pa
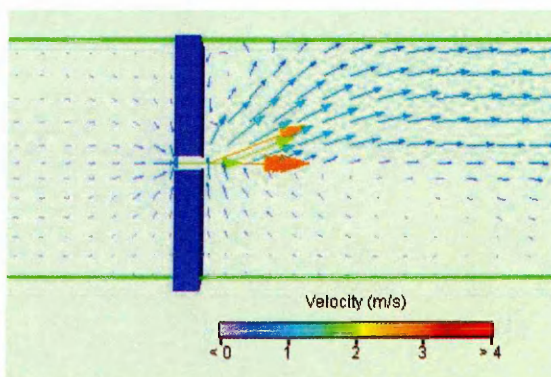
Figure 6.33: Velocity vectors forSlotA1 without mesh-screen at ΔP = 5Pa
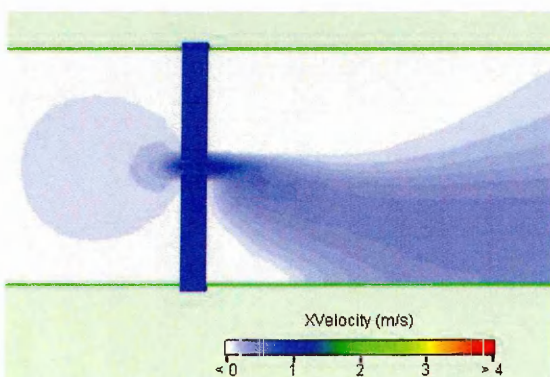
Figure 6.34: X-Velocity contour forSlotA1 with mesh-screen at ΔP = 5Pa
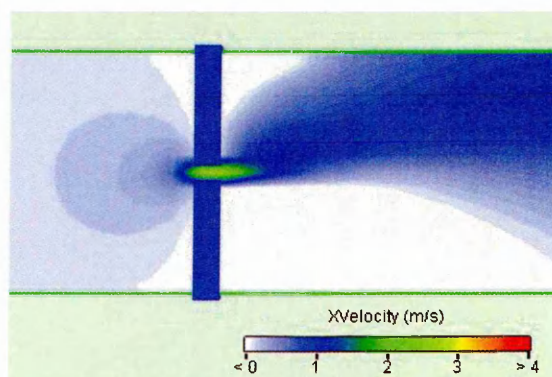
Figure 6.35: X-Velocity contour forSlotA1 without mesh-screen at ΔP = 5Pa
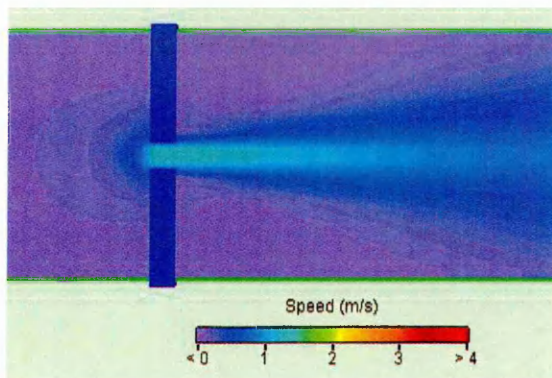
Figure 6.36: Speed contour forSlotA2 with mesh-screen at ΔP = 5Pa
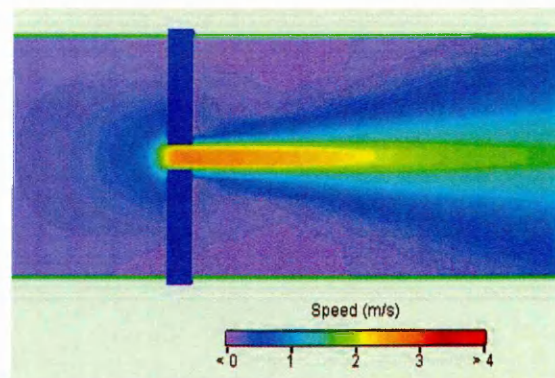
Figure 6.37: Speed contour forSlotA2 without mesh-screen at ΔP = 5Pa
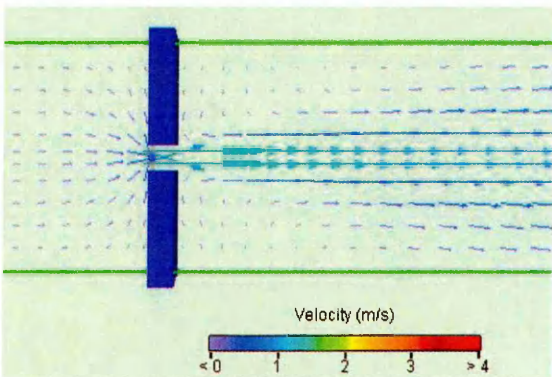
Figure 6.38: Velocity vectors forSlotA2 with mesh-screen at ΔP = 5Pa
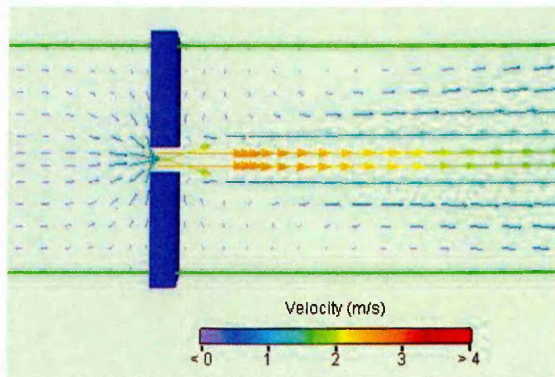
Figure 6.39: Velocity vectors forSlotA2 without mesh-screen at ΔP = 5Pa
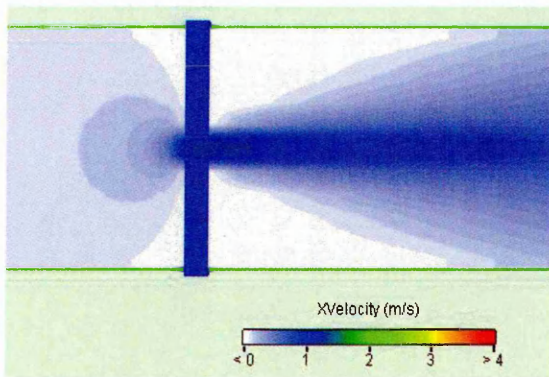
Figure 6.40: X-Velocity contour forSlotA2 with mesh-screen at ΔP = 5Pa
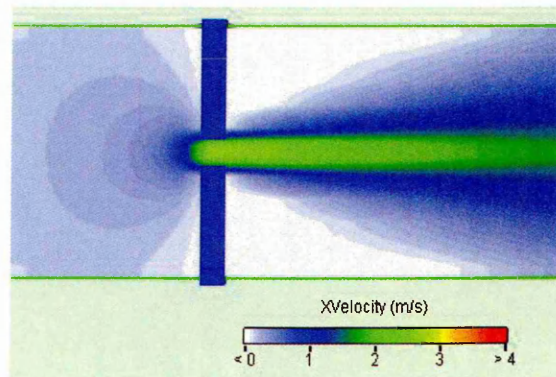
Figure 6.41: X-Velocity contour forSlotA2 without mesh-screen at ΔP = 5Pa
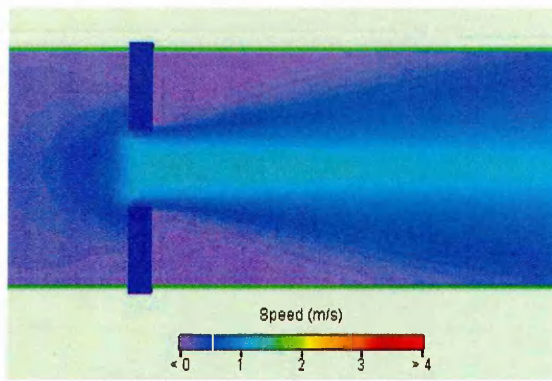
Figure 6.42: Speed contour forSlotA6 with
mesh-screen at ΔP = 5Pa
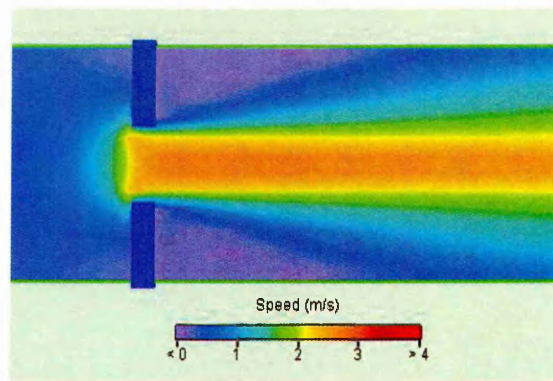
Figure 6.43: Speed contour forSlotA6 without
mesh-screen at ΔP = 5Pa
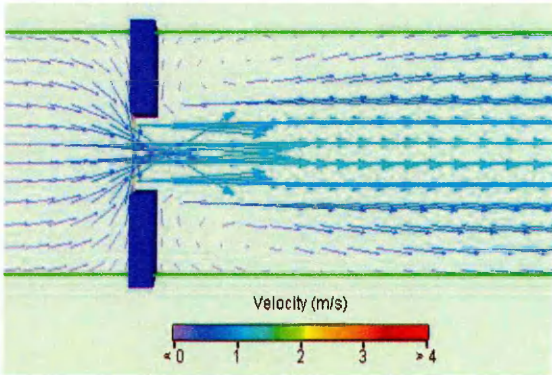
Figure 6.44: Velocity vectors forSlotA6 with
mesh-screen at ΔP = 5Pa
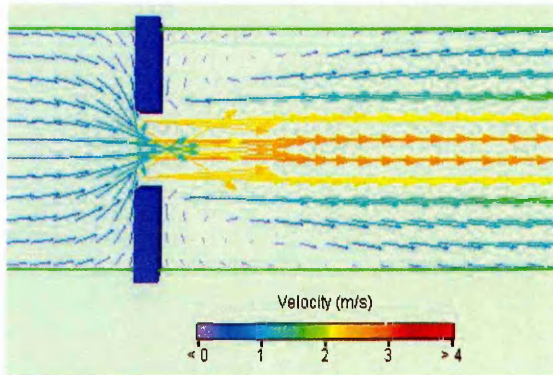
Figure 6.45: Velocity vectors forSlotA6 without
mesh-screen at ΔP = 5Pa
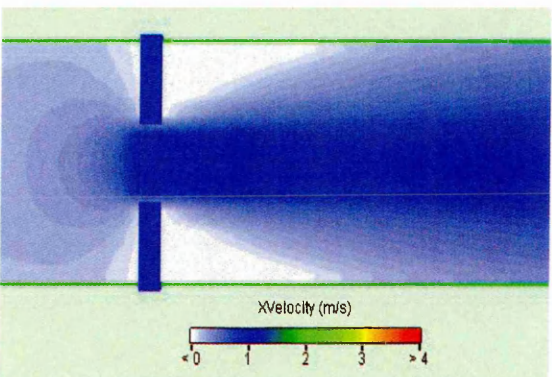
Figure 6.46: X-Velocity contour forSlotA6 with
mesh-screen at ΔP = 5Pa
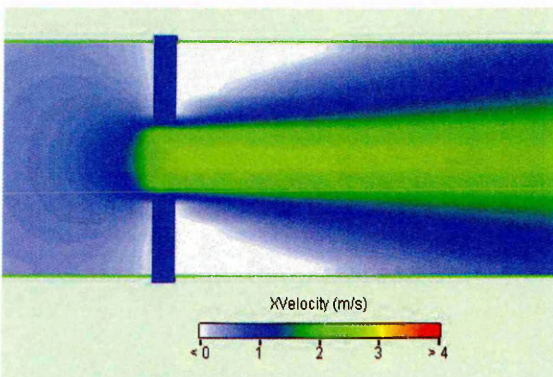
Figure 6.47: X-Velocity contour forSlotA6
without mesh-screen at ΔP = 5Pa

Here again some insight into the airflow characteristics of the slots can be obtained from graphical plots of vectors and contours in planes cutting through the computational domain. Figure 6.30 to Figure 6.47 show plots of air speed, velocity vectors and the X-velocity (velocity in direction of flow) for a central Z-plane for Slot A1, Slot A2 and Slot A6 when the pressure differential across the slots was 5 Pa. The old numbered figures show the results for slots without a mesh-screen whilst the even numbered figures show the results when the slots were used with a fine mesh-screen. As expected

-184-

the effect of the mesh-screen on the airflow was a reduction in airflow velocity on the discharge side of the slot. It is clear from the figures, with and without a mesh-screen, that at a pressure difference of 5 Pa the highest velocity on the discharge side of the slots reduced from approximately 2.5 m/s to about 1 m/s when a fine mesh-screen was added to the slots. Further, with a mesh-screen, the airflow discharges from the slots with uniform velocity whilst without the mesh-screen there is a central core of airflow with a high velocity which is surrounded by relatively low velocity flow. Figures 6.31, 6.33 and 6.35 for Slot A1 without a mesh-screen show that after flowing through the slot the air turns steeply upwards. On the other hand, with a mesh-screen (Figures 6.30, 6.32 and 6.34) the air discharges from the slot with a steep downward flow. As can be seen from Figure 6.33 and Figure 6.32 the upward and downward, respectively, shifts in flow can be attributed to a pressure gradient caused by re-circulating flow developed at the upper and lower portions of the simulation model on the discharge side of the slot. The shift of the re-circulation zone from top to bottom following the addition of a mesh-screen could have resulted from a change in vertical momentum immediately after the air discharges from the slot.
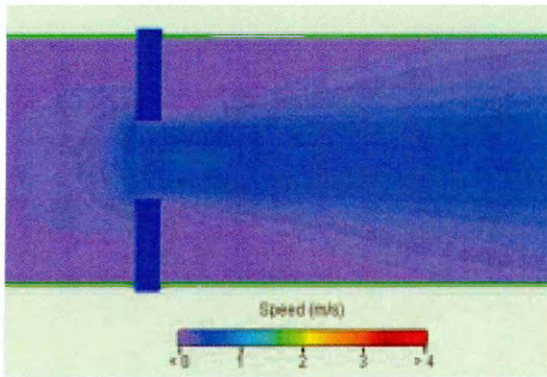
Figure 6.48: Speed contour forSlotA6 with mesh-screen at $\Delta P = 1Pa$
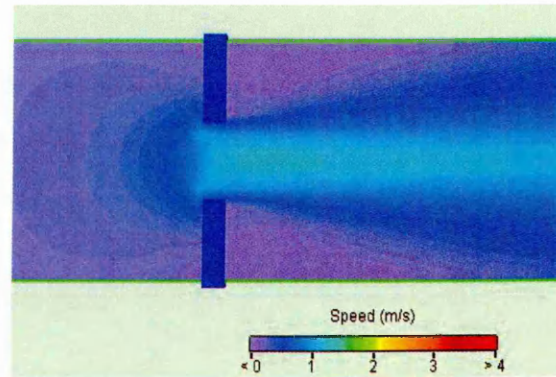
Figure 6.49: Speed contour forSlotA6 without mesh-screen at $\Delta P = 1Pa$
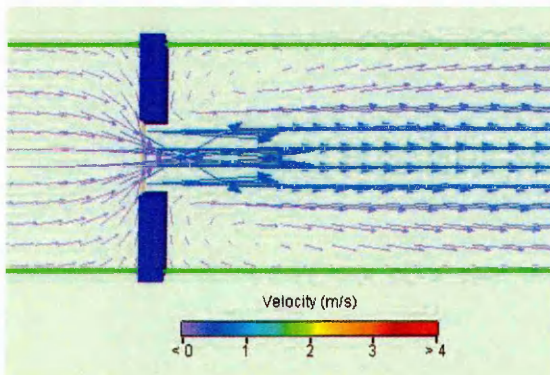
Figure 6.50: Velocity vectors forSlotA6 with mesh-screen at $\Delta P = 1Pa$
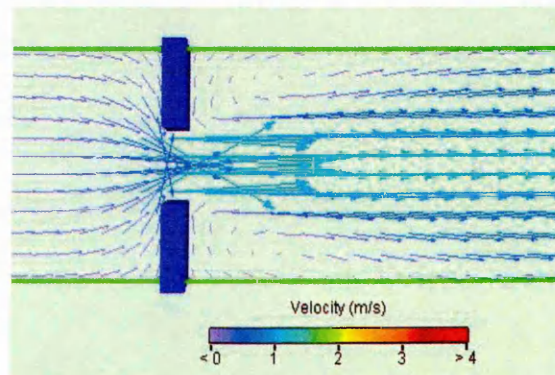
Figure 6.51: Velocity vectors forSlotA6 without mesh-screen at $\Delta P = 1Pa$
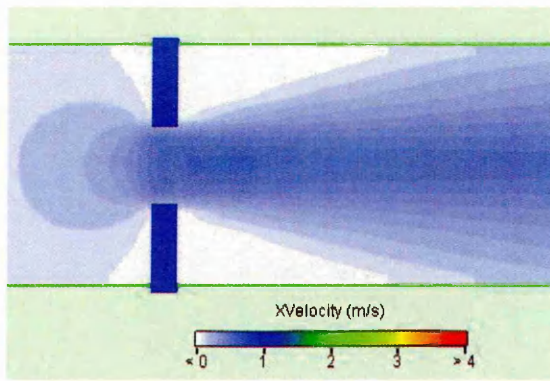
Figure 6.52: X-Velocity contour forSlotA6 with mesh-screen at ΔP = 1Pa
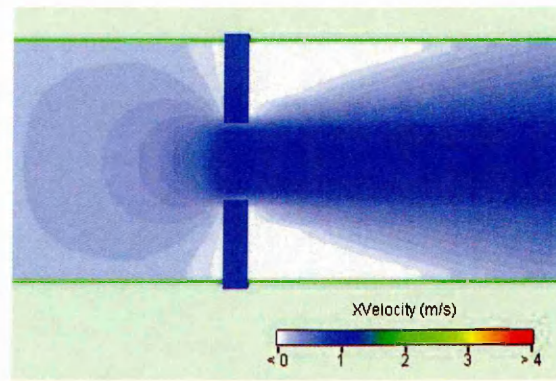
Figure 6.53: X-Velocity contour forSlotA6 without mesh-screen at ΔP = 1Pa
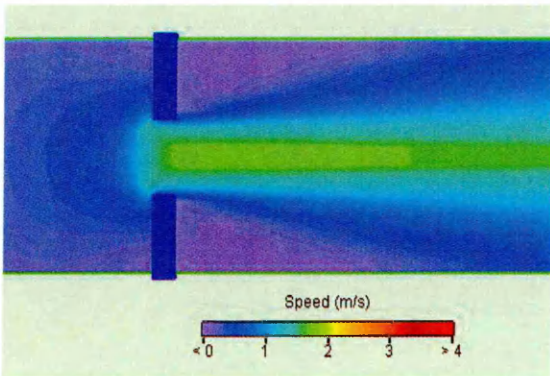
Figure 6.54: Speed contour forSlotA6 with mesh-screen at ΔP = 10Pa
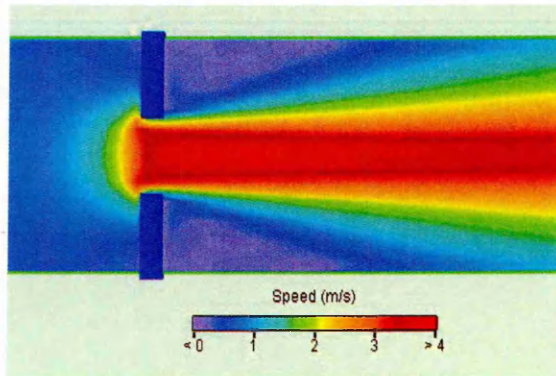
Figure 6.55: Speed contour forSlotA6 without mesh-screen at ΔP = 10Pa
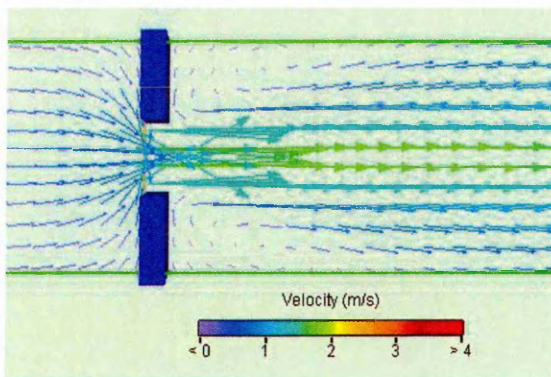
Figure 6.56: Velocity vectors forSlotA6 with mesh-screen at ΔP = 10Pa
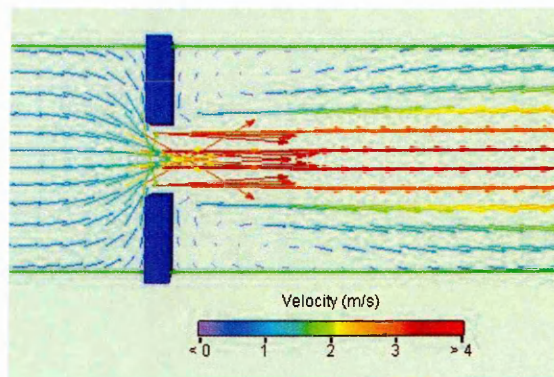
Figure 6.57: Velocity vectors forSlotA6 without mesh-screen at ΔP = 10Pa

-186-
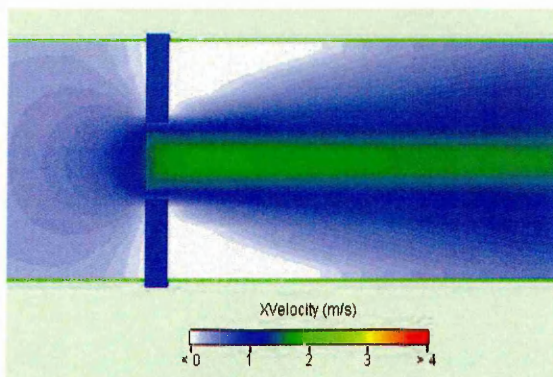
Figure 6.58: X-Velocity contour for SlotA6 with mesh-screen at ΔP = 10Pa
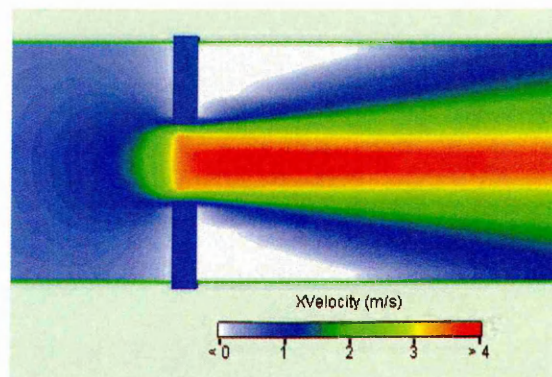
Figure 6.59: X-Velocity contour for SlotA6 without mesh-screen at ΔP = 10Pa

Figure 6.48 to Figure 6.53 show plots of air speed, velocity vectors and the X-velocity (velocity in direction of flow) for a central Z-plane for Slot A6 when the pressure differential across the slots was 1 Pa. Figure 6.54 to Figure 6.59 show plots of air speed, velocity vectors and the X-velocity (velocity in direction of flow) for a central Z-plane for Slot A6 when the pressure differential across the slots was 10 Pa. Here again the old numbered figures show the results for slots without a mesh-screen whilst the even numbered figures show the results when the slots were used with a fine mesh-screen.

As expected the effect of the mesh-screen on the airflow was a reduction in airflow velocity on the discharge side of the slot. It is clear from the figures, with and without a mesh-screen), that at a pressure difference of 1 Pa the highest velocity on the discharge side of the slots reduced from just under 1.5m/s to about approximately 0.5m/s when a fine mesh-screen is added to the slots. At pressure differences of 5 Pa (Figure 6.42 to Figure 6.47) and 10 Pa (Figure 6.54 to Figure 6.59) the highest velocity on the discharge side of the slots reduced from about 2.5m/s to 1m/s and from approximately 3.5 m/s to just under 2m/s respectively when a fine mesh-screen is added to the slots. Further, with a mesh-screen, the airflow discharges from the slots with uniform velocity whilst without the mesh-screen there is a central core of airflow with a high velocity which is surrounded by relatively low velocity flow.

EFFECT OF VARYING HEIGHT-TO-DEPTH RATIO

The effect of varying the height-to-depth (H/D) ratio of the slots is shown in Figure 6.60. Three basic performance parameters were used in the discussion of the results i.e. airflow rate level (low, medium and high), relative pressure differential ($\Delta P/\Delta P_{12}$) and H/D. The $\Delta P/\Delta P_{12}$ ratio was examined in this investigation because it represents a

relative resistance to airflow through slots of varying dimensions and therefore can be used as a measure to represent the airflow performance of the slots.
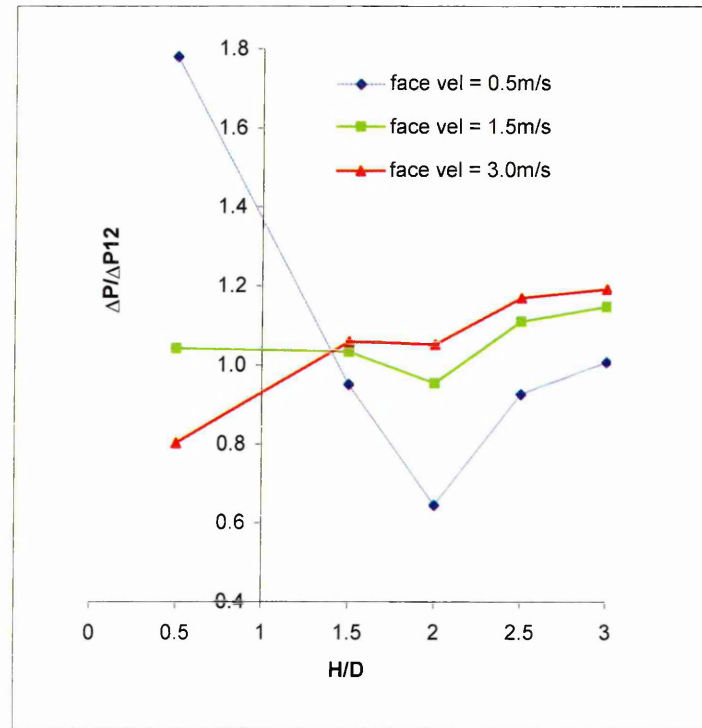
Figure 6.60: Variation of relative ΔP/ΔP₁₂ with
slot height-to-depth (H/D) ratio

The variation of the CFD predicted relative pressure differential ($\Delta P/\Delta P_{12}$) with slot height-to-depth ratio (H/D) is shown in Figure 6.60. Here again the variation was assessed for three levels (low, medium and high) of airflow rates through the slots, corresponding to face velocities of approximately 0.5 m/s, 1.5 m/s and 3 m/s respectively. For each slot height airflow rates corresponding to each face velocity were substituted into quadratic function airflow characteristics given in Table 6.5 to determine the predicted ΔP at the respective face velocity. It can be seen from the trends in Figure 6.60 that the greatest variation of $\Delta P/\Delta P_{12}$ with H/D occurred at H/D = 0.5 as the level of airflow increased from low to high. This suggests that at H/D = 0.5 there is significant impact on the airflow performance as the flow varies from low to medium and slightly less impact as the flow changes from medium to high. The low flow level trend initially decreased with increasing H/D reaching a minimum at H/D = 2 and then rose with increasing H/D. The medium flow trend was approximately constant (horizontal line) as H/D increased from 0.5 to 1.5. It then dropped to a minimum at H/D = 2. On the other hand, the high flow trend had the lowest $\Delta P/\Delta P_{12}$ ratio at H/D = 0.5

and increased with increasing H/D. The high flow trend attained a constant $\Delta P/\Delta P_{12}$ ratio between H/D = 1.5 and H/D = 2. The three flow levels exhibited a similar trend as H/D increased from 2 to 3. With reference to natural ventilation this suggests that to avoid penalties in ventilator airflow performance due to fluctuations over the range of operation, care must be taken when designing the airflow path with low H/D ratio to ensure that the airflow performance remains as uniform/constant as possible.

The variation of the CFD predicted relative pressure differential ($\Delta P/\Delta P_{12M}$) with slot height-to-depth ratio (H/D) when the slots were used in combination with a mesh-screen is shown in Table 6.7 and Figure 6.61. Table 6.7 is included to highlight the degree to which the three trends are superimposed where applicable.

Table 6.7

Variation of relative ΔP with slot height-to-depth ratio
(slots with mesh-screen)

H/D	low flow (=0.5m/s)	medium flow (=1.5m/s)	High flow (=3m/s)
0.5	0.561	0.499	0.484
1.5	0.998	0.997	0.997
2	1.226	1.226	1.226
2.5	1.176	1.179	1.180
3	1.009	1.149	1.195
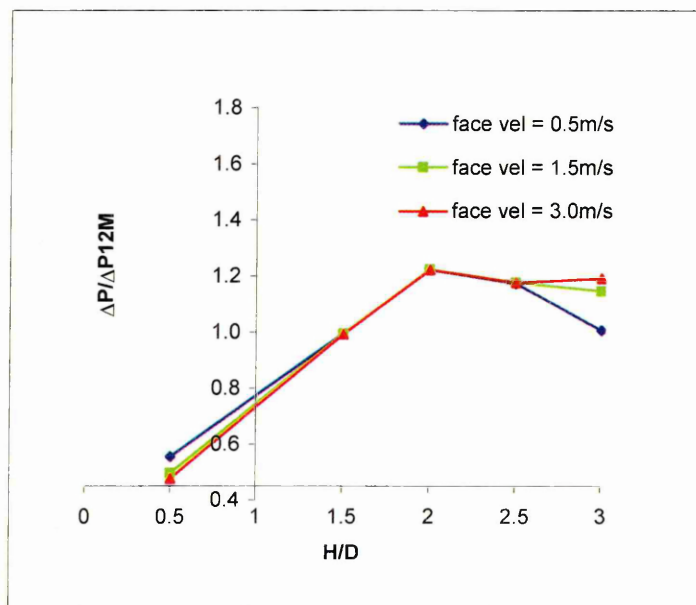
Figure 6.61: Variation of relative $\Delta P/\Delta P_{12M}$ with slot height-to-depth (H/D)

ratio for slots used in combination with a mesh-screen

It can be seen from Figure 6.61 that addition of a mesh-screen to the slots transformed the low and medium flow curves to a trend similar to the high flow curve as H/D increased from 0.5 to 1.5. A possible explanation of this is that the resistance presented by the slots at high flow level is little affected by the addition of a mesh-screen to the slots. Whereas on the other hand, the resistance to low and medium flow is significantly influenced by addition of a mesh-screen to the slots. The variation of $\Delta P/\Delta P_{12M}$ was now greatest at H/D = 3 compared to the case when the slots had no mesh which exhibited greatest variation of the relative pressure differential at H/D = 0.5. The medium and high flow trends were only marginally different for all H/D ratios from 0.5 to 2.5. Between H/D = 1.5 and H/D = 2.5 the three trends (low, medium and high) were superimposed, implying that between these limits the relative pressure differential was not influenced by the flow level change from low through medium to high, and attained the maximum $\Delta P/\Delta P_{12M}$ ratio and H/D = 2. The degree to which the trends varied can be seen in the values presented in Table 6.7 where it can be seen that the difference occurred only in the third decimal place between these limits. The graph suggests that for H/D ratios between 1.5 and 2.5 the behaviour of the slot/mesh combinations between various levels of flow rate (low, medium and high) was constant/uniform. The significance and interpretation of the intersection points of the curves in Figures 6.29, 6.60 and 6.61 has intentionally not been referred to in the above discussions and will be delayed until the next chapter. In the meantime, it must be pointed out that the trends shown in Figure 6.29, 6.60 and 6.61 were derived from a limited number of data points. Therefore, further investigations to confirm, dispute or improve on these findings are strongly recommended.

6.8 Steady-State Simulations of Airflow through Commercial Louvers

This section describes and presents details of steady-state simulations that were conducted on the airflow through commercial louvers described in *Section 5.3.3*. Basic CFD simulations where conducted in 3-D and for flow only (with thermal calculations disabled) on full-size louver banks with and without mesh-screens described in *Section 5.3.4* and *Section 5.3.5*. The simulations were carried out using FLOVENT which was used as a numerical wind tunnel. This analysis assessed the feasibility of integration of CFD and CAD as a tool for designing and optimising the performance of ventilators. The approach employed was to compare the computational results with experimentally measured pressure differentials across the ventilators.

6.8.1 Simulated cases

Commercial louvers used in combination with the insect-screen and bird-guard (described in *Sections 5.3.4* and *5.3.5* of this thesis) were subjected to pressure differentials resulting in velocities of 0.05, 0.25 and 0.5m/s on the louver face. Airflow rates corresponding to these face velocities were used as boundary conditions to predict pressure differentials across the ventilators (louver/mesh combinations). The pressure differentials predicted from the simulation model will be compared with experimental data in the following chapter.

6.8.2 Simulation domain

The computational domain and part of the base grid system used in this investigation are shown in Figure 6.62. The grid system is described in *Section 6.8.3* below. The computational domain consisted of a wind tunnel to represent the actual plenum chamber on which experimental measurements were carried out. The computational wind tunnel had a free stream outlet at one end coinciding with the domain boundary; an intermediate solid partition with an opening of dimensions 480 mm x 320 mm (corresponding to the overall dimensions of the commercial louvers) into which various ventilators were inserted; and a fixed flow inlet of 100% free area located on the domain boundary at a distance of one metre away from the partition.
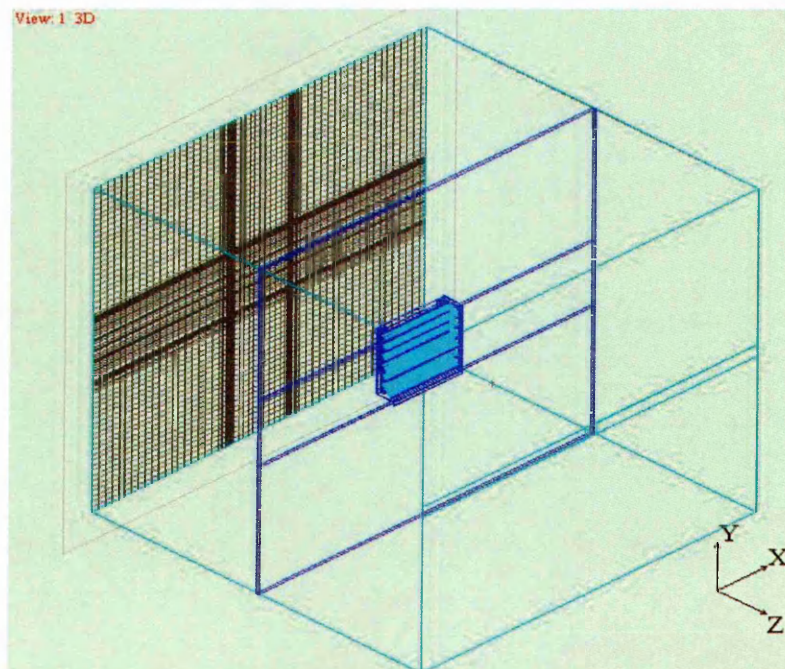
Figure 6.62: Computational domain and base grid

system for commercial louvers

Location of the inlet in this manner avoided the need to specify a velocity profile onto the louver face and enabled FLOVENT to establish its own boundary conditions (approaching velocity profile) at the ventilator inlet face. The inlet represented the airflow resulting from fan pressurisation/depressurisation when the fan was operating at a given speed and was used to vary the airflow rate through the ventilators. The sides of the wind tunnel were modelled as symmetry boundaries because it was assumed that these were far enough so as not to influence the airflow through the ventilator. Therefore, there was no need to specify the friction boundary condition and in addition this led to computational savings being made by avoiding prescription of fine grids at the wind tunnel walls. Two monitor points were included in the base model to represent pressure sensors/probes used during the experimental measurement phase. It is at these monitor points that values of parameters were obtained in order to assess the airflow characteristics of the ventilator components for comparison with experimental data.

6.8.3 Ventilator models

Models of ventilators were created from CAD files of commercial ventilators like the one shown in Figure 6.63. These were obtained in "*.SAT*" file format from the louver manufacturer and were imported into the FLOVENT software for inclusion into the simulation model using the FLO/MCAD module.
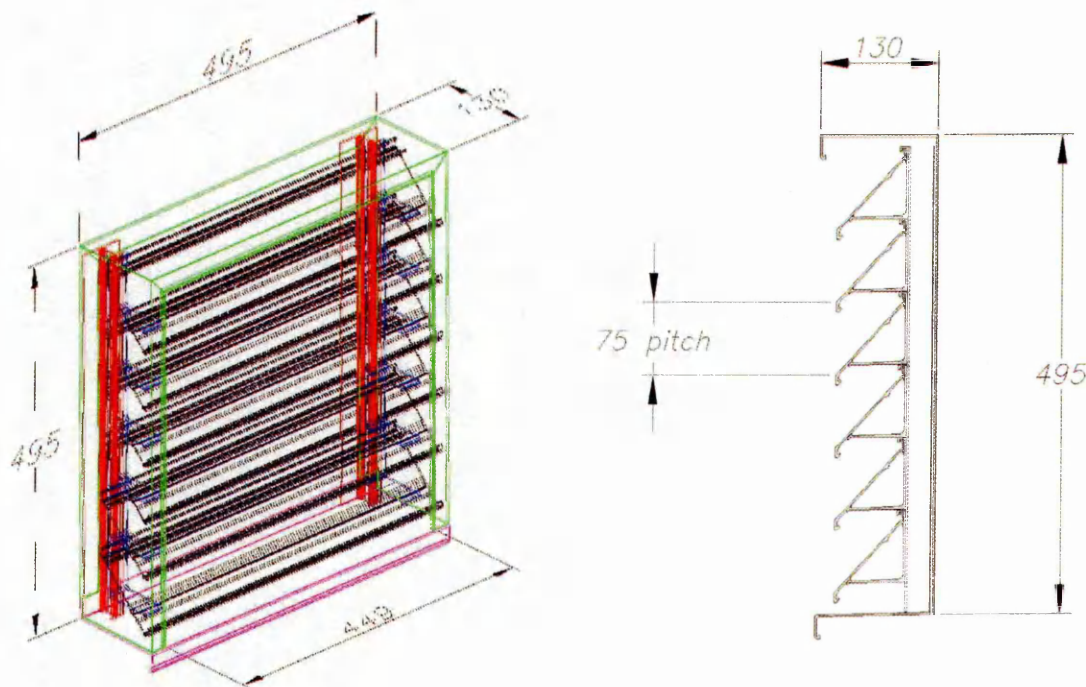
Figure 6.63: Typical CAD model of commercial ventilator

FLO/MCAD is a powerful software tool designed to help the user speed up and automate the geometry acquisition/simplification process leading to greater productivity and faster turnaround in airflow/thermal analysis. Normally the MCAD part geometry includes radii, fillets, draft angles, small holes and other features which are not important from an airflow/thermal standpoint, but which greatly increase the complexity and time required for analysis if included in the simulation [FLOVENT online documentation, *2002*]. A FLO/MCAD model of the louver shown in Figure 6.63 is represented as a solid object (Figure 6.64) after being imported into FLOVENT.
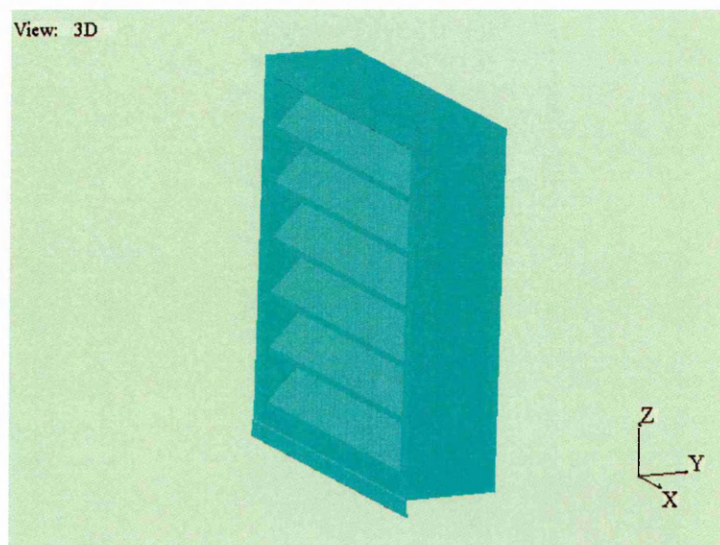
Figure 6.64: FLO/MCAD - louvre imported into FLOVENT

FLO/MCAM takes production quality CAD files and quickly and easily simplifies them for airflow/thermal analysis. It automatically eliminates intricate details surplus to the requirements for airflow/thermal analysis purposes whilst still giving the user exact control on the level of retained detail thus saving time and ensuring simulations accuracy. Using FLO/MCAD, the user can identify and remove unnecessary geometrical features such as non-planar surfaces, blends, fillets, small holes and protuberances, while preserving volume or surface area as appropriate.

6.8.4 Grid

A base grid comprising 100 x 100 x 80 cells was defined to fit the geometry of the plenum box surface and ventilator component. However, the number of cells was slightly adjusted for the different ventilator models used. A refined mesh was necessary around the louver area because in this area large gradients of the solution variables were

-193-

anticipated. The final grid was arrived at by adjusting the number of cells in grid patches and performing grid sensitivity assessments on a number of simulation cases until a difference of less than 5% in ΔP's predicted at a selection of points within the computational domain was achieved. This level of accuracy was considered adequate taking into account the other uncertainties in problem definition likely to be encountered in practice.

6.8.5 Range of investigations (airflow rates and pressure differentials)

Pressure differentials generated across ventilator components during the investigation ranged from 0 to 2 Pa depending on the type of component being tested. It is recognised that the computational work was done using very low pressure differences at the lower end of those typical in natural ventilation systems in buildings. However, as the intent was to compare CFD and experimental results it was necessary to limit the simulation parameters to those achieved during experimental measurements where it was difficult to achieve higher pressure differences because of the relatively open louvers and meshes investigated. Therefore, simulation airflow rates were prescribed so as to achieve pressure differences of a similar magnitude to those obtained experimentally.

6.8.6 Boundary conditions

Laboratory studies are an important first step in establishing appropriate boundary conditions for CFD/ventilator analysis. Hence, some supporting experiments were carried out to establish some of the boundary conditions before any attempt was made to obtain results from CFD simulations. These boundary conditions together with other key simulation parameters are described below:-

THE PRESSURE DROP CAUSED BY THE PRESENCE OF A VENTILATOR

The pressure drop caused by the presence of a ventilator can be split into two major components, namely, the frictional forces resulting from the roughness (see below) of solid surfaces and inertia losses due to velocity changes resulting from angled louvre blades and other variations in size of the flow path within a ventilator. Many CFD studies, for example Maghrabi *[2000]*, neglect roughness of surfaces over which air flows in their simulation models. Although this is acceptable for bulk air movement investigations, for detailed study of airflow on a more or less microscopic scale, as was the case in this investigation, it is important to incorporate the actual roughness of

surfaces to reflect the reality. Detailed discussion and guidance on various aspects relating to surface roughness is beyond the scope of this study. However, the author would direct any interested reader to British Standard BS1134 - 1 [*1988*] and the book "*Exploring Surface Texture*" by Dagnall [*1986*] as excellent starting points or sources of data/information on surface roughness. The roughness of the material (extruded aluminium) used to make the commercial louvers used in this investigation was accurately measured at Sheffield Hallam University (Materials Engineering Laboratory). Roughness measurements were carried out on a Taylor Hobson Laser Form Talysurf MK 1 (2 micron radius stylus) surface texture machine. From several measurements taken on the louvers an average roughness value Ra = 0.3756 micron was adopted for incorporation into the CFD model for all simulations carried on the commercial louvers.

THE PRESSURE DROP CAUSED BY THE PRESENCE OF MESH SCREEN

For the mesh-screens, the flow breaks up into a number of small high velocity jets which coalesce into a small velocity stream and the pressure loss is primarily due to loss of kinetic energy of the high-velocity jets [Kordyban, *2000*]. The insect screen and bird guard, which fall into this category, were modelled as *planar resistances*[B] because the depth/thickness of the meshes was considered very small compared to the overall dimensions of the mesh-screen. Specification of this boundary condition was in the form of a loss coefficient k obtained experimentally and by using the standard equation:

$$\Delta p = 0.5 * k * \rho * v^2$$

(6.6)

A direct benefit of using this approach was significant reduction in the number of grid cells and computing resources gained by not modelling the geometry of the meshes in detail. An empirical formula for the loss coefficient k of a thin walled mesh-screen of perforated sheets or strips with sharp-edged orifices, supported by a large number of measurements is [Idelchik, *1989*]:

[B] *A planar resistance is a simple flow element (available as a smart-part in FLOVENT) that correctly produces a pressure drop related to the airflow rate through it, provided that the flow direction is more or less perpendicular to it.*

$$k = \left(0.707\sqrt{1-f_a} + 1 - f_a\right)^2 \frac{1}{f_a^2} \qquad (6.7)$$

where f_a is the fractional open area of the mesh-screen.

The pressure drop given by this formula agrees well with experimental data obtained in this investigation. The formula gives k values of 1.4 and 2 for the bird guard and insect-screen respectively. The k values derived from the experiments and used in the CFD model were 1.14 and 1.60 for the bird guard and insect-screen respectively.

THERMAL BOUNDARY CONDITIONS

All cases were modelled with constant ambient and airflow temperatures set to match the actual experimental flow conditions after correction to standard temperature and pressure and taking into account background leakages from the test rig. The simulations were carried out for flow only with the thermal calculations disabled.

6.8.7 Simulation results

This investigation has highlighted an example of integrating CAD and CFD models as a tool for analyzing ventilators for natural ventilation applications. In all cases considered the simulations were run till a converged solution was obtained. Solution times ranged from 2 hours (most Louver X cases) to just under 8 hours (Louver Z). A description of Louvers X, Y and Z is given in *Section 5.3.3*. The predicted results of pressure differentials at various louver face velocities simulated are tabulated in Table 6.8.

Table 6.8:
CFD calculated pressure differentials for inlet configurations

Louvre	Mesh type	Predicted ΔP (Pa) at louver face velocity		
		0.05 (m/s)	0.25 (m/s)	0.50 (m/s)
X	no mesh	0.019	0.361	1.453
X	bird guard	0.026	0.454	2.450
X	insect screen	0.030	0.718	2.828
Y	no mesh	0.016	0.362	1.451
Y	bird guard	0.018	0.388	1.555
Y	insect screen	0.019	0.415	1.750
Z	no mesh	0.018	0.379	1.501
Z	bird guard	0.018	0.386	1.527
Z	insect screen	0.021	0.440	1.745

The results in Table 6.8 will be compared with experimental data in the next chapter. Here a comparison was made of the airflow performance of the louver/mesh-screen systems based on the simulation results for louver face velocities of 0.05 m/s (Figure 6.65), 0.25 m/s (Figure 6.66) and 0.5 m/s (Figure 6.67). For a given louver face velocity the pressure differential represents the resistance to airflow through the ventilator, hence the lower the resistance the better the airflow performance.
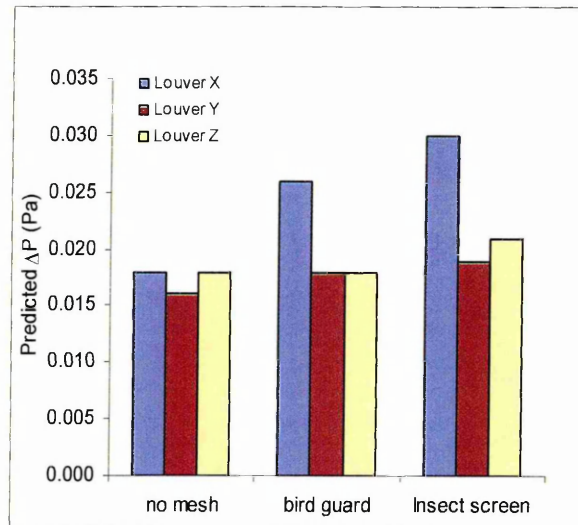
Figure 6.65: Predicted ΔPs at 0.05m/s louver face velocity
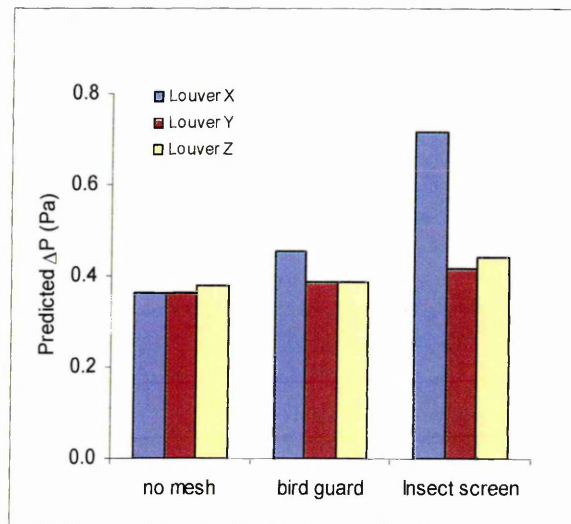
Figure 6.66: Predicted ΔPs at 0.25m/s louver face velocity
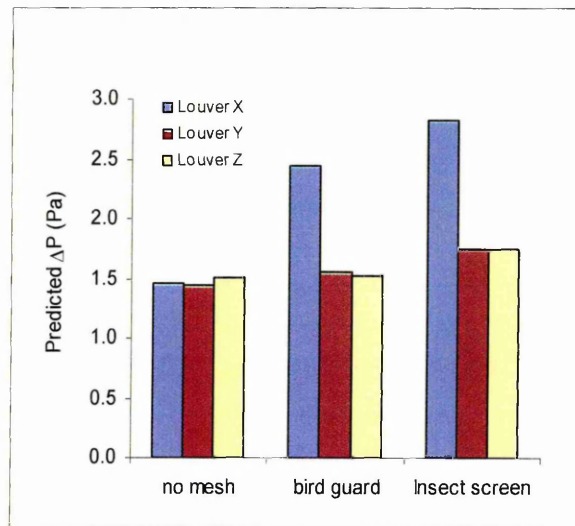
Figure 6.67: Predicted ΔPs at 0.5m/s louver face velocity

It is clear from the above bar charts that the impact of the mesh-screen and bird guard was more significant on Louver X than it was on Louver Y and Louver Z. The predicted ΔPs associated with each louver system for a face velocity of 0.05m/s are shown in Figure 6.65. At this face velocity it can be seen that Louver X gave the worst performance since it had the highest resistance when used in isolation or in combination with an insect-screen and a bird-guard mesh-screen. Louver Y gave better airflow performance than Louver Z when used in isolation or with an insect screen mesh. Used with the bird guard mesh-screen Louver Y and Louver Z achieved the same airflow performance. It can be seen from Figure 6.66 that for a face velocity of 0.25 m/s Louver Z gave a marginally worse airflow performance than the other two louvers when used without any mesh. When used in combination with an insect screen and a bird-guard mesh screen Louver X fared badly compared to other two louvers which again achieved similar airflow performance when used with a bird-guard. Louver Y marginally performed better than Louver Z when used with an insect screen. The predicted ΔPs associated with each louver system for a face velocity of 0.5 m/s are shown in Figure 6.67. For this face velocity Louver X again exhibited the worst airflow performance compared to the other two louvers when used with either type of mesh. On the other hand Louver Y and Louver Z achieved approximately the same performance when used in combination with an insect-screen or bird guard mesh-screen. The airflow performance of Louver Z was marginally worse than the other two louvers when used in isolation.

The above findings suggest that Louver X had the highest resistance to airflow, hence the worst performance, for all face velocities considered. Not surprisingly Louver Y and Louver Z generally gave a similar airflow performance for all face velocities considered. This was expected because Louver Y and Louver Z were very similar to each other geometrically with the only difference being that Louver Z incorporated an additional offset or "rain hook" on each blade which is intended to provide additional protection against water ingress during operation in actual buildings. The expected negative impact of the rain hooks on the airflow performance of Louver Z compared to Louver Y was detectable from the simulation results when the louvers were used without any mesh-screen for all face velocities considered. This was also evident when the louvers where used in combination with an insect-screen at the lower face velocities. However, when used with a bird-guard mesh-screen at 0.05 and 0.25 m/s face velocities, and also when used with an insect screen at 0.5 m/s the detrimental effect of the rain hooks was undetectable from the simulation results. The results given in Table 6.8 will be compared with experimental findings (see also *Chapter 5*) in the following chapter.

6.9 Problems Encountered and Limitations

Some discrepancies from expectation are inevitable when a physical situation is simulated by a theoretical model. With CFD sometimes the discrepancies can be small and their exact cause can be difficult to ascertain. It must be remembered that in CFD the solution is strictly a solution of the numerical problem, not of the physical problem, and that differences between these two could be due to such things as an inadequate grid or a poor turbulence model. Apart from the usual inaccuracies resulting from the application of turbulence models (k - ε model in this case) there were some minor problems encountered in this investigation in relation to achieving full convergence of the simulated situations within reasonable time-frames. Another problem stemmed from the preparation of CAD drawings. The drawings obtained from the ventilator manufacturer were excellent and very detailed for production/fabrication purposes. Although these CAD files could easily be simplified using FLO/MCAD some ventilator elements were inevitably lost whilst some that had no impact on airflow performance could not be left out during simplification. The ideal situation would be to prepare CAD models sufficiently detailed with a specific intention of being used in CFD models. This

would reduce the number of grid cells necessary and hence reduce on the computing resources required during simulations.

On the other hand a major limitation with the simulation models used related to the modelling of mesh-screens. Although CAD models of the mesh-screens were available, these could not be imported into FLOVENT using the FLO/MCAD module since the files were excessively huge because of the large number of tiny openings and thin dimensions of the mesh-screen materials. In addition it would not have been feasible to handle the large number of grid cells resulting from the "physical" representation of the mesh-screens. Following discussions with the FLOVENT user-support team it was decided that the mesh-screens would be modelled as planar resistances which, although they correctly produce a pressure drop related to the airflow rate, they do not reflect the actual airflow interactions and effects resulting from air flowing around solid objects such as the woven round wires or thin plates from which mesh-screens are fabricated. This could have contributed to the discrepancies in the computational results obtained since the airflow models used were representing flow situations on a more or less microscopic scale.

6.10 Concluding Remarks

This chapter described how CFD was used as tool to predict parameters from simulations of airflow through ventilator components. This involved the identification of a suitable model and validating this for use in the current investigation. The validation process involved the comparison of FLOVENT predictions with well known standard analytical solutions and also a solution obtained using a different CFD software package (PHOENICS). The k - ε turbulence model was selected for use in this investigation following discussions/recommendations from the FLOVENT user-support team and its wide use in research and design applications. The investigation highlighted an example of integrating CAD and CFD models as a tool for analyzing commercial ventilators for natural ventilation applications. The range of investigation of the modelling task was determined based on experimental findings. During the course of the investigation the following observations were made:-

- A literature review revealed that there has been very little work done on CFD studies of the airflow performance of ventilators and their associated components for natural ventilation applications.

- Although there is an increased application of CFD to predict airflows in buildings, there is still limited availability/evidence of supportive validation studies particularly in relation to airflow in building components.

- By making appropriate assumptions and carefully selecting boundary conditions, CAD/CFD modelling could be used as a tool for analysing the airflow performance of the ventilators.

- Where CAD drawings are imported into CFD software to speed up geometry generation ventilator drawings need to be simplified at CAD modelling stage, leaving only sufficient detail that would affect the airflow performance at the CFD modelling stage. This reduces on the computing requirements during CFD simulations.

This computational investigation has met its task of analysing the airflow performance of ventilator components using CFD. In so doing substantial data has been obtained which can be used for validation of other studies involving slots, mesh-screens and louvers, and relating to ventilators for natural ventilation in buildings. CFD predicted parameters from this investigation will be compared with experimental results in the following chapter.

Chapter 7

VENTILATOR AIRFLOW PERFORMANCE

OPTIMISATION

7.1 Introduction

This chapter is arranged in two main parts. The first section presents and discusses comparisons of CFD predicted parameters (see *Chapter 6*) and experimental results of some of the components tested in the various experiments described in *Chapter 5*. The intention was to assess whether CFD can be used in the design and analysis of ventilators. The latter part of the chapter utilises the experimental results to derive general equations proposed for application to ventilators for natural ventilation in buildings. Using data from Chapter 5 the trends of the results can be predicted by considering what effects would be expected if combinations of certain components/configurations are used in a ventilator. The aim of the second part of this chapter was to quantify the measured results, identify any trends in the results and ultimately derive simple mathematical models that describe the airflow behaviour of a given ventilator configuration. Multiple regressions were utilised in obtaining relationships between airflow rates, pressure differentials applied across ventilator components, mesh-screen free area, louver blade inclination angles and, where applicable, gaps between louver blades and mesh-screens. An investigation/assessment of the influence of these parameters on the airflow rate through a ventilator is also included using graphical and numerical representations of the variations of the key variables. In addition this chapter relates the findings of the investigations in this thesis to research findings by other investigators.

7.2 Experimental and Computational Comparisons

There is a wealth of information available in the literature about experimental and computational work in the general area of ventilation. Many reports can be found in which air flows in ventilation systems are simulated using CFD methods. Some of them have provided promising results when compared with available experimental data.

However, in the specific area of airflow through ventilators there is a lack of information and several investigators have repeatedly highlighted the need for further research.

CFD affords the opportunity to explore more design possibilities within specified time and budget constraints. More extensive information can be extracted from CFD compared to experimental measurements. For instance, CFD yields values of the computed dependent variables (e.g. velocity, pressure, temperature) at literally thousands or even millions of discrete points in space and time in time-dependent problems. From this high density of information can be extracted qualitative and quantitative pictures of flow streamlines and three dimensional contours of any computed dependent variable. Experimental measurements, on the other hand, traditionally have been limited to global quantities or to values of flow variables at a small number of points in space and /or time. Thus in principle much more complete information is available from CFD to guide the next design iteration. In practice, however, the engineering and scientific community typically accepts measurements from experiments as being more reliable than similar information generated by a CFD calculation. This is the reason for the strong emphasis placed by the profession on "validating" CFD results. Whilst it is true that there are many sources of uncertainty in CFD, the same is true of experiments.

In FLOVENT, as in many other simulation packages, the results obtained are not always directly comparable to quantities which are easily measurable. In other words, the data that are most pertinent to the end user are not easily obtained in a form comparable to measured parameters. Since measured data can only really be obtained at a discrete set of points, points which may or may not have the appropriate data within the model, coupled with the challenge of matching up a physical location with a location in the computational model, and accurately representing the effect of the sensor on airflow pattern [Plunkett, *2000*].

When comparing CFD results with measurements for engineering problems, it is more appropriate to approach the exercise as a "reconciliation" rather than a "validation" as the latter implies that the experiment provides the "correct" values. Naturally some discrepancies exist between computational results and experimental data. As such it is

-203-

important to address the sources of the discrepancies, although this is extremely difficult or impossible in some situations. The advantages of using CFD over conventional experimental studies are many and well documented. Here only a few are highlighted:-

- ability to study systems where experiments are extremely difficult or not possible

- reliable CFD modelling saves time and money

- ease of performing a large range of parametric studies in a shorter time frame than the experimental investigation

- cost of computer hardware is always reducing while its performance is increasing, and software is more user-friendly whilst the cost of materials and full scale models is ever on the increase

- CFD overcomes problems of scale models

Some disadvantages or drawbacks of CFD are:-

- the accuracy of numerical results is strongly dependent on the accuracy and correctness of boundary conditions, therefore if wrong boundary conditions are used wrong results would be obtained, and sometimes it can be time consuming to detect the cause

- Computational techniques rely totally on the validity of the analytical models in the coding. If these are wrong, or the understanding of the physical phenomena is not yet available, simulation techniques can not be used

The experimental study was conducted on test rigs designed and constructed in accordance with CEN standard BS 13141-1:*2004*. A description of the experimental test rigs can be found in *Chapter 5* of this thesis. The standard k - ε turbulence model was used for the computational study using a three-dimensional domain described in *Chapter 6*. The experimental investigation involved subjecting various ventilator components through a range of airflow rates and pressure differentials typical in natural ventilation of buildings applications (see *Chapter 2*). CFD was used to simulate the airflow behaviour of ventilator components, over a range of parameters obtained during the experimental phase of the investigation. Most simulations achieved full convergence as described in *Sections 6.7* and *6.8* of the previous chapter. In the following sections

results of comparisons between CFD predictions of parameters on slots and louvers are presented and discussed. A relative error was used to compare CFD predicted and experimental data and to assess the degree of agreement between the two data sets. The relative error (R.E.) was defined by the following expression:

$$R.E. = \frac{\varphi_{CFD} - \varphi_{Msd}}{\varphi_{Msd}} 100(\%) \tag{7.1}$$

where φ_{CFD} and φ_{Msd} represented predicted and measured parameters respectively. In CFD this type of error can generally be linked to geometric source i.e. in other words, some aspect of the geometry which affects flow phenomena not being represented finely enough to result in the measured parameter [Plunkett, *2000*].

7.2.1 Slots of varying depth

This section includes a discussion of predicted flow characteristics compared with data obtained from experimental measurements on slots of varying depth and fixed height (Slots B1 to B6). A description of these slots and specific dimensions are given in *Section 5.3.1*. Experimental and CFD predicted data for these slots are given in *Section 5.4.4* and *Section 6.7.1* respectively. The comparisons were undertaken from both the power law and quadratic formulation point of view. For the power law, predicted airflow rates at various pressure differentials were compared against experimental data. Whereas for the quadratic formulation predicted pressure differentials corresponding to various airflow rates were compared against experimental findings. The following subsections compare predicted performance quantities against experimental data, and where applicable predicted flow characteristics are compared with experimental flow characteristics. The intention was to demonstrate that CFD can be used to analyse the airflow performance of ventilators. Figure 7.1 to Figure 7.4 show typical predicted and measured airflow rates and pressure differentials for the slots B1 to B6 using both the power law and quadratic formulations. Figure 7.5 and Figure 7.6 illustrate the variation of relative error for all slots with respect to ΔP for the power law and with respect to airflow rate Q for the quadratic formulation. In these graphs the data points for Slots B1 to B6 are plotted together without any distinction since part of the intention was to provide a visual appreciation of the spread of the relative errors. The graphs, discussed below, have been aligned side-by-side for ease of comparison.
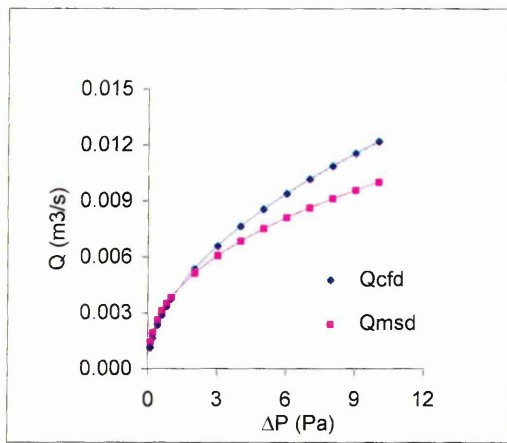
Figure 7.1: Comparison of CFD predicted and experimentally measured airflow rates for slot B4 without a mesh-screen (power law)
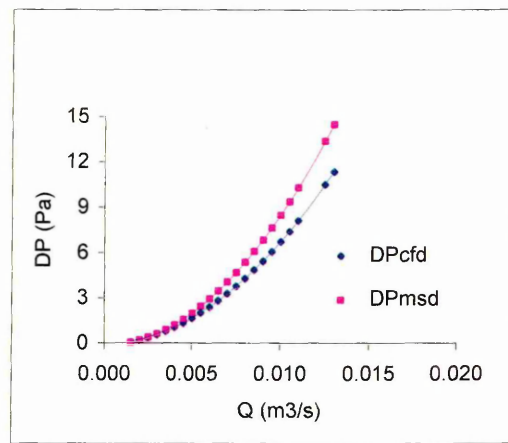
Figure 7.2: Comparison of CFD predicted and experimentally measured ΔPs for slot B4 without a mesh-screen (quadratic)
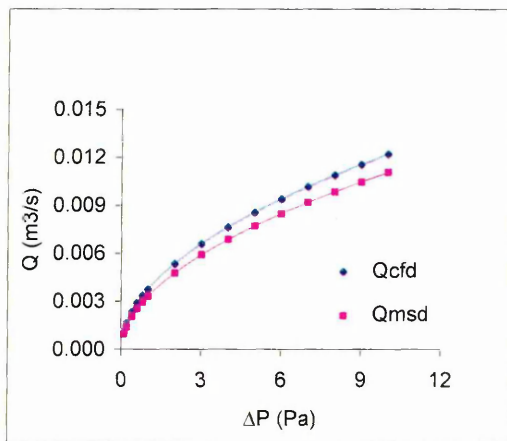
Figure 7.3: Comparison of CFD predicted and experimentally measured airflow rates for slot B6 without a mesh-screen (power law)
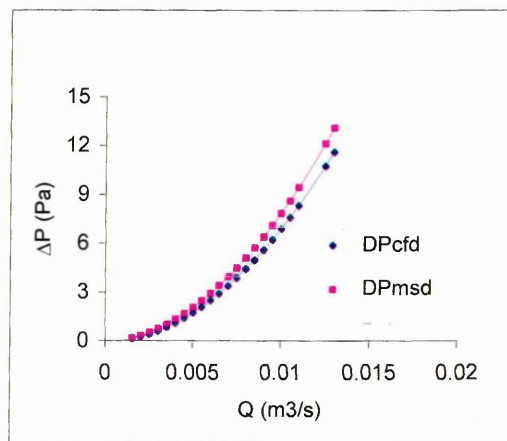
Figure 7.4: Comparison of CFD predicted and experimentally measured ΔPs for slot B4 without a mesh-screen (quadratic)
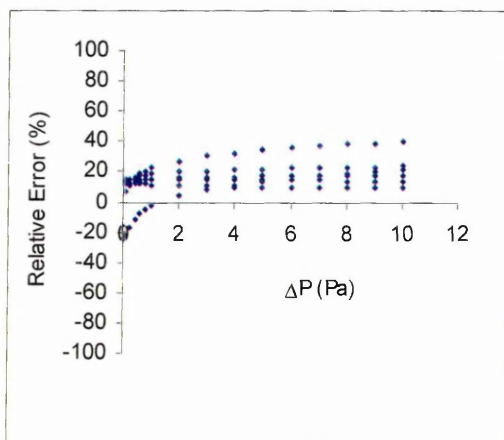
Figure 7.5: Power Law variation of relative error for Slots B1 to B6 without mesh-screen
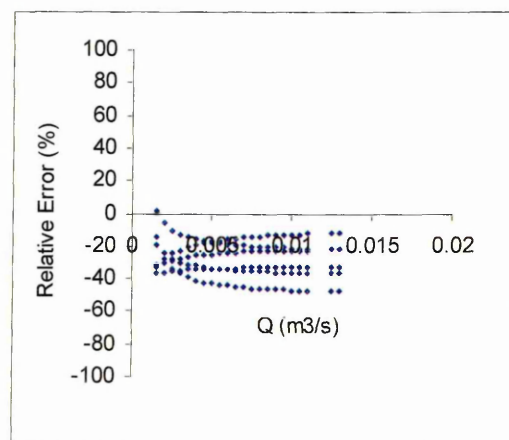
Figure 7.6: Quadratic variation of relative error for Slots B1 to B6 without mesh-screen

-206-

Three categories emerged from the analysis of relative errors for type B slots when examined from the power law point of view. The first which included Slots B1, B2 and B3 exhibited a trend whereby the relative error increased with increasing pressure differential. This could have been caused by an increase in turbulence associated with an increased quantity of air flowing through a restriction of fixed size. At low pressure differentials (below 1Pa) the relative errors ranged from 7% to 14% whilst at high pressure differentials (close to 10Pa) the relative error ranged from 18% to 40%. Slot B4 behaved differently from the other slots in that at pressure differentials below 1Pa the relative error decreased with increasing pressure differential whilst above 1Pa the relative errors increased with increasing pressure differential (Figure 7.1). Slot B5 and Slot B6 (Figure 7.3) formed the third category with the relative error decreasing (only marginally for Slot B5) with increasing pressure differentials. These deeper slots may have introduced a straightening effect on the airflow pattern, compared to Slots B1, B2 and B3, thus reducing the turbulence on the downstream side of the slot. For these slots the relative error ranged from 9% to 16% over the range of pressure differentials considered. The relative error trend for Slot B4 thus initially followed that for Slots B5 and B6 at low pressure differentials and then switched to a trend similar to Slots B1, B2 and B3 at higher pressure differentials. A possible explanation of this can be derived from the vena-contracta phenomena (*Section 3.7.1*). In relation to the slots, a change in slot depth would most likely result in a shift in the location of the vena-contracta for a given airflow rate/pressure differential with a consequent change in airflow pattern upstream and downstream of the slot. Thus the influence of this could have been significant in the computational model during the simulation of the airflow through Slot B4. The CFD model tended to over predict the airflow rates for all slots and all pressure differentials considered except for Slot B4 which revealed under-prediction at pressure differentials below 1Pa (Figure 7.1).
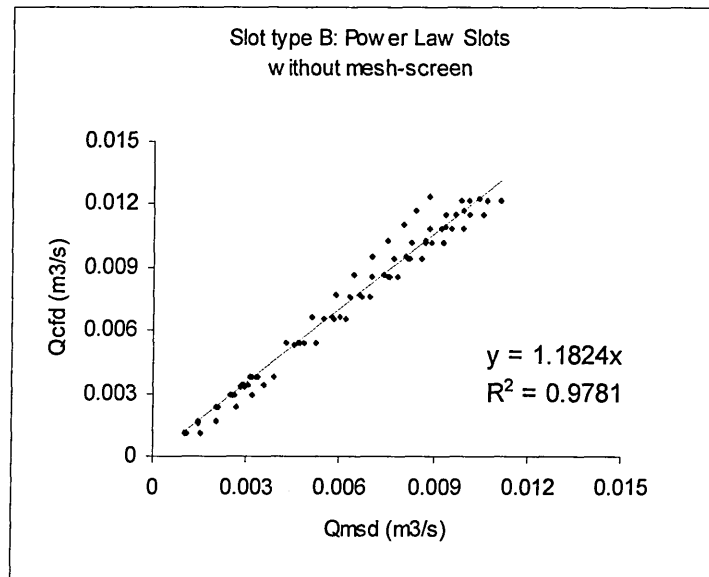
Figure 7.7: Linear regression fit between CFD predicted and experimentally measured airflow rates for Type B slots

The CFD predicted airflow rates shows strong correlation with measured data as can be seen from the correlation coefficient of 0.978. The slope of the regression line was 1.18. This means that the CFD predicted airflow rates were predominantly higher than the measured values.

QUADRATIC - SLOTS OF VARYING DEPTH WITHOUT A MESH-SCREEN

From the quadratic formulation point of view the CFD model under-predicted the pressure differentials for all slots for the range of airflow rates considered. From this point of view the slots followed two trends of variation of relative error with respect to airflow rate emerged. The first, including Slots B1, B2 and B4, had the relative error increasing with increasing airflow rate (Figure 7.2). The second, comprising Slots B3, B5 and B6, had the relative error decreasing with increasing airflow rate (Figure 7.4). For this case the "straightening effect" could be used as a reason for the relative error trends obtained, however this would not hold for Slots B3 and B4 which appear to fall in opposite groups. Overall the relative error ranged from 5.7% to 47% with Slots B1, B2 and B3 showing higher relative errors than Slots B4, B5 and B6. This was attributed to the fact that Slots B4, B5 and B6 had a more airflow straightening effect than Slots B1, B2 and B3 hence the fluctuations in measuring pressure differentials were less.
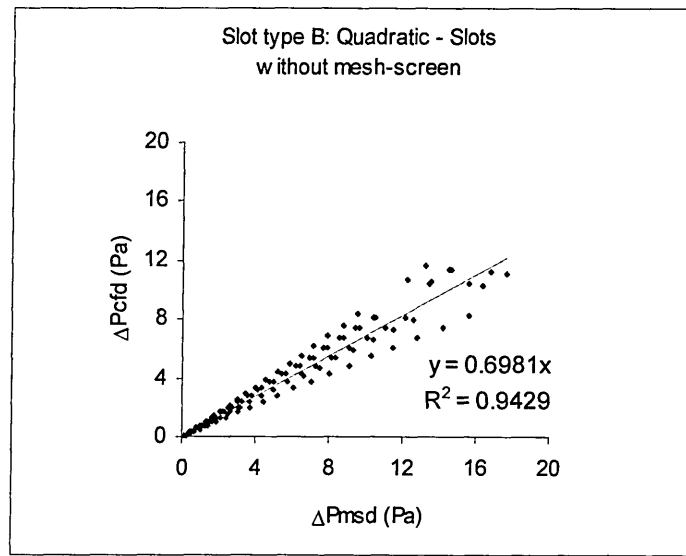
Figure 7.8: Linear regression fit between CFD predicted and experimentally measured ΔPs for Type B slots

The CFD predicted pressure differentials shows strong correlation with measured data as can be seen from the correlation coefficient of 0.943. The slope of the regression line was 0.698. This means that the CFD predicted pressure differentials were predominantly lower than the measured values.

7.2.2 Slots of varying height

This section includes a discussion of predicted flow characteristics compared with data obtained from experimental measurements on slots of varying height and fixed depth (Slots A1 to A6). A description of these slots and specific dimensions are given in *Section 5.3.1*. Experimental and CFD predicted data for these slots are given in *Section 5.4.4* and *Section 6.7.2* respectively. Here again the comparisons were undertaken from both the power law and quadratic formulation point of view. For the power law, predicted airflow rates at various pressure differentials were compared against experimental data. Whereas for the quadratic formulation predicted pressure differentials corresponding to various airflow rates were compared against experimental findings.

The following subsections compare predicted performance quantities against experimental data, and where applicable predicted flow characteristics are compared with experimental flow characteristics. Figure 7.9 to Figure 7.14 show typical predicted

and measured airflow rates and pressure differentials for the slots A1 to A6, without a mesh-screen, using both the power law and quadratic formulation. Figure 7.15 to Figure 7.18 show typical predicted and measured airflow rates and pressure differentials for the slots A1 to A6 used in combination with a mesh-screen, using both the power law and quadratic formulations. Figure 7.19 and Figure 7.21 illustrate the variation of relative error for all slots (without a mesh-screen) with respect to ΔP for the power law and with respect to airflow rate Q for the quadratic formulation. Figure 7.20 and Figure 7.22 illustrate the variation of relative error for all slots (with a mesh-screen) with respect to ΔP for the power law and with respect to airflow rate Q for the quadratic formulation. To visually appreciate the spread of the relative errors the data points of all slot sizes were plotted together without any distinction.
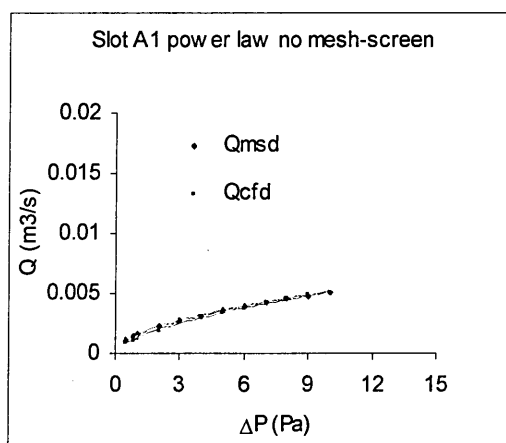
Figure 7.9: Comparison of CFD predicted and experimentally measured airflow rates for slot A1 without a mesh-screen (power law)
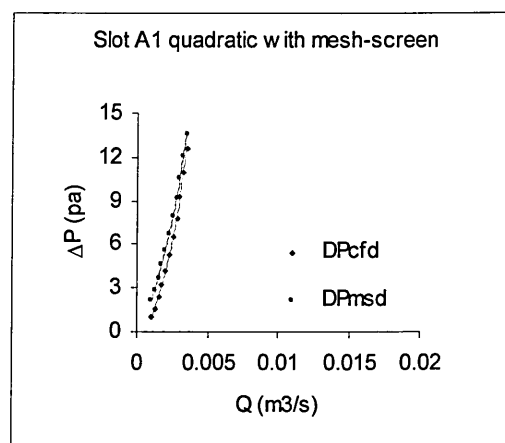
Figure 7.10: Comparison of CFD predicted and experimentally measured ΔPs for slot A1 with a mesh-screen (quadratic)
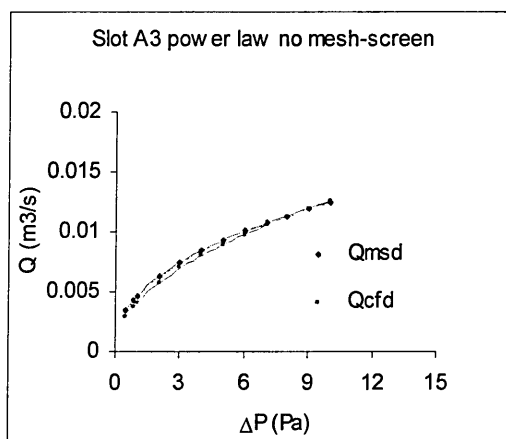
Figure 7.11: Comparison of CFD predicted and experimentally measured airflow rates for slot A3 without a mesh-screen (power law)
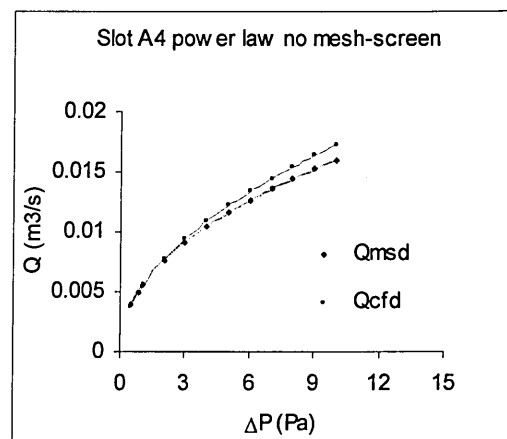
Figure 7.12: Comparison of CFD predicted and experimentally measured airflow rates for slot A4 without a mesh-screen (power law)
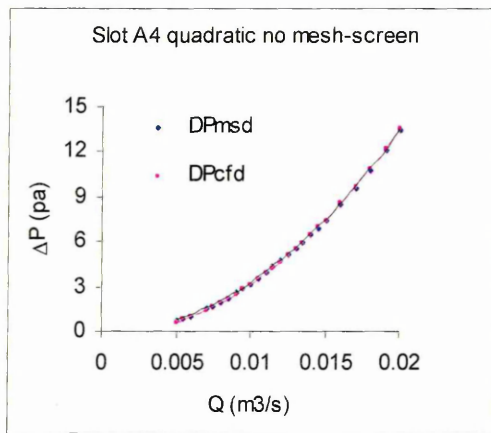
Figure 7.13: Comparison of CFD predicted and experimentally measured ΔP for slot A4 without a mesh-screen (quadratic)
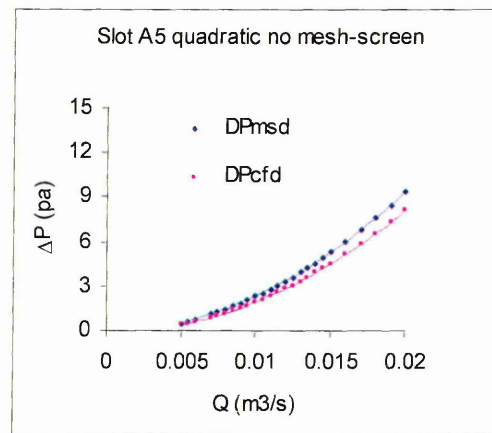
Figure 7.14 Comparison of CFD predicted and experimentally measured airflow rates for slot A5 without a mesh-screen (quadratic)
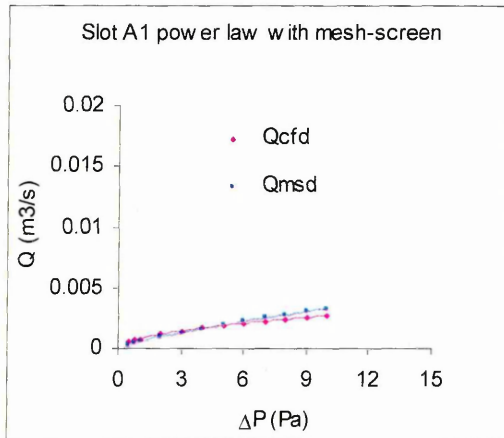
Figure 7.15: Comparison of CFD predicted and experimentally measured airflow rates for slot A1 with a mesh-screen (power law)
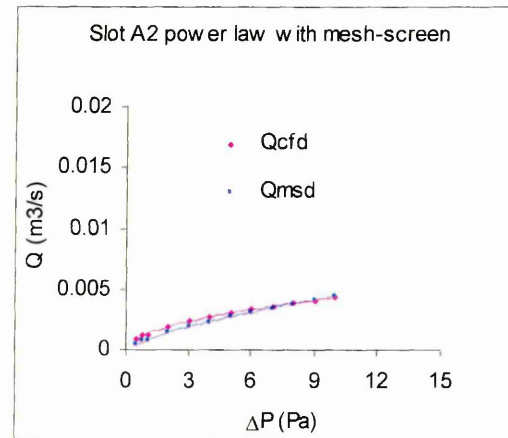
Figure 7.16: Comparison of CFD predicted and experimentally measured airflow rates for slot A2 with a mesh-screen (power law)
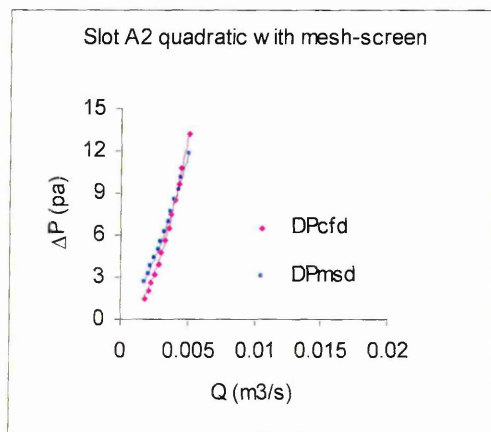
Figure 7.17: Comparison of CFD predicted and experimentally measured ΔPs for slot A2 with a mesh-screen (quadratic)
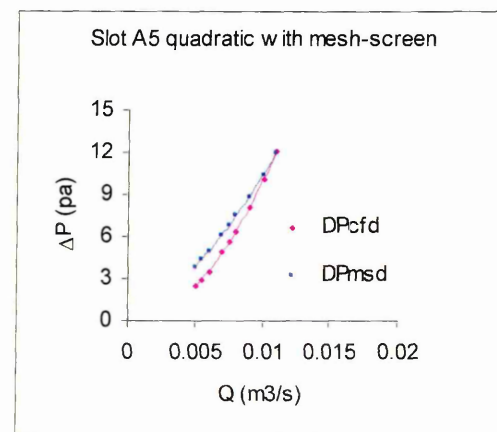
Figure 7.18: Comparison of CFD predicted and experimentally measured ΔPs for slot B6 without a mesh-screen (quadratic)
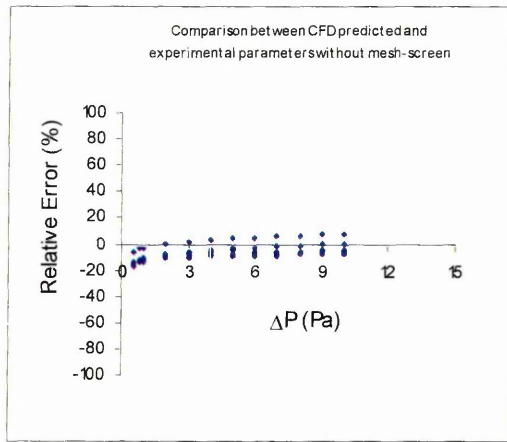
Figure 7.19: Power Law - Comparison between CFD predicted and measured ΔPs for slots of varying height without a mesh-screen
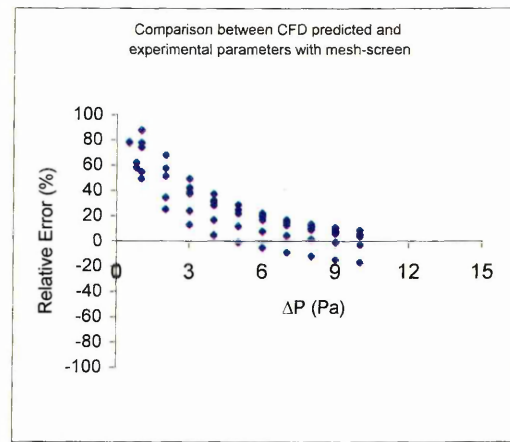
Figure 7.20: Power Law - Comparison between CFD predicted and measured ΔPs for slots of varying height with a mesh-screen
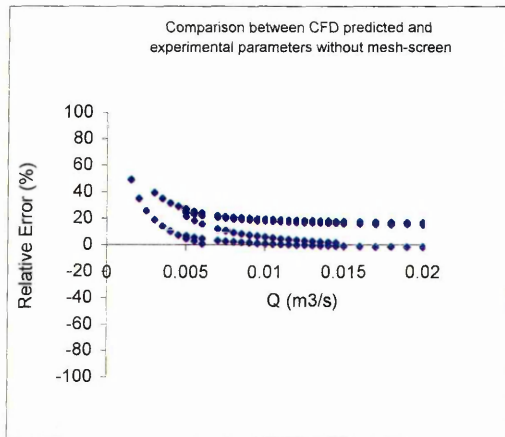
Figure 7.21: Quadratic - Comparison between CFD predicted and measured airflow rates for slots of varying height without a mesh-screen
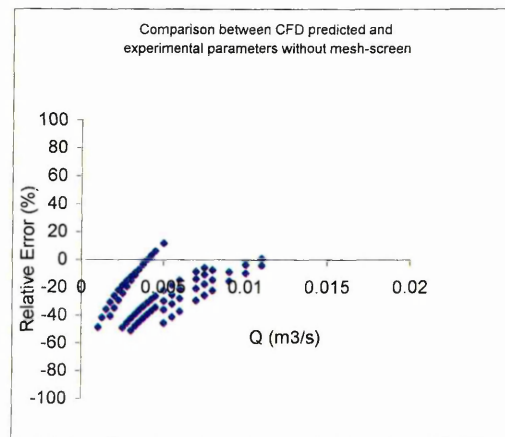
Figure 7.22: Quadratic Comparison between CFD predicted and measured airflow rates for slots of varying height with a mesh-screen

POWER LAW - SLOTS OF VARYING HEIGHT WITHOUT A MESH-SCREEN

From the results of the analysis on Slots type A without a mesh-screen it was observed that relative to the pressure differential, the relative error between CFD predicted airflow rates and experimentally measured ones generally reduced with increasing pressure differential. This was attributed to the airflow through the slots becoming more established with increasing pressure differential with a consequent result of reduced turbulence/fluctuations in the measured data. The CFD model generally under-predicted the airflow rates for all slots. The only exception was for Slot A4 which had the relative error increasing with pressure differentials and the CFD model indicating an over-

-212-

prediction of pressure differentials above 2 Pa (Figure 7.13). Overall the relative error between CFD predicted and experimentally measured pressure differentials for slots A1 to A6 ranged from 0.6% to -16.2% (Figure 7.19). For all slots the highest relative errors were observed for very low pressure differentials.
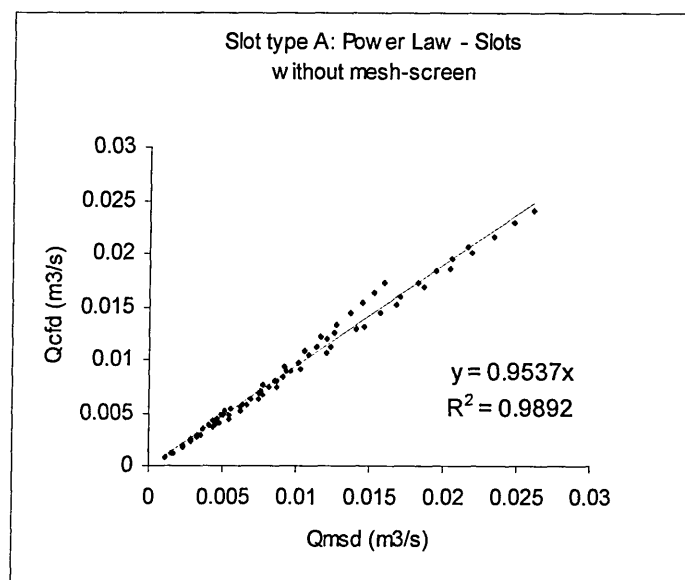
Figure 7.23: Linear regression fit between CFD predicted and experimentally measured airflow rates for Slots type A

The CFD predicted airflow rates shows strong correlation with measured data as can be seen from the correlation coefficient of 0.989. The slope of the regression line was 0.954. This means that the CFD predicted airflow rates were predominantly lower than the measured values.

POWER LAWS - SLOTS OF VARYING HEIGHT WITH A MESH-SCREEN

Addition of a mesh-screen to the slots generally increased the relative errors between predicted and experimentally measured parameters. The most likely reason for this was the inadequate representation of the mesh-screen boundary condition in the CFD model. This was represented by a pressure loss coefficient following consultation/discussion with the FLOVENT User-support Team. The full geometric description of the mesh-screens would have required the use of very fine grids incorporating numerous (millions) of nodes/cells for which it would not have been easy to solve efficiently whilst having a computationally "cheap" model. As such the pressure loss approach could have resulted in significant departure from the actual physical situation thus

-213-

leading to increased deviation between predicted and experimental parameters. The addition of the mesh-screen resulted in a significant increase of relative errors at low pressure differentials with the CFD model over-predicting the airflow rates at various pressure differentials. All slots exhibited the same trend whereby the relative error reduced with increasing pressure differential.
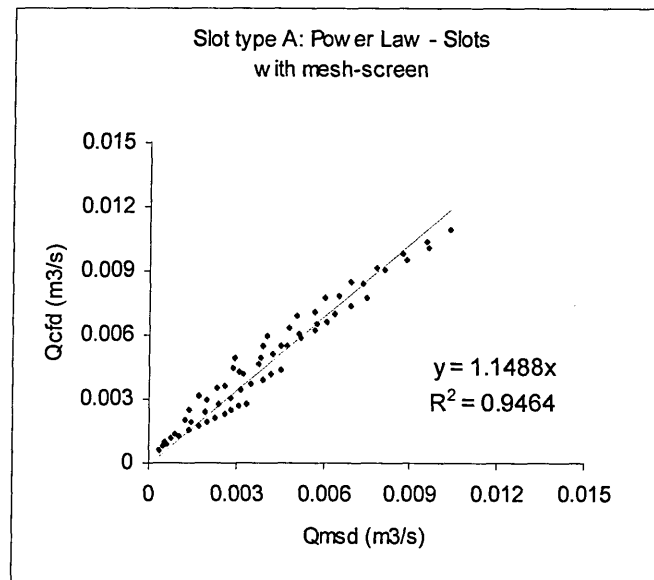
Figure 7.24: Linear regression fit between CFD predicted and
experimentally measured airflow rates for
Slots type A with mesh-screen

For all cases of the slots used in combination with a mesh-screen the CFD model tended to over-predict the airflow rates. The relative error ranged from -20% to as high as 88% with the high values been observed at low pressure differentials (Figure 7.20).

The CFD predicted airflow rates shows strong correlation with measured data as can be seen from the correlation coefficient of 0.9464. The slope of the regression line was 1.149. This means that the CFD predicted airflow rates were predominantly higher than the measured values.

QUADRATIC - SLOTS OF VARYING HEIGHTS WITHOUT A MESH-SCREEN

From the results of the analysis on Slots A1 to A6 used without a mesh-screen it was observed that the relative error between CFD predicted and experimentally measured pressure differentials at various airflow rates generally reduced with increasing airflow rate. The CFD model generally over-predicted the pressure differentials for all slots.

The only exception was for Slot A4 which had the relative error increasing with airflow rates and the CFD model indicating an under-prediction of pressure differentials at airflow rates above 0.013 m^3/s (Figure 7.13). Slot A4 gave the best agreement between computational and experimental parameters with the relative error ranging from 1.3% to 7.3% (Figure 7.13) whereas the worst case was for slot A5 (Figure 7.14) with relative errors at various airflow rates consistently falling between 15.5% and 25%. For all slots the highest relative errors were observed at very low airflow rates.
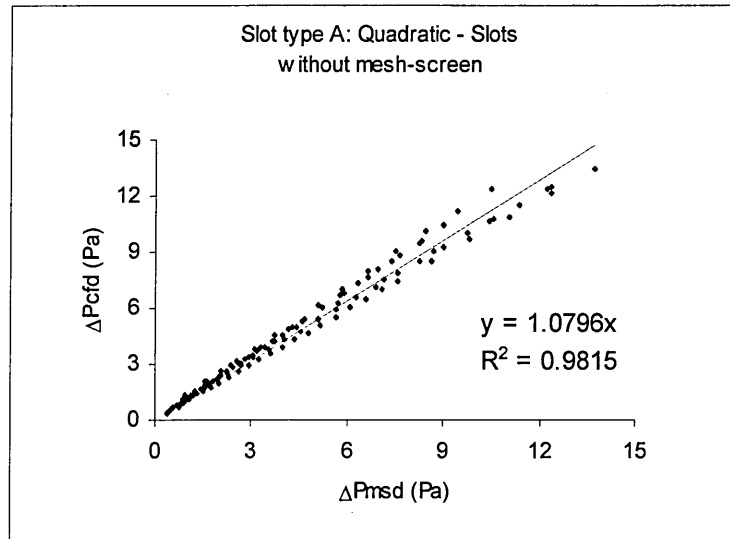
Figure 7.25: Linear regression fit between CFD predicted and experimentally measured ΔPs for Slots type A

The CFD predicted airflow rates shows strong correlation with measured data as can be seen from the correlation coefficient of 0.982. The slope of the regression line was 1.08. This means that the CFD predicted airflow rates were predominantly higher than the measured values.

QUADRATIC - SLOTS OF VARYING HEIGHTS WITH A MESH-SCREEN

Addition of a mesh-screen to the slots generally increased the relative errors between predicted and experimentally measured parameters. The addition of the mesh-screen generally resulted in an increase of relative errors and caused the CFD model to under-predict the pressure differentials at various airflow rates. Generally all slots exhibited the same trend whereby the relative error reduced with increasing airflow rate. The only exception was Slot A2 which over-predicted the pressure differentials at airflow rates above 0.004 m^3/s and resulted in the relative error increasing with increasing airflow rate (Figure 7.17).
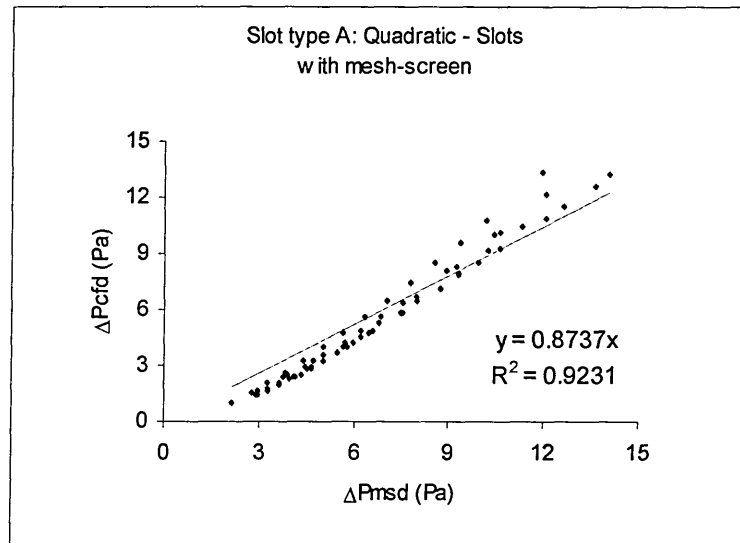
Figure 7.26: Linear regression fit between CFD predicted and experimentally measured ΔPs for Slots type A with mesh-screen

The CFD predicted airflow rates shows strong correlation with measured data as can be seen from the correlation coefficient of 0.923. The slope of the regression line was 0.874. This means that the CFD predicted airflow rates were predominantly lower than the measured values.

7.2.3 Commercial louvers

Simulations were carried out on louvres X, Y and Z used in combination meshes an insect screen and a bird guard (see *Section 5.3.5*) for airflow rates resulting in velocities of 0.05, 0.25 and 0.5 m/s on the louvre face. Table 7.1 shows a comparison between experimental results and CFD calculated ΔP values for inlet configurations.

Table 7.1:
Experimental results and CFD calculated pressure differentials for inlet configurations

Louvre	Mesh type	Louvre face velocity 0.05m/s			Louvre face velocity 0.25m/s			Louvre face velocity 0.5m/s		
		Measured ΔP (Pa)	CFD calculated ΔP (Pa)	$\frac{M-C}{M}$ (%)	Measured ΔP (Pa)	CFD calculated ΔP (Pa)	$\frac{M-C}{M}$ (%)	Measured ΔP (Pa)	CFD calculated ΔP (Pa)	$\frac{M-C}{M}$ (%)
X	no mesh	0.018	0.019	-5.6	0.382	0.361	5.5	1.448	1.453	-0.3
	bird guard	0.030	0.026	13.3	0.552	0.454	17.8	1.951	2.450	-25.6
	insect screen	0.048	0.030	37.5	0.607	0.718	-18.3	1.828	2.828	-54.7
Y	no mesh	0.018	0.016	11.1	0.336	0.362	-7.7	1.187	1.451	-22.2
	bird guard	0.034	0.018	47.1	0.512	0.388	24.2	1.659	1.555	6.3
	insect screen	0.031	0.019	38.7	0.527	0.415	21.3	1.801	1.750	2.8
Z	no mesh	0.017	0.018	-9.1	0.346	0.379	-9.5	1.298	1.501	-15.6
	bird guard	0.046	0.018	60.0	0.473	0.386	18.4	1.306	1.527	-16.9
	insect screen	0.048	0.021	56.3	0.487	0.440	9.7	1.332	1.745	-31.0

The results indicate that there is reasonable agreement between the two sets of data. Although the deviations extend over a wide range nearly two-thirds of the cases considered were under ±20%.

It is clear from Table 7.1 that only the CFD model for louvre Y used in combination with meshes consistently under-predicted the ΔP's. The results also show that the models used tended to over-predict the ΔP at the higher louvre face velocity i.e. 0.5 m/s and under-predicted ΔP's at 0.05 m/s. Generally better agreement was achieved when no mesh-screen was included in the model.
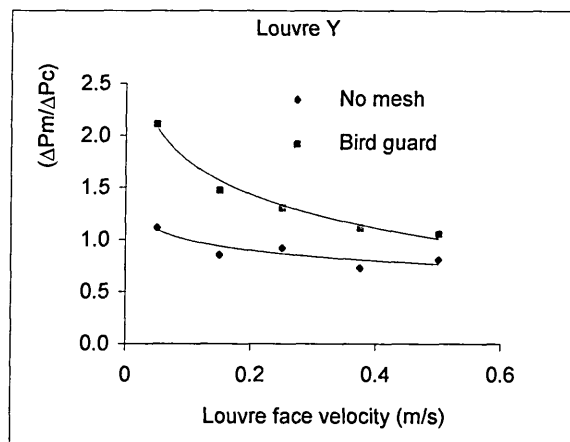
Figure 7.27: Ratio of measured to calculated pressure differentials as a function of louvre face velocity

It can be seen from Figure 7.27 that agreement between measured and CFD calculated pressure differentials improved with increasing louvre face velocities. A possible reason for this trend is that at higher louvre face velocities the pressure differentials were larger and more firmly established, hence, making it easier to measure experimentally i.e. less variation than at low face velocities.

7.2.4 General discussion of CFD/experimental results

Although CFD can quickly and easily be utilised to predict airflow and to carry out parametric studies, its accuracy and quality of results rely heavily on accurate setting up of the simulation model and specification of boundary conditions governing the flow field. Consequently, discrepancies from expectation are inevitable when a physical situation is simulated by a theoretical model. With CFD sometimes the discrepancies can be small and their exact cause can be difficult to ascertain. It must be remembered that in CFD the solution is strictly a solution of the numerical problem, not of the physical problem, and that differences between these two could be due to such things as an inadequate grid, difficulties in achieving full convergence of some simulated situations within reasonable time-frames, or the usual inaccuracies resulting from the application of turbulence models (k - ε model in this case). In this investigation grid and convergence associated issues were adequately dealt with. However, the quantitative differences observed between the computational and the experimental results cannot be attributed entirely to the approximations included in the used turbulence $(k$ - $\varepsilon)$ model, since modelling limitations such as the representation of the mesh-screen during computer simulations also influenced the numerical results.

Generally, over-prediction of airflow rates was very high at low pressure differentials. This large deviation at low pressure differentials was expected and can be attributed to the following reasons:

- Experimentally measured airflow rates were not well established through the test rig, resulting in high levels of fluctuation, hence recorded parameters possibly incorporated a relatively large error

- Some CFD simulations were generally not fully converged at low pressure differentials, in addition parameters obtained from the numerical solution were for central planes/centre of cells hence small error in gridding was possibly carried over to the final result

Further, experimental measurements also share the blame for the deviations between predicted and expected parameters. For physical measurements accuracy/reliability

-218-

depends on three main types of uncertainties which undoubtedly were present in this investigation:-

i) Boundary condition uncertainty: These include errors in measurement and control of the test boundary conditions and deviations of boundary conditions from steady state values.

ii) Fluctuations of the flow pattern: which are normally associated with the stability of flow pattern. For instance, fluctuations in the fan-motor speed also affect the general airflow through the experimental test rigs.

iii) Airflow and ΔP measurement uncertainties: closely associated with accuracy of measuring instruments and disturbances caused by the measuring system. The errors were addressed by calibration of the instruments and locating the probes so as to reduce their influence on the flow pattern.

The study has highlighted an example of integrating CAD and CFD models as a tool to analyse ventilators for natural ventilation applications. Since data for CFD validation of airflow through louvres/meshes is extremely scarce or non-existent it follows that studies such as this generate important data which would hopefully lead to ventilator manufacturers having better design guidelines and design tools for the production of efficient and effective natural ventilation ventilators. In turn such information would improve the confidence in natural ventilation design methods to a level where they can match the design methods of similar components in mechanical ventilation applications.

7.3 Overview of Comparison with other Research Results

This section presents comparisons between the results obtained from tests on some of the components used in this investigation and those derived from models proposed, or experimental results obtained by other researchers. The intention of the comparisons was to relate the present findings to other work and also to put it into context with the overall on-going research in the general field of natural ventilation components. A lack of similar studies in the literature restricted the comparisons to components (slots and louver banks) used without any mesh-screens.

It was mentioned in *Section 2.4.1* that purpose-provided openings such as ordinary slots represent trickle ventilators in there simplest form as found in natural ventilation applications. In addition, ordinary slots represent a type of real leakage path typically found around doors and windows in buildings. Several researchers including Etheridge [1977, *1984*], Baker *et al.* *[1987]*, Sherman *[1992]* and Walker *et al.* *[1998]* have previously focussed their attention on cracks and simple ordinary slots and employed similar approaches in order to gain an understanding of the airflow characteristics of these components. The study by Baker *et al.* *[1987]* was selected for comparison of properties of airflow through slots tested in this investigation. Using the quadratic model proposed by Baker *et al.* (described in *Section 4.6.1* - Equations 4.7 to 4.9, repeated here for ease of reference) theoretical curves derived from coefficients calculated for each slot, using the slot dimensions and experimental ambient conditions, were drawn and compared with results obtained from experiments carried out in this investigation.

$$\Delta P = AQ^2 + BQ \tag{4.7}$$

$$A = \frac{\rho C}{2d^2 l^2} \tag{4.8}$$

$$B = \frac{12\mu z}{ld^3} \tag{4.9}$$

According to Baker *et al.* the pressure difference (ΔP) is the total pressure drop allowing for edge effects due to skin friction along the dimension z in the direction of flow (Q), d is the gap thickness between plates, l is the breadth of the plates, μ is the dynamic viscosity (Pa s), ρ is the fluid density and C is a dimensionless constant which for straight-through cracks such as the slots used in this investigation assumes a value of 1.5. The theoretical, experimental and CFD predicted values of the coefficients are presented in Table 7.2.

Slot Ref.	Slot dimensions			Theoretical (Baker et al.)		Experimental (this investigation)		CFD predicted (this investigation)	
	l (m)	d (mm)	z (mm)	A	B	A	B	A	B
A1	0.3	6	12	277778	40.82	318987	142.67	256442	544.49
A2	0.3	12	12	69444	5.10	107486	-28.78	119115	53.05
A3	0.3	18	12	30864	1.51	61879	-55.15	57853	20.12
A4	0.3	24	12	17361	0.64	36068	-37.07	34777	-20.22
A5	0.3	30	12	11111	0.33	20972	-8.66	23631	1.81
A6	0.3	36	12	7716	0.19	14429	-1.34	16498	6.50
B1	0.3	12	6	69444	2.55	136604	-87.50	68299	-1.06
B2	0.3	12	12	69444	5.10	106418	-28.25	65384	9.11
B3	0.3	12	18	69444	7.65	97226	28.68	66252	11.01
B4	0.3	12	24	69444	10.21	88445	-28.13	67070	6.11
B5	0.3	12	30	69444	12.76	82507	45.21	66119	14.76
B6	0.3	12	36	69444	15.31	73253	60.41	67826	9.78

Table 7.2:
Theoretical, experimental and CFD predicted values of the coefficients in the quadratic solution

It can be seen from Table 7.2 that for slots of varying height (Slot type A) the coefficients obtained from experiments and CFD predictions in this investigation were more or less similar. When compared to the theoretical model the experimental and CFD predicted coefficients were within 15% and 35% of the values calculated from the model by Baker *et al.* for the slots with heights 6 mm and 12 mm respectively. The agreement worsened with increasing slot height with the experimental and CFD predicted values being bigger than the theoretical values by a constant factor of approximately 2 at slot heights of 18 mm and above. However, bearing in mind that the theoretical model is for crack-type leakage paths this large deviation was not unexpected. The airflow characteristics for Slots A1, Slot A3 and Slot A6 derived from the coefficients given in Table 7.2 are shown graphically in Figure 7.28, Figure 7.29 and Figure 7.30 respectively. The large deviation between theoretical and experimental/CFD predicted airflow characteristics as the slot height was increased is evident from these figures. The most obvious meaning of these results is that the airflow characteristics of slots with heights greater than 12 mm may be better estimated by other models such as those based up on large openings.
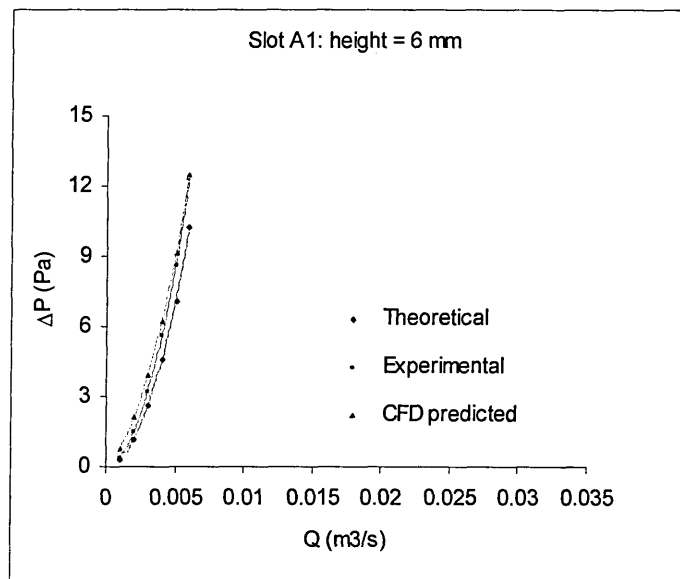
Figure 7.28: Theoretical, experimental and CFD predicted airflow characteristics for slot A1
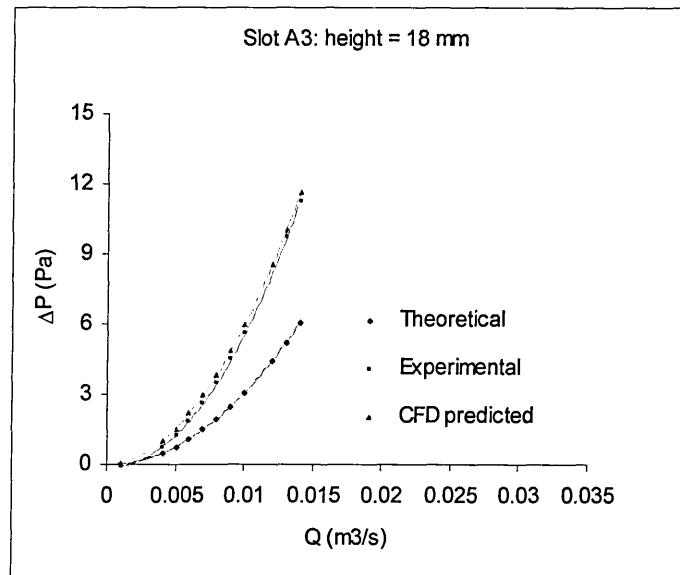
Figure 7.29: Theoretical, experimental and CFD predicted airflow characteristics for slot A3
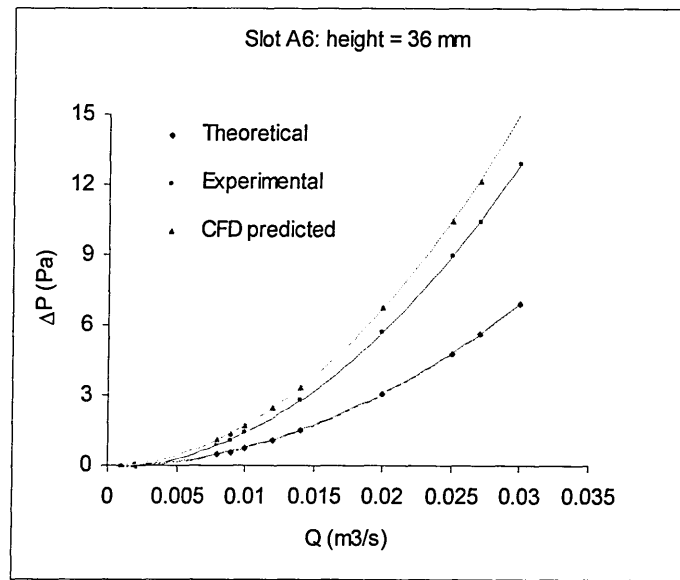
Figure 7.30: Theoretical, experimental and CFD predicted airflow characteristics for slot A6

The slots of varying depth (Slot type B) appear to give better agreement with the theoretical coefficient "A" for both measured and CFD predictions. As expected the CFD predicted values of the coefficient "A" were approximately constant. Further, CFD predicted values of the coefficient "B" were closer to the theoretically calculated values than those obtained experimentally. On the other hand, experimentally obtained values of coefficient "A" varied with slot depth with the agreement relative to theoretically calculated value improving with increasing slot depth as can be seen from Figure 7.31, Figure 7.32 and Figure 7.33. The deviation between theoretical and experimental coefficients varied from just under 50% for the slot with depth equal to 6 mm to 5% for the slot with depth equal to 36 mm.
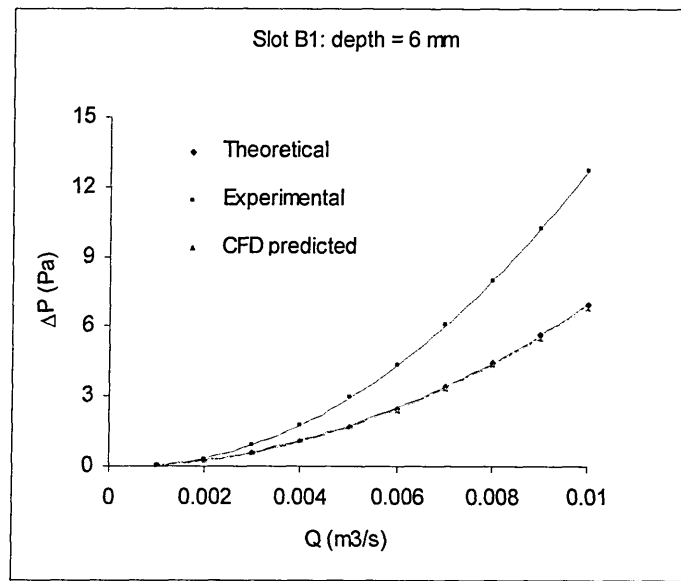
*Figure 7.31: Theoretical, experimental and CFD predicted
airflow characteristics for slot B1*
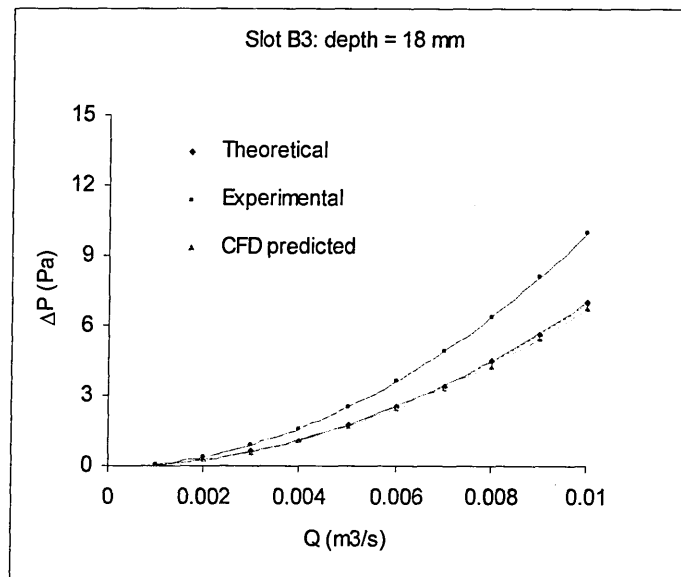
*Figure 7.32: Theoretical, experimental and CFD predicted
airflow characteristics for slot B3*
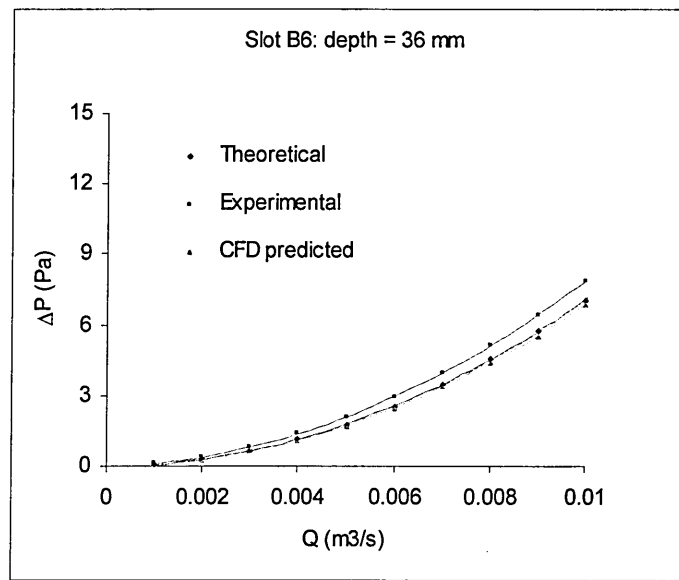
Figure 7.33: Theoretical, experimental and CFD predicted airflow characteristics for slot B6

That the theoretical and CFD predicted coefficient "A" is more or less constant is not surprising because the theoretical and CFD predicted values are based up on slots of a given roughness whereas in reality, as was the case with the fabricated slots, the roughness of the various slots may differ due to several factors such as fabrication finish and natural defects of the material used. The improvement in agreement with increasing slot depth was also expected and possibly resulted from the flow getting more fully developed as the slot depth was increased. Another factor which could be attributed to for the relatively large deviations between experimental/CFD predicted airflow characteristics and the theoretical ones in some of the cases considered is that the expressions proposed by Baker *et al.* originate from pipe flow experiments. Hence, the assumptions therein and the associated value of 1.5 for the constant C may not necessarily be true for rectangular cross-section cracks or slots such as those used in this investigation.

AIRFLOW THROUGH WOODEN LOUVERED VENTILATORS

The lack of studies from the literature on the airflow characteristics of combinations of ventilator components such as those used in this investigation was highlighted in Section 4.6.3. Available studies that could be used for comparisons were limited in scope with studies by Yakubu and Sharples *[1991]*, Oliveira and Bittencourt *[1998]*, Maghrabi and Sharples *[1999]* and Maghrabi *[2000]* being the only ones that used

-225-

louvered ventilators of configurations similar to the ones used in this investigation. It is of interest to note that a common call found in all these studies was the need for more research into the impact of various ventilator components on the airflow characteristics.

In contrast to previous research in the above mentioned studies which were generally limited to assessing the airflow characteristics for only one flow direction (Oliveira and Bittencourt considered only the inlet configuration whilst Yakubu and Sharples and Maghrabi and Sharples discussed ventilators used in an outflow configuration), this investigation assessed and compared the airflow characteristics for both flow directions with the results indicating that differences between the two flow directions can be significant.

Oliveira and Bittencourt *[1998]* attempted to show the significant variation and resistance to the airflow produced by horizontal louvered inlets used with and without mesh-screens. The only quantifiable parameter in their study that could tentatively be compared with the results of this investigation was the impact of the mesh-screen which they found to reduce the flow in their louver system by as much as 40%. The impact of mesh-screens on the overall airflow performance of ventilators used in this investigation was discussed in Section 5.4.7. However, without specific information about the type or dimensions of the mesh-screen used by Oliveira and Bittencourt the basis of comparison does not exist.

Because of significant differences in the type/dimensions of louvers used by Yakubu and Sharples and those used in this investigation a direct quantitative comparisons was only applied in relation to the airflow patterns based up on the indices obtained by using the power law - recalling in relation to the power law that the flow pattern can be deduced from the value of the exponent, i.e. 0.5 (fully turbulent) $\leq n \leq 1.0$ (fully laminar). Yakubu and Sharples obtained exponents of the order of 0.9 for their louver system with horizontal blades. The exponent reduced to 0.87, 0.78 and 0.7 respectively for louver blade inclination angles of 30°, 60° and 75° thus indicating that the flow shifted from a laminar pattern towards a turbulent pattern as the inclination angle was increased. A similar shift in airflow pattern with changing louver blade inclination angle was observed in the present investigation. However, this investigation, and also Maghrabi *[2000]* and Sharples and Chilengwe *[2001]* who used louver systems with the

same dimensions as those used in the present study, observed relatively less laminar and more turbulent flow patterns for horizontal and inclined louver blades respectively based on the values of power law exponents (see for example Table 5.5 for louvers without mesh-screens).

The experimental work of Yakubu and Sharples *[1991]*, Maghrabi and Sharples *[1999]* and Maghrabi *[2000]* found that the quadratic formulation resulted in better curve fits compared with the power law. In contrast this investigation concluded that the two formulations were only marginally different. A possible source of greater differences between power law and quadratic curve fits obtained by Yakubu and Sharples, Maghrabi and Sharples and, Maghrabi could be in the way the background leakage from the test rigs was treated which as mentioned earlier (see Section 4.8.1 which also indicates how the background leakage was handled in this and the other investigations) could influence the derived airflow characteristics of components tested in the laboratory. Further, the ranges of pressure differences achieved (typically 0 to 2 Pa for Yakubu and Sharples and Maghrabi and Sharples and, 0 to 6 Pa for this investigation) could have affected the magnitudes of the differences between power law and quadratic formulations. For example Etheridge *[1984]*, see also Figure 4.11 in this thesis, indicated that differences between power law and quadratic equations can be significant (as much as 40 - 50%) at low pressure differences.

Part of Maghrabi's [2000] work included some components with dimensions the same as those used in this investigation hence these can facilitate a direct comparison of the results. Some quantitative/graphical comparisons between results from this investigation and those obtained by Maghrabi are given in *Section 7.6* of this thesis.

7.4 Ventilator Airflow Performance Optimisation

7.4.1 Optimisation approach

In many natural ventilation applications the quantity of prime interest is the air volume flow rate (Q) through the ventilator resulting from a pressure differential (ΔP) across it. Over the past several years independent researchers have investigated some of the factors that influence the overall airflow rate through ventilators [Ayad, *1999* and Heiselberg *et al. 2001*] whilst others have focussed on isolated individual elements or

ventilator components, for example White *et al.* [*1998*] and Maghrabi and Sharples [*1999*]. Maghrabi [*2000*] extensively investigated parameters such as louver blade inclination angles, number of blades in a ventilator, depth of blades and the gap between louver blades and assessed their impact on pressure differentials and velocities in louver banks similar to the ones used in this investigation. This investigation (*Chapter 5* and *Chapter 6*) has to some extent shown how a combination of various parameters such as louver blade inclination angle, free-area ratio as well as geometries of mesh-screens and, the gap between louver blades and mesh-screens have an impact on the overall airflow rate through a given ventilator. The impact of these elements on the overall airflow performance of a ventilator was quantified (to some extent) in *Chapter 5* of this thesis. In this chapter the intention is to further explore and understand these issues in addition to deriving some general equations to represent the relationships between various elements under a number of scenarios typical in natural ventilation applications. The following situations were considered:

- louvers of different blade inclinations without mesh-screens

- mesh-screens of different free areas

- horizontal louvers with mesh-screens

- inclined louvers with mesh-screens

- horizontal louvers with a gap between louver blades and mesh-screen

- inclined louvers with a gap between louver blades and mesh-screen

- combinations of all variables

The starting point to this analysis was the results of experiments reported in Chapter 5, in particular the standard practice, previously adopted by several researchers including Walker *et al*, [*1998*], Liddament [*1987*] and, Sharples and Chilengwe [*2001*], of power law formulations. The power law was used to fit trend-lines to raw experimental data points which were used to obtain power law equations of the form (described in *Chapter 5* and repeated here for ease of reference):

$$Q = \alpha \, (\Delta P)^n \qquad\qquad (7.2)$$

The results for various scenarios presented in *Chapter 5* indicated that the power law curves fitted to the data were valid approximations of the actual experimental results judging from the correlation coefficients obtained which were generally of the order of 0.99. Hence this justified the use of derived data in place of raw experimental results in the subsequent analysis. A second multiple regression analysis was then conducted on Q-ΔP data sets derived from power law formulations to obtain overall relationships between various variables included in a given scenario. The underlying principles of the analysis used here were very similar to the one used in ALTAS -a software package which the author recently designed for an engineering firm HRS Services Ltd (Sheffield, England) and which is used to analyse data from air-leakage tests on buildings. Core to the analysis was the approach of using the natural logarithm to convert the power law parameters Q and ΔP to linear form $\log_e(Q)$ and $\log_e(\Delta P)$. Designing ventilators of good airflow characteristics or any improvement on airflow performance requires a detailed understanding of the ventilator components and their interaction with each other and external environmental factors. It is therefore of vital importance to characterise the behaviour of each component. An earlier experimental study [Sharples and Chilengwe, *2001*] that investigated the interaction of louver geometries and blade inclination angles with meshes of different hole sizes lay the foundation of the work described in this chapter. In the following sections of this chapter is presented a different approach in which several parameters that may influence the components behaviour in a ventilator were segregated and the effects of individual variables that would affect the ventilator behaviour were studied. Using the derived equations the influence of various parameters on the overall airflow performance of the ventilator was examined by varying one or more variables at a time whilst keeping the rest of the variables constant.

7.4.2 Parameters for optimisation

Traditionally the process of optimising the airflow through or over solid objects has been associated with the physical geometry of the object through which or over which the air flows. In this regard the approach has been to configure the shape of the object in such a way as to minimise significant or abrupt changes in geometry with the intended

result of attaining an "optimised" airflow profile or pattern which smoothly varies with small changes in the shape of the object. The most common examples that impact everyday life are the shape of the aeroplane wing and, the artistic and creative configurations of modern streamlined cars. In relation to ventilators such an approach would focus the attention to the shape of the airflow path within a ventilator taking into account components such as louvers. Some studies such as Maghrabi [*2000*] have previously attempted to assess the influence of parameters such as the thickness of louver blades, gap between louvers and depth of louver blades etc on airflow through ventilators. In this investigation optimisation is not viewed from the "shapes" point of view but the focus is rather on the impact of the combination of components of given geometry on the overall airflow performance of a ventilator taking into account the driving forces (pressure differentials) available to effect the airflow. Therefore in this investigation, the following are the parameters that were used in the optimisation analysis:-

- magnitude of pressure differential ΔP (Pa)
- airflow rate Q (m^3/s)
- louver blade inclination angle θ (degrees)
- mesh-screen fractional free-area f_a
- gap between louver blades and mesh-screen L (mm)

The equation derivations and analysis in the following sections were primarily based on a smooth pinewood louver bank system such as the one shown in Figure 7.34 with overall frame dimensions of 480 mm high x 320 mm wide. Components of similar dimensions have previously been used in investigations by Maghrabi [*2000*], Yakubu and Sharples [*1999*] and, Pitts and Georgiadis [*1994*]. The louver bank system comprised 15 blades with a gap of 20 mm between blades measured when the blades were in a horizontal position. Each blade measured 60 mm deep and was 10 mm thick.

Figure 7.34: Pinewood louver bank

The louver bank was fitted with a mechanism that allowed louver blades to be inclined and adjusted to the desired angle. Although results on other louver banks are not specifically referred to in the following analyses, these contributed in the development of the analysis and reaching of conclusions. As the focus in this investigation was on the interaction of combinations of different ventilator components, Louver 1 was used in conjunction with the woven-square mesh-screen lattices formed from round wires evenly spaced in both the vertical and horizontal directions such as the one shown in Figure 7.35. These were locally obtained from a commercial supplier.
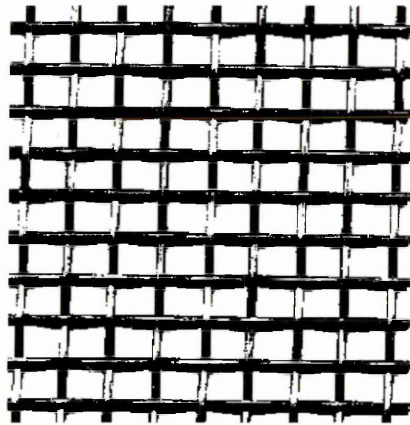
Figure 7.35: Square grid round-wire meshes

Three types of wire-mesh-screens of free-areas 35%, 50% and 70% (detailed in Table 7.3) were used in the investigation. For consistence a "mesh-screen with 100% free-area" was used to imply the case when the louver was used without any mesh-screen.

		Table 7.3:			
		Details of round wire meshes used in investigation			
Mesh	Construcion type	Average wire dia (mm)	Holes in 320mm x 480mm	Equivalent open area (m2)	Free Area (%)
1	woven square	0.599	95256	0.056	35
2	woven square	0.921	34126	0.077	50
3	woven square	1.618	8475	0.104	70

The effect of locating a mesh-screen with a gap relative to louver blades and how this affected the overall airflow performance of the ventilator was investigated by inserting wooden spacer frames (Figure 7.36) of identical width and height to the wooden louver frame dimensions.

Figure 7.36: Spacer between louver and mesh

Spacer frames of thickness 3, 6, 9, 12 and 15 mm were used in combination with Louver 1 at various louver blade inclination angles and the round-wire mesh-screens. Measurements were also taken when the mesh-screen was placed adjacent to the louver frame without a spacer in-between ("0 mm spacer").

7.4.3 Optimisation criteria

This investigation adopted a simplified technique to be used in an attempt to optimise the airflow performance of ventilators in relation to a set of identified variables such as the louver blade angle or gap between the louver and mesh-screen for a given situation. Since there are a number of different parameters involved in any scenario it is obvious that several conflicting quantities each with different dimensional units had to be taken into account in the attempt to optimise the airflow performance. The criteria followed in this study was to initially consider only the parameters associated with a given scenario

to establish any trends and, to quantify the effect of varying a particular variable on the resulting airflow rate for that particular scenario. This was based on mathematical characteristic equations derived from experimental data to suitably describe the passage of air through the ventilator based on a particular combination of parameters associated with a given situation. Once this was done, the analysis then considered the combination of all the variables and attempted to determine a good compromise solution by considering trade-offs between various competing parameters. Unfortunately no commercial software/tool with automatic search and optimisation procedures was available to facilitate this exercise hence, the treatment in this investigation was rather simplistic and was performed on an Excel spreadsheet.

The key objective was to derive a relationship relating the airflow rate (Q) to various variables influencing it in a ventilator using expressions of the form:

$$Q = f\{\Delta P, \theta, f_a, L\} \tag{7.3}$$

An earlier attempt to find such a relationship can be found in Maghrabi [*2000*] where the pressure drop through a ventilator was related to the various variables that influence the airflow through it by the expression:-

$$\Delta P = c + \alpha Q + \beta_i d_\theta + \chi_i A_f + d_i N + \varepsilon_i L_\theta +$$
$$[(\alpha\beta)_{ij}.Qd_\theta + (\alpha\chi)_{ij}.QA_f + (\alpha\delta)_{ij}.QN + (\alpha\varepsilon)_{ij}.QL_\theta] \tag{7.4}$$

where c was the intercept defined from linear curve estimates, α was a constant value for volume flow rate and the parameters $\beta, \chi, \delta, \varepsilon$ were numerical representations of the variables relating to the geometry of the louver. This equation is included here just as an example and hence no attempt was made to interpret it or compare it with expressions derived in this investigation.

7.5 Optimisation Case Studies and Results

The following sections describe case studies and presents results of the approach described above when applied to a number of situations common in natural ventilation applications. It must be remembered that a general solution applied to a wide range of scenarios is likely to result in unacceptably wide variations/differences relative to

expected values. For time and economy on the number of pages, it would be unrealistic to present all possible variations on the combinations of parameters or situations typical in natural ventilation applications. As such only a few selected examples are included here together with likely limits of application of the proposed equations. Although not all results are specifically referred to in the course of the analysis, these contributed in the development of the analysis and reaching conclusions. That aside this investigation appears to be the most comprehensive study to date on the impact/interaction of components in a ventilator on the airflow performance with no comparable results to refer to.

7.5.1 Louvers at different blade inclinations

The general expectation for louvers with inclined blades is that the airflow rate (Q) is proportional to the pressure differential (ΔP) for a given angle, and Q is inversely proportional to the angle of inclination for a given ΔP. For this situation power law data for wooden Louver 1 at blade angles 0°, 30° and 60° were used as the starting point for these derivations. The raw experimental data and subsequently derived power law factors for the 0° and 60° louver blade inclination angles are given in Table 5.5 of Chapter 5 of this thesis. A second regression performed on $\log_e Q$ and $\log_e \Delta P$ and the cosine of the angle of inclination from horizontal resulted in the relationship given by Equation 7.5 with statistical parameters associated with this equation given in Table 7.4:

$$\log_e Q = 0.57\log_e \Delta P + 2.36\cos\theta - 4.41 \qquad (7.5)$$

Table 7.4: Statistical Parameters for Equation 7.5			
Equation parameters			
R square			0.9988
Adjusted R square			0.9986
Standard Error			0.0272
Multiple Regression Equation			
	coefficients		standard error
intercept	-4.406		0.023
loge DP	0.569		0.009
cosθ	2.36		0.024
observations			20

Equation 7.5 was then transformed to linear format by inverting the natural logarithms to obtain the expression:

$$Q = \frac{\Delta P^{0.57} * 10.591^{\cos\theta}}{82.269}$$

(7.6)

where Q is the airflow rate resulting from a pressure differential ΔP across a ventilator with louver blades inclined at an angle θ from horizontal.

To assess the degree of agreement between airflow rates predicted from Equation 7.6 and those expected from experimental data using the power law formulation a linear regression line for the two sets of data was plotted. Figure 7.37 shows the linear regression comparison between airflow rates predicted by Equation 7.6 ($Q_{predicted}$) and those expected (as given by power law curve fit to raw experimental data) ($Q_{expected}$) for various ΔPs. For this situation only 20 data points were used, however even for this low number of points agreement between predicted and expected parameters was excellent based on the correlation coefficient of 0.999 obtained. An effect of increasing the number of data points was assessed and indicated that even doubling the number of observations had no impact on the correlation coefficient. This was expected because data used was previously correlated to a power law equation and as such all data points would lie on the same trend-line.
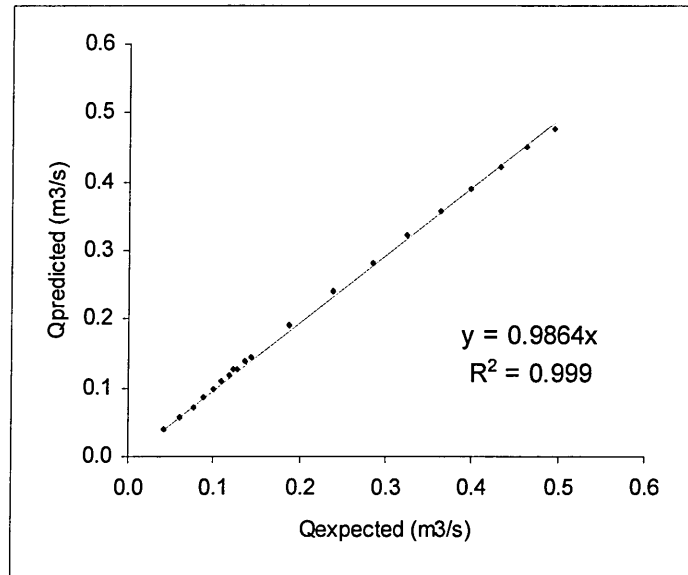
Figure 7.37: Variation of airflow rates predicted from Equation 7.6 with expected airflow rates

The predicted airflow rates shows strong correlation with measured data as can be seen from the correlation coefficient of 0.999. The slope of the regression line was 0.986. This means that the predicted airflow rates were predominantly lower than the measured values.

PARAMETER VARIATION FOR LOUVERS AT VARIOUS BLADE INCLINATION ANGLES

Figure 7.38 shows the effect of varying the louver blade inclination angle on the predicted airflow rate (Equation 7.6) at a given angle as a ratio of the predicted airflow rate through the ventilator with horizontal blades (Q/Q_0). As expected the trend line shown in Figure 7.38 was independent of the pressure differential across the ventilator (see also Figure 7.39). As can be seen from Figure 7.38 the trend between various angles was not perfectly linear through the data points. The most likely explanation of this is that the experimental data (used as source data for deriving Equation 7.6) was influenced by turbulence or changes in airflow patterns associated with changes in the louver blade inclination angle. Recalling that the flow pattern changes from fully laminar at n= 1 to fully turbulent at n = 0.5 [Liddament, *1998*] it was evident, from the power law index "n" which for instance changed from 0.6054 at 0° to 0.5335 at 60° (see Column 9 in Table 5.5 of *Chapter 5*) that the flow turbulence increased with increasing louver blade inclination angle. Experimentally derived data gave a similar trend of the variation of (Q/Q_0) with louver blade inclination. However, experimental data was slightly dependant on the pressure differential. Comparison between experimental values and those derived from Equation 7.6 for the 60° blade angle gave a deviation of 10% at pressure differentials of 1 Pa and 10Pa with the experimental values being higher. At 5Pa the deviation was 0.7% with the value obtained from Equation 7.6 giving an over-prediction. The variation in deviation as the pressure difference increased can be attributed to fluctuations in the measurements of flow properties resulting from the not strongly established flow at low ΔP whereas for high ΔP the high flow rates creates more turbulence which again led to fluctuations in measured flow properties.
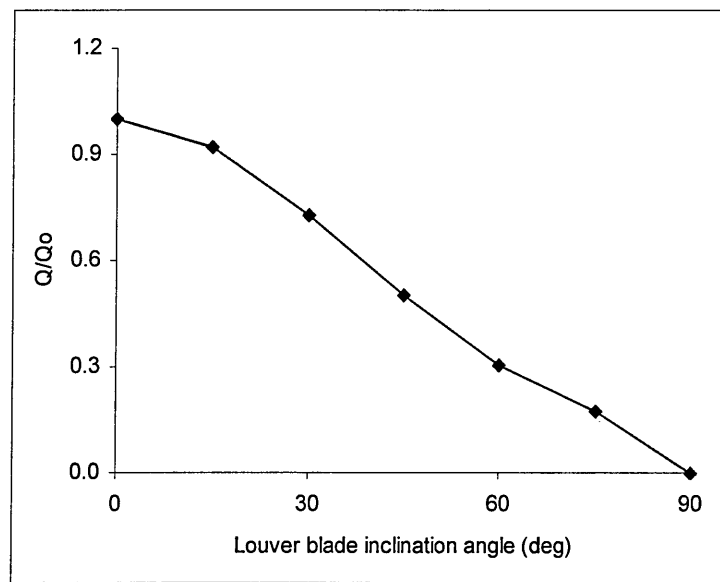
*Figure 7.38: Variation of airflow rate as a ratio of the airflow
rate through the ventilator with horizontal blades*

Figure 7.39 shows that the ratio of the predicted airflow rate through the ventilator at a given angle relative to that predicted with ventilator louver blades in a horizontal position was independent of the pressure differential. The solid line shown on the graph represents experimental variation of the airflow rate ratio with pressure differential for louvers inclined at $60°$. The graph for the $60°$ louver blades shows that the predicted and expected parameters closely agreed with each other. Similar results were obtained for other louver blade inclinations hence they are excluded from the graph for clarity. The impact of louver blade angle on the airflow (Q) was assessed by considering the rate of reduction of the airflow rate ratio (Q/Q_0). Although the ratio of the airflow rates reduced with increasing louver blade inclination angle at all pressure differentials, the rate of reduction was different between the various angles. For instance, by changing the louver blade inclination angle from $30°$ to $75°$ the rate of reduction of the ratio of airflow rates progressively changed from 31% between $30°$ and $45°$, to 38% between $45°$ and $60°$ and, 43% between $60°$ and $75°$.
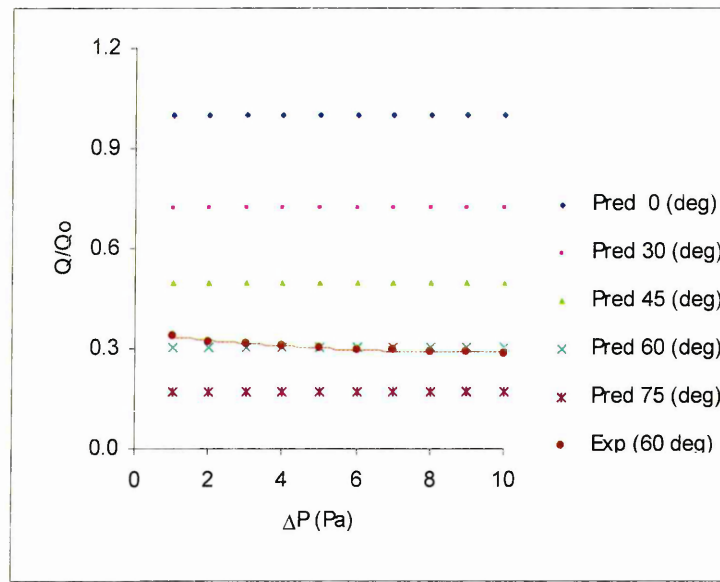
Figure 7.39: Variation of airflow rate ratio with pressure differential based on Equation 7.6

The higher rate of reduction of airflow rate ratio at angles above $60°$ imply that there was greater influence on the airflow properties. These findings are in line with previous independent studies by Yakubu and Sharples [*1991*] and also by Maghrabi and Sharples [*1999*] whose results of investigations on similar components concluded that louver blade angles above $60°$ strongly influence airflow properties.

7.5.2 Mesh-screens

For mesh-screens it is generally expected that the airflow rate (Q) is proportional to the pressure differential (ΔP) for a given mesh-screen free area and that Q is proportional to the mesh-screen free area for a given ΔP. Power law derived parameters of mesh-screens given in Table 7.3 were used as the starting point in deriving a general relationship:

$$Q = f\{\Delta P, f_a\} \tag{7.7}$$

A second regression performed on $\log_e$ Q and $\log_e$ ΔP and the mesh-screen free area resulted in the relationship given by Equation (7.8) with statistical parameters associated with this equation given in Table 7.5:

$$\log_e Q = 0.81\log_e \Delta P + 4.42*f_a - 3.53 \tag{7.8}$$

-238-

Table 7.5: Statistical Parameters for Equation 7.8		
Equation parameters		
R square		0.8234
Adjusted R square		0.8172
Standard Error		0.4296
Multiple Regression Equation		
	coefficients		standard error
intercept	-3.527		0.23
loge DP	0.814		0.07
cosθ	4.419		0.387
observations			60

Equation 7.8 was then transformed to linear format by inverting the logarithms to obtain the expression:

$$Q = \frac{\Delta P^{0.81} * 83.096^{f_a}}{34.124}$$

(7.9)

where Q is the airflow rate resulting from a pressure differential ΔP across a mesh-screen with free area f_a. Figure 7.40 shows a linear regression comparison between airflow rates predicted by Equation 7.9 and those expected (given by power law curve fit to raw experimental data) for various ΔPs. For this situation 60 data points were used, however the regression comparison between airflow rates predicted by Equation 7.9 and those expected was relatively poor based on the correlation coefficient of 0.6592.

y = 0.9335x
R² = 0.6592
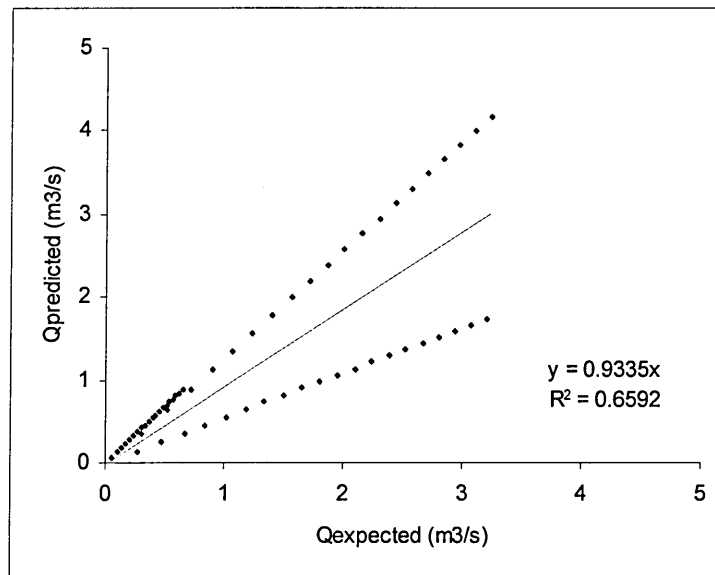
Figure 7.40: Variation of airflow rates predicted from Equation 7.9
with expected airflow rates for mesh-screens

-239-

The predicted airflow rates show a relatively poor correlation with measured data as can be seen from the correlation coefficient of 0.659. The slope of the regression line was 0.934. Two distinct sets of data points emerged from this correlation. Further investigation and checks concluded that the data points above the regression line related to airflow rates predicted for the 35% and 70% free area mesh-screen whilst those below the line were due to the 50% free area mesh-screen. What this means is that Equation 7.9 over predicts the airflow rates for the 35% and 70% mesh-screens and on the other hand under-predicts the airflow rates for the 50% mesh-screen. An assessment of the degree of over-/under-prediction showed that on average the airflow rates through the 35% mesh-screen were over-predicted by 39% whilst those for the 70% free area mesh-screen were over-predicted by 28%. The equation under-predicted the airflow rates through the 50% free area mesh-screen at an average of 45%. Initially the author suspected the data for the 50% free-area mesh-screen was entered wrongly into the statistical analysis spreadsheets. However, a re-check of the input and measured parameters did not reveal any mistakes. Possible explanations of the 50% mesh-screen behaviour are that:-

- The geometric effects resulting from the mesh-screen wire diameters, ignored in the derivation of the equations, could have had a significant influence on the airflow pattern through the mesh-screen

- Indeed in line with previous findings, for example [White *et al. 1999*], the flow characteristics of simple airflow components such as mesh-screens do not necessarily always follow established theoretical expectations thus leading to pressure-flow behaviour different from what one would intuitively expect

Without further investigation and detailed study of the effects of mesh-screen wire diameters on airflow properties/patterns, it is not possible to state for certain the reasons for the behaviour observed. As can be seen from Figure 7.40 the data points fall on opposite sides of the regression line. Initial thoughts to reduce the deviations between the two data sets involved adjustments to the ΔP index (0.81) and the f_a coefficient (38.096). It was observed that by making small adjustments to the index and coefficient, the magnitudes of the over-prediction and under-prediction are affected in opposite ways. As such by employing a search procedure values can be found of the ΔP index

and f_a coefficient that would reduce the spread between the data points for the 50% free-area mesh-screen and those for the 35% and 70% free-area mesh-screens. This would then collapse the two sets of data points onto or closer to the regression line. Time constraints and the lack of a dedicated search/optimisation tool did not permit this task to be completed. However, the author hopes to pursue this task at a later stage.

7.5.2 Horizontal louvers with mesh-screens

The power law data (given in Table 5.5 of *Chapter 5*) for Louver 1 used in combination with mesh-screens of various free-areas was used as the starting point in establishing the relationship:

$$Q = f\{\Delta P, f_a\} \tag{7.10}$$

relating the airflow rate (Q) through a louver with horizontal blades used in combination with a mesh-screen of free-area f_a to the pressure differential ΔP.

A second regression performed on $\log_e Q$ and $\log_e \Delta P$ and the fractional free-area of the mesh-screen resulted in the relationship given by Equation 7.11 with statistical parameters associated with this equation given in Table 7.6:

$$\log_e Q = 0.67\log_e \Delta P + 0.31 f_a - 2.51 \tag{7.11}$$

Table 7.6: Statistical Parameters for Equation 7.11			
Equation parameters			
R square	0.9657		
Adjusted R square	0.9639		
Standard Error	0.0924		
Multiple Regression Equation			
	coefficients		standard error
intercept	-2.509		0.052
loge DP	0.669		0.021
f_a	0.315		0.06
observations			40

Equation 7.11 was then transformed to linear format by inverting the natural logarithms to obtain the expression:

$$Q = \frac{\Delta P^{0.67} * 1.363^{f_a}}{12.305}$$

(7.12)

where Q is the airflow rate resulting from a pressure differential ΔP across a ventilator with horizontal louver blades used in combination with a mesh-screen of free area f_a. For this situation there was no gap between the louver blades and the mesh-screen. Figure 7.41 shows a linear regression comparison between airflow rates predicted by Equation 7.12 and those expected (given by power law curve fit to raw experimental data) for various ΔPs. For this situation 40 data points were used and resulted in close agreement based on the correlation coefficient of 0.9639 obtained.
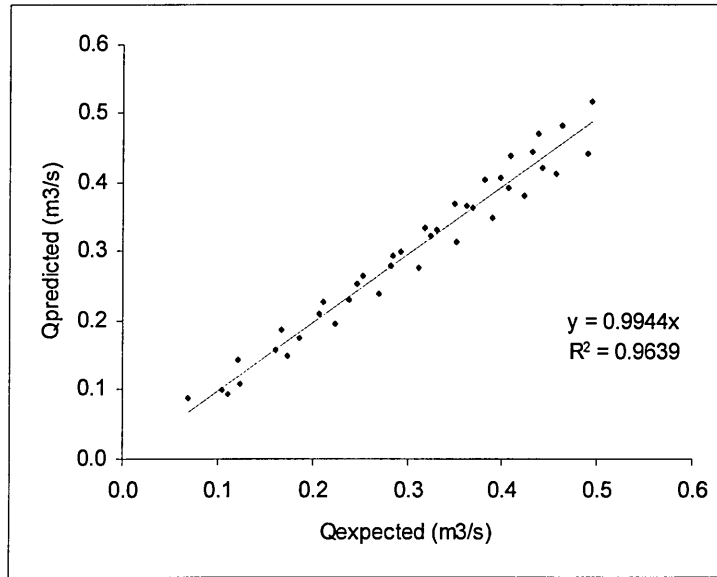
Figure 7.41: Variation of airflow rates predicted from Equation 7.12 with expected airflow rates for mesh-screens

The predicted airflow rates shows a strong correlation with measured data as can be seen from the correlation coefficient of 0.964. The slope of the regression line was 0.994. This means that the predicted airflow rates were predominantly lower than the measured values.

Findings from a comparison between airflow rates predicted from Equation 7.12 and those derived from experimental data at selected pressure differentials in the range 0 to 10 Pa for each mesh-screen are tabulated in Table 7.7 and discussed below.

mesh-screen free area	ΔP (Pa)	Qpredicted (m3/s)	Qexpected (m3/s)	standard error (%)
0.35	1	0.0906	0.0691	31.1
	5	0.2663	0.2526	5.4
	10	0.4236	0.4414	-4.0
0.5	1	0.0949	0.1106	-14.2
	5	0.2789	0.3123	-10.7
	10	0.4438	0.4883	-9.1
0.7	1	0.1009	0.1046	-3.5
	5	0.2967	0.2839	4.5
	10	0.4721	0.4363	8.2
1	1	0.1108	0.1223	-9.4
	5	0.3256	0.324	0.5
	10	0.5181	0.493	5.1

Table 7.7: Comparison of typical predicted and expected airflow rates at selected ΔPs for horizontal louvers used with various mesh-screens

HORIZONTAL LOUVERS WITH A 35% FREE-AREA MESH-SCREEN

An assessment of the results obtained indicated that Equation 7.12 over-predicted the airflow rates at pressure differentials below 7Pa and under-predicted the airflow rates at pressure differentials above 7Pa. It was observed that the over-prediction decreased with increasing ΔP whilst the under-prediction increased with increasing ΔP. This was most likely due to the measurements at low ΔP (flow not strongly established) and those at high ΔP (increased turbulence) suffering more significant fluctuations than those taken for ΔP in the middle range of pressure differentials.

HORIZONTAL LOUVERS WITH A 50% FREE-AREA MESH-SCREEN

Airflow rates predicted from Equation 7.12 and those expected gave the poorest agreement for horizontal louvers used in combination with a 50% free-area mesh-screen. The equation under-predicted the airflow rates throughout the range of pressure differentials (0 to 10 Pa) with the deviation ranging from 14% at 1Pa and decreasing with increasing ΔP to 9% at 10Pa.

HORIZONTAL LOUVERS WITH A 70% FREE-AREA MESH-SCREEN

Although there was an under-prediction of the airflow rates at ΔPs close to 1 Pa, Equation 7.12 generally over-predicted the airflow rates for horizontal louvers used in combination with a 70% free-area mesh-screen. The over-prediction increased with increasing pressure differentials when the overall pressure differential range was

considered. The increase in deviation with increasing ΔP (and hence increasing airflow rate) was possibly caused by increased turbulence of flow leading to fluctuations in measured parameters. A maximum deviation of 8% occurred at $\Delta P = 10Pa$.

HORIZONTAL LOUVERS WITH A 100% FREE-AREA MESH-SCREEN

Equation 7.12 applied to this situation (corresponding to horizontal louvers used without any mesh-screen) resulted in under-prediction of airflow rates at pressure differentials less than 5 Pa. A deviation of 9% was observed at 1Pa and reduced with increasing ΔP to 1% at 4 Pa. On the other hand the equation over-predicted the airflow rates above 5 Pa with a deviation that increased with increasing ΔP ranging from 1% at 5Pa to 5.1% at 10 Pa.

PARAMETER VARIATION FOR HORIZONTAL LOUVERS WITH MESH-SCREENS

The effect of varying the mesh-screen free-area ratio on the airflow rate through the ventilator with horizontal blades is shown numerically in Table 7.8 and also graphically in Figure 7.42. The trend predicted from Equation 7.12 is shown together with experimental data for selected pressure differentials.

Table 7.8: Variation of Q/Q_{100} with fa for horizontal louvers				
fa	Q_{pred}/Q_{100}	1Pa	5Pa	10Pa
		Q_{exp}/Q_{100}	Q_{exp}/Q_{100}	Q_{exp}/Q_{100}
0.35	0.82	0.6	0.78	0.89
0.5	0.86	0.9	0.96	0.99
0.7	0.91	0.85	0.87	0.88
1	1	1	1	1

As expected, the trend obtained by using Equation 7.12 was independent of the pressure differential across the ventilator. The results obtained show that experimental data had some dependence on pressure differential and that the trend lines for $\Delta P = 1$, 5 and 10 Pa all followed a similar profile. A possible reason for the difference between the trends predicted from the equation and those from experimental data is that the influence of the mesh-screen wire diameters, ignored in the derivation of the proposed equation, was appreciable. It can be seen from Figure 7.42 that the greatest variation of the airflow rate ratios occurred when the louver was used with the mesh-screen of 35% free-area. This was contrary to the expectation that the mesh-screen with lower free area would

provide a more straightening effect on the airflow which would lead to less variation as the pressure differential is increased.
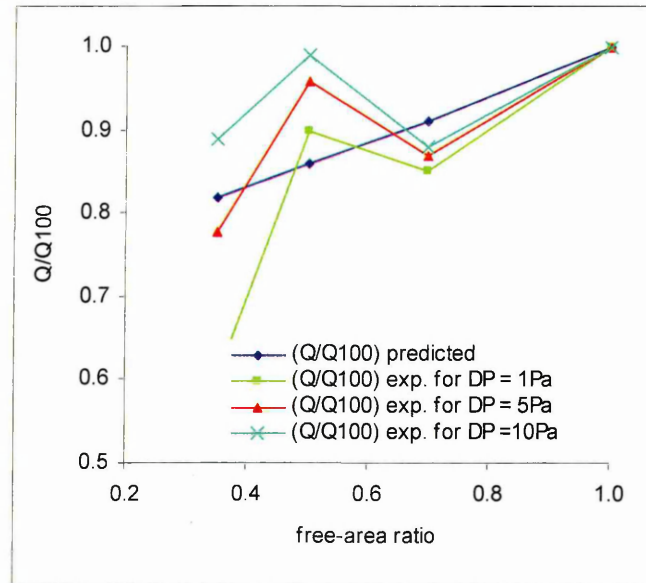
Figure 7.42: Variation of airflow rate ratio with mesh-screen free-area for horizontal louverblades

On the other hand it can be argued that the smaller holes in the mesh-screen with low free-area did in fact enhance turbulence thus leading to more fluctuations. It can be seen from the graph that as the mesh-screen free-area is increased the impact on the airflow between various pressure differential levels decreases. For instance by varying ΔP from 1 Pa to 5 Pa the impact of the meshes with 0.35, 0.5 and 0.7 free-areas progressively reduced with the numerical values of the impact (Table 7.8) being respectively 23%, 6.3% and 2.3%. However, over a similar range of pressure differentials but at higher pressure levels, i.e. varying ΔP from 5 Pa to 10 Pa, the impact of the mesh-screens was found to be 12%, 3% and 1% respectively for the same mesh-screens. The reduction in impact on airflow with increasing free-area ratio was expected as was the reduction in impact with increasing pressure differential levels. These findings are supported by an earlier independent study [Chilengwe and Sharples, *2003*] which concluded that the airflow characteristic of a ventilator comprising louvers and mesh-screens are influenced by the pressure range from which it was derived. However, it is further interesting to note that the impact of each mesh-screen is reduced by a factor of half in switching the pressure range from 1 - 5 Pa to 5 - 10 Pa.

Figures 7.43 and 7.44 respectively show the experimental and predicted variation of the airflow rate ratio with pressure differential for various mesh-screen free-areas. The graphs for the trends predicted from Equation 7.12 and those obtained experimentally are aligned side-by-side for ease of comparison.
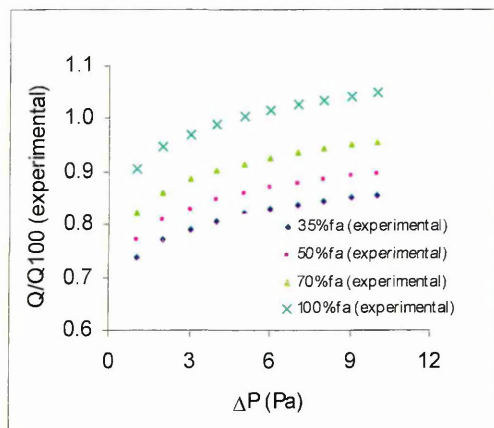
Figure 7.43: Variation of experimental airflow rate ratio with ΔP for different mesh free-areas for horizontal louver blades
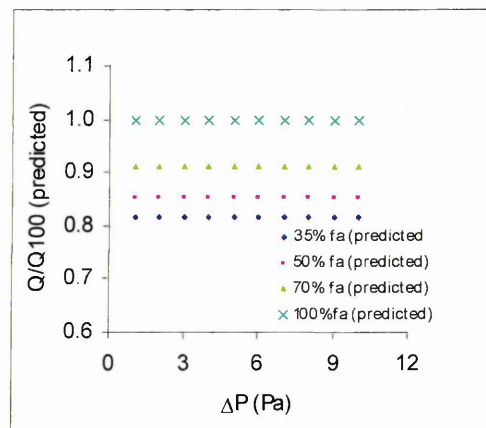
Figure 7.44: Variation of predicted airflow rate ratio with ΔP for different mesh free-areas for horizontal louver blades

It can be seen from Figure 7.43 and 7.44 that the predicted trends for various mesh-screen free-areas were independent of the pressure differential across the ventilator whilst those obtained experimentally revealed an increase with increasing pressure differential. The variation of the trends with pressure differential obtained from the experimental data can be partly attributed to the variation in turbulence levels associated with increasing ΔP and partly to the influence of the mesh-screen wire diameters which were ignored during the proposed equation formulation. An assessment of the impact of wire diameters on airflow properties of the mesh-screens was beyond the scope of this investigation, and so it is not dealt with here. As such the author recommends this aspect of investigation for further research. A visual inspection of Figures 7.43 and 7.44 suggests that the magnitudes of the impact of various mesh-screens on the airflow through horizontal louvers for the range of pressure differentials considered can be determined from either graph, implying that although the trend profiles are different the two graphs give approximately similar numerical values. This can be interpreted to mean that the proposed equation is an excellent numerical approximation of the experimental data.

7.5.3 Inclined louvers with mesh-screens

For this scenario power law data for wooden Louver 1 at blade angles $0°$, $30°$ and $60°$ were used as the starting point for these derivations. The raw experimental data and subsequently derived power law factors for the $0°$ and $60°$ louver blade inclination angles are given in Table 5.5 of *Chapter 5*. Louver 1 in combination with mesh-screens of various free-areas was used to establish the relationship:

$$Q = f\{\Delta P, \theta, f_a\} \tag{7.13}$$

relating the airflow rate (Q) through a louver with blades inclined at an angle θ to the horizontal used in combination with a mesh-screen of free-area f_a to the pressure differential (ΔP).

A second regression performed on $\log_e Q$, $\log_e \Delta P$, f_a and the cosine of the angle of inclination from horizontal resulted in the relationship given by Equation 7.14 with statistical parameters associated with this equation given in Table 7.9:

$$\log_e Q = 0.63\log_e \Delta P + 2.15\cos\theta + 0.18f_a - 4.52 \tag{7.14}$$

Table 7.9: Statistical Parameters for Equation 7.14			
Equation parameters			
R square			0.9866
Adjusted R square			0.9861
Standard Error			0.0832
Multiple Regression Equation			
	coefficients		standard error
intercept	-4.52		0.043
loge DP	0.635		0.013
Cosθ	2.146		0.037
f_a	0.184		0.038
observations			80

Equation 7.14 was then transformed to linear format by inverting the natural logarithms to obtain the expression:

$$Q = \frac{\Delta P^{0.63} * 8.585^{\cos\theta} * 1.197^{f_a}}{91.8356} \tag{7.15}$$

where Q is the airflow rate resulting from a pressure differential ΔP across a ventilator with louver blades inclined at $\theta°$ from horizontal used in combination with a mesh-

screen of free area f_a. For this situation there was no gap between the louver blades and the mesh-screen.

Figure 7.45 shows a linear regression comparison between airflow rates predicted by Equation 7.15 and those expected (given by power law curve fit to raw experimental data) for various ΔPs. For this situation 82 data points were used and these resulted in close agreement between predicted and experimental data as can be judged from the correlation coefficient of 0.985 obtained.
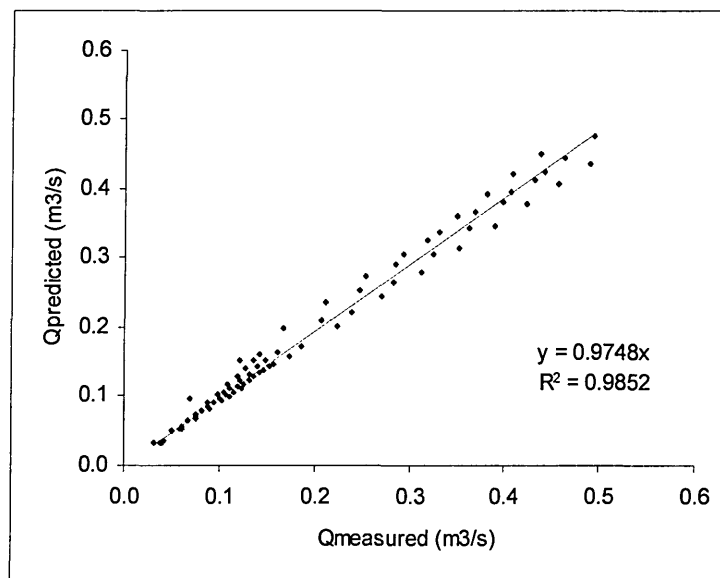
Figure 7.45: Variation of airflow rates predicted from Equation 7.15 with expected airflow rates for mesh-screens

The predicted airflow rates show a strong correlation with measured data as can be seen from the correlation coefficient of 0.985. The slope of the regression line was 0.975. This means that the predicted airflow rates were predominantly lower than the measured values.

PARAMETER VARIATION FOR INCLINED LOUVERS WITH MESH-SCREENS

Figure 7.46 shows the experimental variation of the airflow rate through a ventilator with louver blades inclined at $60°$ relative to the airflow rate through a ventilator of horizontal blades with pressure differential. Experimental results for various mesh-screen free-areas are given on the graph. The solid line shown in the graph represents the airflow rate ratio (= 0.34) predicted from Equation 7.15. The predicted airflow rate

ratio remained constant for all mesh-screen free-areas. However, comparison with experimental data shows that the prediction from the equation can only be regarded as a close approximation for the mesh-screens with 50% and 70% free-areas for the whole range of pressure differentials considered. On the other hand, in relation to the 35% and 100% free-area mesh-screens the prediction from the equation is only a close approximation low ΔP for the 100% free-area mesh-screen and at high ΔP for the 35% free-area mesh-screen.
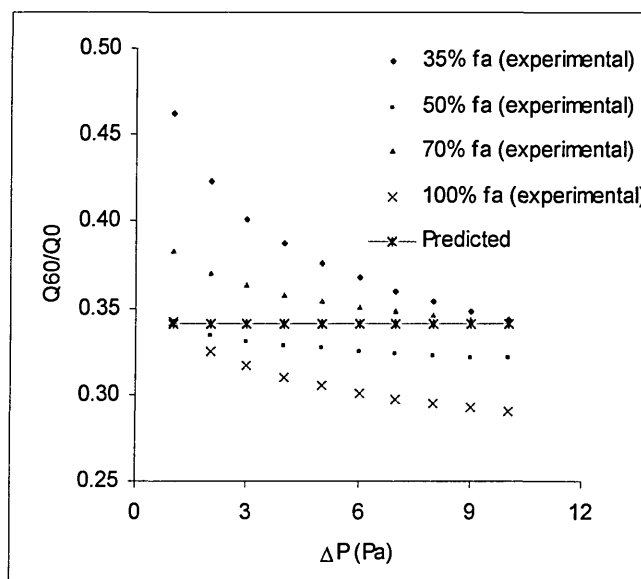
Figure 7.46: Variation of airflow rate ratio (Q_{60}/Q_0) with ΔP
for inclined louver blades with various mesh-screens

Comparison between the predicted ratio and those obtained from experimental data revealed that for the 35% free-area mesh-screen the deviation at 1 Pa was 26% with the proposed equation under-predicting the airflow rate ratio. For the 70% free-area mesh-screen the deviation was 10% at 1 Pa pressure differential across the ventilator. On the other hand, the highest deviations for the mesh-screens with 50% and 100% free-area occurred at 10 Pa with the proposed equation over-predicting the airflow rate ratio. Figure 7.47 shows the variation of airflow rate ratio at various louver blade inclination angles with pressure differential for a mesh-screen free area of 0.35. The solid line shown in Figure 7.47 represents the experimental variation of airflow rate ratio for a ventilator with louver blades inclined at 60°. The graph shows that there was some deviation between the predicted and experimental parameters at low pressure differentials. However, the deviation steadily decreased to attain an exact match at high

pressure differentials. Similar trends were obtained for various louver blade inclination angles and also when the 50% and 70% mesh-screens were used.

1.2

1.0 · · · · · · · ·

0.8 · · · · · · · ·

Q /Q0 (deg)

0.6

0.4

0.2

0.0

0   3   6   9   12

ΔP (Pa)

· 0 deg (pred)

· 30 deg (pred)

▲ 60 deg (pred)

● 60 deg (exper)
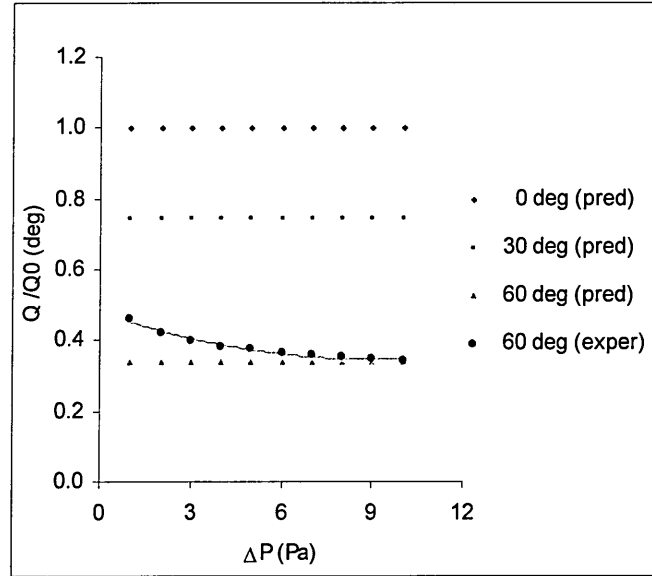
Figure 7.47: Variation of airflow rate ratio (Q/Q₀) with ΔP for
35% free-area mesh-screen for various louver blade angles

7.5.4 Horizontal louvers with gap between blades and mesh-screen

The power law source data for the case where horizontal louvers were used in combination with various mesh-screens and included a variation of the gap between the louver blades and the mesh-screen is given in Tables A6, A7 and A8 in the appendices of this thesis. For this scenario the objective was to establish a relationship:

$$Q = f\{\Delta P, f_a, L\} \tag{7.16}$$

relating the airflow rate (Q) resulting from a pressure differential (ΔP) across a ventilator incorporating a mesh-screen with free-area f_a located at a distance L from louver blades. A second regression performed on $\log_e Q$, $\log_e \Delta P$, mesh-screen fractional free-area f_a and separation/gap L resulted in the relationship given by Equation 7.17 with statistical parameters associated with this equation given in Table 7.10:

$$\log_e Q = 0.75 \log_e \Delta P + 2.32 f_a + 0.02L - 3.4 \tag{7.17}$$

Table 7.10: Statistical Parameters for Equation 7.17		
Equation parameters		
R square		0.8318
Adjusted R square		0.8287
Standard Error		0.2869
Multiple Regression Equation		
	coefficients	standard error
intercept	-3.399	0.100
loge DP	0.753	0.032
f_a	2.321	0.149
L	0.016	0.004
observations		170

Equation 7.17 was then transformed to linear format by inverting the logarithms to obtain the expression:

$$Q = \frac{\Delta P^{0.75} * 10.176^{f_a} * 1.0202^{L}}{29.923} \qquad (7.18)$$

where Q (m3/s) is the airflow rate resulting from a pressure differential ΔP (Pa) across a ventilator used in combination with a mesh-screen of free-area f_a with a gap L (mm) between the louvers and the mesh-screen. Figure 7.48 shows a linear regression comparison between airflow rates predicted by Equation 7.18 and those expected (given by power law curve fit to raw experimental data) for various ΔPs. For this situation 170 data points were used and resulted in a correlation coefficient of 0.648.

Figure 7.48: Variation of airflow rates predicted from Equation 7.18 with expected airflow rates

The predicted airflow rates show a relatively poor correlation with measured data as can be seen from the correlation coefficient of 0.648. The slope of the regression line was 0.875. This means that the predicted airflow rates were predominantly lower than the measured values.

PARAMETER VARIATION FOR HORIZONTAL LOUVERS WITH A GAP BETWEEN LOUVER BLADES AND THE MESH-SCREEN

The results from a comparison between predicted and experimental airflow rates, for various mesh-screen free-areas, as a ratio of airflow rates without any mesh-screen (Q/Q_{100}) for gap size = 3mm are shown graphically in Figure 7.49 and tabulated for selected pressure differentials in Table 7.11.

fa	$\Delta P = 1Pa$		$\Delta P = 5Pa$		$\Delta P = 10Pa$	
	Q/QL0exp	Q/QL0pred	Q/QL0exp	Q/QL0pred	Q/QL0exp	Q/QL0pred
0.35	0.26	0.22	0.28	0.22	0.29	0.22
0.5	0.57	0.31	0.59	0.31	0.6	0.31
0.7	0.56	0.5	0.55	0.5	0.55	0.5

Table 7.11:
Predicted and experimental variation of airflow rate ratio with DP for L = 3mm
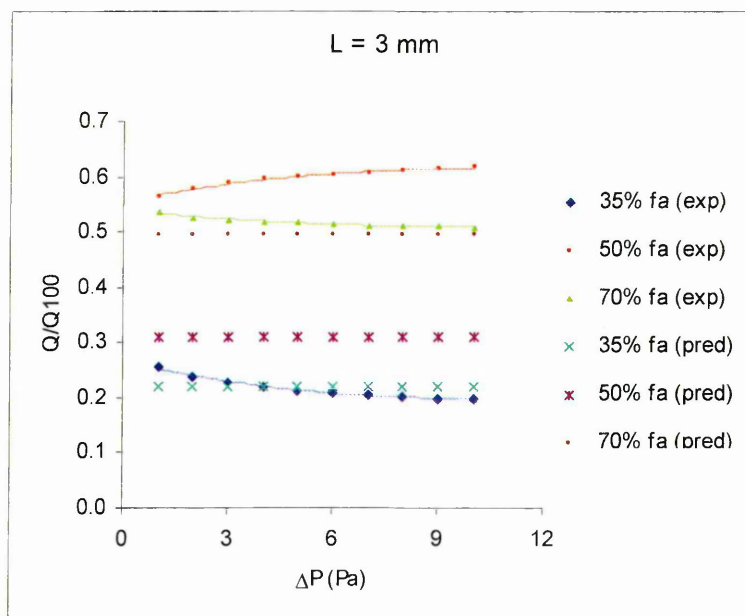
Figure 7.49: Variation of airflow ratio (Q/Q_{100}) with ΔP for horizontal louver blades with various mesh-screens for L = 3 mm

A visual assessment of Figure 7.49 shows that the predicted airflow rate ratios for the ventilator with mesh-screens of free-area ratio equal to 0.35 and 0.7 were in very good agreement with the expected parameters derived from experiments. The closeness of the predicted parameters to the experimental data can be judged from Table 7.11. On the other hand, the departure of the experimental airflow rate ratio from the predicted trend for the 50% free-area mesh-screen was rather large - approximately double that obtained from Equation 7.18. Further, the results obtained for the mesh-screen with 50% free-area did not follow the logical expectation of its experimental trend-line falling somewhere between the ones for the mesh-screens with 35% and 70% free-areas. At this stage in the analysis this can only be attributed to the "weird" behaviour of the 50% free-area mesh-screen initially detected and highlighted in *Section 7.5.2*. That aside, what this means physically is that the ventilator with 50% mesh-screen free-area performed better than when the louver was used in combination with a 70% free-area mesh-screen.

Although the variation of the predicted airflow rate ratios was independent of pressure differentials, the variation observed from experimental data exhibited some dependence on pressure differential. However, close examination of the experimental trends did not reveal any consistence as to how the airflow ratio was affected relative to ΔP. Generally the findings described above also held when the gap between louvers and mesh-screen was increased. However, it was noted that the deviation between predicted and expected parameters for the mesh-screens with free-areas of 35% and 70% increased with increasing gap size.

Figures 7.50 to 7.53 show the variation of the predicted and experimental airflow rates through the ventilator used in combination with a mesh-screen of 35% free-area, as a ratio of the airflow rates through the ventilator with no gap between the louver blades and the mesh-screen for separations L = 3, 6, 9 and 12 mm.
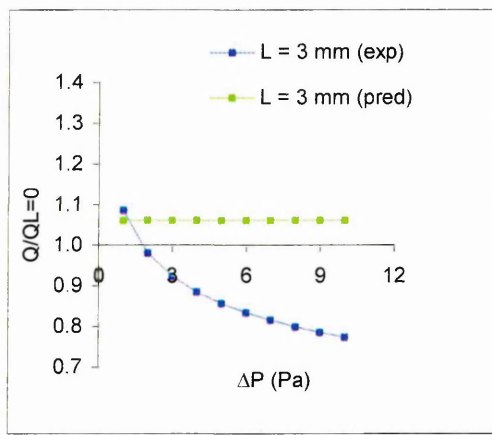
Figure 7.50: Variation of airflow rate ratio
($Q/Q_{L=0}$) with ΔP for $L = 3$ mm
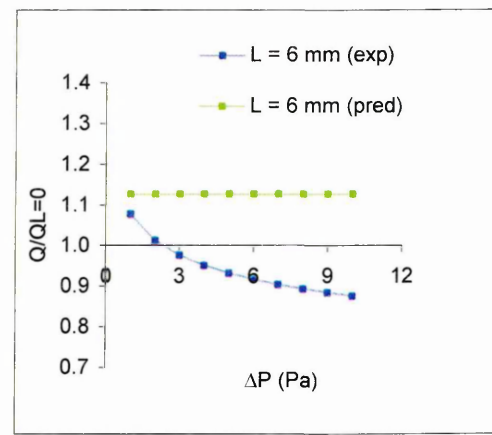
Figure 7.51: Variation of airflow rate ratio
($Q/Q_{L=0}$) with ΔP for $L = 6$ mm
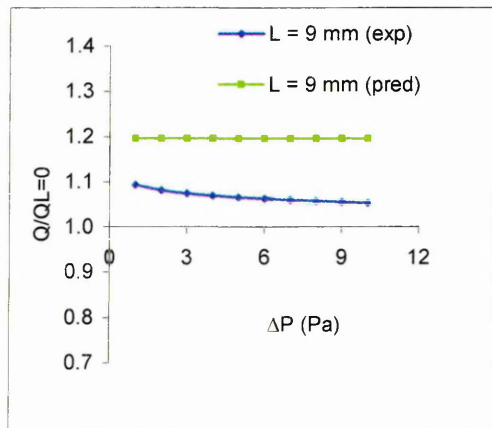
Figure 7.52: Variation of airflow rate ratio
($Q/Q_{L=0}$) with ΔP for $L = 9$ mm
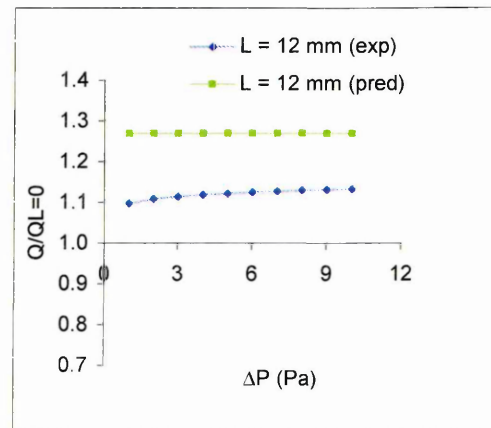
Figure 7.53: Variation of airflow rate ratio
($Q/Q_{L=0}$) with ΔP for $L = 12$ mm

It can be seen from the graphs that the prediction from the equation indicated improvements in the airflow properties which increased as the gap between the louver blades and the mesh-screen was increased. These improvements remained constant with increasing pressure differential across the ventilator. Experimental data on the other hand showed that the airflow ratio was dependent on the pressure differential. Figure 7.50 and Figure 7.51 show that at 3 mm and 6 mm the gap between the louver blades and the mesh-screen initially had a positive influence on the airflow properties of the ventilator. This influence decreased with increasing pressure differential and turned into an adverse effect at pressure differentials just above approximately 2 Pa. Higher separations however, revealed improvements throughout the range of pressure differentials considered. The positive influence on airflow properties varied slightly with increasing ΔP. For instance for the 9 mm gap the improvement marginally decreased with increasing ΔP whilst at 12 mm it marginally increased with increasing

ΔP. From the experimental trends point of view two possible explanations can be applied to these findings. The first is that the findings suggest that there is a minimum separation or gap between the louver blades and mesh-screen at which the airflow properties begin to be enhanced. The second reason is that at low gap size between the louver blades and mesh-screen the turbulence created by the mesh-screen introduces a resistance which hinders the overall airflow through the ventilator.

The experimental and predicted variation of airflow rate ratio ($Q/Q_{L=0}$) with separation between the louver blades and the mesh-screens is shown in Figure 7.54 for selected pressure differentials and the mesh-screen with 35% free-area.
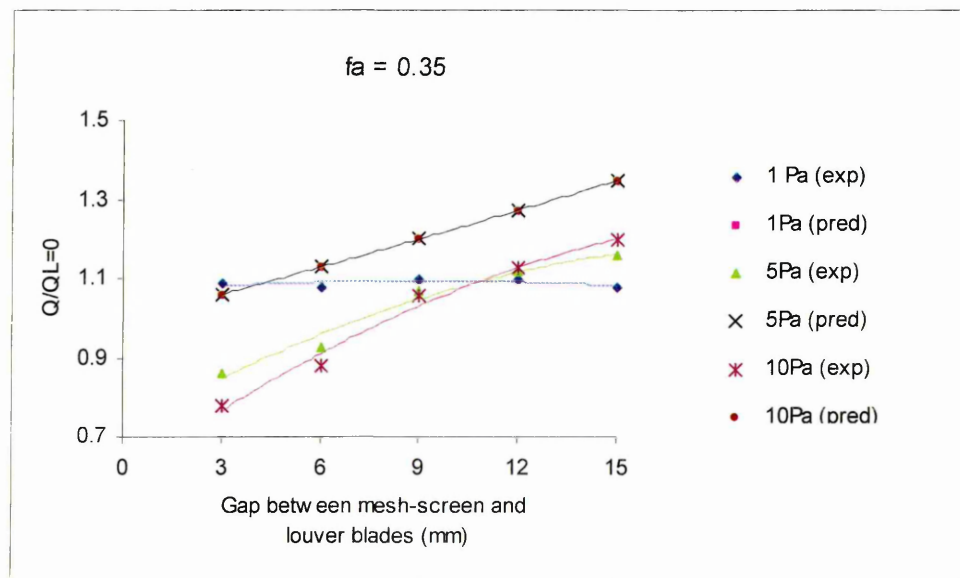
Figure 7.54: Variation of airflow rate ratio ($Q/Q_{L=0}$) with gap size between louver blades and mesh-screen for various ΔPs

The predicted parameters at various gap sizes were found to be independent of the pressure differential hence the trend-lines for ΔP = 1, 5 and 10 Pa were superimposed on the graph. The graph also shows that the predicted airflow rate ratios increased with increasing gap size. This was also generally true for the experimental airflow rate ratios at ΔP = 5 and 10 Pa. Relative to experimental data the airflow rate predicted by Equation 7.18 resulted in over-prediction of parameters. The degree of over-prediction can be determined from Table 7.12. For instance at 5 Pa the over-prediction was 19% at L = 3 mm, 11% at L = 9 mm and 14% at L = 15 mm.

L (mm)	ΔP = 1 Pa		ΔP = 5Pa		ΔP = 10Pa	
	$Q_L/Q_{L=0}$ (exp)	$Q_L/Q_{L=0}$ (pred)	$Q_L/Q_{L=0}$ (exp)	$Q_L/Q_{L=0}$ (pred)	$Q_L/Q_{L=0}$ (exp)	$Q_L/Q_{L=0}$ (pred)
3	1.09	1.06	0.86	1.06	0.78	1.06
6	1.08	1.13	0.93	1.13	0.88	1.13
9	1.1	1.2	1.07	1.2	1.06	1.2
12	1.1	1.27	1.12	1.27	1.13	1.27
15	1.08	1.35	1.16	1.35	1.2	1.35

Table 7.12:
Experimental and predicted airflow rate ratios at various gap sizes

However, at ΔP = 1Pa the experimental airflow ratio remained approximately constant for all gap sizes. Here again this was attributed to the airflow at low ΔP = 1 Pa not being as strongly established as that for ΔP = 5 Pa and 10 Pa.

7.5.5 Inclined louvers with gap between blades and mesh-screen

This scenario represented the case that integrated all variables. The power law source data for wooden Louver 1 with louver blade inclination angles 0°, 30° and 60° with various mesh-screen free-areas and gap sizes (Tables A6 to A8 in the appendices) was used as starting point for establishing the relationship:

$$Q = f\{\Delta P, \theta, f_a, L\} \tag{7.19}$$

for the airflow rate (Q) resulting from a pressure differential (ΔP) across a ventilator with louver blades inclined at an angle θ to the horizontal. For this case the ventilators incorporated mesh-screens of fractional free-area f_a located with a gap/separation of size L away from the louver blades. A second regression performed on $\log_e$ Q, $\log_e$ ΔP, the cosine of the angle of inclination of the louver blades (θ) from horizontal, mesh-screen fractional free-area f_a and separation L resulted in the relationship given by Equation 7.20 with statistical parameters associated with this equation given in Table 7.13:

$$\log_e Q = 0.71\log_e \Delta P + 2.66\mathrm{Cos}\theta + 1.47f_a + 0.02L - 5.58 \tag{7.20}$$

Table 7.13: Statistical Parameters for Equation 7.20			
Equation parameters			
R square	0.8353		
Adjusted R square	0.8341		
Standard Error	0.3503		
Multiple Regression Equation			
	coefficients		standard error
intercept	-5.581		0.089
loge DP	0.708		0.022
Cosθ	2.664		0.072
f_a	1.474		0.105
L	0.018		0.003
observations			530

Equation 7.20 was then transformed to linear format by inverting the natural logarithms to obtain the expression:

$$ Q = \frac{\Delta P^{0.71} * 14.296^{Cos\theta} * 4.349^{f_a} * 1.0202^{L}}{265.072} \qquad (7.21) $$

where Q (m3/s) is the airflow rate resulting from a pressure differential ΔP (Pa) across a ventilator with louver blades inclined at θ° from horizontal used in combination with a mesh-screen of free area f_a which was located at a distance L (mm) away from the louver blades. Figure 7.55 shows a linear regression comparison between airflow rates predicted by Equation 7.21 and those expected (given by power law curve fit to raw experimental data) for various ΔPs. For this situation 532 data points were used and resulted in a correlation coefficient equal to 0.7586.
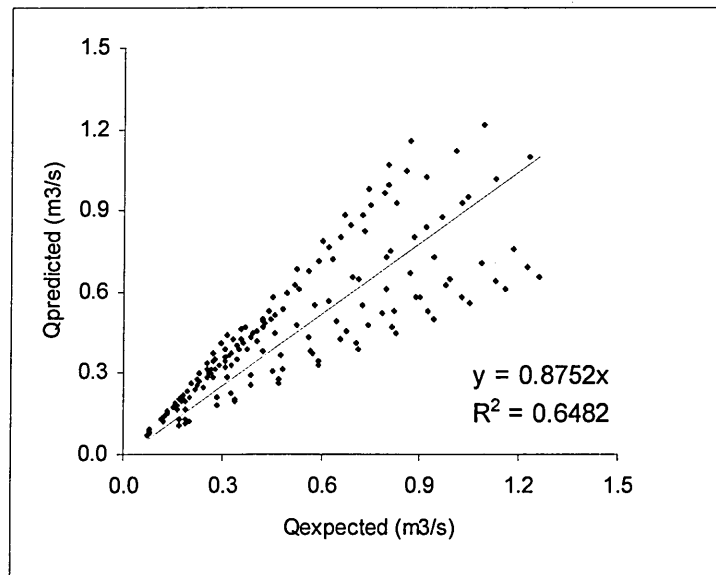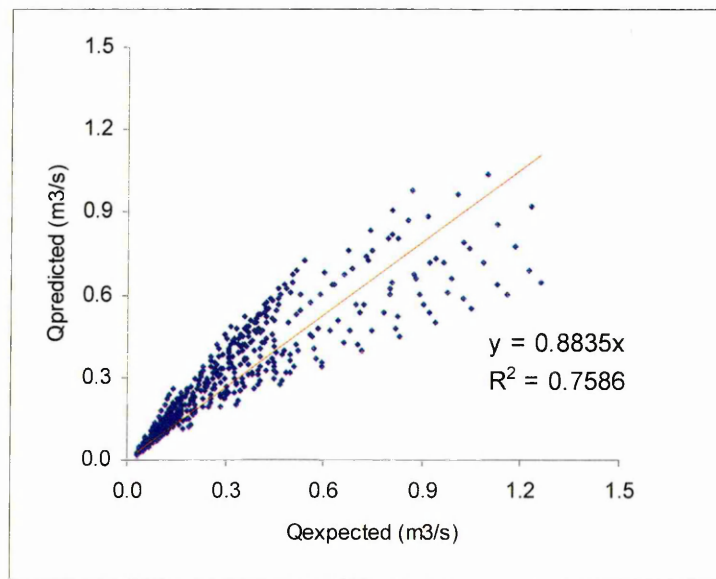

Figure 7.55: Variation of airflow rate ratio predicted from Equation 7.21 with expected airflow rate ratio

The predicted airflow rates show a good correlation with measured data as can be seen from the correlation coefficient of 0.7586. The slope of the regression line was 0.884. This means that the predicted airflow rates were predominantly lower than the measured values.

PARAMETER VARIATION FOR A VENTILATOR WITH INCLINED LOUVERS WITH GAP BETWEEN LOUVER BLADES AND THE MESH-SCREEN

Several interesting variations of the combinations of the five variables included in this case can be derived and analysed. However, for time and economy, only a few selected examples of variations and comparisons between experimental parameters and those predicted by utilising Equation 7.21 are included here. Figure 7.56 shows the ratio of the experimental airflow rate through a ventilator with horizontal blades and incorporating a 35% free-area mesh-screen located at separation L, to the airflow rate through the ventilator when L was equal to zero, and how the airflow rate ratio varied with respect to the pressure differential across the ventilator. Whilst the experimental airflow rate ratios varied with increasing ΔP for each gap size the ratios predicted by the equation were independent of ΔP and resulted in values of 1.06, 1.13, 1.20, 1.27 and 1.35 for L = 3, 6, 9, 12 and 15 mm respectively. It can be seen from Figure 7.56 that there was significant deviation between airflow rate ratios for various gap sizes at high pressure differentials for the ventilator with horizontal (0 deg) louver blades. However, inclining the louver blades to 60° decreased the deviations in airflow rate ratios for various gap sizes. Figure 7.56 suggests that locating the mesh-screen at L = 9, 12 and 15 mm enhanced the airflow performance throughout the range of pressure differentials considered. On the other hand, tilting the louver blades to 60° had a negative impact on the ventilator with L = 12 mm at pressure differentials less than 3 Pa and also for the ventilators with L = 3mm and L = 15mm at pressure differentials greater than approximately 5 Pa (Figure 7.57).
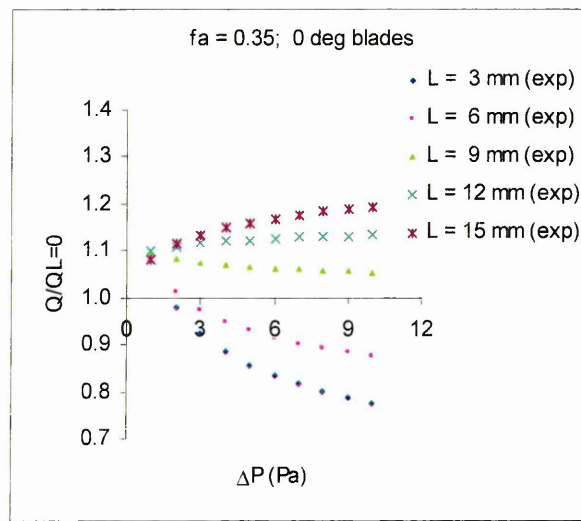
Figure 7.56: Variation of airflow rate ratio (Q/Q$_{L=0}$) with ΔP
for ventilator with 0.35 free-area mesh-screen
and horizontal louver blades
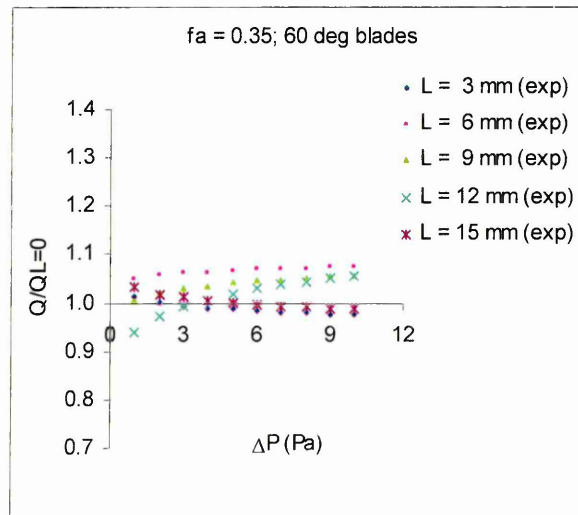
Figure 7.57: Variation of airflow rate ratio (Q/Q$_{L=0}$) with ΔP
for ventilator with 0.35 free-area mesh-screen
and louver blades inclined at 60°

The variation of the airflow rate ratios with louver blade inclination angle is also shown graphically in Figures 7.58 to 7.60 and numerically in Table 7.14 for selected pressure differentials to further gain an insight into how different gap sizes between louver blades and mesh-screens influenced the airflow performance of the ventilator.
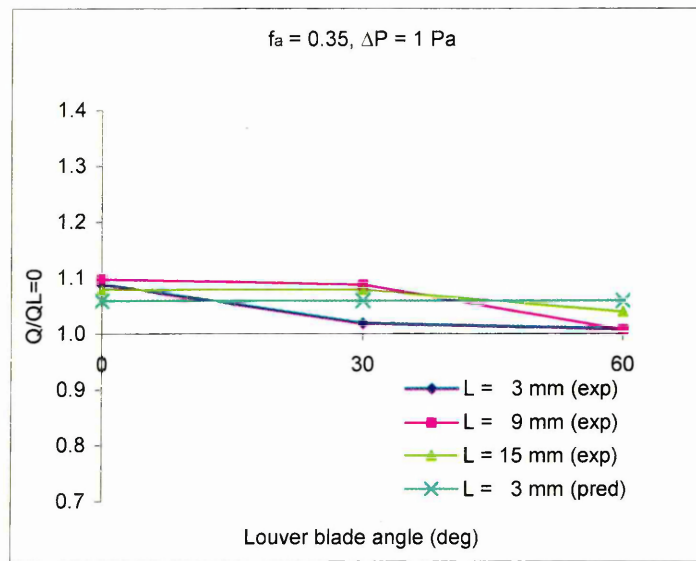
Figure 7.58: Variation of airflow rate ratio (Q/Q_{L=0}) with louver blade angle for ΔP = 1 Pa
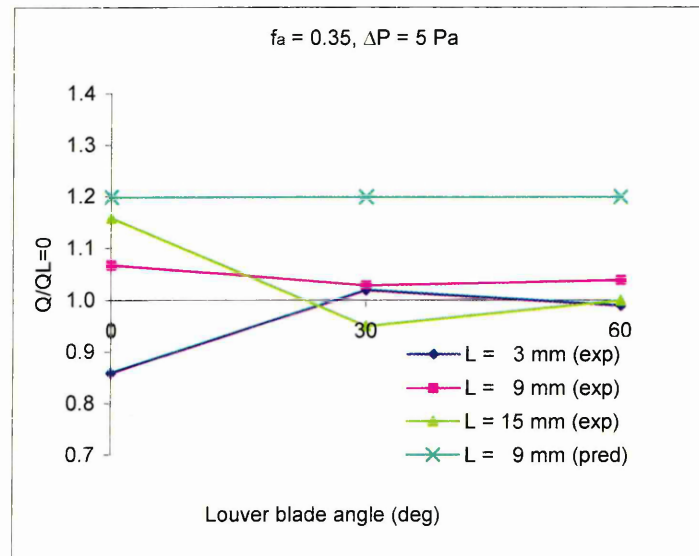
Figure 7.59: Variation of airflow rate ratio (Q/Q_{L=0}) with louver blade angle for ΔP = 5 Pa
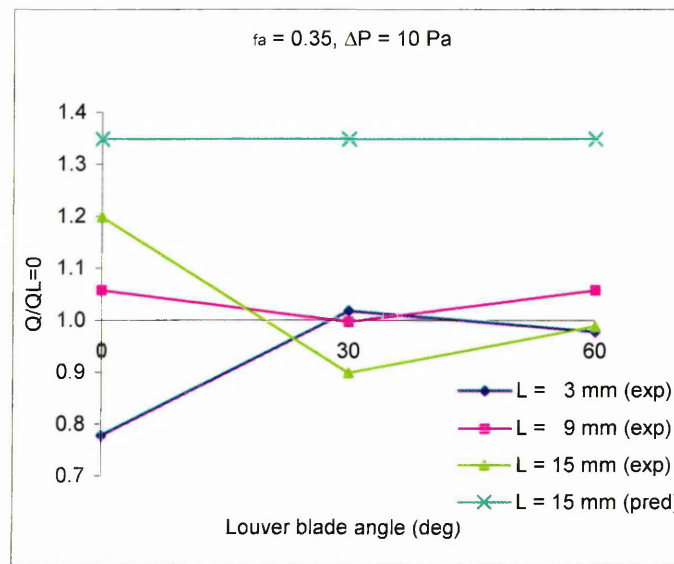
Figure 7.60: Variation of airflow rate ratio ($Q/Q_{L=0}$) with louver blade angle for $\Delta P = 10$ Pa

θ (deg)	ΔP = 1 Pa			ΔP = 5 Pa			ΔP = 10 Pa		
	3 mm	9 mm	15 mm	3 mm	9 mm	15 mm	3 mm	9 mm	15 mm
0	1.09	1.10	1.08	0.86	1.07	1.16	0.78	1.06	1.20
30	1.02	1.09	1.08	1.02	1.03	0.95	1.02	1.00	0.90
60	1.01	1.01	1.04	0.99	1.04	1.00	0.98	1.06	0.99

Table 7.14: Variation of airflow rate ratio for inclined louver blades

Numerous deductions can be made from Figures 7.58 to 7.60, however only a few key observations from the graphs are highlighted here:-

- at low ΔP ($\Delta P = 1$ Pa) all gap sizes appear to enhance the airflow performance of the ventilator at the three louver blade angles (0°, 30° and 60°) considered

- at $\Delta P = 5$ Pa only the ventilator with louver blade/mesh-screen gap size L = 9 mm exhibited a positive influence for the three louver blade angles considered

- at high ΔP ($\Delta P = 10$ Pa) the gap size L = 9 mm appeared to improve the airflow performance at 0° and 60° blade angles by an equal amount (= 6%) whilst for θ = 30° gap size L = 9 mm appeared to result in an airflow performance equal to that when there was no gap between the louver blades and mesh-screen

-261-

An obvious possible application of such findings is the manufacture of fixed blade ventilators where an assessment could be carried out to determine the gap size between louver blades and the mesh-screen that would result in the most efficient airflow performance. Previous discussions with some ventilator manufacturers revealed that no particular attention is currently paid to the location of mesh-screens from a point of view of airflow performance in ventilators for natural ventilation applications.

The airflow rate through ventilators with $30°$ and $60°$ inclined louver blades relative to the airflow rate through a ventilator with horizontal blades incorporating a 35% free-area mesh-screen is shown in Figures 7.61 to 7.63 as a function of the pressure differential for selected gap sizes L between the louver blades and mesh-screen. The experimental trend points are joined by solid lines for no special reason other than choice of presentation. A comparison between predicted and experimental trend lines shows that for the $\theta = 30°$ the deviation between the two data sets increased with increasing ΔP but decreased with increasing gap size L. On the other hand, for $\theta = 60°$ the deviation was almost constant for all pressure differentials at L = 3 mm, and decreased with increasing ΔP for L = 9 and 15 mm. It is clear from Figures 7.62 and 7.63 that agreement between experimental parameters and those predicted improved with increasing pressure differential.
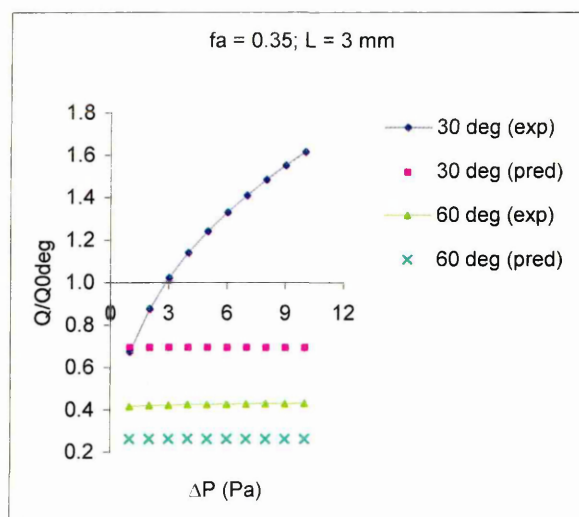
Figure 7.61: Variation of airflow rate ratio ($Q/Q_{\theta=0}$) with ΔP for $\theta = 30°$ and $60°$, $f_a = 0.35$ and L = 3 mm
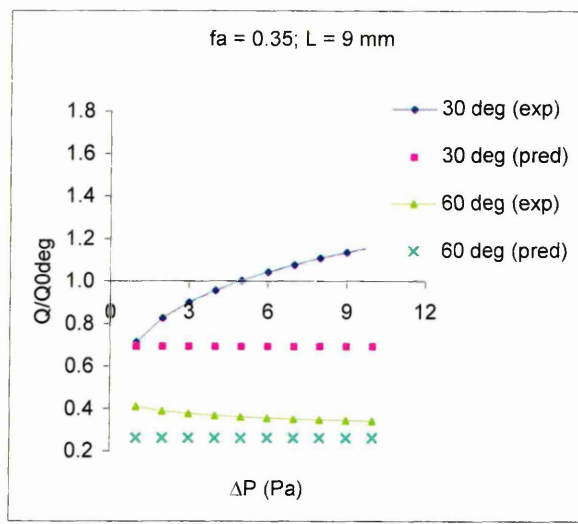
Figure 7.62: Variation of airflow rate ratio (Q/Q$_{\theta=0}$) with ΔP for θ = 30° and 60°, f$_a$ = 0.35 and L = 9 mm
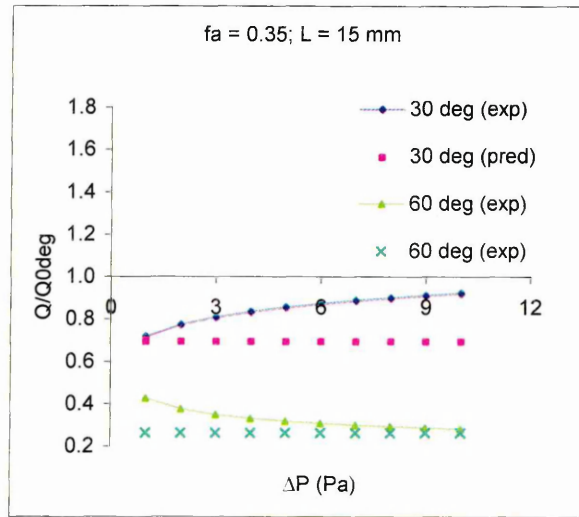
Figure 7.63: Variation of airflow rate ratio (Q/Q$_{\theta=0}$) with ΔP for θ = 30° and 60°, f$_a$ = 0.35 and L = 15 mm

The influence of the mesh-screen free-area on the airflow performance was assessed by considering the variation of airflow rate ratio $\left(\dfrac{Q}{Q_{f_a=1}}\right)$ with pressure differential for louver blade angles of 0°, 30° and 60°. $\left(\dfrac{Q}{Q_{f_a=1}}\right)$ is the ratio of the airflow rate through a meshed ventilator with inclined blades to the airflow rate when the ventilator was unmeshed. The results for mesh-screens with 35% and 70% free-areas are shown in Figures 7.64 to 7.69 for selected separations between the louver blades and the mesh-screens.
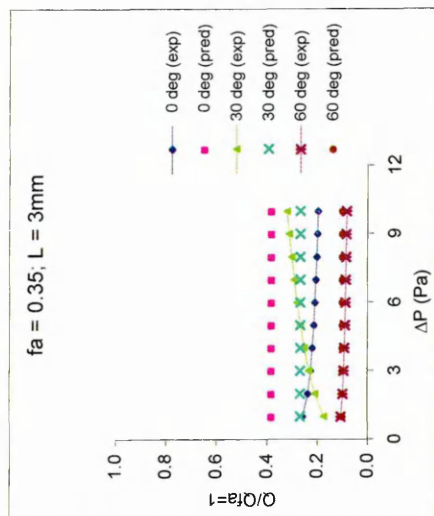
Figure 7.64: Variation of airflow rate ratio
($Q/Q_{fa=1}$) with ΔP for $f_a = 0.35$ and $L = 3$ mm
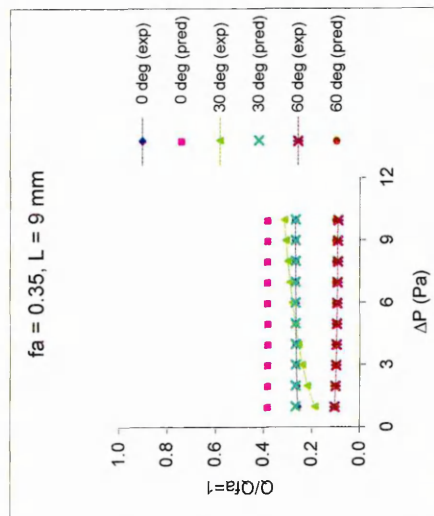
Figure 7.65: Variation of airflow rate ratio
($Q/Q_{fa=1}$) with ΔP for $f_a = 0.35$ and $L = 9$ mm
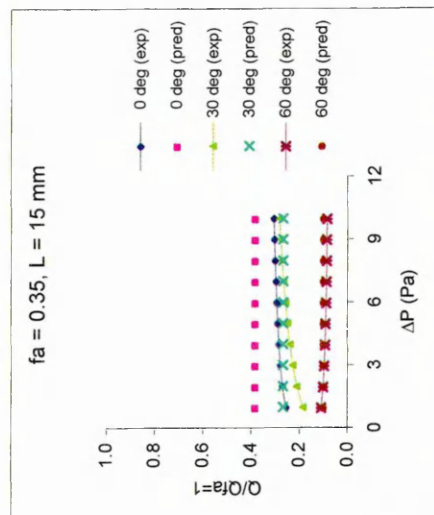
Figure 7.66: Variation of airflow rate ratio
($Q/Q_{fa=1}$) with ΔP for $f_a = 0.35$ and $L = 15$ mm
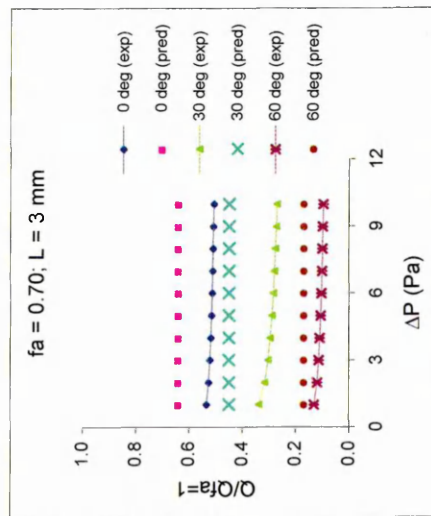
Figure 7.67: Variation of airflow rate ratio
($Q/Q_{fa=1}$) with ΔP for $f_a = 0.70$ and $L = 3$ mm
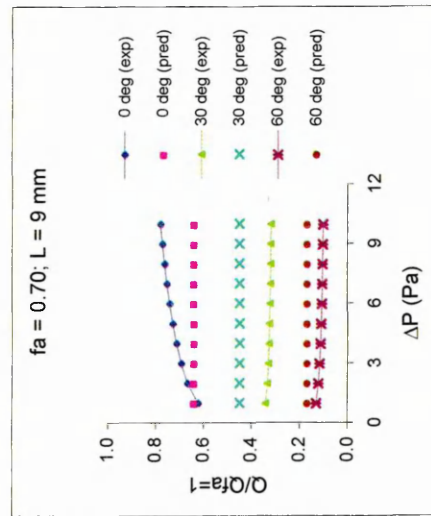
Figure 7.68: Variation of airflow rate ratio
($Q/Q_{fa=1}$) with ΔP for $f_a = 0.70$ and $L = 9$ mm
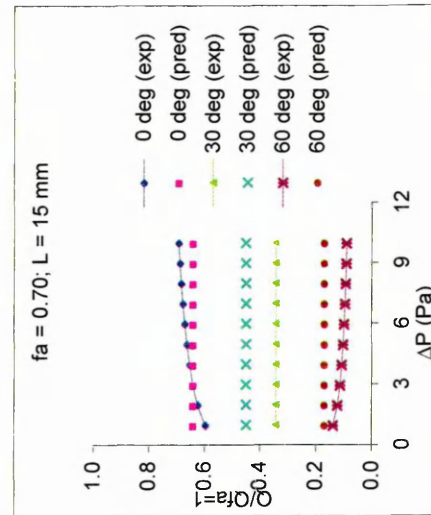
Figure 7.69: Variation of airflow rate ratio
($Q/Q_{fa=1}$) with ΔP for $f_a = 0.70$ and $L = 15$ mm

Comparison between experimental parameters and those predicted from the proposed equation revealed some interesting features. For instance, there was close agreement of airflow parameters at $\theta = 60°$, for both mesh-screens and also for all gap sizes. At $\theta = 30°$, the deviation between experimental and predicted parameters was approximately constant for $L = 9$ mm and $L = 15$ mm when the fractional free-area of the mesh-screen was equal to 0.7 with the proposed equation giving an over-prediction of the airflow rate ratios. For the 35% free-area mesh-screen, agreement between experimental and predicted parameters appeared to improve with increasing gap size between the mesh-screen and louver blades. The case with horizontal blades gave the worst deviations between predicted and experimental parameters.

7.6 Evaluation of Proposed Equations

The various equations derived in the preceding sections can be thought of as merely different choices of the function $Q = f\{\Delta P, f_a, \theta, L\}$ relating the airflow rate to the prevailing driving force (ΔP) and constituent components of a ventilator. The expressions for Q for various scenarios considered are listed in Table 7.15 together with proposed ranges of application of various variables for ease of reference. In addition to the ranges of application listed in the table the pressure differentials were limited to those typical in natural ventilation of buildings (i.e. $0 < \Delta P \leq 10Pa$). It is worth mentioning here that the parameters indicated in Column 3 of Table 7.15 are generally those that were used in the derivation of the proposed equations. Hence although the equations are intended for these ranges, they can possibly hold to a limited extent outside the limits given. Determination of this extent was outside the scope of this investigation although the author intends to pursue this out of interest. The degree of satisfaction of each equation can be judged by comparison with the expected solution some examples of which are included in the previous sections. Based on the results from comparisons between predictions and experimental data the proposed equations can be said to generally give what may be termed a physically realistic solution. A word of caution! The equations proposed in this investigation are not intended to replace the judgement and insight of the ventilation designer. Rather, they should properly be viewed as an enabling tool that allows the designers to focus their effort on the overall ventilation design, by relieving them of the need to spend large amounts of time exploring the effects of small variations on the overall airflow performance of natural ventilation systems.

Table 7.15:

Summary of Proposed Equations

CASE DESCRIPTION	PROPOSED EQUATION	RANGE OF APPLICATION
Ventilator with louver blades inclined at an angle to the horizontal	$$Q = \frac{\Delta P^{0.57} * 10.591^{\cos\theta}}{82.269}$$	$0° \le \theta \le 60°$
Round wire woven-square mesh-screen lattice	$$Q = \frac{\Delta P^{0.81} * 83.096^{f_a}}{34.124}$$	$0.35 \le f_a \le 0.7$
Ventilator with horizontal blades incorporating mesh-screen (described above)	$$Q = \frac{\Delta P^{0.67} * 1.363^{f_a}}{12.305}$$	$0.35 \le f_a \le 0.7$
Ventilator with inclined louver blades with and mesh-screen	$$Q = \frac{\Delta P^{0.63} * 8.585^{Cos\theta} * 1.197^{f_a}}{91.8356}$$	$0° \le \theta \le 60°$ $0.35 \le f_a \le 0.7$
Ventilator with horizontal louver blades with gap between blades and mesh-screen	$$Q = \frac{\Delta P^{0.75} * 10.176^{f_a} * 1.0202^{L}}{29.923}$$	$0.35 \le f_a \le 0.7$ $3mm \le L \le 15mm$
Ventilator with inclined louver blades with gap between blades and mesh-screen	$$Q = \frac{\Delta P^{0.71} * 14.296^{Cos\theta} * 4.349^{f_a} * 1.0202^{L}}{265.072}$$	$0° \le \theta \le 60°$ $0.35 \le f_a \le 0.7$ $3mm \le L \le 15mm$

A comparison was performed between Maghrabi's [*2000*] experimental data and the results predicted from Equation 7.6 for the same louver system with horizontal louver blades and those inclined at 30°. Figure 7.70 shows quadratic curve fits to data for horizontal louvers with Maghrabi's data points plotted with ± 20% X-axis error bars.
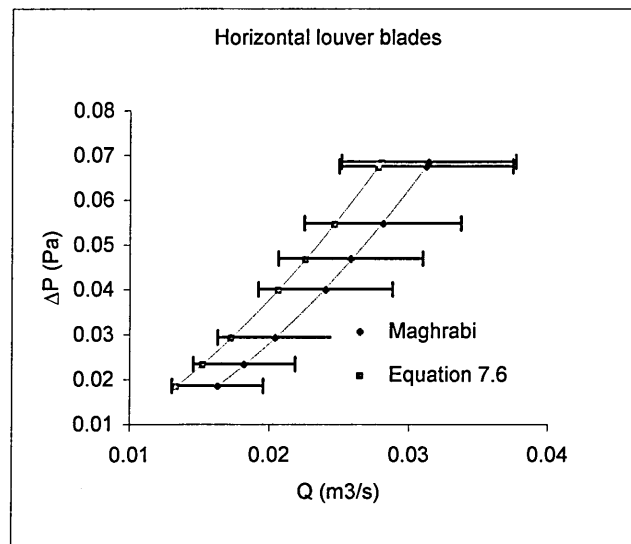
Figure 7.70: Quadratic formulation comparison between data
from Maghrabi [2000] and that predicted from Equation 7.6
for a louver system with horizontal

By inspection of Figure 7.70, the curve predicted from the proposed equation gave an under-prediction within 20% of Maghrabi's experimental data. Figure 7.71 shows quadratic curve fits to data for $30°$ inclined louver blades with Maghrabi's data points plotted with $\pm 10\%$ X-axis error bars.
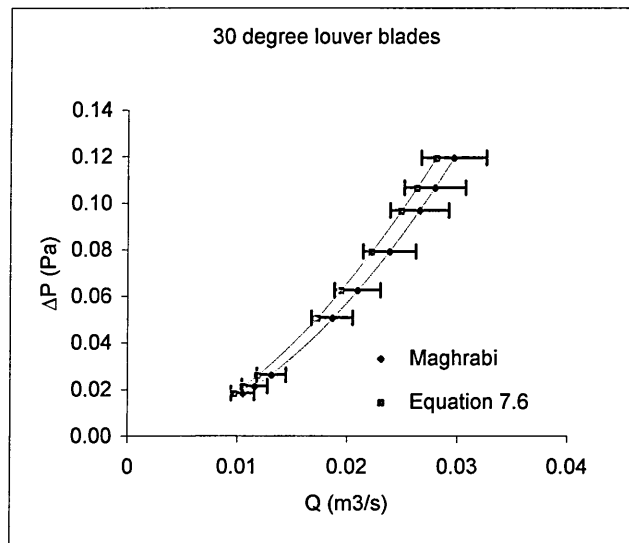
Figure 7.71: Quadratic formulation comparison between data
from Maghrabi [2000] and that predicted from Equation 7.6
for a louver system with $30°$ inclined louver blades

Similarly, inspection of Figure 7.71 shows that the curve predicted from the proposed equation gave an under-prediction within 10% of Maghrabi's data points. It can be seen that the theoretical curves give satisfactory fit to the experimental data from a totally independent study on components with the same dimensions/configuration. As such, by taking the margins indicated as arbitrary limits of acceptability there was therefore reasonable justification for adopting the proposed equation as giving a physically realistic equation. Comparisons for other configurations such as louvers with mesh-screens could not be carried out simply because there was no data in the literature that could be used.

IMPORTANCE OF PROPOSED EQUATIONS

Lack of simple equations such as those derived here (previously unavailable) has denied designers and ventilator manufacturers tools with which they can quickly assess the impact of various components on the airflow performance of ventilators. There is no doubt as to the potential benefits of the equations proposed here. For instance, designers' main feature of interest is likely to be departure of flows from design specification. Posed with this situation, designers can use these equations to easily predict operating conditions in the absence of experimental data. In addition these equations can be used as a method to adapt airflow rates in ventilation models to estimate the variation in the airflow produced by different ventilator configurations. Hence the designer can assess the amount of air through a ventilator of given components under specified conditions in early stages of the design. For instance the equations can be used to provide boundary conditions for CFD simulations or allow CFD simulations to be assessed for various scenarios of ventilator operation before the design is fixed. As a consequence, they can thus be applied to study impact of user operation on overall airflow performance and resulting indoor comfort and air quality. In addition the equations can be used to check the sensitivity of the airflow rate Q to possible changes in ventilator elements.

More often than not manufacturers design ventilators by using empirical guidelines based upon experience and limited measurements. These guidelines do not consider the complex combination of parameters that influence the airflow through the ventilator components. Consequently, the ventilators do not always produce the expected airflow characteristic. Frequently, considerable trial and error measurements are required in identifying adjustments that would yield the desired changes in the airflow

characteristics. This practice is usually time consuming and expensive, and often the resulting arrangement rarely optimum. Therefore, equations such as those proposed here can aid ventilator manufacturers for instance, in predicting the characteristics of different models prior to manufacture. Further, from a manufacturer's point of view these equations can significantly reduce the amount of component testing required.

7.8 Limitations of Proposed Equations

Although the potential of the proposed equations has been highlighted the following are some of the difficulties that would limit their application to some extent:-

1. The proposed equations were derived based on louvers banks of typical dimensions 380 mm wide x 420 mm high x 130 mm deep, hence they might need scaling/modification to be applicable to dimensions significantly different from these.

2. Mesh-screen wire diameters were not taken into account hence, geometric effects of the wires are not accounted for in the equations. In addition only a limited range of mesh-screen free-areas were included, therefore, more tests on a wide range of mesh-screens are necessary.

3. Currently the proposed equations do not have an easy physical interpretation that directly relates them to the dimensions of the ventilator in a manner similar to the well known relationships between the coefficients from the quadratic formulation and the dimensions of the airflow path (see *Section 4.6.1*).

4. In practice pressure differences acting across ventilators are seldom steady, contrary to the simplification used in deriving the equations. In this regard the proposed equations do not take into account the influence of instantaneous fluctuating or unsteady effects of the pressure driving forces. A possible approach to account for such effects would be to describe the pressure differential by a harmonic oscillation with mean $\overline{p_o}$ and amplitude p_p [Kronvall, *1980*] which would then give a revised power law function of the form:

$$Q = A(\overline{p_o} + p_p Sin\omega t)^B \qquad (7.22)$$

as source data for establishing the relationship $Q = f\{\Delta P_{unsteady}, \theta, f_a, L\}$.

7.9 Concluding Remarks

This chapter presented and discussed results of comparisons between experimental results and CFD predictions of airflow properties for some of the ventilator components tested during the experimental phase of the investigation. In addition, some general equations were established to represent the relationships between airflow rates through a ventilator to the pressure differential driving the flow by taking into account a variety of combinations of ventilator constituent components. No similar expressions were found in the literature as such; this work marks the first major step in the *new approach to understanding the airflow performance of ventilator components for natural ventilation applications*[1].

The quantitative comparisons between experimental and predicted data were generally very good. The 3-D computational domain and representation of turbulence effects by using the k - ε turbulence model provided good prediction of airflow performance quantities and of flow characteristics for the ventilator components investigated.

The general solution equations proposed essentially encompassed the range of parameters attained in the experiments. Comparison between numerical results predicted from the equations and experimental data for all cases considered was generally reasonable and acceptable. In addition, the accordance between trends predicted from the equations and those derived from measured data was quite satisfactory for all cases considered. Whilst on one hand the validity of the general equations presented in this work needs to be checked and possibly improved by more experiments, on the other hand, by means of the relationships presented in this chapter quantitative predictions maybe made of flow modifications to be expected as a result of variations in parameters of components constituting a ventilator.

---

[1] *A paper with this title and based on the work described in this chapter is currently being prepared for journal publication.*

Clearly the physical processes involved in natural ventilation airflows are much more complex than has been given credit for in this chapter and to this effect some limitations of the proposed equations are highlighted. Therefore, although the present study provides sufficient indication of the magnitudes of airflow properties which may be generated in natural ventilation applications, the extension of the results to other dimensionally different ventilators or to components in real buildings depends on further analysis and experiment. For instance, there is need to determine more precisely the effects of the mesh-screen hole shape, diameter of wires forming the mesh-screen lattice, in addition to the effects originating from the instantaneous nature of airflows occurring in practice.

Chapter 8

FINAL REMARKS

8.1 Introduction

The prediction of airflow characteristics of ventilators in naturally ventilated buildings is very important for the calculation of the thermal response of the buildings. This thesis closes here with a review of the aims and objectives of the investigation, followed by an overview of the main findings of the investigation including suggestions of design guidelines for ventilator manufacturers. Some proposed recommendations for future work in the quest of making ventilators more efficient for natural ventilation applications are also presented.

8.2 Review of Aims and Objectives of the Research

The overall aim of this study was to investigate the airflow performance of ventilators through a parametric analysis based upon experimental measurements and Computational Fluid Dynamics (CFD) modelling.

The specific objectives were as follows:

- To investigate experimentally how individual components in ventilators affect airflow performance

- To develop flow equations to describe the airflow through ventilators

- To compare experimental data with CFD predicted values and develop CFD as a potential design tool for ventilators

- To develop a methodology to design ventilators with the aim of optimising the overall airflow performance

8.3 Overview of Main Findings

The prediction of airflow through ventilators is a difficult task. From the available literature a good agreement does exist on the prediction of airflow characteristics through individual components (such as louvers, mesh screens etc) using power law and quadratic formulations/regressions. Nevertheless, a large uncertainty due to lack of sufficient studies remains on the impact of various ventilator components on the overall performance of ventilators. A real lack of knowledge exists on the behaviour of ventilators (combinations of components) or airflow characteristics especially in relation to low pressure differentials typical in natural ventilation applications. However, some studies/experiments do exist on individual components and these save as an excellent starting point in any attempt to investigate and quantify the impact of individual components on the overall airflow performance of ventilators.

A key contribution of this study (unavailable until now) was the quantification of the impact of combinations of components/configurations on the overall airflow performance of ventilators for natural ventilation in buildings. The methodology adopted in analysing various components was a combination of experimental and numerical parametric approaches.

The following are the key points developed in this thesis:-

DIRECTIONAL AIRFLOW

One feature of natural ventilation is that depending upon the prevailing climatic or thermal conditions the airflow through a ventilator can be bi-directional. Aerodynamically, the ventilator, depending upon its construction may not perform in the same way for the two different flow directions. The geometry of the internal flow-path, the inclination of louver blades and the location of meshes and acoustic linings are features that stop the ventilator being aerodynamically symmetrical for different flow directions. The findings of this investigation revealed that airflow through ventilators is influenced by the flow direction, with the influence being more pronounced at low pressure differentials than at high pressure differentials. Therefore, where prevailing climatic conditions are reasonably consistent it might prove beneficial in naturally ventilated buildings to have differently designed inlet and outlet ventilators. Hence, it is

essential to treat the inlet and outlet configurations as independent elements in any attempt to optimise the airflow performance of the overall natural ventilation system.

EFFECT OF SEPARATION

Generally little or no particular attention is paid to the location of mesh-screens incorporated in to ventilators. This investigation observed that inserting a spacer between louvers and mesh screens always influenced the airflow performance of the ventilator. The relative overall improvement in airflow performance of a ventilator was found to be dependent on interactions between the following main factors:-

- Pressure differential across the ventilator

- Size of separation/gap between louvers and a mesh-screen

- Type of mesh-screen used

- Louver blade inclination angle

LOW AND HIGH PRESSURE AIRFLOW CHARACTERISTICS

The airflow characteristic of ventilators is influenced by the pressure range from which it was generated. The results obtained indicate that the characteristic equation derived to represent airflow through a ventilator was not only influenced by the constituent components of the ventilator but also the pressure range from which it was generated. This study highlighted the need to understand how the airflow characteristic of a ventilator is influenced by the pressure range from which it was generated. Although only a basic arrangement was used it was still sufficient enough to bring to light the dependence of the characteristic of a ventilator on pressure range under consideration and the components that make up the ventilator - louvers and mesh-screen in this case.

CFD MODELLING OF VENTILATORS

The current study was successful in utilising CFD model and integrating CAD as tools for analysing ventilator components for natural ventilation applications. However, it was noted that attention to the geometric details (e.g. mesh-screens, rain-hooks, and louver shapes) can be important in order to get accurate pressure/flow details. As such to some extent FLOVENT had some limitations to adequately represent the geometry of the louver systems that were modelled. Comparison of simulation and experimental

results was assessed from two perspectives, namely, power law and quadratic formulation. In both cases agreement between CFD predicted parameters and those obtained from experiments was reasonable and acceptable taking the above comments into account. Broadly speaking, the computational investigation met its task of analysing the airflow performance of ventilator components using CFD by making some necessary simplifications. In so doing substantial data has been obtained which can be used for validation of other studies involving slots, mesh-screens and louvers, and relating to ventilators for natural ventilation in buildings.

MESH-SCREEN ORIENTATION WITH RESPECT TO HOLE CONFIGURATION

Discussions with some ventilator manufacturers indicated that no particular attention is paid to the orientation of geometrically non-square mesh-screens incorporated in to ventilators. As such an assessment was carried out to establish how uneven mesh-screens performed when the orientation of the mesh-screen holes was changed. The results from this investigation show that the orientation of uneven mesh-screens in ventilators can result in significant differences in airflow performance (as high as 36%), hence this requires careful consideration by ventilator designers.

VENTILATOR AIRFLOW PERFORMANCE OPTIMISATION

Various equations derived in this investigation present different choices of the function $Q = f\{\Delta P, f_a, \theta, L\}$ relating the airflow rate to the prevailing driving force (ΔP) and constituent components of a ventilator. Based on the results from comparisons between predictions and experimental data the proposed equations can be said to generally give what may be termed a physically realistic solution. Lack of simple equations such as those derived here (previously unavailable) has denied designers and ventilator manufacturers tools with which they can quickly assess the impact of various components on the airflow performance of ventilators. There is no doubt as to the potential benefits of the equations proposed here. Therefore, equations such as those proposed here can aid ventilator manufacturers for instance, in predicting the characteristics of different models prior to manufacture. Further, from a manufacturer's point of view these equations can significantly reduce the amount of component testing required. The general solution equations proposed essentially encompassed the range of parameters attained in the experiments. Comparison between numerical results predicted from the equations and experimental data for all cases considered was

generally reasonable and acceptable. In addition, the accordance between trends predicted from the equations and those derived from measured data was quite satisfactory for all cases considered. Whilst on one hand the validity of the general equations presented in this work needs to be checked and possibly improved by more experiments, on the other hand, by means of the relationships presented in this chapter quantitative predictions maybe made of flow modifications to be expected as a result of variations in parameters of components constituting a ventilator.

Equations such as those proposed in this investigation can be used to establish a combination of values for various elements included in the equations that would result in an optimised solution and hence the most efficient airflow performance of a given ventilator. This would possibly require the use of a dedicated "search and optimisation" tool. A key criterion for the optimisation would for instance be the production of airflow through the ventilator with components configured to present the least resistance.

8.4 Design Methodology of Ventilators for Natural Ventilation

Design of buildings with increased air tightness for the sake of energy conservation is re-focussing scientific and public concerns on probable health risk with a consequent requirement of efficient ventilation systems. However, at present there is a lack of guidelines to provide manufacturers with background information to enable them to be in a position to develop ventilators with improved aerodynamic performance. Traditionally the process of selecting ventilator variables has been carried out by trial and error, relying on the intuition and experience of the designer. It is not at all likely that repeated trials in an interactive design and analysis procedure can lead to a truly optimum design. As such there is a need for guidelines for the design and manufacture of ventilators that are optimised for airflow performance.

Establishing guidelines is a tough process involving thorough review and careful consideration of all relevant information available. It is fairly obvious that, unfortunately in relation to ventilators for natural ventilation, such information is currently unavailable. Further, comprehensive guidelines can only be established by taking an integrated approach in which all design parameters and their interaction with building and system components are considered concurrently.

It is obvious that ventilators for natural ventilation applications cover a wide range of dimensions, configurations, types and include individual components which also vary significantly. Hence, it is impossible to prescribe tight guidance which would apply to all types/varieties of ventilators. However, based on the findings of this investigation, although based up on a limited number/types of ventilator components a design methodology was deduced and is presented here to guide designers and ventilator manufacturers. The following are the key aspects:-

- It is desirable to distinguish between ventilators to be used as air inlets and those to be used as air outlets. Consequently airflow performance needs to be assessed and indicated for the particular intended application. Alternatively, manufacturers should seek to develop ventilators that are aerodynamically symmetrical for the two flow directions.

- For a given ventilator configuration (combination of louver blades and mesh-screens) the ventilator performs better in outlet configuration than in the corresponding inlet configuration.

- Where mesh-screens are incorporated into ventilators the orientation of mesh-screen holes in non-square mesh types needs to be assessed and the configuration resulting in the most efficient airflow performance established and adopted for a given type of ventilator.

- Locations of mesh-screens relative to louver blades need to be assessed and the most efficient separation/gap for passage of air through a given ventilator established taking into account the overall pressure range to which the ventilator would be subjected and also the louver blade inclination angles.

- For a given separation/gap between louver blades and mesh-screen the overall improvement in airflow performance is higher for horizontal louver blades compared to inclined louver blades.

- Louver/mesh-screen combinations do not necessarily follow linear arithmetic rules. For instance doubling the mesh-screen free area does not result in double the initial airflow rate at a given pressure differential.

- Even for simple airflow openings such as rectangular slots combined with mesh-screens the airflow performance do not always follow linear trends. Hence, where such components are incorporated in ventilators appropriate ranges of aspect ratios need to be established for which airflow characteristics deviate from or follow the linear trends.

- Where a characteristic equation is used to represent the airflow properties of a ventilator, the pressure range from which it was generated needs to be indicated.

- Appropriate CFD boundary conditions need to be established from tests on typical components rather than based on data from standard text books equations which rarely distinguish parameters such as the orientation of holes in non-square mesh-screens.

- For CFD modelling and simulation of airflow through ventilators the ability of the selected software to adequately represent the geometric details such as rain-hooks, mesh-screens, louver blade shapes etc. which can be important to obtain accurate pressure-flow parameters needs to be assessed and understood.

- For given ranges of ventilators with associated constituent components appropriate generic equations of the form $Q = f\{\Delta P, f_a, \theta, L \text{ etc.}\}$ can be quickly established from a relatively limited number of tests. Such equations can then be used to select suitable dimensions/parameters of variables that would result in ventilators configured to provide optimised airflow performance characteristics.

8.5 Recommendations for Future Work

As a direct follow on to this research the following are some aspects that could be investigated further in the quest of furthering the application of sustainable natural ventilation to building design:-

- Develop and test ventilator prototypes based on findings from the theoretical/analytical models described in this thesis

- Develop Artificial Intelligence logic for ventilators to automatically vary the configuration of a ventilator (e.g. vary mesh-screen/louver separation in relation to pressure range) with the aim of maintaining an optimum airflow performance

- Derive equations for an "Intelligent" ventilator incorporating adaptive factors necessary to account for variations in pressure differentials and airflow rates resulting from different ranges of operation. This would ensure that the intelligent ventilator maintains a consistent airflow pattern over the whole range of parameters encountered when incorporated in ventilation models

- Extend the proposed equations to assess the impact on various ventilator components on airflow performance by taking into account the random instantaneous variations of pressure differentials/airflow rates

- Conduct investigations that directly link the airflow performance characteristics of ventilators to indoor comfort, air quality and energy usage in buildings

- Extend the findings of this investigation to hybrid ventilation systems in the quest to develop dedicated ventilators that could be used over the whole range of parameters encountered in these two mode systems

- Carry out more experimental/parametric investigations on a wider variety of ventilator components to extend the range of application of the equations developed in this investigation

- Develop more accurate/reliable methods of fully prescribing the geometric and resulting airflow properties of ventilator components such as mesh-screens

8.6 Concluding Remarks

This investigation provides an indication of the magnitudes of the impact of various components on the airflow performance of ventilators. The extension of the results to real buildings depends on further analysis and experiments to incorporate more precisely the effects of shape, size, number and spacing of openings, interactions within a building due to the inter-connecting airflow paths and other relevant variables. Parametric studies coupled with experiments on other types of ventilators are now necessary to check the validity of the solutions proposed here and to show the effect of the different parameters involved in the model. Clearly the physical processes involved in this type of airflow analysis are much more complex and only a limited assessment has been presented in this investigation (see recommendations for further research).

However, this investigation has developed and established a comprehensive CFD methodology to obtain detailed information for airflow performance analysis of ventilators for natural ventilation applications. The approach proposed in this thesis has shown to provide credible results that could be used by designers and ventilator manufacturers as a suitable means of predicting the airflow properties of ventilators to achieve an optimised airflow based design. Thus it offers a level of influence during the crucial stages of the natural ventilation design process where significant components of the indoor environmental performance are determined.

The importance of this work is represented by the high confidence in the results obtained. For this reason the huge amount of data obtained in this investigation could clearly be used to validate CFD models in order to analyse the airflow performance of ventilators for natural ventilation applications. The overall direct benefit of this research can be summed up as offering an efficient method for ventilator design and analysis with regard to achieving an optimised airflow performance taking into account the low driving forces available for natural ventilation.

BIBLIOGRAPHY

Allard F. *Natural ventilation in buildings - A design handbook.* James & James, London, 1998.

Alamdari F., Edwards S.C., Hammond G.P. *Microclimate performance of an open atrium office building: a case study in thermo-fluid modelling.* Proc. IMechE Seminar, pp 81 - 92, Inst. Mechanical Engineers, London, 1991.

Alamdari F. and Seymour M. *CFD and the built environment - applications.* Proc. IMechE Seminar, pp 133 - 137, Mechanical Engineers, London, 1993.

Alexander G. *The most energy efficient building ever.* Building, October 20, pp 24 -25, 2000.

Alloca C., Chen Q. and Glicksman L.R. *Design analysis of single-sided natural ventilation, Energy and Buildings.* Vol. 35, pp 785 - 795, 2003.

Annand W.J.D. *The resistance to air flow of wire gauzes.* Journal of the Royal Aeronautical Society, Vol. 57, pp 141 - 146, 1953.

Ajiboye P.J. *An Air inlet device suitable for noisy and polluted urban environments.* NATVENT Report. EC Contract: JOR3-CT95-002(DG XII), 1998.

ASHRAE *Fundamentals Handbook* ISBN 1883413885. American Society of Heating, Refrigeration & Air conditioning, 2001.

ASTM E783, *Testing method for field measurements of air leakage through installed exterior windows and doors.* Philadelphia: American Society for Testing and Materials, 1993.

Ata P.K. *Investigation into the thermal comfort and indoor air quality of rooms in low energy homes using a combined heating and ventilation system.* PhD thesis, Dept of Mechanical Engineering, University College London, February 1997.

Awbi H.B. *Design considerations for naturally ventilated buildings.* Renewable Energy, Vol. 5 Part II, pp 1081 - 1090, 1994.

Awbi H.B. *Chapter 7 - Ventilation.* Renewable and Sustainable Energy Reviews Vol. 2, pp 157 - 188, 1998.

Ayad S.S. *Computational Study of natural ventilation.* Journal of Wind Engineering & Industrial Aerodynamics, Vol. 82, pp 49 - 68, 1999.

Aynsley R.M. *A resistance approach to estimating airflow through buildings with large openings due to wind.* ASHRAE Transactions 94, second edition , pp 1661 - 1669, 1988.

Aynsley R.M. *A resistance approach to analysis of natural ventilation airflow networks.* J Wind Ind. Aerodyn. Vol. 67 and 68, pp 711 - 719, 1997.

Baines W.D. and Peterson E.G. *An investigation of flow through screens.* Transactions of the ASME, Vol. 73, pp 467 - 480, 1951.

Baker P.H., Heap R.D. and Sharples S. *Airflow through perforated screens at small pressure differences.* Building Services Engineering Research and Technology, Vol. 7 (2) , pp 96 - 97, 1986A.

Baker P.H., Sharples S. and Ward I.C. *Airflow through asymmetric building cracks.* Building Services Engineering Research and Technology, Vol. 7 (3), pp 107 - 108, 1986B.

Baker P.H., Sharples S. and Ward I.C., *Airflow through cracks.* Building and Environment, Vol. 22 (4), pp 293 - 304, 1987.

Bedford T. and Warner G.C. *Observations on natural ventilation.* Journal of the Royal Institute of British Architects, Vol. 51 (7), 1943.

Bevan R. *Birth of the Cool.* Building Design, May 1997.

BS 1134 - 1: *Assessment of surface texture: Methods and instrumentation.* 1988.

BS 5925: *Code of practice for ventilation principles and designing for natural ventilation.* 1991.

BS EN 13141-1, *Ventilation for buildings - Performance testing of components/products for residential ventilation - (Externally and internally mounted air transfer devices)*, 2004.

CADserver *Online resource for the CAD community - MCAD feature*, http://www.cadserver.co.uk, accessed November 2004.

Chilengwe N. *Investigation of air movement in rooms using computational fluid dynamics.* MSc dissertation, Dept. of Mechanical Engineering, University College London, 1994.

Chilengwe N. and Sharples S. *Parametric analysis of air flow through ventilators.* International Journal of Ventilation, Vol. 1 (2), pp 109 - 117, 2002.

Chilengwe N. and Sharples S. *Low and high pressure experimental analysis of ventilators for natural ventilation in buildings.* International Journal of Ventilation, Vol. 2, September 2003A.

Chilengwe N. and Sharples S. *CFD and experimental analysis of ventilators to improve airflow performance for natural ventilation.* Proc. First Scottish Conference for Postgraduate Researchers in the Built & Natural Environment (PRoBE), Glasgow, Scotland, 18 - 19 November, 2003B.

Chilengwe N. and Sharples S. *Airflow performance characteristics of ventilators in hybrid ventilation systems*. Proc. 25th AIVC Conference, Paper 2004050, Prague, Czech Republic, 15 - 17 September, 2004.

CIBSE: AM10, *Natural ventilation in non-domestic buildings*. The Chartered Institution of Building Services Engineers, London UK, 1997.

CIBSE: AM13, *Mixed Mode Buildings*. The Chartered Institution of Building Services Engineers, London UK, 2000.

CIBSE: TM23, *Testing Buildings for Air Leakage*. The Chartered Institution of Building Services Engineers, London UK, 2000.

CIBSE: *Guide C, Reference Data*. The Chartered Institution of Building Services Engineers, London UK, 2001.

Cockroft J.P. and Robertson P. *Ventilation of an enclosure through a single opening*, Building & Environment. Vol. 11, pp 29 - 29, 1976.

Cornell W.G. *Losses in flow normal to plane screens*. Transactions of the ASME, Vol. 80, pp 791 - 799, 1958.

Cousin S. *Some aspects relating to the design of natural ventilation systems for buildings.* The South African Mechanical Engineer, pp 253 - 256, April 1969.

Dagnall H. *Exploring surface texture*. Taylor Hobson Ltd, 1997.

Dascalaki E., Santamouris M. and Asimakopoulos D.N. *On the use of deterministic and intelligent techniques to predict the air velocity distribution on external openings in single-sided natural ventilation configurations*. Solar Energy, Vol. 66, pp 223 - 43, 1999.

Douglas J.F., Gasiorek J.M. and Swaffield J.A. *Fluid Mechanics*. 2nd edition, Pitman, 1985.

DEFRA *Sustainable Buildings Initiative*, http://www.defra.gov.uk/environment/energy, accessed December 2003.

De Gidds W.F. *An overview of the availability, performance and application of inlets for natural supply of ventilation air and the consequences on indoor air quality and comfort.* NATVENT WorkPackage 3, Activity 2 Project Report, May 1997A.

De Gidds W.F. *Controlled Airflow Inlets*. Proc. 18th AIVC Conf. Athens, Greece, 23 - 26 September 1997B.

De Salis M.H.F. Oldham D.J. and Sharples S. *Noise control strategies for naturally ventilated buildings*. Building and Environment, Vol. 37, pp 471 - 484, 2002.

Dick J.B. *Experimental studies in natural ventilation of houses*. J. Inst. Heating and Ventilation Engineers, Vol. 17, pp 419 - 466, 1949.

Dick J B, *The Fundamentals of natural ventilation of houses*. J. Inst. Heating and Ventilation Engineers, Vol. 18, pp 123 - 134, 1950.

Eckert B. and Pfluger F. *The resistance coefficient of commercial round wire grids*. N.A.C.A. Technical Memo No. 1003 A.R.C. 7466, January 1942.

Eley Associates, *Hawaii Commercial Building Guidelines for Energy Efficiency - Natural ventilation*. 2003.

Etheridge D.W. *Air leakage characteristics of houses - a new approach*. Building Services Engineering Research and Technology, Vol. 5 (1), pp 32 - 36, 1984.

Etheridge D.W. *Crack flow equations and scale effect*. Building and Environment, Vol. 12, pp 181 - 189, 1977.

Etheridge D.W. *A note on crack flow equations for ventilation modelling*. Building and Environment, Vol. 33 (5), pp 325 -28, 1998.

Etheridge D.W. *Non-dimensional methods for natural ventilation design*. Building and Environment, Vol. 37, pp1057 - 1072, 2002.

Etheridge D.W. and Sandberg M. *A simple parametric study of ventilation*. Building and Environment, Vol. 19 (3), pp 163 - 173, 1984.

Etheridge D.W. and Sandberg M. *Building Ventilation*, John Wiley and Sons. 1996.

Etheridge D.W. and Stanway R.J. *A parametric study of ventilation as a basis for design,* Building and Environment, Vol. 23 (2), pp 81 - 93, 1988.

Evans B.H. *Energy conservation with natural air flow through windows*. ASHRAE Transactions 5 (2nd edition), pp 641 - 650, 1979.

Fanger P.O., Melikov A.K., Hanzawa H. and Ring J. *Air turbulence and sensation of draught*. Energy and Buildings. Vol. 12, pp 21 - 39, 1988.

Flourentzou F. Van der Maas J. and Roulet C A, *Natural ventilation for passive cooling: Measurement of discharge coefficients*. Energy and Buildings, Vol. 27, pp 283 - 292, 1998.

FLOMERICS website, *www.flomerics.com,* accessed October 2002.

FLOVENT online documentation, *www.flovent.co.uk,* accessed November 2002.

FLOVENT *Introduction to FLOVENT version 3.2,* Document No. FLOVENT/LC/11/01/V32Isuue1.2, 2001.

FLOVENT Manual, 1999.

Fracastoro G.V., Mutani G. and Perino M. *Numerical simulation of transient effects of window openings*. Proc. RoomVent2000 Conf. Reading (UK), July 2000.

Gosman A.D. *Developments in CFD for industrial and environmental applications in wind engineering.* Journal of Wind Engineering & Industrial aerodynamics, Vol. 81, pp 21 - 39, 1999.

Gonzalez M.A. *On the Aerodynamics of Natural Ventilators.* Building & Environment, Vol. 19 (3), pp 179 - 189, 1984.

Gratia E., Bruyere I., and De Herde A. *How to use natural ventilation to cool narrow office buildings.* Building and Environment, Vol. 39, pp 1157 - 1170, 2004.

Gratia E. and De Herde A. *Design of low energy office buildings.* Energy and Buildings, Vol. 35, No. 5, pp 473 - 491, 2003.

Grosso M., Marino D. and Parisi E. *Wind pressure distribution calculation program for multi-zone airflow models.* Proc. Building Simulation Conference, Madison, 1995.

Haghighat F. and Rao J. *Computer aided building ventilation - a system-theoretic approach.* Energy and Buildings, Vol. 17, pp 147 - 155, 1991.

Haines R.W. and Wilson C.L. *HVAC Systems Design Handbook.* McGraw-Hill Inc. 1994.

Heisbelberg P., Svidt K. and Nielsen P.V. *Windows - measurement of airflow capacity.* Proc. RoomVent2000 Conf. Reading (UK), July 2000.

Heisbelberg P., Svidt K. and Nielsen P.V. *Characteristics of airflow from open windows.* Building and Environment, Vol. 36, pp 859 - 869, 2001.

Heiselberg P., Bjorn E. and Nielsen P.V. *Impact of open windows on room air flow and thermal comfort.* International Journal of Ventilation, Vol. 1 (2), pp 91 - 100, 2002.

Hitchin E.R. and Wilson C.B. *A review of experimental techniques for the investigation of natural ventilation in buildings.* Building Science, Great Britain, Vol. 2, pp 59 - 82, 1967.

Holmes M.J. and Whittle G.E. *How accurate are predictions of complex air movement models?* Building Services Research and Technology, Vol. 8, pp 29 - 31, 1987.

Hopkins L.P. and Hansford B. *Airflow through cracks.* Building Services Engineer, Vol. 42, September 1974.

Howarth A.T. *The prediction of air temperature variations in naturally ventilated rooms with convective heating.* Building Services Research and Technology, Vol. 6 (4), pp 169 - 175, 1985.

Hunt and Linden *The fluid mechanics of natural ventilation - displacement ventilation by buoyancy-driven flows assisted by wind.* Building and Environment, Vol. 34, pp 707 - 720, 1999.

Huo Y., Hahighat F., Zhang J.S. and Shaw C.Y. *A systematic approach to describe the air terminal device in CFD simulation for room air distribution analysis.* Building and Environment, Vol. 35, pp 563 - 576, 2000.

Idelchik I.E. and Fried E. *Flow Resistance: A design guide for engineers.* ISBN: 0-89116-435-9 Hemisphere Publishing Corporation 1989.

Iannone F. *Natural Ventilation and sustainability: designing with Computational Fluid Dynamics.* Proc. of Sharing Knowledge on Sustainable Building Conference, Bari, Italy Dec 16 - 17, 1999.

Jiang Y. and Chen Q. *Study of natural ventilation in buildings by large eddy simulation.* Journal of Wind Engineering & Industrial Aerodynamics, Vol. 89, pp 1155 - 1178, 2001.

Jones P.J. and Whittle G.E. *CFD for building airflow prediction - current status and capabilities.* Building & Environment, Vol. 27 (3), pp 321 - 338, 1992.

Joro S. *Noise ingress through vents.* Building Services, November 1991.

Kang J. and Broclesby M.W. *Application of micro-perforated absobers in developing window systems for optimum acoustic, ventilation and daylightng performance.* Proc. Inst. of Acoustics, Vol. 25, Pt. 7, pp 47 - 54, 2003.

Karava P., Stathopoulos T. and Athienitis A.K. *Investigation of the performance of trickle ventilators.* Building and Environment, Vol. 38, pp 981 - 993, 2003.

Kato S., Murakami S., Shoya S., Hanyu F. and Zeng J. *CFD analysis of flow and temperature fields in atrium with ceiling height of 130m.* ASHRAE Transactions: symposia, SD-95-14-5, 1995.

Kolokotroni M., White M.K. and Perera M.D.A.E.S. *Trickle Ventilators: Field Measurements in Refurbished Offices.* Building Services Engineering Research and Technology, Vol. 18 (4), pp 193 - 199, 1997.

Kordyban T. *Fan Swirl and Planar Resistances don't mix.* 9th International FLOTHERM Users conference, May 2000.

Kreider J.F. and Rabi A. *Heating and Cooling of Buildings - Design for Efficiency.* McGraw-Hill International Editions, 1994.

Kronvall J. *Airflow in building components.* Report TVBH - 1002, LUND Sweden, 1980.

Lee H. and Awbi H.B. *Effect of internal partitioning on indoor air quality of rooms with mixing ventilation - A basic study.* Building and Environment, Vol. 39, pp 127 - 141, 2004.

Liddament M.W. *A Guide to Energy Efficient Ventilation.* AIVC, Coventry, UK, 1996.

Liddament M.W. *A Review of Building Airflow Simulation.* AIVC TN33, 1991.

Liddament M.W. *Power law rules - ok?* Air Infiltration Review, Vol. 8:2, pp 4 - 6, 1987.

London HMSO: Approved Document F, *Ventilation - Means of Ventilation.* The Building Regulations, 1995.

Lu W., Howarth A.T., Adam N. and Riffat S.B. *Modelling and Measurement of Airflow and Aerosol Particle Distribution in a Ventilated Two-Zone Chamber.* Building and Environment, Vol. 31 (5), pp 417 - 423, 1996.

Lu W. and Howarth A.T. *Numerical Analysis of Indoor Aerosol Particle Deposition and Distribution in Two-Zone Ventilation System.* Building and Environment, Vol. 31 (1), pp 41 - 50, 1996.

Lu W., Howarth A.T. and Jeary A.P. *Prediction of Airflow and Temperature Field in a Room with Convective Heat Source,* Building and Environment. Vol. 32 (6), pp 541 - 550, 1997.

Maghrabi A.A. and Sharples S. *Airflow characteristics through modulated louvred windows.* Proc. 16th International Conf. on Passive & Low Energy Architecture, pp 507 - 514, Brisbane, 22 - 24 September, 1999.

Maghrabi A.A. *Airflow characteristics of modulated louvered windows with reference to the Rowshan of Jeddah, Saudi Arabia.* PhD thesis, School of Architecture, University of Sheffield, 2000.

Martin A. and Fitzsimmons J. *Making natural ventilation work.* BSRIA Guidance Note GN 7/2000, 2000.

Massey B.S. *Mechanics of Fluids.* 7th ed. Stanley Thornes, 1998.

Mathew E.H. and Rousseau P.G. *A new integrated design tool for naturally ventilated buildings Part 1: Ventilation Model.* Building and Environment, Vol. 29 (4), pp 461 - 471, 1994.

McGrath P.T. and Howarth A.T. *Measurements of airflows through cracks between building components.* Building Services Engineering Research and Technology, Vol. 5 (2), pp 43 - 48, 1984.

Miguel A.F. *Airflow through porous screens: from theory to practical considerations.* Energy and Buildings, Vol. 28, pp 63 - 69, 1998.

Miguel A.F. and Silva A.M. *Effect of aperture characteristics on the mean and turbulent heat and mass flows within enclosures.* Proc. RoomVent2000 Conf. Reading (UK), July 2000.

Miguel A.F., Van de Braak N.J. and Bot G.P.A. *Analysis of the airflow characteristics of greenhouse screening materials.* Journal of Agricultural Engineering Research, Vol. 67, pp 105 - 112, 1997.

Miguel A.F., Van de Braak N.J, Silva A.M. and Bot G.P.A. *Physical modelling of natural ventilation through screens and windows in greenhouses.* Journal of Agricultural Engineering Research, Vol. 70, pp 165 - 176, 1998.

Miguel A.F., Van de Braak N.J., Silva A.M. and Bot G.P.A. *Wind-induced airflow through permeable materials Part I: the motion equation.* J. Wind Eng. Ind. Aerodyn. Vol. 89, pp 45 - 57, 2001.

Miguel A.F., Van de Braak N.J., Silva A.M. and Bot G.P.A. *Wind-induced airflow through permeable aterials Part II: air infiltration in enclosures.* J. Wind Eng. Ind. Aerodyn. 89, pp 59 - 72, 2001.

Morgan P.G. *Fluid flow through screens of low solidity.* Journal of the Royal Aeronautical Society, Vol. 66, pp 54 - 56, 1962.

NATVENT, *Natural ventilation for offices.* Guide published as part of DETR Best Practice Programme, 1999.

NATVENT, *Over-coming technical barriers to low energy natural ventilation in office type buildings in moderate and cold climates.* 1998.

Nielsen P.V., Dam H., Lars C.S, Svidt K. and Heisbelberg P. *Characteristics of buoyant flow from open windows in naturally ventilated rooms.* Proc. RoomVent2000, Conf. Reading (UK), July 2000.

Oliveira F. and Bittencourt L. *Air flow through louvered windows in small rooms,* Proc. PLEA '98, Lisbon, Portugal, pp 393 - 396, June 1998.

O' Rourke P.J., Haworth D.C. and Ranganathan R. *Computational Fluid Dynamics.* ASM Handbook Volume 20, December 1997.

Palmer J. *First contact.* CIBSE Building Services Journal, pp 31 - 34, October 1999.

Papadakis G., Mermier M., Meneses J.F. and Boulard T. *Measurement and analysis of air exchange rates in a greenhouse with continuous roof and side openings.* Journal of Agricultural Engineering Research, Vol. 63, pp 219 - 228, 1996.

Parrot L. *An environmental perspective on UK Construction materials.* CIB World Building Conference Proc., Sweden, 1998.

Patankar S.V. *Numerical Heat Transfer and Fluid Flow.* Hemisphere Publishing Corporation. 1980.

Peppes A.A., Santamouris M. and Asimakopoulos D.N. *Airflow through horizontal openings.* Proc. 18th AICV Conference, pp 513 - 521, September 1997.

Peterson F. *On flow in narrow slots applied to infiltration.* Proc. 3rd AIC Conf. London (UK), Sept 20 -23, 1982.

Perera M.D.A.E.S., Marshall S.G. and Solomon E.W. *Controlled background ventilation for large commercial buildings.* Building Services Engineering Research and Technology, Vol. 14 (3), pp 81 - 86, 1993.

Pitts A.C. and Georgiadis S. *Ventilation airflow through window openings in combination with shading devices.* Proc. 15th AIVC Conference, pp 432 - 439, Buxton, September 1994.

Plunkett JW. *An airspeed measurement technique for accurate correlation to CFD simulation results.* International Conference on high density interconnect and systems packaging, 2000.

Pollock G. and Stribling D. *A real application of arflow modelling in optimising cleanroom design.* FLOVENT Registered User Online documentation, http://www.flovent.co.uk, 1989.

Raja I.A., Nicol J.F., McCartney K.J. and Humphreys M.A. *Thermal Comfort: use of controls in naturally ventilated buildings.* Energy and Buildings, Vol. 33, pp 235 - 244, 2001.

Reardon J.T., Shaw C.Y. and Chown G.A. *Ventilation strategies for small buildings.* Building Science Insight, Canada, 1990.

Richards P.J and Robinson M. *Wind loads on porous structures.* J Wind Eng Ind. Aerodyn. Vol. 83, pp 455 - 465, 1999.

Roache P.J. *Fundamentals of Computational Fluid Dynamics.* Hermosa Publishers, Albuquerque, 1998.

Rosenberg H. *Reducing energy usage in green buildings.* Proc. WRI Bell Conference, USA, July 2002.

Ross D.I., Stephen R.K. and Pierce J.B.M. *Background ventilators for dwellings.* BRE Information Paper IP2/03, 2003.

Sahin B., Ward-Smith A.J. and Lane D. *The pressure drop and flow characteristics of wide-angle screen diffusers of large area ratio.* J. Wind Eng. Ind. Aerodyn. Vol. 58, pp 33 - 50, 1995.

Satwiko P., Locke N. and Donn M. *Reproducing the real pressure coefficient using a computational fluid dynamics program - How close is close enough?* ANZAScA Annual Conf. June 1998.

Schubauer G.B. Spangenberg W.G. and Klebanoff P.S. *Aerodynamic characteristics of damping screens.* NACA, Technical Note 2001, January 1950.

Sekhar S.C. and Willem H.C. *Impact of airflow profile on indoor air quality - a tropical study.* Building and Environment, Vol. 39, pp 255 - 266, 2004.

Sharples S. *Eaves and roof ridge pressure coefficients on an isolated low-rise dwelling. Wind tunnel study*. Building Services Engineering, Research and Technology, Vol. 18, No. 1, pp 47 - 58,1997.

Sharples S. and Chilengwe N. *Directional airflow performance of ventilators for natural ventilation*. Proc. 24th AIVC Conf. Washington DC, USA, 12 - 14 October, 2003.

Sharples S. and Chilengwe N. *Parametric analysis of the airflow performance of ventilators*. Proc. 22nd AIVC Conference, Paper 33, Bath, UK, 11 - 13 September, 2001.

Sharples S. and Chilengwe N. *Optimising the design of ventilators for natural ventilation*. Proc. 9th Int. Conf. on Indoor Air Quality and Climate, Monterey, California, USA, June 30, 2002.

Sharples S. and Goodacre C. *Air leakiness of non-standard housing: Impact of upgrading measures*. Proc. 25th AIVC Conference, pp 37 - 42, Prague, Czech Republic, September 2004.

Sharples S. and Maghrabi A.A. *Airflow through Louvers: an experimental and CFD study*. Proc. 21st AIVC Conf. Paper 16, The Hague, Netherlands, 26 - 29 September, 2000.

Shaw C.T. *Using Computational Fluid Dynamics*. 1st Edition, Prentice Hall, 1992.

Shaw W.N. *Air currents and laws of ventilation*. Cambridge University Press, 1907.

Sherman M.H. *A power law formulation of laminar flow in short pipes*. J. Fluids Eng. Vol. 114, LBL Report 29414, Lawrence Berkeley Laboratory, University of California, CA, pp 601 - 605, 1992.

Simmons L.F.G. and Cowdrey C.F. *Measurements of the Aerodynamic forces acting on porous screens*. Reports & Memoranda No. 2276, August 1945.

Southall R.G. and McEvoy M. *Results from a validated CFD simulation of a supply air ventilated window*. Proc. RoomVent Conf. Reading, July 2000.

SPG Media website, *http://www.port-technology.com/projects*, London, UK, accessed May, 2004.

Straw M.P., Baker C.J. and Robertson A.P. *Experimental measurements and computations of wind-induced ventilation of a cubic structure*. J. wind Engineering and Industrial Aerodynamics, Vol. 88, pp 213 - 230, 2000.

Taylor G.I. and Batchelor G.K. *The effect of wire gauze on small disturbances in a uniform stream*. Quart. Journ. Mech and Applied Math. Vol. 2, pp 1 - 29, 1949.

Taylor G.I. and Davies R.M. *The Aerodynamics of porous sheets*. Reports & Memoranda No. 2237, April 1944.

Tipping J.C. and Tickner J. *New developments in ventilator design*. Building Services, Vol. 42, pp 99 - 105, August 1974.

Tutt R.D. *Principles of Air Distribution*, Tuttle and bailey Inc. New Britain, Connecticut, 1955.

Van dyke M. *Album of fluid motion*. ISBN: 0915760037, Parabolic Press, 1982.

Vincent D., Annesi I., Festy B. and Lamrozo J. *Ventilation system, indoor air quality and health outcomes in Parisian modern office workers*. Environmental Research, Vol. 75, pp 100 - 112, 1997.

WBDG website Sustainable Committee, *Minimize Energy Consumption*. http://www.wbdg.org/design, accessed December 2004.

Walker I.S., Wilson D.J. and Sherman M.H. *A comparison of the power law to quadratic formulations for air infiltration calculations*. Energy and Buildings, Vol. 27, pp 293 - 299, 1998.

Webb B. and Kolokotroni M. *Night cooling a 1950's office*. Architects Journal, 13 June, pp 54 - 55, 1996A.

Webb B. and Kolokotroni M. *In the cool of the night*. Building Services Journal, Vol. 18 (12), pp 39 - 40, December 1996B.

Webb B., Kolokotroni M., White M. and Hesketh M. *Testing a prototype night ventilator*. Building Services Journal, Vol. 2, pp 47 - 48, February 1998.

White M.K., Kolokotroni M. and Perera M.D.A.E.S. *Trickle Ventilators in Offices*. BRE Information Paper, IP 12/98, BRE, August 1998.

White M.K., Mc Cann., Stephen R. and Chandler M. *Ventilators: Ventilation and acoustic effectiveness*. BRE Information Paper, IP 4/99, BRE, November 1999.

Yakubu G.S. and Sharples S. *Airflow through modulated louvre systems*. Building Services Engineering Research and Technology, Vol. 12 (4), pp 151 - 155, 1991.

Vincent D., Annesi I., Festy B. and Lambozo J. *Ventilation system, indoor air quality and health outcomes in Parisian modern office workers*. Environmental Research, Vol. 75, pp 100 - 112, 1997.

Veersteeg H.K. and Malalasekera W. *An introduction to computational fluid dynamics - The finite Vol.ume method*. McGraw Hill, 1995.

Appendix A:

Experimentally Measured, CFD Predicted and Derived Parameters

Table A.1: Experimental and derived data for aluminium louvers (pressurisation)

Louver Type	Insect-screen ΔP	Insect-screen Q	Bird guard ΔP	Bird guard Q	No Mesh ΔP	No Mesh Q	Derived Insect-screen	Derived Bird guard	Derived No Mesh	Regression coefficient	Regression type
X	0.034	0.0049	0.027	0.0124	0.058	0.0210	0.075	0.0772	0.0911	α	Power Law
X	0.058	0.0123	0.079	0.0196	0.131	0.0298					Power Law
X	0.123	0.0203	0.210	0.0300	0.270	0.0416	0.7042	0.5411	0.5469	β	Power Law
X	0.237	0.0302	0.372	0.0406	0.506	0.0562					Power Law
X	0.385	0.0408	0.583	0.0526	0.717	0.0716	98.04	98.63	98.75	R	Power Law
X	0.667	0.0545	0.938	0.0695	0.986	0.0868	62.908	67.986	58.884	a	Quadratic
X	0.991	0.0694	1.296	0.0873	1.173	0.1001					Quadratic
X	1.271	0.0832	1.562	0.1020	1.284	0.1088	8.895	7.7515	5.3596	b	Quadratic
X	1.610	0.1007	1.851	0.1180	1.436	0.1167					Quadratic
X	1.953	0.1198	2.030	0.1284	1.556	0.1270	99.15	98.95	98.86	R	Quadratic
X	2.130	0.1295									
Y	0.025	0.0124	0.023	0.0119	0.011	0.0130	0.076	0.0831	0.0957	α	Power Law
Y	0.089	0.0205	0.066	0.0205	0.064	0.0227					Power Law
Y	0.188	0.0307	0.140	0.0298	0.133	0.0320	0.5177	0.5288	0.5555	β	Power Law
Y	0.356	0.0418	0.313	0.0413	0.295	0.0436					Power Law
Y	0.574	0.0535	0.530	0.0530	0.489	0.0579	99.16	99.04	98.19	R	Power Law
Y	0.879	0.0686	0.744	0.0648	0.687	0.0724	64.912	66.037	47.923	a	Quadratic
Y	1.102	0.0806	1.035	0.0809	0.915	0.0889					Quadratic
Y	1.344	0.0940	1.269	0.0937	1.089	0.1023	7.4539	6.4188	5.2968	b	Quadratic
Y	1.662	0.1081	1.485	0.1079	1.286	0.1183					Quadratic
Y	1.716	0.1172	1.621	0.1160	1.439	0.1300	98.61	98.73	98.69	R	Quadratic
Y	1.888	0.1268	1.785	0.1267							
Z	0.037	0.0127	0.017	0.0132	0.017	0.0126	0.0845	0.0874	0.1025	α	Power Law
Z	0.085	0.0217	0.068	0.0206	0.029	0.0212					Power Law
Z	0.184	0.0306	0.161	0.0311	0.081	0.0314	0.5832	0.5074	0.4903	β	Power Law
Z	0.327	0.0416	0.284	0.0424	0.183	0.0420					Power Law
Z	0.585	0.0561	0.513	0.0558	0.357	0.0562	99.18	97.98	98.47	R	Power Law
Z	0.882	0.0721	0.779	0.0721	0.589	0.0703	50.944	55.71	53.926	a	Quadratic
Z	1.171	0.0898	1.026	0.0866	0.815	0.0884					Quadratic
Z	1.351	0.1028	1.274	0.1028	1.000	0.1040	7.4031	5.9835	3.498	b	Quadratic
Z	1.595	0.1190	1.514	0.1200	1.160	0.1197					Quadratic
Z	1.741	0.1300	1.625	0.1295	1.294	0.1290	98.59	98.61	98.31	R	Quadratic

Slot Reference and details	Experimental data				Derived data		Regression coefficients	
	Without mesh-screen		With mesh-screen		Without mesh-screen	With mesh-screen		
	Q (m3/s)	ΔP (Pa)	Q (m3/s)	ΔP (Pa)				
Slot A1: height = 6mm, depth = 12mm	0.00172	1.083	0.00143	3.403	0.0016	0.0006	α	Power Law
	0.00248	2.251	0.00169	4.395				
	0.00337	4.081	0.00250	8.095	0.5098	0.6474	β	
	0.00482	8.234	0.00290	10.141				
	0.00544	10.330	0.00379	15.392	99.99	100	R	
	0.00668	15.063			318987	6.88E+05	a	Quadratic
					142.67	1475	b	
					99.96	99.96	R	
Slot A1: height = 12mm, depth = 12mm	0.00185	0.296	0.00155	2.285	0.0032	0.0009	α	Power Law
	0.00222	0.451	0.00242	4.154				
	0.00264	0.662	0.00383	8.033	0.4751	0.7017	β	
	0.00290	0.801	0.00451	10.268				
	0.00326	1.019	0.00587	15.231	99.96	99.94	R	
	0.00447	2.058			107486	251408	a	Quadratic
	0.00639	4.232						
	0.00883	8.155			-28.776	1125.1	b	
	0.00993	10.264			99.99	99.98	R	
Slot A1: height = 18mm, depth = 12mm	0.00157	0.062	0.00163	1.623	0.0047	0.0012	α	Power Law
	0.00245	0.220	0.00206	2.211				
	0.00320	0.424	0.00326	4.108	0.4262	0.7058	β	
	0.00361	0.644	0.00526	8.168				
	0.00410	0.822	0.00608	10.175	99.47	99.93	R	
	0.00495	1.242	0.00809	15.836	61879	144900	a	Quadratic
	0.00654	2.323						
	0.00858	4.026			-55.15	787.61	b	
	0.01194	8.197						
	0.01332	10.220			99.99	100	R	

Table A.3: Measured and derived parameters for slots A4 to A6

Slot Reference and details	Experimental data				Derived data		Regression coefficients	
	Without mesh-screen		With mesh-screen		Without mesh-screen	With mesh-screen		
	Q (m3/s)	ΔP (Pa)	Q (m3/s)	ΔP (Pa)				
Slot A4: height = 24mm, depth = 12mm	0.00184	0.077	0.00174	1.407	0.0056	0.0014	α	Power Law
	0.00312	0.242	0.00231	2.082				
	0.00418	0.456	0.00391	4.092	0.456	0.7278	β	
	0.00498	0.665	0.00654	8.342				
	0.00555	0.862	0.00756	10.765	99.96	99.93	R	
	0.00661	1.321	0.01007	15.761	36068	8.33E+04	a	Quadratic
	0.00821	2.154						
	0.01119	4.100			-37.072	741.96	b	
	0.01553	8.274						
	0.01754	10.335			99.97	99.87	R	
Slot A5: height = 30mm, depth = 12mm	0.00187	0.049	0.00175	1.072	0.0074	0.0017	α	Power Law
	0.00359	0.222	0.00313	2.137				
	0.00497	0.432	0.00546	4.401	0.4652	0.7503	β	
	0.00597	0.680	0.00837	8.016				
	0.00686	0.802	0.01275	15.103	99.87	99.78	R	
	0.00750	1.107			20972	51976	a	Quadratic
	0.00993	2.084						
	0.01420	4.065			-8.6602	522.46	b	
	0.01957	8.067						
	0.02271	10.481			99.92	100	R	
Slot A6: height = 36mm, depth = 12mm	0.00192	0.042	0.00173	1.063	0.0086	0.0017	α	Power Law
	0.00417	0.246	0.00314	2.067				
	0.00577	0.455	0.00552	4.128	0.4813	0.7844	β	
	0.00713	0.674	0.00917	8.192				
	0.00813	0.856	0.01113	10.837	99.9	99.78	R	
	0.00986	1.269	0.01402	15.126	14429	38647	a	Quadratic
	0.01194	2.085						
	0.01776	4.687			-1.337	539.05	b	
	0.02357	8.115						
	0.02668	10.083			99.92	100	R	

Table A.4: Measured and derived parameters for slots B1 to B3

Slot Reference and details	Without mesh-screen Q (m3/s)	Without mesh-screen ΔP (Pa)	With mesh-screen Q (m3/s)	With mesh-screen ΔP (Pa)	Derived Without mesh-screen	Derived With mesh-screen	Regression coefficients	
Slot B1: height = 12mm, depth = 6mm	0.00174	0.287	0.00148	2.035	0.0031	0.0009	α	Power Law
	0.00219	0.462	0.00252	4.333				
	0.00262	0.660	0.00389	8.071	0.4546	0.6887	β	
	0.00283	0.844	0.00455	10.206				
	0.00322	1.101	0.00595	15.412	99.93	99.98	R	
	0.00440	2.181			136604	2.58E+05	a	Quadratic
	0.00614	4.532						
	0.00800	8.491			-87.498	1061.5	b	
	0.00920	10.482			99.74	99.99	R	
Slot B2: height = 12mm, depth = 12mm	0.00176	0.274	0.00152	2.293	0.0033	0.0009	α	Power Law
	0.00217	0.425	0.00242	4.223				
	0.00269	0.661	0.00378	8.002	0.5003	0.7078	β	
	0.00303	0.844	0.00444	10.132				
	0.00334	1.074	0.00578	15.164	99.97	99.9	R	
	0.00456	2.123			106418	260497	a	Quadratic
	0.00648	4.369						
	0.00903	8.385			-28.248	1122.7	b	
	0.00992	10.192			99.99	100	R	
Slot B3: height = 12mm, depth = 18mm	0.00179	0.301	0.00151	1.800	0.0032	0.001	α	Power Law
	0.00211	0.429	0.00211	3.034				
	0.00262	0.639	0.00258	4.460	0.4877	0.6394	β	
	0.00292	0.822	0.00389	8.106				
	0.00327	1.047	0.00453	10.222	99.92	99.86	R	
	0.00448	2.050	0.00601	15.460	97226	268265	a	Quadratic
	0.00614	4.072						
	0.00895	8.258			28.679	988.99	b	
	0.01047	10.742			99.85	99.77	R	

Table A.5: Measured and derived parameters for slots B4 to B6

Slot Reference and details	Experimental data				Derived data		Regression coefficients	
	Without mesh-screen		With mesh-screen		Without mesh-screen	With mesh-screen		
	Q (m3/s)	ΔP (Pa)	Q (m3/s)	ΔP (Pa)				
Slot B4: height = 12mm, depth = 24mm	0.00236	0.229	0.00146	2.041	0.0039	0.0009	α	Power Law
	0.00302	0.548	0.00246	4.318				
	0.00341	0.773	0.00396	8.392	0.4122	0.7045	β	
	0.00433	1.482	0.00453	10.051				
	0.00505	2.338	0.00590	15.039	98.42	99.98	R	
	0.00676	4.064			88445	2.38E+05	a	Quadratic
	0.00972	8.140						
	0.01118	10.627			-28.127	1149.4	b	
					99.8	99.97	R	
Slot B5: height = 12mm, depth = 30mm	0.00169	0.261	0.00151	1.773	0.0033	0.001	α	Power Law
	0.00210	0.408	0.00277	4.046				
	0.00255	0.609	0.00451	8.225	0.5096	0.6953	β	
	0.00298	0.853	0.00531	10.521				
	0.00323	1.001	0.00675	15.312	99.95	99.93	R	
	0.00483	2.210			82507	203047	a	Quadratic
	0.00669	4.023						
	0.00987	8.515			45.213	899.3	b	
	0.01104	10.515			99.99	100	R	
Slot B6: height = 12mm, depth = 36mm	0.00170	0.231	0.00151	1.792	0.0034	0.001	α	Power Law
	0.00216	0.442	0.00279	4.127				
	0.00255	0.607	0.00446	8.033	0.5159	0.7069	β	
	0.00305	0.828	0.00523	10.158				
	0.00334	1.001	0.00681	15.215	99.82	99.94	R	
	0.00479	2.020			73253	190051	a	Quadratic
	0.00717	4.259						
	0.01012	8.141			60.412	944.82	b	
	0.01168	10.651			99.98	99.99	R	

Louver Blade Inclination (deg)	Regression coefficients		Spacer thickness (mm) between mesh-screen and louver					
			0	3	6	9	12	15
0	α	Power Law	0.0701	0.0763	0.0757	0.0768	0.0771	0.076
	β		0.76	0.6131	0.6702	0.7438	0.7736	0.8028
	R		99.38	98.07	98.55	99.08	99.49	99.46
	a	Quadratic	14.441	32.763	13.415	7.2491	9.2662	-3.4696
	b		12.937	10.06	11.362	11.835	11.844	13.209
	R		99.59	98.72	99.26	99.47	99.49	97.27
30	α	Power Law	0.0506	0.0516	0.0543	0.0551	0.0547	0.0549
	β		0.99	0.9922	0.9616	0.955	0.9141	0.9104
	R		99.3	98.96	99.01	99.24	99.46	99.54
	a	Quadratic	10.307	12.879	19.233	17.383	19.051	22.43
	b		19.383	18.812	17.499	17.37	17.587	17.265
	R		99.79	99.72	99.71	99.7	99.62	99.65
60	α	Power Law	0.0314	0.0318	0.033	0.0316	0.0295	0.0325
	β		0.6436	0.6284	0.6541	0.6651	0.6947	0.6239
	R		99.71	99.64	99.69	99.72	99.8	99.54
	a	Quadratic	154.65	160.02	143.42	138.82	140.89	156.82
	b		40.267	39.952	36.304	38.714	41.257	39.019
	R		99	99.04	98.82	99.02	99.06	99.06

The following power law equations (pressurisation) were also used in the analysis:

Louver 1 with horizontal blades without a mesh-screen:

$$Q = 0.2954 \, \Delta P^{\,0.7268} \qquad (A.1)$$

$$R = 99.36\%$$

Louver 1 with louver blades inclined at 30° without a mesh-screen:

$$Q = 0.1387 \, \Delta P^{\,0.9301} \qquad (A.2)$$

$$R = 98.6\%$$

Louver 1 with louver blades inclined at 60° without a mesh-screen:

$$Q = 0.0374 \, \Delta P^{\,0.5326} \qquad (A.3)$$

$$R = 99.88\%$$

Louver Blade Inclination (deg)	Regression coefficients		Spacer thickness (mm) between mesh-screen and louver					
			0	3	6	9	12	15
0	α	Power Law	0.0702	0.0705	0.0717	0.0729	0.0742	0.0746
	β		0.8139	0.7756	0.7744	0.7866	0.7694	0.7801
	R		99.81	99.69	99.76	99.74	99.64	99.37
	a	Quadratic	34.686	19.794	17.839	14.827	18.856	13.171
	b		12.021	12.72	12.662	12.61	11.91	12.386
	R		99.39	99.47	99.31	99.33	99.41	99.32
60	α	Power Law	0.032	0.0333	0.0321	0.033	0.0323	0.0333
	β		0.6767	0.6802	0.6771	0.671	0.6859	0.6607
	R		88.83	99.8	99.79	99.76	99.78	99.61
	a	Quadratic	157.82	152.62	157.75	152.77	155.25	155.1
	b		33.32	31.899	34.035	33	33.347	33.307
	R		99.12	99.1	99.13	99.09	99.11	99.04

Table A.8:
Derived data for Louver 1 with 50% and 70% free-area mesh-screens (pressurisation)

Louver Blade Inclination (deg)	Regression coefficients		Spacer thickness (mm) between mesh-screen and louver					
			0	3	6	9	12	15
0	α	50% FA mesh-screen	-	0.1674	0.1895	0.196	0.1686	0.1861
	β		-	0.7649	0.8225	0.7948	0.7463	0.802
	R		-	99.8	99.52	99.53	98.79	99.78
	α	70% FA mesh-screen	0.1843	0.1583	0.1608	0.1843	0.1661	0.1766
	β		0.7518	0.7044	0.7245	0.8244	0.7172	0.7914
	R		99.75	99.36	99.15	99.75	99.38	99.84
30	α	50% FA mesh-screen	0.096	0.0944	0.1018	0.0949	0.1	0.098
	β		0.696	0.6393	0.7385	0.6214	0.6426	0.6662
	R		99.86	99.07	99.86	99.42	99.63	99.51
	α	70% FA mesh-screen	0.1016	0.0996	0.0996	0.1008	0.1002	0.1014
	β		0.6167	0.6314	0.6984	0.6975	0.7085	0.7268
	R		98.55	99.25	99.59	99.64	99.75	99.59
60	α	50% FA mesh-screen	0.0385	0.0387	0.038	0.0387	0.0366	0.0413
	β		0.5729	0.5636	0.6289	0.6181	0.6313	0.5273
	R		99.16	99	99.63	99.58	99.72	98.21
	α	70% FA mesh-screen	0.0407	0.0391	0.0404	0.0392	0.0422	0.0412
	β		0.5603	0.5977	0.6139	0.6162	0.5122	0.5411
	R		99.02	99.44	99.69	99.47	98.33	99.59

Slot Reference and details	CFD predicted data				Derived data		Regression coefficients	
	Without mesh-screen		With mesh-screen		Without mesh-screen	With mesh-screen		
	Q (l/s)	ΔP (Pa)	Q (l/s)	ΔP (Pa)				
Slot A1: height = 6mm, depth = 12mm	1.5	1.076	1.0	1.330	0.0014	0.0009	α	Power Law
	2.5	3.040	1.5	3.009	0.5719	0.4954	β	
	3.5	5.282	2.0	5.578	99.53	99.94	R	
	4.5	7.447	2.5	8.613	256442	1.00E+06	a	Quadratic
	5.0	9.364	3.0	11.981	544.49	120.01	b	
	5.5	10.606			99.6	99.9	R	
Slot A1: height = 12mm, depth = 12mm	1.5	0.308	2.0	2.140	0.0028	0.0014	α	Power Law
	2.5	0.777	2.5	3.342	0.5082	0.5005	β	
	3.5	1.645	3.0	4.808	99.92	100	R	
	5.0	3.078	4.0	8.543	119115	533745	a	Quadratic
	7.5	7.398	4.5	10.820	53.045	1.8677	b	
	10.8	14.393			99.91	100	R	
Slot A1: height = 18mm, depth = 12mm	1.5	0.137	1.5	0.535	0.0042	0.0021	α	Power Law
	2.5	0.241	2.0	0.950	0.4779	0.5007	β	
	3.5	0.728	3.0	2.132	99.12	100	R	
	5.0	1.477	3.5	2.903	57853	236416	a	Quadratic
	7.5	3.317	5.0	5.920	20.123	1.819	b	
	10.0	6.313	6.2	9.099	99.88	100	R	
	15.0	13.211						

Table A10: CFD predicted and derived parameters for slots A4 to A6

Slot Reference and details	CFD predicted data				Derived data		Regression coefficients	
	Without mesh-screen		With mesh-screen		Without mesh-screen	With mesh-screen		
	Q (l/s)	ΔP (Pa)	Q (l/s)	ΔP (Pa)				
Slot A4: height = 24mm, depth = 12mm	2.0	0.132	1.5	0.355	0.0055	0.0025	α	Power Law
	3.5	0.401	2.5	1.027	0.4986	0.4951	β	
	5.0	0.814	3.5	2.009	99.99	99.99	R	
	7.5	1.831	5.0	4.102	34777	163572	a	Quadratic
	10.0	3.260	7.5	9.206	-20.223	1.0967	b	
	15.0	7.299			99.9	100	R	
	17.0	9.874						
Slot A5: height = 30mm, depth = 12mm	2.0	0.098	2.0	0.403	0.0065	0.0032	α	Power Law
	3.5	0.295	3.0	0.907	0.5034	0.4999	β	
	5.0	0.598	5.5	3.050	100	100	R	
	10.0	2.386	8.0	6.458	23631	100878	a	Quadratic
	15.0	5.341	10.0	10.084	1.8121	-0.5818	b	
	20.0	9.490			100	100	R	
Slot A6: height = 36mm, depth = 12mm	2.5	0.108	1.5	0.182	0.0076	0.0035	α	Power Law
	3.5	0.211	3.0	0.729	0.5027	0.4962	β	
	5.0	0.418	5.5	2.454	99.97	99.99	R	
	7.5	1.024	8.0	5.198	16498	87870	a	Quadratic
	20.0	6.711	10.0	8.468	6.4968	-38.571	b	
	25.0	10.483			100	99.95	R	

Table A11: CFD predicted and derived parameters for slots B1 to B3

Slot Reference and details	CFD predicted data Without mesh-screen		Derived data Without mesh-screen	Regression coefficients	
	Q (l/s)	ΔP (Pa)			
Slot B1: height = 12mm, depth = 6mm	1.5	0.16950	0.0038	α	Power Law
	2.0	0.29540	0.5133	β	
	2.5	0.45680	99.92	R	
	3.5	0.81810	68299	a	Quadratic
	5.0	1.75620	-1.0587	b	
	7.5	3.73630	99.96	R	
	10.5	7.55630			
Slot B2: height = 12mm, depth = 12mm	1.5	0.16948	0.0038	α	Power Law
	2.0	0.27697	0.5122	β	
	2.5	0.42837	99.97	R	
	3.0	0.61323			
	3.5	0.83158	65384	a	Quadratic
	5.0	1.68120	9.1112	b	
	7.5	3.74930	100	R	
	10.5	7.30330			
Slot B3: height = 12mm, depth = 18mm	1.5	0.15870	0.0038	α	Power Law
	2.0	0.27740	0.5062	β	
	2.5	0.42930	99.89	R	
	3.0	0.69210	66252	a	Quadratic
	3.5	0.83480	11.008	b	
	5.0	1.69180	99.99	R	
	10.5	7.42200			

Table A12: CFD predicted and derived parameters for slots B4 to B6

Slot Reference and details	CFD predicted Without mesh-screen		Derived data Without mesh-screen	Regression coefficients	
	Q (l/s)	ΔP (Pa)			
Slot B4: height = 12mm, depth = 24mm	1.5	0.16190	0.0038	α	Power Law
	2.0	0.28200	0.5076	β	
	2.5	0.43480	100	R	
	3.0	0.62150	67070	a	Quadratic
	3.5	0.84330	6.112	b	
	5.0	1.70500	100	R	
	10.5	7.45860			
Slot B5: height = 12mm, depth = 30mm	1.5	0.16335	0.0038	α	Power Law
	2.0	0.28012	0.507	β	
	2.5	0.43380	100	R	
	3.5	0.85481			
	5.0	1.71500	66119	a	Quadratic
	10.5	3.88100	14.764	b	
	12.0	9.69825	100	R	
Slot B3: height = 12mm, depth = 36mm	2.0	0.28897	0.0038	α	Power Law
	3.0	0.63861	0.5081	β	
	3.5	0.86473	100	R	
	5.0	1.74495	67826	a	Quadratic
	7.5	3.89140	9.777	b	
	10.5	7.58100	100	R	
	12.3	10.52710			

Appendix B:

Published Academic Papers based on Investigations Detailed in this Thesis

Published Papers

Journal Papers

Chilengwe N. and Sharples S. *Parametric analysis of air flow through ventilators.* International Journal of Ventilation, Vol. 1 (2), pp 109 - 117, October 2002.

Chilengwe N. and Sharples S. *Low and high pressure experimental analysis of ventilators for natural ventilation in buildings.* International Journal of Ventilation, Vol. 2 (2), pp 149 - 158, September 2003.

Conference Papers

Chilengwe N. and Sharples S. *Airflow performance characteristics of ventilators in hybrid ventilation systems.* Proceedings of the 25th AIVC Conference, Paper 050, Prague, Czech Republic, 15 - 17 September, 2004.

Chilengwe N. and Sharples S. *CFD and experimental analysis of ventilators to improve airflow performance for natural ventilation.* Proceedings of the First Scottish Conference for Postgraduate Researchers in the Built & Natural Environment (PRoBE), Glasgow, Scotland, 18 - 19 November, 2003.

Sharples S. and Chilengwe N. *Directional airflow performance of ventilators for natural ventilation.* Proceedings of the 24th AIVC Conference, Paper 024, Washington DC, USA, 12 - 14 October, 2003.

Sharples S. and Chilengwe N. *Optimising the design of ventilators for natural ventilation.* Proceedings of the 9th International Conference on Indoor Air Quality and Climate, Monterey, California, USA, June 30 - July 5, 2002.

Sharples S. and Chilengwe N. *Parametric analysis of the airflow performance of ventilators.* Proceedings of the 22nd AIVC Conference, Paper 33, Bath, UK, 11 - 13 September, 2001.

Papers in Preparation

Chilengwe N. and Sharples S. *A new approach to understanding the airflow performance of ventilator components for natural ventilation applications.*

Chilengwe N. and Sharples S. *Airflow through combinations of slots and mesh-screens at low and high pressure differentials.*

Sharples S. and Chilengwe N. *An Application of Computational Fluid Dynamics to the Design and Analysis of Airflow through Ventilators for Natural Ventilation in Buildings.*

Sharples S. and Chilengwe N. *Generic equations for optimising the airflow performance of ventilators for natural ventilation in buildings.*